Outburst floods from moraine-dammed lakes in the Himalayas

Detection, frequency, and hazard

Georg Veh

Cumulative dissertation submitted for obtaining
the degree "Doctor of Natural Sciences" (Dr. rer. nat.)
in the research discipline Natural Hazards

Institute of Environmental Science and Geography
Faculty of Science
University of Potsdam

submitted on March 26, 2019
defended on August 12, 2019

First supervisor: PD Dr. Ariane Walz
Second supervisor: Prof. Oliver Korup, PhD

First reviewer: PD Dr. Ariane Walz
Second reviewer: Prof. Oliver Korup, PhD
Independent reviewer: Prof. Dr. Wilfried Haeberli

Published online at the
Institutional Repository of the University of Potsdam:
https://doi.org/10.25932/publishup-43607
https://nbn-resolving.org/urn:nbn:de:kobv:517-opus4-436071

Declaration of Authorship

I, Georg Veh, declare that this thesis entitled “Outburst floods from moraine-dammed lakes in the Himalayas: Detection, frequency, and hazard” and the work presented in it are my own. I confirm that:

- This work was done completely or mainly while in candidature for a research degree at the University of Potsdam.
- Where any part of this dissertation has previously been submitted for a degree or any other qualification at the University of Potsdam, or any other institution, this has been clearly stated.
- Where I have consulted the published work of others, this is always clearly attributed.
- Where I have quoted the work of others, the source is always given. With the exception of such quotations, this thesis is entirely my own work.
- I have acknowledged all main sources of help.
- Where the thesis is based on work done by myself jointly with others, I have made clear exactly what was done by others and what I have contributed myself.

_____ _____

Location & Date Georg Veh

Abstract

High mountain regions are the water towers of the Earth. They can store snow and ice over seasons to years, and their meltwater is a vital resource of freshwater for humans and ecosystems. Clearly, the benefits from mountain runoff are manifold, from its primary use as drinking water, to irrigation, and hydropower generation. Human activity and settlements thus gradually moved into river headwaters over the past centuries, accepting that this environment hosts many sources of natural hazards. Weather and topography can change frequently over short distances, so that single events, such as avalanches, flash floods and debris flows have resulted in dramatic loss of human lives and damages to infrastructure. One prominent notion is that ongoing global atmospheric warming will express most severely in high mountains. Disasters from snow- and ice-related processes may hence become more frequent, with possibly higher magnitudes.

The Himalayas are a region that is most dependent, but also frequently prone to hazards from changing meltwater resources. This mountain belt hosts the highest mountain peaks on earth, has the largest reserve of ice outside the polar regions, and is home to a rapidly growing population in recent decades. One source of hazard has attracted scientific research in particular in the past two decades: glacial lake outburst floods (GLOFs) occurred rarely, but mostly with fatal and catastrophic consequences for downstream communities and infrastructure. Such GLOFs can suddenly release several million cubic meters of water from naturally impounded meltwater lakes. Glacial lakes have grown in number and size by ongoing glacial mass losses in the Himalayas. Theory holds that enhanced meltwater production may increase GLOF frequency, but has never been tested so far. The key challenge to test this notion are the high altitudes of >4000 m, at which lakes occur, making field work impractical. Moreover, flood waves can attenuate rapidly in mountain channels downstream, so that many GLOFs have likely gone unnoticed in past decades. Our knowledge on GLOFs is hence likely biased towards larger, destructive cases, which challenges a detailed quantification of their frequency and their response to atmospheric warming. Robustly quantifying the magnitude and frequency of GLOFs is essential for risk assessment and management along mountain rivers, not least to implement their return periods in building design codes.

Motivated by this limited knowledge of GLOF frequency and hazard, I developed an algorithm that efficiently detects GLOFs from satellite images. In essence, this algorithm classifies land cover in 30 years (~1988–2017) of continuously recorded Landsat images over the Himalayas, and calculates likelihoods for rapidly shrinking water bodies in the stack of land cover images. I visually assessed such detected tell-tale sites for sediment fans in the river channel downstream, a second key diagnostic of GLOFs. Rigorous tests and validation with known cases from roughly 10% of the Himalayas suggested that this algorithm is robust against frequent image noise, and hence

capable to identify previously unknown GLOFs. Extending the search radius to the entire Himalayan mountain range revealed some 22 newly detected GLOFs. I thus more than doubled the existing GLOF count from 16 previously known cases since 1988, and found a dominant cluster of GLOFs in the Central and Eastern Himalayas (Bhutan and Eastern Nepal), compared to the rarer affected ranges in the North. Yet, the total of 38 GLOFs showed no change in the annual frequency, so that the activity of GLOFs per unit glacial lake area has decreased in the past 30 years. I discussed possible drivers for this finding, but left a further attribution to distinct GLOF-triggering mechanisms open to future research.

This updated GLOF frequency was the key input for assessing GLOF hazard for the entire Himalayan mountain belt and several subregions. I used standard definitions in flood hydrology, describing hazard as the annual exceedance probability of a given flood peak discharge [$m^3\ s^{-1}$] or larger at the breach location. I coupled the empirical frequency of GLOFs per region to simulations of physically plausible peak discharges from all existing ~5,000 lakes in the Himalayas. Using an extreme-value model, I could hence calculate flood return periods. I found that the contemporary 100-year GLOF discharge (the flood level that is reached or exceeded on average once in 100 years) is $20{,}600^{+2{,}200}/_{-2{,}300}$ $m^3\ s^{-1}$ for the entire Himalayas. Given the spatial and temporal distribution of historic GLOFs, contemporary GLOF hazard is highest in the Eastern Himalayas, and lower for regions with rarer GLOF abundance. I also calculated GLOF hazard for some 9,500 overdeepenings, which could expose and fill with water, if all Himalayan glaciers have melted eventually. Assuming that the current GLOF rate remains unchanged, the 100-year GLOF discharge could double ($41{,}700^{+5{,}500}/_{-4{,}700}$ $m^3\ s^{-1}$), while the regional GLOF hazard may increase largest in the Karakoram.

To conclude, these three stages–from GLOF detection, to analysing their frequency and estimating regional GLOF hazard–provide a framework for modern GLOF hazard assessment. Given the rapidly growing population, infrastructure, and hydropower projects in the Himalayas, this thesis assists in quantifying the purely climate-driven contribution to hazard and risk from GLOFs.

Zusammenfassung

Hochgebirge bilden die Wassertürme unserer Erde. Sie können Schnee und Eis über viele Jahre hinweg speichern, und ebenso wieder als Schmelzwasser abgeben. Der Abfluss aus Hochgebirgen ist daher eine wichtige Süßwasserquelle für Ökosysteme und seit den letzten Jahrhunderten zunehmend auch für den Menschen. Der Nutzen von Schmelzwasser reicht von seiner ursprünglichen Bedeutung als Trinkwasserressource, über Bewässerung in der Landwirtschaft, bis zur Gewinnung von Wasserenergie. Menschliches Handeln und Siedeln dehnte sich daher immer weiter in die Oberläufe der Flüsse aus, wohlwissend, dass diese Umgebung auch eine Vielzahl an Naturgefahren birgt. Wetter und Topographie ändern sich hier schnell auf engstem Raum, sodass einzelne Ereignisse wie Lawinen, Sturzfluten oder Murgänge in der Vergangenheit immer wieder zu tragischen Verlusten an Menschenleben und Schäden an Infrastruktur führten. Heutzutage deutet vieles darauf hin, dass der weltweit beobachtete Klimawandel am stärksten in Hochgebirgen zum Ausdruck kommen könnte. Gerade solche Prozesse, die durch das Abschmelzen von Schnee und Eis entstehen, könnten dadurch häufiger und eventuell mit einer stärkeren Intensität auftreten, was auch vermehrt Katastrophenfälle zur Folge hätte.

In kaum einer anderen Region treten Abhängigkeit, Nutzen und Gefährdung von Gletscher- und Schneeschmelze so deutlich zu Tage wie im Himalaya. Diese Gebirgskette beherbergt die höchsten Berge und das größte Eisvolumen außerhalb der Polregionen weltweit, und bietet Lebensraum und natürliche Ressourcen für eine jüngst rasch wachsende Bevölkerung. Naturgefahren sind hier allgegenwärtig, wobei eine die Wissenschaftler in den vergangen zwei Jahrzehnten besonders beschäftigte: Ausbrüche von Gletscherseen traten in der Vergangenheit zwar selten, aber meist mit katastrophalen Konsequenzen für die darunterliegenden Berggemeinden auf. Gletscherseeausbrüche (englisches Akronym GLOFs – *glacial lake outburst floods*) beschreiben den plötzlichen Ausfluss von teils mehreren Millionen Kubikmetern Wasser aus natürlich gedämmten Schmelzwasserseen. Anhaltender Gletscherrückgang in vergangenen Jahrzehnten schuf mehrere tausend Hochgebirgsseen, mit ununterbrochenem Wachstum in Anzahl und Fläche, was den Schluss auf ein möglicherweise vermehrtes Auftreten von GLOFs nahelegte. Diese suggerierte Zunahme von GLOFs konnte jedoch bisher weder getestet noch bestätigt werden, vor allem weil Seen überwiegend jenseits von 4,000 m üNN entstehen, was Feldstudien dort erschwert. Zudem schwächen sich diese Flutwellen meist schnell ab, sodass einige davon wahrscheinlich unentdeckt blieben. Unser Wissen über GLOFs ist daher möglicherweise zu größeren, schadensreichen Ereignissen verschoben, wodurch ihre aktuelle Frequenz, und letztlich auch ihr Zusammenhang mit dem Klimawandel, nur schwer quantifizierbar sind. Mit welcher Wiederkehrrate GLOFs auftreten ist nicht zuletzt

entscheidend für Risikoanalyse und -management entlang von Flüssen, um beispielsweise Gebäude entsprechend sicher gegenüber der zu erwartenden Häufigkeit und Magnitude von GLOFs zu planen.

Um einer Unterschätzung der tatsächlichen GLOF-Aktivität entgegenzuwirken, entwickelte ich einen Algorithmus, der GLOFs automatisch aus Satellitenbildern detektiert. Der Algorithmus greift auf etwa 30 Jahre kontinuierlich aufgenommene Landsat-Bilder (~1988-2017) zu, klassifiziert die Erdoberfläche in jedem einzelnen Bild und berechnet letztlich die Wahrscheinlichkeit, ob Wasserkörper rasch innerhalb dieser Bildzeitreihe geschrumpft sind. An solch gekennzeichneten Stellen suchte ich nach Anzeichen für Sedimentverlagerung im Gerinne flussabwärts, was ein zweites Hauptkriterium für GLOFs ist. Tests und Validierung in etwa 10% des Himalayas bestätigten, dass die Methode robust gegenüber häufig auftretenden atmosphärischen Störeffekten ist. Mit dem Ziel bisher unbekannte GLOFs zu entdecken, wendete ich daher diesen Algorithmus auf den gesamten Himalaya an. Die Suche ergab 22 neu entdeckte GLOFs, was das bestehende Inventar von 16 bekannten GLOFs seit 1988 mehr als verdoppelt. Das aktualisierte räumliche Verbreitungsmuster bestätigte einmal mehr, dass GLOFs vermehrt im Zentral- und Osthimalaya (Bhutan und Ost-Nepal) auftraten, wohingegen im Norden deutlich weniger GLOFs stattfanden. Entgegen der häufigen Annahme stellte ich jedoch fest, dass die jährliche Häufigkeit von GLOFs in den letzten drei Jahrzehnten konstant blieb. Dadurch hat das Verhältnis von GLOFs pro Einheit See(-fläche) in diesem Zeitraum sogar abgenommen. Ich diskutiere mögliche Gründe für dieses Ergebnis, lasse aber eine tiefergehende Analyse von möglichen Ausbruchsfaktoren offen für zukünftige Forschung.

Dieses räumlich aufgelöste GLOF-Inventar bot nun die Möglichkeit, das Gefährdungspotential durch GLOFs für den gesamten Himalaya und einzelne Regionen zu berechnen. Dafür verwendete ich die in der Hochwasseranalyse gebräuchliche Definition von Gefährdung, welche die jährliche Überschreitungswahrscheinlichkeit einer gewissen Abflussmenge, in diesem Fall des Spitzenabflusses [m^3 s^{-1}] am Dammbruch, beschreibt. Das GLOF-Inventar liefert demnach die zeitliche Wahrscheinlichkeit für das Auftreten von GLOFs, während Simulationen von möglichen Spitzenabflüssen für alle heute existierenden ~5,000 Seen im Himalaya die zu erwarteten Magnituden beisteuerten. Mit Extremwertstatistik lässt sich so die mittlere Wiederkehrzeit dieser Spitzenabflüsse errechnen. Ich fand heraus, dass der 100-jährliche Abfluss (die Flutmagnitude, die im Durchschnitt einmal in 100 Jahren erreicht oder überschritten wird) derzeit bei rund $20{,}600^{+2{,}200}/_{-2{,}300}$ m^3 s^{-1} für den gesamten Himalaya liegt. Entsprechend der heutigen räumlichen und zeitlichen Verteilung von GLOFs ist die Gefährdung im Osthimalaya am höchsten und in Regionen mit wenig dokumentierten GLOFs vergleichsweise niedrig. Für ein Szenario, in dem der gesamte Himalaya in Zukunft eisfrei sein könnte, errechnete ich zudem das Gefährdungspotential von ~9,500 Übertiefungen unterhalb der heutigen Gletschern, die sich nach deren Abschmelzen mit

Wasser füllen könnten. Angenommen, dass die zukünftige GLOF-Rate der heutigen entspricht, könnte der 100-jährliche Abfluss sich mehr als verdoppeln ($41{,}700^{+5{,}500}/_{-4{,}700}$ m^3 s^{-1}), wobei der stärkste regionale Anstieg für den Karakorum zu erwarten wäre.

Zusammenfassend formen diese drei Schritte–von der Detektion von GLOFs, über die Bestimmung derer Frequenz, bis zur regionalen Abschätzung von Spitzenabflüssen–das Grundgerüst, das ein moderner Ansatz zur Gefahrenabschätzung von GLOFs benötigt. Angesichts einer wachsenden Exposition von Bevölkerung, Infrastruktur und Wasserkraftanlagen liefert diese Arbeit einen entscheidenden Beitrag, den Anteil des Klimawandels in der Gefährdung und Risiko durch GLOFs zu quantifizieren.

Acknowledgments

Many people have accompanied me through three and a half exciting, diverse, and not least challenging years. Clearly, without their help and support, I would not have realised this thesis and wish therefore to express my deep gratitude.

First, I want to thank my supervisors, Ariane Walz and Oliver Korup, for their commitment and patience, pushing me when necessary, giving me feedback and being open to my concerns at any time. I feel honoured that I could (and will) work with you, and will never forget about your inspiring attitude towards life in- and outside academia.

Special thanks go to my mentor Sigrid Roessner for constructive meetings and very detailed reviews to my manuscripts. I also thank Wilfried Haeberli for reviewing this thesis.

Then there is the whole graduate school *NatRiskChange*, which simply overwhelmed me with regards how diverse and fruitful work in academia can be. Each of the many meetings, retreats and conferences will stay in good memory. Special thanks go to (in alphabetical order) Ankit Agarwal, Berry Boessenkool, Irene Crisologo, Jennifer von Keyserlingk, Jonas Laudan, Ugur Öztürk, Erwin Rottler, Tobias Sieg, Sebastian von Specht, and Dadiyorto Wendi – you're awesome! I also want to thank the spokespersons of *NatRiskChange*, Axel Bronstert and Annegret Thieken, given that "*NatRiskChange* will pay!" was indeed true for all my demands on computational power.

My gratitude also goes to the members of the working groups *Landscape Management* and *Geohazards* for their feedback during team meetings, not to forget about the annual team building events at the Potsdamer Weihnachtsmarkt.

I also wish to emphasize my old and new flatmates, and friends in and far away from Potsdam–Lisa A., Paula, Lisa L., Amelie, Moriz, Kerstin, and Arnt–for lots of fun outside the office.

And finally, I would like to thank my parents, my brothers and sisters, and above all, my dear Steffi, for their endless support, trust and love at any time.

Table of Contents

1. Introduction

1.1. Climate Change in the Himalayas

The Himalayas and its adjacent mountain ranges, the Hindu Kush, Karakoram, Nyaiqentanglha and Hengduan Shan, form one of Earth's largest mountain belts, spanning >3,000 km across eight countries: Afghanistan, Pakistan, India, Nepal, Bhutan, Myanmar and China (Figure 1-1). Ten major rivers, including the Indus, Ganges and Brahmaputra, drain this region and sustain the livelihood of 240 million people in the mountains and their foothills. Another 1.4 billion people downstream depend at least partly on the runoff that these rivers provide for households, agriculture, and hydropower operations. Approximately 45,600 glaciers cover ~52,200 km^2 in the headwaters of these rivers today (Arendt et al., 2015), and their meltwater plays a key role in modulating stream flow throughout the year. Glacial runoff from the Himalayas is an important buffer against drought in regions with hot and dry summers such as the upper Indus Basin, during which storages from snow and rainfall are declining or have already depleted (Kaser et al., 2010; Lutz et al., 2014). Not least the growing trends in population and economy in recent decades underline the benefits, but also the dependency from glacial melt in the Himalayas (Wester et al., 2019).

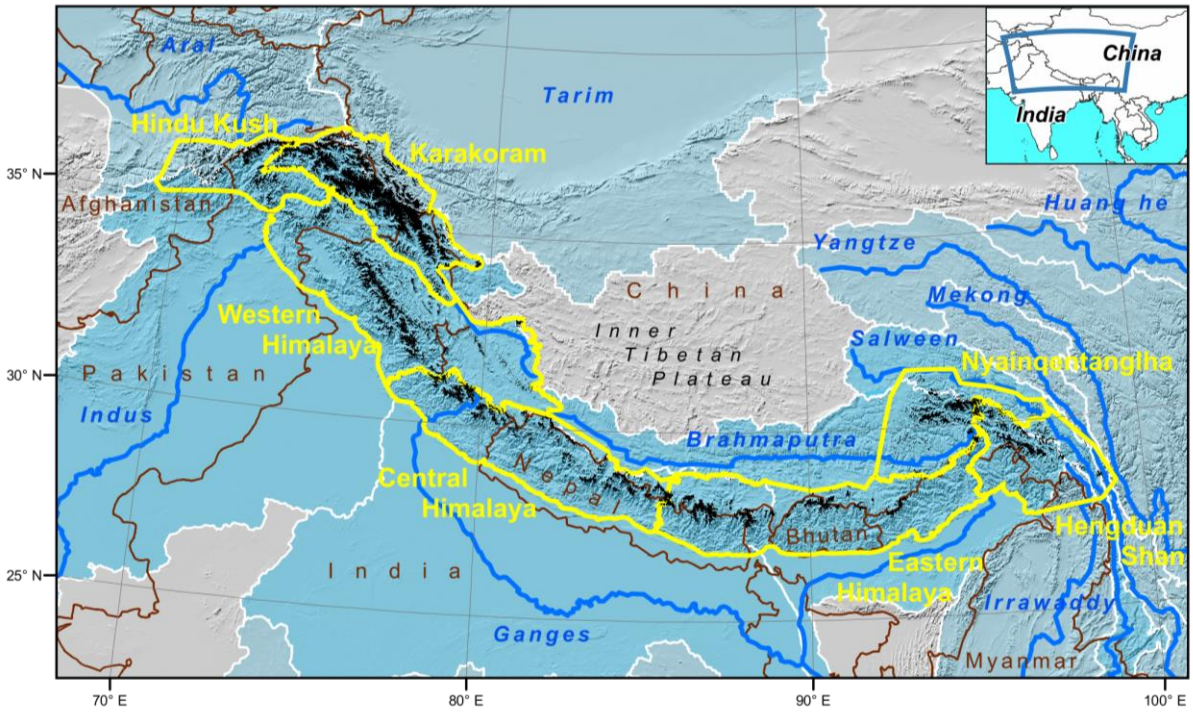

Figure 1-1: The Himalayas and the main river basins draining the Tibetan Plateau. *Basins are light blue with dark blue rivers and labels; subregions of the Himalayas are yellow; country borders and labels are brown; and glaciers are black.*

We may thus understand the stir that arose from the Fourth Assessment Report of the Intergovernmental Panel on Climate Change (IPCC) in 2007. Then, the experts noted that Himalayan glaciers are retreating faster than in any other mountain range, and would likely be gone by 2035, if warming continued as before (IPCC, 2007). Though these statements were rather quickly convicted of erroneous referencing (Cogley et al., 2010), it took five years to summarise for the first time the current state of Himalayan glaciers (Bolch et al., 2012; Kääb et al., 2012). Apart from the general conclusion that Himalayan glacier mass balances are mostly negative and far from uniform, scientists realized that knowledge on glacier processes in this and neighbouring mountain ranges was limited with large uncertainties about the impacts of climate change. After a decade of minutely quantifying historic glacier changes, evidence has substantiated that the region-wide glacier mass balance has likely been negative since at least the 1970s (Bolch et al., 2019). Several studies independently provided estimates of mass balances for the 21st century, accentuating the highest mass losses in the Western Himalayas (or Spiti Lahaul) and the Nyainqentanglha Mountains (Brun et al., 2017; Kääb et al., 2015, 2012), and more stable ice volumes for the Karakoram (Bolch et al., 2017; Gardelle et al., 2012) (Figure 1-2).

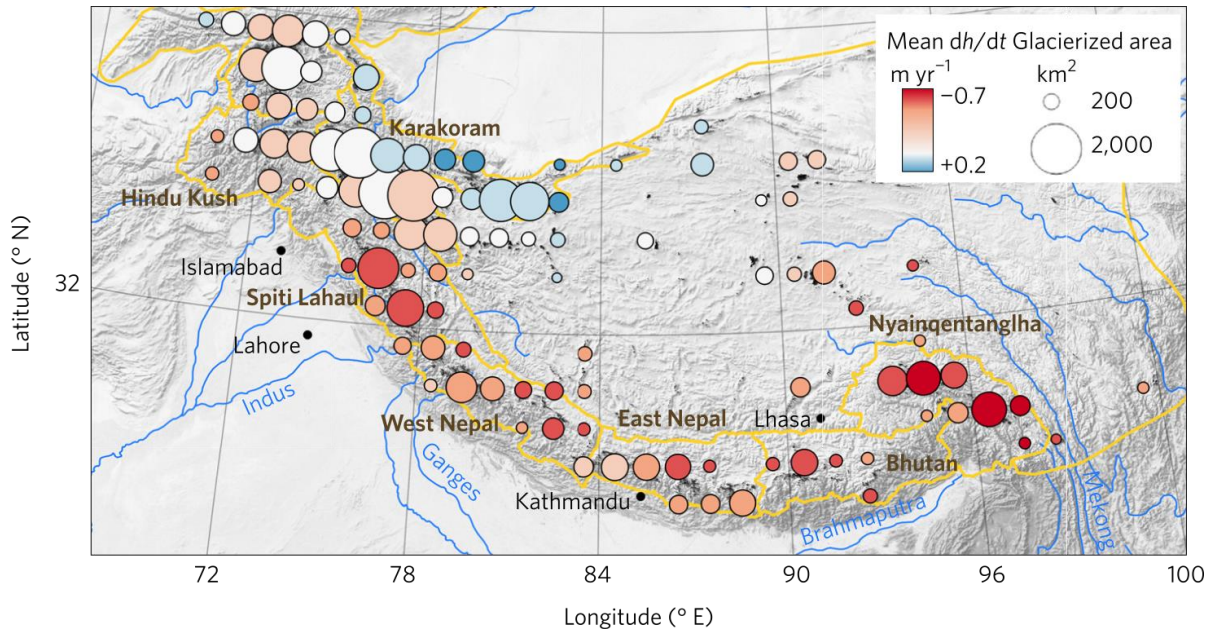

Figure 1-2: Glacier elevation changes and mass balance for High Mountain Asia (2000–2016). *Glacier elevation change is averaged over the study period (dh/dt) and aggregated on a 1° × 1° grid. Modified after Brun et al. (2017).*

Glacier changes are challenging to capture locally, because ice flow responds with delay to climatic changes. A glacier's annual mass budget can be out of balance for years, until measurable fluctuations of the glacier terminus–a conventional indicator for long-term mass change–indicate

either advance (mass accumulation) or "retreat" (mass loss) (Jóhannesson et al., 1989). Glacial lakes, by contrast, are an appropriate archive of negative mass balances, and hence atmospheric warming, because they form and grow when glaciers waste back from their former frontal position and expose accumulation space for meltwater (Grabs and Hanisch, 1993; Mool, 1995; Yamada and Sharma, 1993). Thousands of such glacial lakes have thus appeared behind moraines or in bedrock depressions and cirques, and many more are recently forming as supraglacial ponds (Benn et al., 2012; Miles et al., 2017; Thompson et al., 2012; Watson et al., 2016). Mapping glacial lakes from satellite imagery, assessing their geometric and topographic properties, and tracking their changes over time has become a core field of research in Himalayan glaciology (Table 1.1). The International Centre for Integrated Mountain Development (ICIMOD) generated a first consistent glacial lake inventory for the entire Himalayas from Landsat images between 2004 and 2007, covering 25,614 glacial lakes >0.003 km^2 between 3,500 and 6,000 m a.s.l. (Maharjan et al., 2018) (Figure 1-3). Contemporary lake density per unit area is similarly high in the Hindu Kush, the Eastern Himalayas, the Nyainqentanglha, and the Hengduan Shan, while most lake area (and hence water volume) has accumulated in the Eastern Himalayas. Quantifying lake changes on regional scales is challenging and difficult to compare between studies, because multi-temporal inventories cover different periods, basins, lake types, data sources, and mapping conventions (Table 1.1). A synopsis of 15 regional multi-temporal inventories (Table 1.1) suggests that recorded lake numbers have increased less consistently than lake areas. Since 1990, lakes areas have grown largest in the Central Himalayas (+23%), and lowest in the Northwestern Himalayas (+5.0%) (Nie et al., 2017).

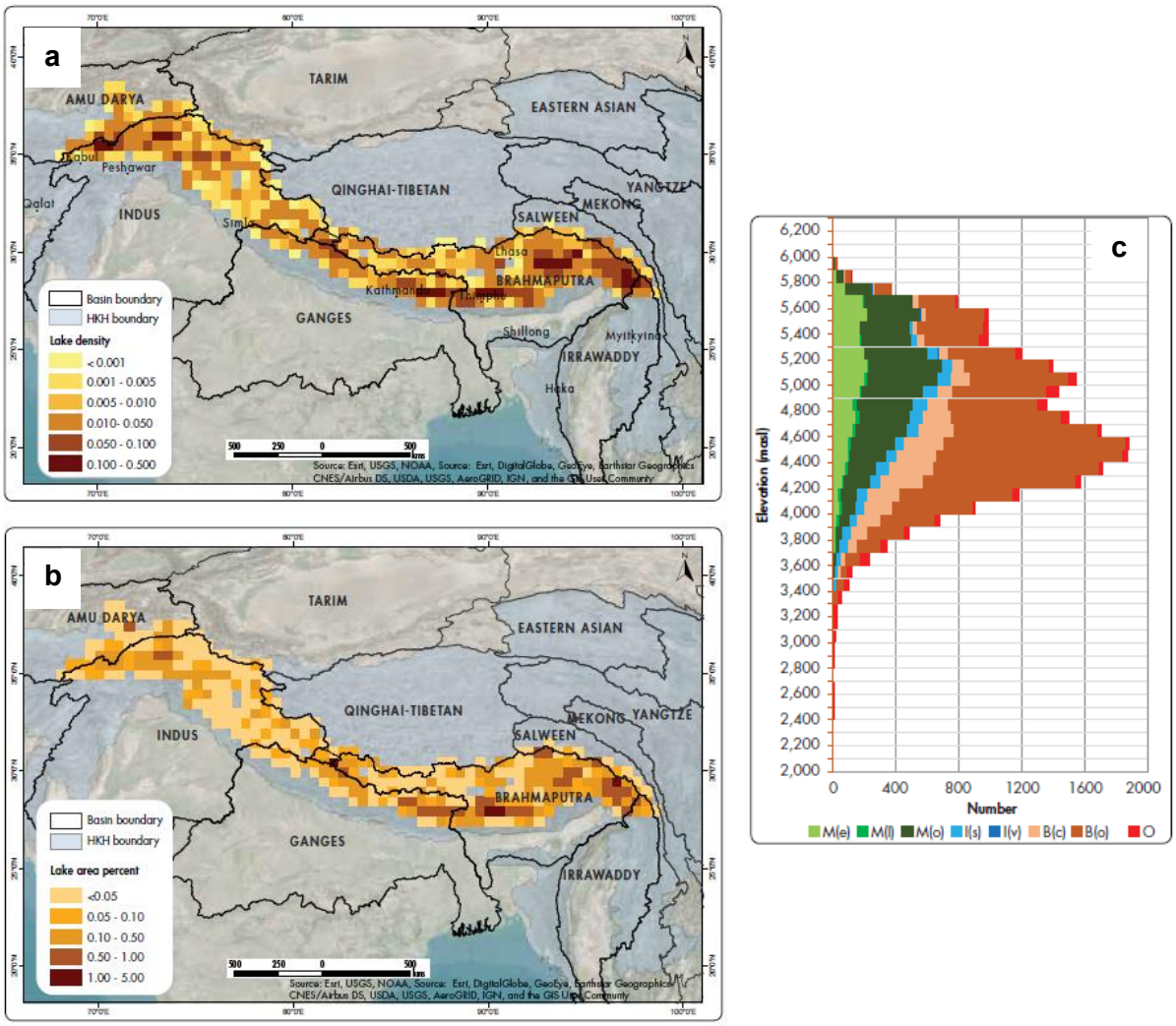

Figure 1-3: Lake abundance in the Himalayas. a, *Lake density, calculated as the number of glacial lakes occurring in a grid of 0.5° × 0.5°.* ***b,*** *Lake area, given as the percentage of the grid area covered by lakes.* ***c,*** *Elevation distribution of glacial lakes by dam type: M(e) Terminal moraine; M(l) Lateral moraine, M(o) Other moraine-dammed lakes; I(s) Supraglacial lakes; I(v) Glacier-dammed lakes; B(c) Cirque; B(o) Other bedrock-dammed lakes; O Others. Most of the lakes formed in bedrock depressions. Adapted from Maharjan et al. (2018).*

Table 1.1: Glacial lake inventories for the entire Himalayas and subregions. *Inventories are classified into static snapshots (mapped for a specific year) and multi-temporal inventories.*

Period	Period of mapping	Authors	Region	Number of lakes reported	Area covered by glacial lakes [km^2]	Minimum mapping unit [km^2]	Data sources for mapping
static	2004-2007	(Maharjan et al., 2018) / ICIMOD	Hindu Kush Himalaya	25,614	1,444	0.003	Landsat ETM+
	1999-2005	(Ives et al., 2010) / ICIMOD	Himalayas without Afghanistan, Arunachal Pradesh, Jammu and Kashmir, Myanmar	8,790	801.83	NA	Topographic maps; remote sensing: Landsat, IRS, LISS3, SPOT
	2015	(Chen et al., 2017)	Tibetan Plateau (including Himalayas)	8,215	832.19	0.0081	Landsat OLI
	2009	(Wang et al., 2011a)	Boshula Range (Tibet)	78	NA	0.02	Topographic maps, Landsat TM, ALOS AVNIR-2
	2001	(Ashraf et al., 2012)	Hindu Kush, Karakoram and Himalaya in Pakistan	2,420	126.35	0.02	Landsat ETM+
	2013	(Senese et al., 2018)	Central Karakoram National Park	202	3.56	NA	Landsat OLI
	2000-2002	(Worni et al., 2013)	Indian Himalayas	251	NA	0.01	Landsat ETM+, Google Earth imagery
	2000s	(X. Wang et al., 2012)	Chinese Himalayas	1,680	68.13	NA	Remote sensing analysis
	2008	(Salerno et al., 2012)	Mount Everest region	624	7.43	0.0001	AVNIR-2
	2000-2010	(Fujita et al., 2013)	Himalaya	2,276	233.3	0.005	ASTER
multitemporal	nearly annually 1975-2017	(Haritashya et al., 2018)	Nepal Himalaya	1975: 3 2017: 3	1975: 0.63 2017: 4	NA	Landsat MSS, TM, ETM+, OLI
	~1990, ~2010	(Nagai et al., 2017)	Bhutan Himalaya	~1990: ? ~2010: 733	~1990: ? ~2010: 82.6	0.01	ALOS
	2000, 2015	(Rounce et al., 2017)	Nepal Himalaya	2000: 131 2015: 131	2000: 37.8 2015: 41.3	0.1	Landsat ETM+, OLI
	1990, 2000, 2009	(Gardelle et al., 2011)	Hindu Kush, Karakoram, Spiti Lahaul, Garhwal, West Nepal, Everest and Bhutan	?	?	0.0036	Landsat ETM+
	1970s, 2000s	(Xin et al., 2012)	Chinese Himalaya	1970s: 1,750 2000s: 1,680	1970s: 166.48 2000s: 215.28	NA	ASTER
	2002, 2008, 2014	(Prakash and Nagarajan, 2017)	Chandra-Bhaga basin (Western Himalaya)	2002: 26 2008: 29 2014: 30	2002: 2.45 2008: 2.75 2014: 3.62	0.005	Landsat TM, ETM+, OLI
	2000, 2014	(Song et al., 2017)	Himalayas	2000: 151 2014: 151	2000: ? 2014: ?	0.5	Landsat scenes, IceSat
	1970, 1988, 2001, 2009	(Wang et al., 2011b)	Boshula Range (Tibet)	1970: 96 1988: 98 2001: 108 2009: 123	1970: 9.24 1988: 9.85 2001: 10.43 2009: 10.96	0.02	Topographic maps, Landsat TM, ETM+, ALOS AVNIR-2
	1988, 2013	(Song et al., 2016)	South Eastern Tibet	1988: 1,278 2013: 1,396	1988: 85.02 2013: 93.09	0.0045	Landsat TM, ETM+, OLI
	1976, 1991, 2000, 2010	(W. Wang et al., 2015)	Poiqu Basin (Central Himalayas)	1976: 52 1991: 55 2000: 63 2010: 69	1976: 10.68 1991: 13.15 2000: 15.67 2010: 19.55	0.01	Landsat MSS, TM, ETM+
	1990, 2010s	(S. Wang et al., 2015)	Chinese Himalaya	1990: ? 2010s: 329	1990: 100.26 2010s: 125.43	0.02	Landsat TM, ETM+
	1990s, 2000s 2009	(Li and Sheng, 2012)	Himalayas	1990s: 11,056 2000s: 12,318 2009:11,289	1990s:256.25 2000s: 272.07 2009: 289.04	0.0045	Landsat TM, ETM+

	~1990, 2000, 2010	(Zhang et al., 2015a)	Third Pole region	~1990: 4,602 2000: 4,981 2010: 5,701	~1990: 553.9 2000: 581.2 2010: 682.4	0.003	Landsat TM, ETM+
	1990, 2000, 2005, 2010	(Nie et al., 2013)	Central Himalaya	1990: 1,191 2000: 1,290 2005: 1,303 2010: 1,314	1990: 168.4 2000: 185.28 2005: 190.84 2010: 197.22	0.0081	Landsat TM, ETM+
	1990, 2000, 2005, 2010, 2015	(Nie et al., 2017)	Himalayas	1990: 4,549 2000: 4,671 2005: 4,691 2010: 4,723 2015:4,950	1990: 389.9 2000: 421.2 2005: 431.4 2010: 442.3 2015:455.3	0.0081	Landsat TM, ETM+, OLI

1.2. Outburst floods from moraine-dammed lakes

The wealth of studies on glacial lakes has had a motive other than changing lake geometries alone, however. Another main reason for the high research attention on glacial lakes is that *"glacier lake outburst floods may become more frequent as glaciers thin and recede because new lakes will form and existing ones might grow"* (Huss et al., 2017). Such glacial lake outburst floods (GLOFs) are single-source hazards that suddenly release meltwater at peak discharges often several times higher than those of hydro-meteorological floods, and entrain, transport and deposit exceptional amounts of sediment (Korup and Tweed, 2007). In this context, one of the earliest systematic studies on this phenomenon in the Himalayas by Richardson and Reynolds (2000) issued confidence that *"the potential for larger and more frequent floods is undoubtedly increasing"*. The ICIMOD similarly expects that the consequence in terms of *"the potential for acceleration of extensive downstream damage and loss of life is high"* (Ives et al., 2010).

Part of these early projections were based on detailed observations of GLOFs, particularly from a series of four large floods from moraine-dammed lakes in Nepal and Bhutan between 1981 and 1998. Among all historic GLOFs since the 20th century, the 1981 GLOF from Lake Zhangzangbo in China still holds the record for the highest estimated peak discharge of ~16,000 m^3 s^{-1} (Xu, 1988). The GLOF from Lake Dig Tsho (Nepal) four years later released ~5 million m^3 of water, transported 3 million m^3 of debris, and destroyed "*a newly built hydroelectric power plant, 14 bridges, about 30 houses, and many hectares of valuable arable land,* [and damaged a] *trail network"* (Vuichard and Zimmermann, 1987). In 1994, the breach of Lake Luggye Tsho (Bhutan) initiated a flood that was two metres deep some 200 km downstream from the source, killing 21 people (Richardson and Reynolds, 2000; Watanabe and Rothacher, 1996). The GLOF from Tam Pokhari in Nepal 1998 had a mean active channel width of >160 m, flow depths of >20 m, and moved ~440,000 m^3 of debris within the first 15 km; a damage of 156 million Nepalese Rupee [~1.25 million € today] was reported even 150 km downstream (Byers et al., 2013; Korup and Tweed, 2007; Osti and Egashira, 2009). With more than 6,000 fatalities, the disaster at Kedarnath (India) in 2013 had the highest death toll from GLOFs worldwide in modern history (Allen et al., 2016), mostly because the town of Kedarnath was located directly downstream of a minor glacial lake. A global assessment of GLOF impacts concludes that *"central Asia is the most vulnerable region to glacier floods causing extreme levels of societal impact,* [and] *Bhutan and Nepal are the countries with the greatest economic consequences of glacier flood impacts"* (Carrivick and Tweed, 2016). Considering their catastrophic downstream impacts and often short warning times, GLOFs have become one of the most emblematic, if not most widely publicised, cryospheric hazard tied to atmospheric warming (Emmer, 2018).

The two main source locations for GLOFs in the Himalayas are glacier- and moraine-dammed lakes (Richardson and Reynolds, 2000). Glacier dams have formed repeatedly in the Karakoram and Hindu Kush Mountains, blocking the discharge from tributary or trunk valleys by gradual or rapid (*surging*) glacier advances (Iturrizaga, 2011). Outbursts occur when the glacier ice begins to float on the dammed lake or the dam is eroded laterally, subglacially or superficially by the impounded water (Iturrizaga, 2011). The Upper Yarkant and Indus rivers (Karakoram) had a series of >100 outburst floods from glacier-dammed lakes from the mid-19th century until the 1960s, but fewer cases afterwards (Hewitt, 2014; Hewitt and Liu, 2010; Iturrizaga, 2005). Some 27 glacier-dammed lakes existed between 2004 and 2007 in the Karakoram (Maharjan et al., 2018), and Kyagar glacier has been the only flood source there in recent decades (Round et al., 2017; Yan et al., 2017). While future work may prod deeper into the mechanics of how glacier-dammed lakes form and fail, I focus here on >7,300 moraine-dammed lakes that currently dot the Himalayas (Maharjan et al., 2018). This focus is motivated by the conclusion of many previous studies that establishing a *"hypothetical link between climate change, glacier response, moraine-dammed lake formation and GLOF production* [is] *more straightforward compared to the range of processes driving GLOFs from ice- and bedrock-dammed lakes"* (Harrison et al., 2018).

Several conditioning factors and triggering mechanisms can make moraine-dammed lakes prone to outburst (Figure 1-4). Dams are often unvegetated, narrow and steeper than the angle of repose (Costa and Schuster, 1988), and contain loose, poorly sorted debris across a wide spectrum of clast sizes, from silt to large boulders (Clague and Evans, 2000). Some moraines also have ice cores that melt and thus create conduits for water to percolate through the dam (*piping*), weakening the stability of the dam (Richardson and Reynolds, 2000). Settlement of the dam, in turn, can decrease the vertical distance to the dam crest (*freeboard*), allowing overspill and breach initiation or decreasing the minimum wave height to overtop the dam (Westoby et al., 2014). Lake levels may also rise rapidly by water input from heavy rainfall or after periods of intense snow melt, reducing the shear resistance of the dam against the growing hydrostatic pressure (Worni et al., 2012). Other triggers for moraine-dam failures are mass movements such as calving glaciers, ice or rock avalanches, and debris flows or (outburst) floods from upstream. Such impacts induce displacement (*seiche*) waves that overtop, incise, and erode dams with otherwise sufficient freeboard (Korup and Tweed, 2007). Ice avalanches are the most prominent GLOF trigger in the Himalayas, initiating 34 of 38 cases with known triggers (Nie et al., 2018). In most cases, though, triggers happened unnoticed (Richardson and Reynolds, 2000), or are estimated without further field validation, given the remote locations of many lakes, far from human settlements. Once water overtops the dam, the initial breach channel erodes and enlarges progressively. Physical and geometric properties of the

dam (clast size, cohesion, slope, height, width, etc.) ultimately control whether the dam fails partially or completely and how rapidly it does so (Westoby et al., 2014). These properties also constrain the maximum possible discharge from a moraine-dammed lake, whereas the valley geometry and gradient define how rapidly the flood waves attenuate (Kershaw et al., 2005; Schwanghart et al., 2016b).

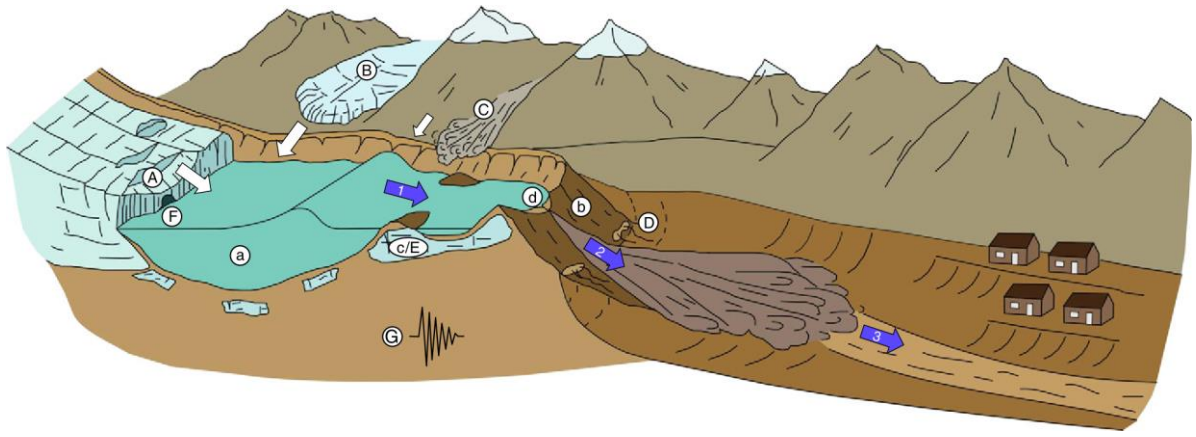

Figure 1-4: GLOF triggers, conditioning factors and key stages of flood propagation. *Capital letters are plausible triggers for GLOFs such as A) calving glaciers; B) snow and ice avalanches from hanging glaciers; C) rockfall, debris flows and landslides; D) dam settlement and/ or piping; E) melting ice-cores in the moraine; F) rapid water input from supra-, en-, or subglacial sources; G) seismic shaking weakening the cohesion of the moraine dam or triggering secondary gravitational mass movements. Lower case letters are conditioning factors for dam failure, including a) large lake volumes; b) low width-to-height dam ratio; c) degrading moraines from melting ice cores; d) brim-full lake basins. Numbers are key stages of GLOF propagation: 1) displacement or seiche waves on the lake; 2) breach initiation, dam erosion and incision; 3) propagation of the flood wave(s) downstream. Adapted from Westoby et al. (2014).*

1.3. Frequency of Himalayan GLOFs

The catastrophic impacts from moraine-dammed GLOFs have prompted calls to drain glacial lakes artificially in a controlled manner before they burst out (Kattelmann and Watanabe, 1997). Yet the thousands of glacial lakes in the Himalayas forbid such logistically challenging countermeasures, mainly because it is difficult to identify those lakes that are most prone to catastrophic outburst. Modern hazard assessment relies on quantifying the frequency and magnitude of a potentially damaging process, and hence the (annual) probability of a lake outburst of a given size, measured for example by the amount of water and sediment released or the peak discharge through the failing dam. Rigorously appraising and predicting changes in GLOF hazard requires baseline data, such as the current GLOF frequency, but suffers from the few reliable cases that enter scientific reports. Compiling inventories and estimating average GLOF rates has thus occupied scientists for more than two decades. Yamada and Sharma (1993), for example, reported that *"severe floods caused by glacier outburst have been frequent in the Nepal Himalayas, occurring more than every three years over the*

approximately thirty years since the 1960s". Bajracharya and Mool (2010) projected lower rates with *"at least one GLOF event occurring every 3–10 years in the Himalayan region"*. Four GLOFs in 1935, 1964, 1981, and 2016 in the Bhotekoshi River, Nepal, indicate return periods of about 30 years for this particular basin (Cook et al., 2018), whereas Harrison et al. (2018) recorded a total of 54 GLOFs for the entire Himalayas between 1878 and 2018. The most recent Himalayan GLOF inventory by Nie et al. (2018; Figure 1-5a) concluded that *"out of the 51 persuadable Himalayan GLOF events, 35 are known with specific occurrence years, while the other 16 events are perceived to have occurred before 1975"*. Clearly, the study periods and the compiled cases vary substantially in previous work, so that apparent mean annual GLOF rates can be anywhere around 0.39 (Harrison et al., 2018), 0.47 (Nie et al., 2018), or 0.52 (Richardson and Reynolds, 2000). Trends in GLOF frequency have been rarely analysed, given the few dozens of documented cases. Richardson and Reynolds (2000) speculated that *"historical records* [...] *of 33 Himalayan GLOFs* [from the past six decades] *indicate that the frequency of events appears to be increasing."* (Figure 1-5). In contrast, Nie et al. (2018) interpreted from 35 cases in their inventory (Figure 1-5a) *"that GLOF hazards increased from 1975 to 1995 and slightly decreased from 1995 to 2015."*

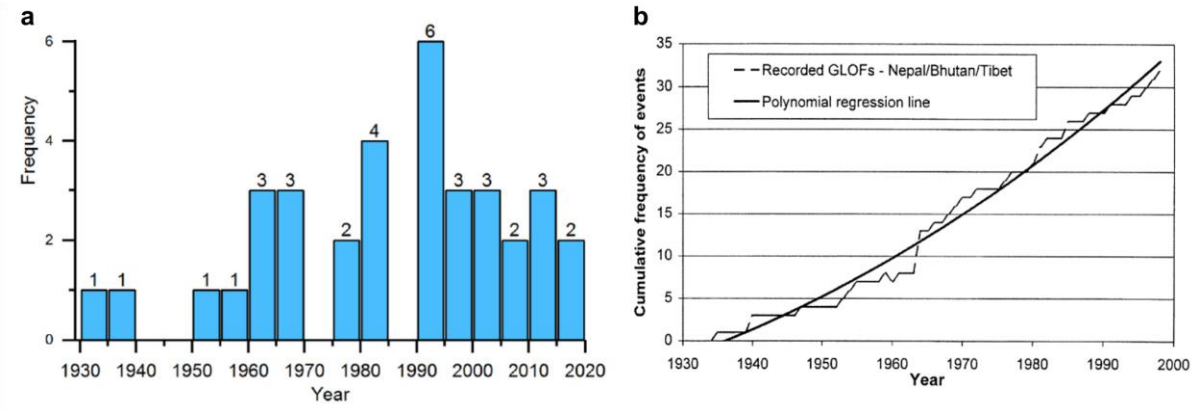

Figure 1-5: Historic GLOF inventories. a, *GLOFs with known year of occurrence between 1935 and 2017, modified after Nie et al. (2018).* ***b,*** *Cumulative frequency of GLOFs between the 1930s and 1990s, given in Richardson and Reynolds (2000). The authors underline their notion of an increasing GLOF trend with a polynomial regression fit to the cumulative GLOF count, without further details on model choice or goodness of fit.*

The often inaccessible terrain (most lakes lie above 4,500 m a.s.l., Figure 1-3) naturally biases GLOF inventories so that they preferentially include larger cases with commensurate runout and impact (Clague and Evans, 2000). Evidence for GLOFs is collated from highly diverse sources such as eyewitness reports, local chronologies, remote sensing analysis or sedimentology. Though compiling and analysing GLOF inventories have begun to follow standardised and systematic rules (Carrivick and Tweed, 2016; Emmer, 2017), the same principles rarely hold for older or historical

documentation. Sedimentary archives are well-known to include large hiatuses, given that larger cases can eradicate evidence of smaller precursors (Lewin and Macklin, 2003; Wasson et al., 2013). Data from stream gauges may not fully record all GLOF discharges and can be ambiguous, considering that flood waves attenuate rapidly or transform into debris flows (Clague and O'Connor, 2015; Schwanghart et al., 2016b).

Our ability to detect past GLOFs has improved substantially with the advance of spaceborne earth observation. Today, researchers can resort to declassified spy images from the 1960s and

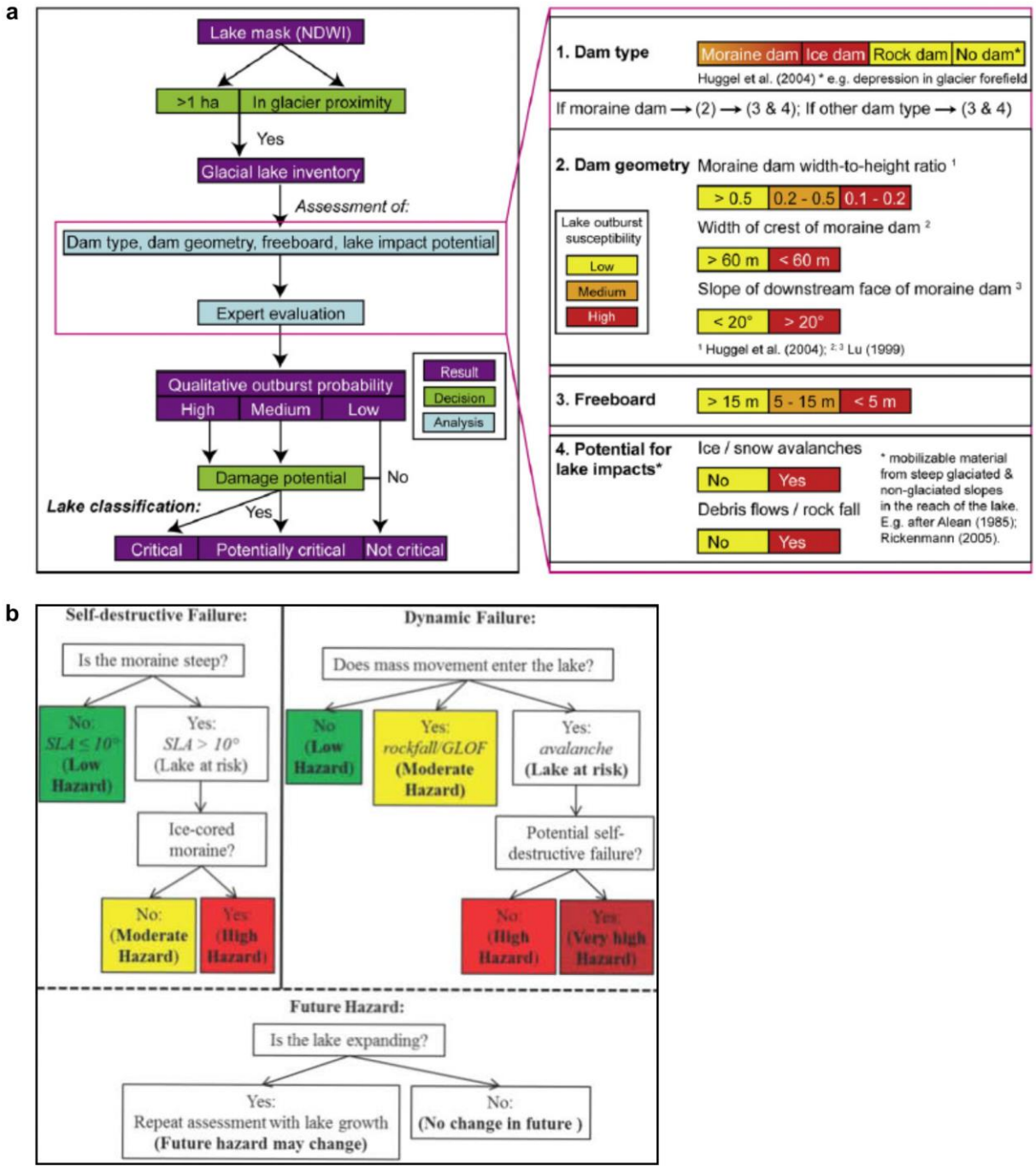

Figure 1-6: Flowcharts for hazard classification of Himalayan glacial lakes. *Adapted from a, Worni et al. (2013) and b, Rounce et al. (2017). NDWI Normalized Difference Water Index, SLA Steep Lake Area.*

1970s, and to continuous monitoring satellite missions such as Landsat or Sentinel at least since the late 1980s (Komori et al., 2012). Selective reporting has thus been assumed negligible in recently compiled global GLOF inventories (Carrivick and Tweed, 2016; Harrison et al., 2018), although this assumption has not been tested systematically. Indeed, the analysis of multi-temporal satellite imagery has lately revealed many unnoticed, even large, GLOFs in the Patagonian Andes (Wilson et al., 2018), the Cordillera Blanca of Peru (Emmer, 2017), and the Coast Mountains of British Columbia (McKillop and Clague, 2007). The first evidence of such a reporting bias in the Himalayas were three newly detected GLOFs from Landsat images (Komori et al., 2012; Nie et al., 2018), but triggered no further detailed follow-up investigation.

Clearly, establishing a more complete inventory and learning from past GLOFs is essential for improving our knowledge about the response of GLOFs to atmospheric warming in the Himalayas. Moreover, accurately estimating the frequency and the maximum discharges of GLOFs provides essential data on the average recurrence and intensity of GLOFs, thus supplying two key diagnostics for modern flood hazard assessment. The structure of this PhD thesis addresses some of these basic requirements: in Chapter 2, I offer a full workflow that covers the systematic detection of GLOFs from Landsat satellite images in the Himalayas and adjacent mountain belts. I apply this approach at the mountain-belt scale to obtain a bulk probabilistic estimate of GLOF frequency for the past three decades that serves as a measure of the current GLOF activity (Chapter 3). This first consistently and objectively derived GLOF inventory provides vital input for estimating contemporary GLOF return periods and hazard for the Himalayas and its neighbouring regions (Chapter 4).

1.4. GLOF hazard assessment in the Himalayas

Despite our censored knowledge on GLOF rates and triggers, scientists and regional planners have been concerned with providing and improving frameworks for GLOF hazard assessment (Table 1.3). The current practice of appraising GLOF hazard heavily relies on experts who select and evaluate a set of indicators that make lakes likely prone to outburst (Figure 1-6). Emmer and Vilímek (2013) compiled 35 of such stability parameters from previous studies that chiefly capture geometric properties of the moraine dam; the condition of the surrounding topography and its proneness to shed mass movements into the lake; lake size and past growth rates; or characteristics of the parent glacier (Table 1.2). While local hazard assessment incorporates fieldwork in some cases, remote sensing datasets have substantially advanced the digital mapping and extraction of tell-tale sources of GLOF triggers on basin and regional scales (Table 1.3).

Table 1.2: Stability parameters of glacial lakes. *Compiled by Emmer and Vilímek (2013).*

Moraine parameters	Glacier parameters	Parameter describing lake surrounding	Lake parameters	Downstream parameters
Slopes of lateral moraine/possibility of its fall into the lake	Crevassed glacier snout above lake	Possibility of landslide/ rockfall into the lake	Lake freeboard-to-moraine crest height ratio	Debris-flow occurrence after GLOF
Armoured overflow channel (natural or technical)	Slope between lake and glacier snout	Possibility of dynamic slope movements into the lake (ice, rock material)	Lake area	Flash flood occurrence after GLOF
Moraine slopes stabilised by vegetation	Glacier shrinkage	Possibility of snow/ice avalanche into the lake	Lake volume	
Moraine width-to-height ratio	Glacier snout steepness	Seismic activity	Lake area change	
Piping/ seepage through moraine dam	Distance between lake and glacier	Evidence of recent small GLOFs	Lake depth	
Distal flank steepness of the dam	Glacier advance	Compound risk present	Lake freeboard	
Top width of dam	Stagnant ice at the terminus	Hydro-meteorological situation		
Dam type	Glacier area			
Buried ice present in moraine dam	Supra-/englacial drainage			
Moraine height-to-width ratio				
Main rock type forming moraine				

The general workflow of GLOF hazard assessment can be a decision tree with mostly four or more stability parameters that are examined in sequence (Figure 1-6, Table 1.3). For each lake, the expert either answers yes-or-no queries, given that a specific condition is met (e.g. ice core in a moraine) or that a trigger (e.g. rockfalls) is likely to occur; or she or he examines whether the parameter exceeds an empirical threshold (e.g. slope of the moraine dam) (Figure 1-6). The more of such criteria are met, the higher is the rank of GLOF hazard from a given lake. The expert then assigns the lake into a certain hazard category, which may be *"critical", "potentially critical", "not critical"* (Worni et al., 2013) or *"very high", "high", "moderate", "low", "no"* (Rounce et al., 2017). Such classification metrics are not standardised, and assessments of whether a lake is *"potentially dangerous"* (Bolch et al., 2008; Wang et al., 2011a) can be conflicting due to mixing subjective beliefs and fixed thresholds. For example, Imja Lake in the Mt. Everest region, Nepal, and has been attributed both "high" and "low" GLOF hazard, because researchers selected different stability parameters for their hazard appraisals (Rounce et al., 2016). The lake has a volume of 78.4×10^6 m^3 (Haritashya et al., 2018), but has even been deemed to have zero potential flood volume in another assessment that *"guarantees repeatability to assess the possibility of GLOF hazards because it requires no particular expertise to carry out"* (Fujita et al., 2013). Such diverging appraisals may intend to be objective and reproducible, but eventually confuse scientists, practitioners, and the public.

Much of this controversy results from the vague, if not missing, definition of GLOF hazard. Research on other natural hazards such as landslides, wildfires or earthquakes rigorously defines hazard as the probability that an event of a given intensity or higher occurs. A fundamental concept in flood hydrology and engineering is then to express hazard by an average return period for a given flood level, measured for example by peak discharge (Katz et al., 2002). Transferring this concept to GLOFs, an objective diagnostic of hazard can be the product of the exceedance probability for a given outburst size, for example peak discharge at the breach location, and the outburst probability in a specific time interval, assuming that location and frequency are independent of each other. We can thus express GLOF hazard as the peak discharge that occurs (or is exceeded) once on average in 10, 50, or 100 years or any other chosen return period, in any basin or region of interest.

The rapidly growing literature of GLOFs shows very few attempts at sufficiently producing such an objective hazard appraisal for the Himalayas. Recent studies applied numerical and statistical models to quantify the magnitude of GLOF-related processes, such as the size of impacts into the lake (Byers et al., 2018; Lala et al., 2018; Rounce et al., 2016); the parameters during dam failure such as breach depth, rate, and peak discharge (Westoby et al., 2014; Westoby et al., 2015); or the propagation of flood waves downstream (Somos-Valenzuela et al., 2015; Watson et al., 2015). These studies offer no hazard assessment in a probabilistic sense, but could be expanded easily and usefully by estimates of the frequency, or better probability, at which GLOFs or their triggers occur. Wang et al. (2012) considered occurrence probabilities of triggers in their hazard appraisal for lakes in the Chinese territory of the Himalayas; yet they obtained these figures from expert judgement instead from empirically measured rates. Moreover, most estimates of peak GLOF discharge are tied to mean or end-member scenarios, relying on a fixed set of breach hydrographs or outburst volumes (Shrestha et al., 2010, 2013; Wang et al., 2018), so that the physically plausible range of flood magnitudes remains widely unexplored. More advanced, physically-based models of dam failure and flood runout require extensive parameterisation with field data (Westoby et al., 2014), which is logistically challenging in the Himalayas; in many cases the computational costs to solve these models also still run high. Practitioners, however, demand large numbers of outburst simulations to understand and cater for model reliabilities and uncertainties, particularly when it comes to implement remedial works and precautionary measures.

Especially for regions with numerous meltwater lakes with a known history of GLOFs, hazard assessment must find a way beyond traditional, labour-intense, and overly subjective expert judgement. In Chapter 4 of this thesis, I propose a first consistent framework to estimate regional GLOF hazard in the Himalayas and neighbouring mountains based on flood return periods. I estimate contemporary GLOF rates from a new, consistent GLOF inventory and link these rates to a physically

motived model to predict credible (in the Bayesian statistical sense) distributions of peak discharge from present and likely future meltwater-lake geometries. Completely reproducible in essence, this approach is intended to robustly quantify the contemporary GLOF hazard. Assuming that future lake abundance will change with ongoing glacier melt, I also assess the physically plausible range of changes in future GLOF hazard, taking into account the worst-case scenario of a completely ice-free Himalayan region.

Table 1.3: Types of hazard assessments for Himalayan glacial lakes on local, basin and regional scales. *The data used may be obtained from remote sensing (RS) or fieldwork (FW). Results from hazard classification typically identify the "Potentially Dangerous Glacial Lakes" (PDGL) in a given region.*

Scale	Location/ Region	Authors	Data used	Method	Number and specific variables used for hazard assessment	Result
Local	Longbasaba and Pida Lake, China	(Xin et al., 2008)	RS/ FW	Expert-based rating of breaching risk, breach simulations for estimating peak discharge	**5** (Stability of moraine dam; State of mother glacier; Climatic setting; Lake water level and dam height relation; Lake and mother glacier relation)	High risk of failure for Longabasa and Pida Lake
	Cirenmaco Lake	(Wang et al., 2018)	RS/ FW	Bathymetric survey; flood modelling	**NA**	Outburst volumes range from 0.05 to 0.30 and 5 to 18 million m^3
	Imja Lake	(Watanabe et al., 2009)	RS/ FW	Qualitative expert judgement	**6** (Lake area and lake-area expansion rate; Up-glacier and down-valley expansion rate; Dead-ice melting; Seepage; Lake water level change; Surge wave by rockfall and/or slide and ice calving)	Imja Tsho is not in immediate danger of producing an outburst flood
	8 lakes in Nepal	(Rounce et al., 2016)	RS	Expert-based classification of failure mechanisms	**4** (Mass movement trajectories; Lake expansion; Hydrostatic pressure; Buried ice)	GLOF hazard is 5x very high, 2x high, 1x low
Basin	8 lakes in the Mt. Everest region, Nepal	(Bolch et al., 2008)	RS	Expert judgement of potentially dangerous lakes	**9** (Lake volume, rate of lake formation and growth; Reaction of the glacier to climate change; Activity of the glacier; Morphometric characteristics of the glacier; Possibility of mass movements into the lakes; Stability, width and height of the moraine dam; Freeboard between lake and crest of moraine ridge; Presence of dead ice in the moraine; Situation down-valley)	PDGL: 1x none, 2x low; 1x low to medium; 2x medium
	473 lakes in the Mt. Everest region, Nepal	(Bajracharya and Mool, 2010)	RS/ FW	Expert judgement of potentially dangerous lakes	**NA** (lake expansion and distance to glaciers?)	10 PDGL
	78 lakes in the Boshula Mountain Range, Tibet	(Wang et al., 2011a)	RS	Weighting of variables with fuzzy consistent matrix	**5** (Mother glacier area; Distance between lake and glacier terminus; Slope between lake and glacier; Mean slope of moraine dam; Mother glacier snout steepness)	8 potentially very highly dangerous glacial lakes
	254 lakes in the Pumqu River Basin, Tibet	(Che et al., 2014)	RS	Weighting parameters based on how frequently they were cited	**10** (Type of glacial lake; Area of lake; Distance to mother glacier; Slope of glacier; Slope downstream; Top width of dam; Area of glacier; Slope between lake and mother glacier; Change of lake area; Elevation of lake)	19 dangerous glacial lakes
Regional	1680 lakes in the Chinese Himalayas	(Wang et al., 2012)	RS	Calculating breach probabilities from an event tree model	**5** (Avalanches from glaciers; Glacier motion; Seepage enlarging; Overflow incision)	142 PDGL: 4x very low, 24x low, 24x medium, 47x high, 43 very high
	251 lakes in the Indian Himalayas	(Worni et al., 2013)	RS/ FW (for 3 lakes)	Qualitative classification by thresholds in variables, breach simulations; Runout modelling	**4** (Dam type; Dam geometry; Freeboard; Potential for lake impacts)	12 critical lakes; 93 potentially critical lakes; 101 no critical lakes
	733 lakes in the Bhutan Himalayas	(Nagai et al., 2017)	RS	Expert-based selection of candidate variables	**4** (Potential flood volume; Lake expansion factor; Evolution of lake type; Connection with a debris-covered glacier)	two lakes with high GLOF scale and potential
	329 lakes in the Chinese Himalaya	(S. Wang et al., 2015)	RS	Expert-based selection of candidate variables	**4** (Moraine-dammed lake area (>0.02 km^2); Rate of lake area increase (>20%); Distance between lake and glacier snout (<500 m); Availability of settlements downstream)	116 PDGL

1.5. Research questions and structure of the thesis

This overview of meltwater lakes and GLOFs in the Himalayas and adjacent mountain regions has outlined that records of GLOFs are likely incomplete in past decades and biased towards destructive cases with substantial geomorphological and societal impacts. I argue that only a systematic and consistent GLOF inventory guarantees objective input to study GLOF frequency, hazard, and their response to atmospheric warming. In line with the title of this thesis, the detection, frequency and hazard of Himalayan GLOFs form the main body for three key research questions that I address in Chapters 2-4:

1/ How can we systematically detect glacial lake outburst floods in Landsat times series? (Chapter 2)

Before testing my hypothesis of a censoring bias in current GLOF inventories, I establish a framework that robustly detects GLOFs from satellite image time series. The main challenges in this study are frequent image noise from snow and cloud cover; the size of the study area; and the large amount of data (~2,500 Landsat images) that forbid visual interpretation. The core of this work was methodologically motivated, exploring options to automatically process the full seasonal Landsat archive, which is the longest time series of satellite images since the late 1980s. I develop a likelihood-based change point algorithm that independently identifies shrinking water bodies, a key diagnostic of GLOFs, at the pixel scale. The algorithm robustly detects 10 of 11 test cases in an area covering ~10% of the Himalayas, while ten newly found GLOFs support my hypothesis of under-reporting in past decades. I discuss limitations to detecting GLOFs such as insufficient image co-registration, misclassifications or continuous image noise over long periods.

2/ What is the frequency of Himalayan glacial lake outburst floods since the late 1980s? (Chapter 3)

The robust performance of the algorithm developed in Chapter 2 calls for application to the entire Himalayan mountain belt, and demands detecting lake changes in another 6,500 Landsat images. This part of the thesis aims at unravelling the spatial pattern and temporal trends of GLOFs in the Himalayas. I nearly double the known GLOF count, and find that the average GLOF frequency has not changed in any Himalayan region since the late 1980s despite distinct increases in meltwater areas. I discuss underlying climatic and topographic drivers for this invariant GLOF rate, and its implications for hazard assessment.

3/ What is the return period of Himalayan glacial lake outburst floods and how will it change in an ice-free future? (Chapter 4)

With this spatially resolved estimate of GLOF rates, I obtained the minimum requirements to calculate GLOF return periods. Chapter 4 aims at quantifying the contemporary GLOF hazard using the 100-year flood discharge as a standard metric in flood hydrology. I combine regional GLOF rates with simulations of peak discharge from all existing glacial lakes to estimate the GLOF hazard in the entire Himalayas and several key regions. I highlight how regionally varying GLOF rates affect estimates of flood hazard. Additionally, I show how the future GLOF hazard can change within its physically plausible limits by projecting a scenario of ice-free Himalayas in the future.

1.6. Author Contributions

The following three chapters are manuscripts, which I wrote for publication in peer-reviewed journals. I wish to express my gratitude to four co-authors, Oliver Korup, Sigrid Roessner, Sebastian von Specht, and Ariane Walz, who substantially contributed to the production of these manuscripts.

Chapter 2: **Veh, G.**, Korup, O., Roessner, S., Walz, A., 2018. Detecting Himalayan glacial lake outburst floods from Landsat time series. *Remote Sensing of Environment*, 207, 84–97.

G.V., O.K., S.R. and A.W. designed the study. G.V. collected training samples, developed and tested the processing chain and conducted the statistical analysis. All authors interpreted and discussed the results. G.V. wrote the paper with input by all co-authors. G.V. and O.K. wrote the revisions.

Chapter 3: **Veh, G.**, Korup, O., von Specht, S., Roessner, S., Walz, A., 2019. Unchanged frequency of moraine-dammed glacial lake outburst floods in the Himalaya. *Nature Climate Change*. https://doi.org/10.1038/s41558-019-0437-5.

G.V., O.K., S.R. and A.W. designed the study. G.V. performed the Landsat processing with input from S.S., and conducted the statistical analyses with O.K. All authors interpreted and discussed the results. G.V. and O.K. wrote the paper with input by all co-authors. G.V. and O.K. wrote the revisions.

Chapter 4: **Veh, G**., Korup, O., Walz, A. (submitted). Current and future hazard from Himalayan meltwater floods. *Under Consideration for Nature*.

G.V. and O.K. designed the study, and conducted the modelling and statistical analysis. All authors interpreted and discussed the results. G.V. and O.K. wrote the paper with input by A.W.

In addition to these manuscripts, I contributed to the following publications, which are not part of this thesis:

von Specht, S., Ozturk, U., **Veh, G**., Cotton, F., Korup, O., 2019. Effects of finite source rupture on landslide triggering: The 2016 M_W 7.1 Kumamoto earthquake. *Solid Earth Discussions*, https://doi.org/10.5194/se-2018-101, accepted.

Dietze, E., Słowinski, M., Zawiska, I., **Veh, G**, Brauer, A., 2016. Multiple drivers of Holocene lakelevel changes at a lowland lake in northeastern Germany. *Boreas*, 45, 828–845. https://doi.org/10.1111/bor.12190.

Notes

All non-peer reviewed chapters in this thesis (Chapters 1, 5, 6) are written in first person to represent my line of thought in the framework of this thesis. When I refer to contents of published or submitted manuscripts (Chapters 2, 3, 4) in these chapters, the word "I" includes the work of my co-authors, whose contributions I acknowledged above.

The terms **"Himalaya"** and **"Himalayas"** broadly summarize the geographical extent of my study region, including three subregions (Eastern, Central and Western Himalayas), and the mountain ranges attached to what is often referred as the "Main Central Thrust" in a geological context, including the Hindu-Kush and Karakoram in the northwest, and the Nyainqentanglha and Hengduan Shan in the southeast. Definitions on the geographical, geological or political extent of the Himalayas vary widely. Most glaciological studies were guided by the regional naming convention of the Randolph Glacier Inventory (RGI), though adapted this to their particular needs, so that individual use differs between figures and number cited in this thesis.

2. Detecting Himalayan Glacial Lake Outburst Floods from Landsat time series

Authors
Georg Veh
Oliver Korup
Sigrid Roessner
Ariane Walz

Published as
Veh, G., Korup, O., Roessner, S., Walz, A., 2018. Detecting Himalayan glacial lake outburst floods from Landsat time series. *Remote Sensing of Environment* 207, 84–97

Keywords
Random Forest, fuzzy classification, land cover maps, change detection, change points, lakes, sediment tails, Hindu Kush Himalayas (HKH)

ABSTRACT.

Several thousands of moraine-dammed and supraglacial lakes spread over the Hindu Kush Himalayan (HKH) region, and some have grown rapidly in past decades due to glacier retreat. The sudden emptying of these lakes releases large volumes of water and sediment in destructive glacial lake outburst floods (GLOFs), one of the most publicised natural hazards to the rapidly growing Himalayan population. Despite the growing number and size of glacial lakes, the frequency of documented GLOFs is remarkably constant. We explore this possible reporting bias and offer a new processing chain for establishing a more complete Himalayan GLOF inventory. We make use of the full seasonal archive of Landsat images between 1988 and 2016, and track automatically where GLOFs left shrinking water bodies, and tails of sediment at high elevations. We trained a Random Forest classifier to generate fuzzy land cover maps for 2,491 images, achieving overall accuracies of 91%. We developed a likelihood-based change point technique to estimate the timing of GLOFs at the pixel scale. Our method objectively detected ten out of eleven documented GLOFs, and another ten lakes that gave rise to previously unreported GLOFs. We thus nearly doubled the existing GLOF record for a study area covering ~10% of the HKH region. Remaining challenges for automatically detecting GLOFs include image insufficiently accurate co-registration, misclassifications in the land cover maps and image noise from clouds, shadows or ice. Yet our processing chain is robust and has the potential for being applied on the greater HKH and mountain ranges elsewhere, opening the door for objectively expanding the knowledge base on GLOF activity over the past three decades.

2.1. Introduction

Melting glaciers in the Hindu Kush Himalayan (HKH) mountain ranges feed several thousand moraine-dammed and supraglacial lakes (Ives et al., 2010; Nie et al., 2017). Embedded in loose debris and surrounded by sources of falling debris and ice, many of these water bodies are prone to glacial lake outburst floods (GLOFs) (Clague and Evans, 2000). GLOFs can release and transport millions of cubic meters of water and sediment within few hours (Bajracharya et al., 2007; Cenderelli and Wohl, 2001; Wang et al., 2012). Quaternary outburst floods in the HKH have been shaping major valley trains for thousands of years (Korup and Tweed, 2007; O'Connor et al., 2013; Scherler et al., 2014). GLOFs have also killed several hundreds of people in the past decades and caused substantial damage to infrastructure, hydropower stations, livestock and farmland (Kattelmann, 2003; Richardson and Reynolds, 2000; Yamada and Sharma, 1993). Data on loss and damage are crude, though Nepal and Bhutan may have suffered the highest socio-economic impacts by historic GLOFs worldwide (Carrivick and Tweed, 2016). In any case, GLOFs clearly rank among the most publicised glacial hazards in the Himalayas (Richardson and Reynolds, 2000).

Difficult access and high alpine conditions make detailed field-based monitoring of lakes prone to outburst impractical; several studies thus resorted on measuring lake bathymetry, dam material, and the surrounding topography (Fujita et al., 2013; X. Wang et al., 2012; Worni et al., 2013). Moreover, data on historic GLOFs in the HKH are scarce and vague about outburst parameters. Local GLOF inventories often contradict each other, at least judging from data that we collected on 36 GLOFs from moraine-dammed lakes in the Himalayas since the 1950s (Ives et al., 2010; Komori et al., 2012; J.-J. Liu et al., 2014; X. Wang et al., 2012; Table 2.1).

Current research aims at linking global climate warming to glacier melt, and the formation and changes of meltwater lakes, including the probability of catastrophic lake outburst (Harrison et al., 2017). Negative glacier mass balances (Brun et al., 2017) and increases in glacial lake number and area (Nie et al., 2017; Song et al., 2017; Zhang et al., 2015) have characterised many parts of the HKH over the past decades, and thawing permafrost in glacier dams and surrounding rock walls may further destabilise the glacial lake system (Haeberli et al., 2017). While all these observations are in line with a hypothesized increase in GLOF frequency, this remains difficult to test given commonly observed rates of up to one event per year, and only a few dozen reliably documented events (Carrivick and Tweed, 2016; Harrison et al., 2017). This mismatch could reflect a censoring bias such that only extreme events and their impacts have been reported.

Clearly, a database of past events as complete as possible is essential for robust and reliable GLOF hazard assessment (Emmer et al., 2016b). Time series from satellite imagery find widespread use for compiling multi-temporal glacial lake inventories, especially for rapidly expanding lakes that

are thought to have an elevated outburst potential (Nie et al., 2017; Wang et al., 2018, 2011a). To our knowledge, no study has systematically explored the Landsat archive for retrospective GLOF detection in the HKH, although it offers a largely continuous, nearly 30-year time series with regional coverage every 16 days. For tracing past GLOFs, we build on the experience that lakes most often disappeared or shrank abruptly and exposed debris fans and sediment tails in river channels downstream. Only Komori et al. (2012) used these two indicators to visually scan satellite archives for unreported GLOFs in the Bhutan Himalayas. Since glacial lakes often re-fill or re-expand within few years after an outburst, previously used mapping intervals of five to ten years might be too coarse to detect GLOFs from lake inventories (Zhang et al., 2015a). Dense cloud cover during the monsoon, lake freezing in winter, and mountain shadows are the main challenges for pursuing the glacial lake area over time. Multiple noise-free images per year may be desirable to detect reliably sudden lake changes, but remain rare in the Himalayan weather conditions. Expert-based manual mapping from multi-temporal medium to high resolution (<30 m) imagery has so far offered high-quality lake inventories, but is resource-intensive and thus restricted to few selected glacial lakes (Shrestha et al., 2013; Wang et al., 2018; Yao et al., 2012) or single basins (Bolch et al., 2008; Che et al., 2014; Jain et al., 2012). Semi-automatic mapping using chains of decision rules along band and topographic indices allows for monitoring of glacial lakes over larger areas, but requires time-consuming post-processing (Gardelle et al., 2011; Li and Sheng, 2012; Song et al., 2016). Machine learning classifiers such as Random Forests (RF) have rapidly advanced the mapping of changing land cover and water bodies (Mueller et al., 2016; Rover et al., 2012; Tulbure et al., 2016), thereby accompanying a high potential for GLOF detection. Random Forests (Breiman, 2001) are ensemble classifiers that use bagging to grow and aggregate multiple independent decision trees from a bootstrap sample of predictor variables. The classifier can deal with non-monotonic and non-linear relationships between the predictors and response variables, and is robust against overfitting (Rodriguez-Galiano et al., 2012). Hence, RF are a powerful alternative to single, parametric classifiers (Waske and Braun, 2009), especially for spectrally variable target classes such as glacial lakes of differing depth and turbidity. Random Forests offer fuzzy or probabilistic class memberships, which offer richer information about the likelihood of change in land-cover time series (Foody and Boyd, 1999; Metternicht, 1999).

Change detection of water bodies with Landsat time series focused either on long-term trends of lake growth or shrinkage (Fraser et al., 2014; Nitze and Grosse, 2016) or on the estimation of flooding frequencies (Mueller et al., 2016; Tulbure et al., 2016). Automatically extracting distinct events of rapid lake decrease, as is the case for GLOFs, has rarely been of interest (Olthof et al., 2015). Change-point detection in Landsat time series is well-established for forest disturbance mapping,

where pixels of vegetation indices are scanned for level shifts (Hermosilla et al., 2015; Kennedy et al., 2010) or structural breaks in fitted harmonic models (DeVries et al., 2015; Verbesselt et al., 2012). However, alternative techniques are required, as these approaches are difficult to apply to Himalayan glacial lakes where indices such as the Normalized Difference Water Index (NDWI; McFeeters, 1996) share similar spectral characteristics with clouds or shadows (Li and Sheng, 2012).

Our aim is to develop, validate and apply a technique to automatically detect past Himalayan GLOFs. We present a processing chain that traces losses in lake areas from nearly three decades of seasonal Landsat imagery building on (1) a Random-Forest based land cover classification and (2) a novel, likelihood based change-point algorithm to approximate the time stamp of GLOFs. We apply this processing chain to a spatial subset of the HKH, validate our method with documented GLOFs and present newly detected GLOFs. Our search includes sediment tails downstream of drained lakes, allowing us to trace the location, timing, and size of GLOFs, and thus contributing to a more complete GLOF inventory of the Himalayas.

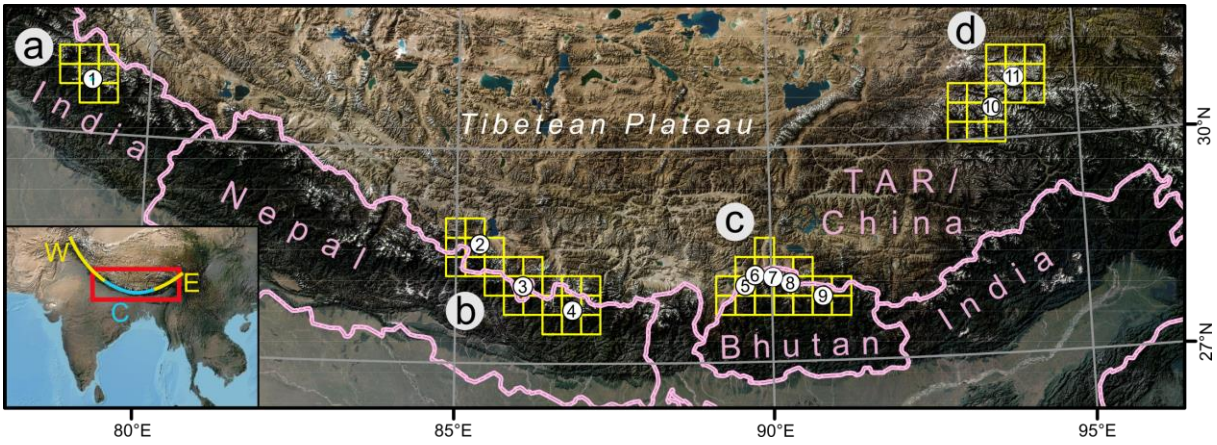

Figure 2-1: Documented GLOFs (1-11, Table 2.1) between 1994 and 2016 in the HKH. *Study regions a-d feature 30 km × 30 km tiles (yellow squares; see Table 2.1 for more details). Inset shows the geographic setting of the HKH, divided into a western (W), central (C) and eastern (E) segment.*

2.2. Study area

Of all 36 documented GLOFs over the past seven decades, we could visually identify eleven GLOFs in Landsat images (Figure 2-1). We obtained information on the date, location, and type of drainage for each GLOF, using the drained lake area as a key metric for comparing pre- and post-GLOF images (Table 2.1).

These GLOFs occurred in four different regions (Figure 2-1) between the central-western Himalayas of northern India (a), the central Himalayas of Nepal and Bhutan (b and c), and the eastern Nyainqentanglha Mountains of China (d). The number of present-day moraine-dammed and

supraglacial lakes in these areas is challenging to establish. Estimates for the whole HKH range from 2,276 (Fujita et al., 2013) to more than 8,000 (Ives et al., 2010), depending on definition, mapping scale, and size of study area. In the central Himalayas, glacial lakes grew by 23% in size between 1990 and 2015. Lakes grow less rapidly in area in the western (5.0-5.4%) and eastern Himalayas (7.7-11.1%) (Nie et al., 2017), and mostly tied to glacier melt (Gardelle et al., 2013; Kääb et al., 2012; Song et al., 2017; Wang et al., 2015b).

Table 2.1: Documented GLOFs between 1988 and 2016. *ID corresponds to labels in Figure 2-1. We visually assessed whether drainage was complete (C) or partial (P).*

ID	Lake	Country	E [°]	N [°]	Elevation [m a.s.l.]	Loss in lake area [m^2]	Date	Type of drainage	Source
1	Chorabari	India	79.06	30.75	3,881	11,700	2013-06-17	C	(Allen et al., 2016; Das et al., 2015)
2	Zanaco	TAR/ China	85.37	28.66	4,737	66,600	1995-06-06	C	Liu et al. (2014)
3	Zhangzangbo 2	Nepal	86.06	28.08	4,501	10,800	2016-07-07	C	(Cook et al., 2017; Gimbert et al., 2017)
4	Sabai Tsho	Nepal	86.84	27.74	4,492	163,800	1998-09-03	P	(Lamsal et al., 2015; Osti and Egashira, 2009)
5	Lemthang Tsho	Bhutan	89.58	28.07	4,273	53,100	2015-06-28	C	(Gurung et al., 2017)
6	Chongbaxia Tsho	TAR/ China	89.74	28.21	5,028	227,700	Spring-Summer 2001	P	(Komori et al., 2012)
7	Tshojo glacier	Bhutan	90.16	28.10	4,273	81,900	2009-07-29	P	(Yamanokuchi et al., 2011)
8	Luggye Tsho	Bhutan	90.28	28.09	4,623	140,400	1994-10-07	P	Fujita et al. (2008); Watanabe and Rothacher (1996)
9	Gangri Tsho III	Bhutan	90.81	27.90	4,826	26,100	Spring-Summer 1998	P	(Komori et al., 2012)
10	Ranzeria Co	TAR/ China	93.53	30.47	5,051	246,600	2013-07-05	P	(Sun et al., 2014)
11	Tsho Ga	TAR/ China	94.00	30.83	4,760	140,400	2009-04-29	P	Y. Nie (pers.comm., 2017)

2.3. Data and Methods

2.3.1. Data

Our processing chain builds on six open-source data sets, including image and topographic data in raster format and two glacier inventories in vector format (Table 2.2). The eleven reference GLOFs are covered by 19 Landsat scenes. We scanned the entire Landsat archive on the *EarthExplorer* web portal for TM, ETM+ and OLI images with <60% cloud cover and time stamps between September and November to avoid excess cloud cover during summer monsoon or snow and ice cover in winter. We downloaded 2,491 images that were radiometrically corrected to Top-

of-Atmosphere (TOA) reflectance, and geometrically corrected to processing level L1T by the ESPA Landsat data processing platform.

Table 2.2: Data sets used in study.

Data set	Temporal coverage	Data format	Resolution [m]	Source
Landsat imagery	1988 - 2016	6 raster bands (TM and ETM+) 9 raster bands (OLI)	30	United States Geological Survey (USGS) https://earthexplorer.usgs.gov
***CFmask* products**	1988 - 2016	Single-raster band	30	Earth Resources Observation And Science (EROS) Center Science Processing Architecture (ESPA) https://espa.cr.usgs.gov
SRTM DEM	2000	Single-raster band	30	USGS https://earthexplorer.usgs.gov
ALOS World 3D DEM	2006 - 2012	Single-raster band	30	Japan Aerospace Exploration Agency (JAXA) http://www.eorc.jaxa.jp/ALOS/en/aw3d30/data/index.htm
Randolph Glacier Inventory, V 5.0, Region 13-15	2006 - 2010	Multipart polygon shape file	-	Global Land Ice Measurements from Space (GLIMS), see (Pfeffer et al., 2014)
ICIMOD Glacier Inventory	2005 ± 3 years	Multipart polygon shape file	-	International Centre for Integrated Mountain Development (ICIMOD), see (Bajracharya et al., 2011)

The first images were acquired in late 1988 by TM, and coverage remained limited in the 1990s. The deployment of ETM+ in 1999 brought more coverage, though the failure of the Scan Line Corrector in 2003 caused image data gaps. The shutdown of TM in 2012 was compensated with the launch of OLI in 2013 (Figure 2-2), so that the time series spans 29 years in total. The central HKH is most densely captured with up to 429 images per pixel (Figure 2-3-A). We used the *CFmask* product, a *C* implementation of the *F*unction of *Mask,* originally designed for detecting clouds in Landsat images (Zhu and Woodcock, 2012). (Zhu et al., 2015) extended *CFmask* to classify each Landsat scene into *Cloud, Shadow, Ice and Snow, Water* and *Clear* (i.e. without atmospheric disturbance), and to assign three categories of classification confidence.

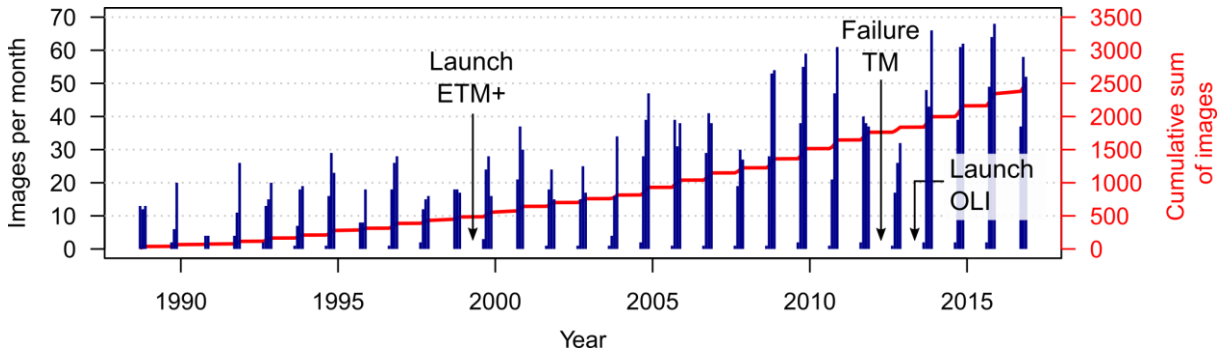

Figure 2-2: Number and approximate time stamps of Landsat images per month for the study period (1988-2016).

We also used the 30m resolution digital elevation model (DEM) from the Shuttle Radar Topography Mission (SRTM) after filling voids with data from the ALOS World 3D–30m digital surface model, and smoothing the data with a 9 × 9 Gaussian filter. For data on glaciers we used the ICIMOD and the Randolph Glacier Inventory (RGI) (Bajracharya et al., 2011; Pfeffer et al., 2014). We filled the missing Chinese territory of the ICIMOD inventory with RGI data, so that our inventory contains more than 50,000 glaciers with a total area of ~9,400 km^2.

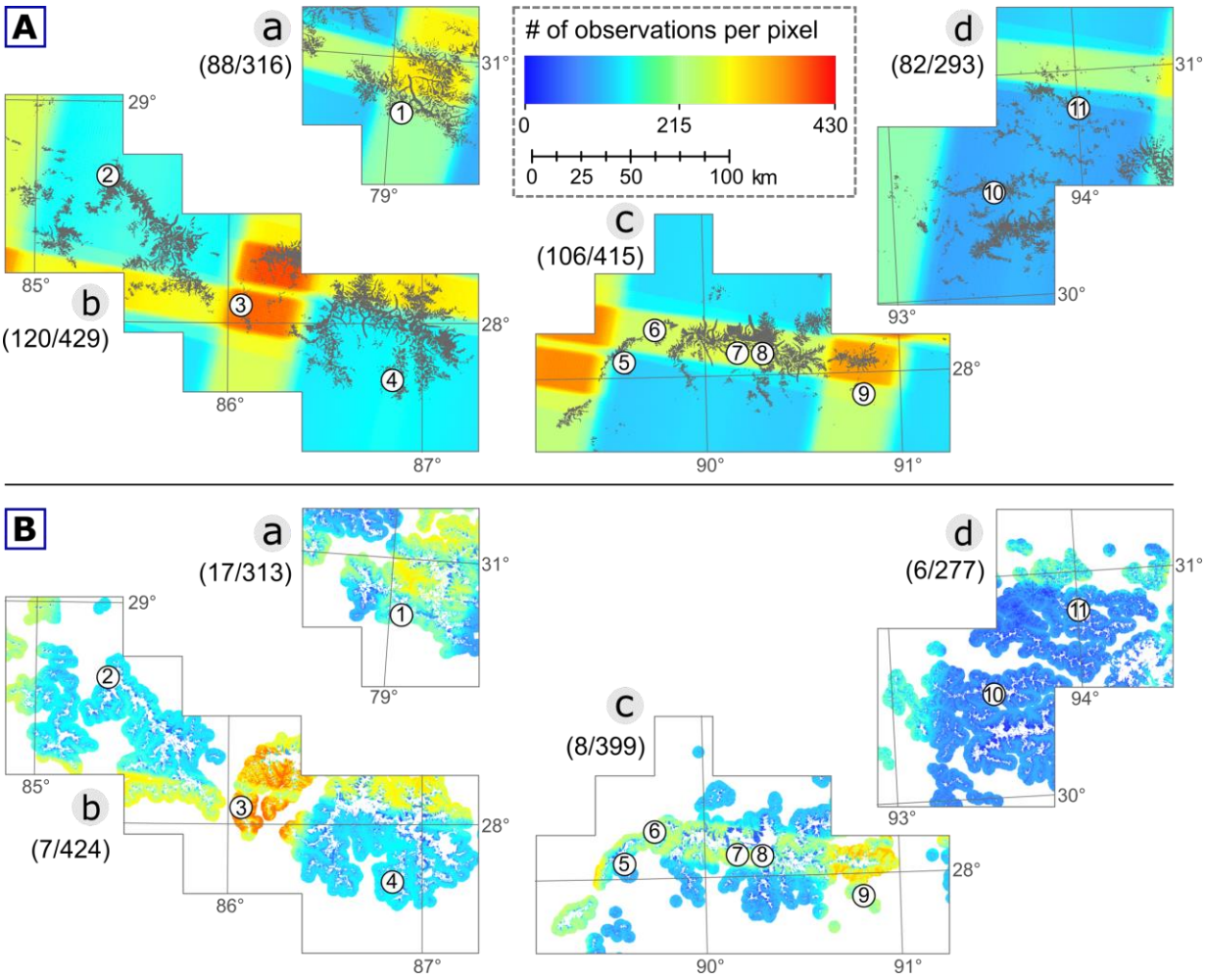

Figure 2-3 A) Total number of Landsat observations per pixel for the four study regions (Figure 2-1); glaciated areas are depicted in grey. B) Remaining observations for time-series analysis after pre-processing and noise removal (Step 2). *Numbers in parentheses are minimum and maximum observations for each study region; numbers 1-11 refer to reference GLOFs in Table 2.1.*

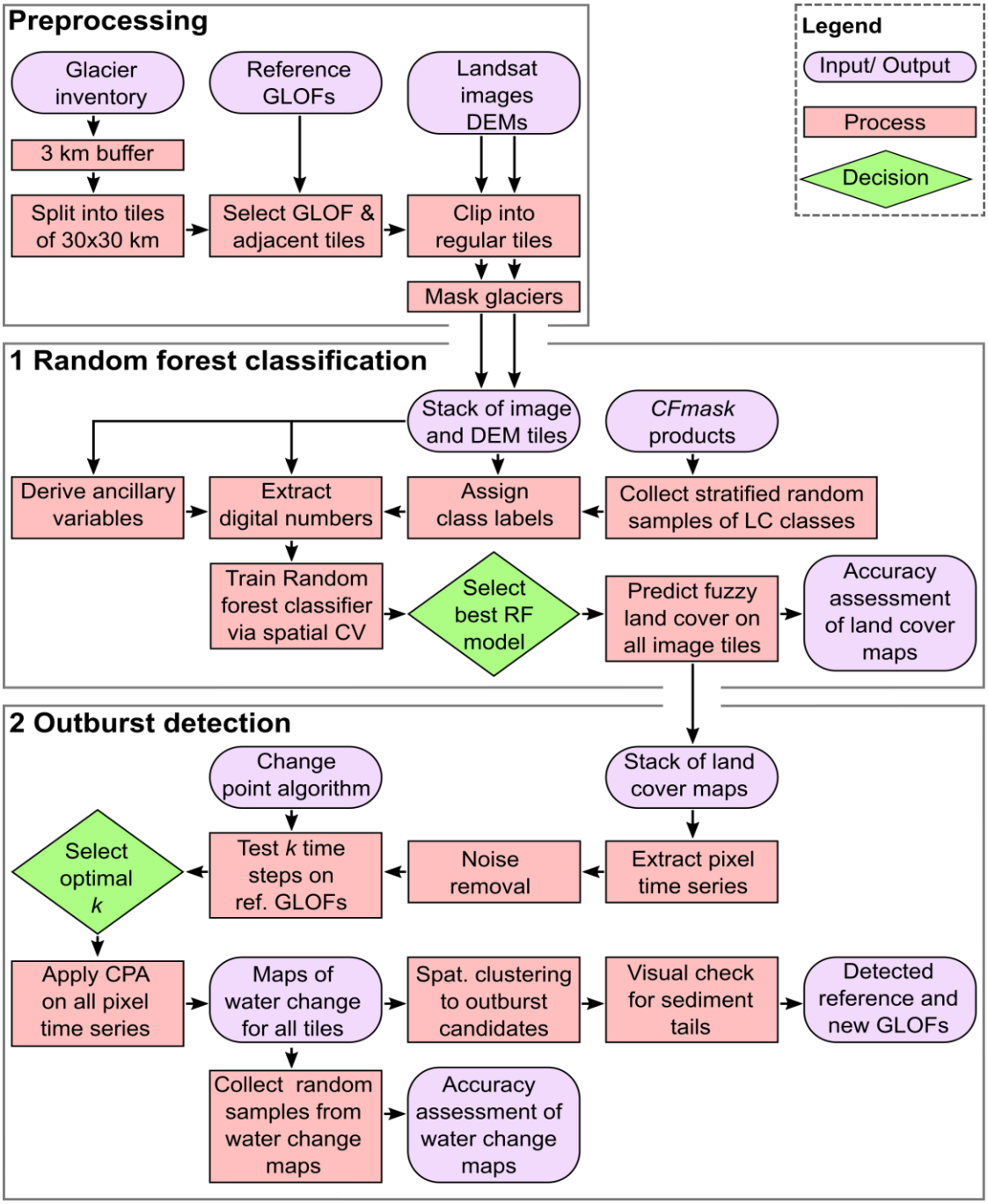

Figure 2-4: Flowchart of processing chain for automated GLOF detection. *Abbreviations: CPA – Change Point Algorithm (see Chapter 2.3.2.3); RF – Random Forest; LC – Land Cover; CV – Cross-validation.*

2.3.2. The processing chain

To automatically detect GLOFs from Landsat time series, we used a two-step approach: first, we trained a Random Forest model to classify land cover in all tiles; second, we used a likelihood-based change-point algorithm to identify GLOF pixels with distinct changes from water to land.

2.3.2.1. Data preprocessing

The study area covers six UTM zones so that we first re-projected the images to the centrally located UTM zone 45N with nearest neighbour resampling to preserve the original digital numbers of the image bands. We divided the study area into 30 km × 30 km tiles to increase data reading speed for parallel processing. We processed those eleven tiles containing documented outbursts, and their 57 neighbouring tiles, resulting in a total of 68 tiles (Figure 2-1). Our analysis focused on lakes impounded by moraines or coalescing on debris-covered glaciers, so that we reduced the search range to valley floors <3 km downstream of glaciers in our inventory. We excluded areas above the median elevation of each glacier, assuming that these steep and rugged areas do not host lakes.

2.3.2.2. Step 1: Random Forest classification

We defined six land cover classes that are potentially relevant for detecting GLOFs. *Water* and *Sediment* were the mandatory classes as we assumed that outbursts of glacial lakes exposes sediments in the lake basin and downstream. Three additional classes (*Ice & Snow, Cloud* and *Shadow*) are sources of image noise in the alpine landscape. Finally, a *Land* class subsumed all other classes not contained in the other five classes. The eleven tiles containing reference GLOFs offered training data for our classification. We chose the first cloud- and ice-free observation after each GLOF and one randomly selected image before. The adjacent 57 tiles supplied test sites for detecting previously unreported GLOFs. We applied a two-fold stratification by land-cover class and confidence band from the *CFmask* product, and distributed 30 random points per stratum. We manually assigned each point to one of the six land cover classes by comparing the Landsat image with Google Earth images without knowing the classification from the *CFmask* product. Classes *Water*, *Cloud* and *Sediment* were undersampled due to misclassifications in the *CFmask* product; we solved this issue with additional random points using the lake inventory of Zhang et al. (2015), and a visually defined threshold of 2,750 in the SWIR1 band for *Sediment* and *Cloud* samples. Sampling the *Sediment* class avoids confusion with the spectrally similar *Cloud* class. We then merged the *Sediment* and *Land* samples into a *Land & Sediment* class, resulting in a total of five land cover classes as response variables for the RF classifier.

Landsat TM and ETM+ share the same spectral band width that differ from OLI. We therefore divided the sampled pixels into TM5/ETM+ and OLI subsets. For TM/ ETM+ (OLI), we collected in total 6573 (5911) point samples, including 617 (633) *Water*, 1822 (2078) *Land & Sediment*, 1324 (1052) *Ice & Snow*, 1088 (945) *Cloud* and 1722 (1203) *Shadow* samples. We extracted the digital numbers from the predictor variables, involving all spectral bands, brightness temperature, and ten ancillary band and topographic indices (Table 2.3).

Table 2.3: Ancillary variables for Random Forest training

Variable	Reference
Normalized Difference Cloud Index (NDCI)	(Martinuzzi et al., 2007)
Modified Soil Adjusted Vegetation Index 2 ($MSAVI_2$)	(Qi et al., 1994)
Normalized Difference Vegetation Index (NDVI)	(Rouse Jr et al., 1974)
Normalized Difference Water Index (NDWI)	(McFeeters, 1996)
Normalized Difference Snow Index (NDSI)	(Riggs et al., 1994)
Hillshade	(Conrad et al., 2015)
DEM	USGS (EarthExplorer)
Slope	(Zevenbergen and Thorne, 1987)
Topographic Position Index (TPI)	(Weiss, 2001)
Aspect	(Zevenbergen and Thorne, 1987)

For fitting the two RF models (one for TM5/ETM+, one for OLI), we grew 1,000 trees and randomly selected four predictors at each split. We assessed the performance of the classifiers via spatial cross-validation: we rearranged the samples into different tile combinations, always using seven tiles as training and four tiles as test data sets. We resampled the training and test data sets to 200 and 100 random instances per class, respectively. In each cross-validation run, the RF models were fitted to the 200 training observations and subsequently used for prediction on the 100 hold-out samples in the test data. We evaluated the classifier performance for each class using a log loss function (1) that penalizes divergences between predictions and manually assigned classes:

$$logloss = -\frac{1}{N}\sum_{i=1}^{N} y_i \log p_i + (1 - y_i) \log(1 - p_i) \quad (1)$$

where N is the number of pixels, y_i is an indicator function of whether pixel i belongs to the target class ($y_i = 1$; $y_i = 0$ otherwise), and p_i is the proportional membership of pixel i over the predicted class. We added a ten and five-fold cost of misclassifying *Water* and *Land & Sediment* to emphasise their importance for GLOF detection.

Labelling mixed pixels with hard classes potentially introduces an interpreter bias during class assignment whose influence can be decreased by cross-validation. We repeated cross-validation 100 times and chose the run with the lowest median log loss as the optimal sample combination. We trained the final RF models with all samples from these tiles and evaluated the accuracy on all samples from the remaining test tiles. For the best two classifiers, we converted the fuzzy class memberships into a hard classification and estimated the error matrices. We report the Overall Accuracy (OA) as well as Producer's Accuracy (PA) and User's Accuracy (UA), and used these two models to predict land cover on all tiles.

2.3.2.3. Step 2: Outburst detection from pixel time series

Our key indicator for GLOFs is the pixel-based change from *Water* to *Land & Sediment*. Each pixel from the stack of land cover maps has a time series of membership probabilities for one of five land-cover classes (Figure 2-5-A). We defined class-membership probabilities of *Cloud, Shadow* or *Ice & Snow* >0.5 as noise and excluded them from further analysis (Figure 2-5-B), resulting in significant spatial differences of valid observations (Figure 2-3-B). Filtered pixel time series with >10% of their original length could potentially include a change event. Yet simply flagging each time step at which the class membership changes from *Water* to *Land & Sediment* would overestimate the number of change points, since we cannot assume correct classifications of water and land throughout the time series. Indeed, most classification errors form irregular spikes in the time series (Figure 2-5-B).

We developed a change-point algorithm (CPA) to remove outliers and to detect major transitions from water to land for each pixel. We approximate the likelihood of change $p(C)$ by multiplying the likelihoods of belonging to the Water and Land & Sediment class before and after each time step i, respectively:

$$p(C) = \prod_{k}^{i-1} P(W) \prod_{i}^{k} P(LS) \quad (2)$$

where $P(W)$ is the predicted probability of belonging to class *Water* for k time steps before i, and $P(LS)$ is the probability of belonging to the *Land & Sediment* class for k time steps after i. The likelihood of change $p(C)$ at time step i must exceed a specified threshold $T(C)$ to qualify as a change point. We set the threshold as

$$T(C) = 0.5^{2k} \quad (3)$$

where 0.5 represents the random chance of belonging to a certain class and $2k$ is the CPA bandwidth. We tested different sizes of k time steps ranging from 2 to 10 to identify optimal values for detecting GLOFs. We then generated maps of water change for each tile where all pixels exceeding $T(C)$ were labelled with the date of the change point.

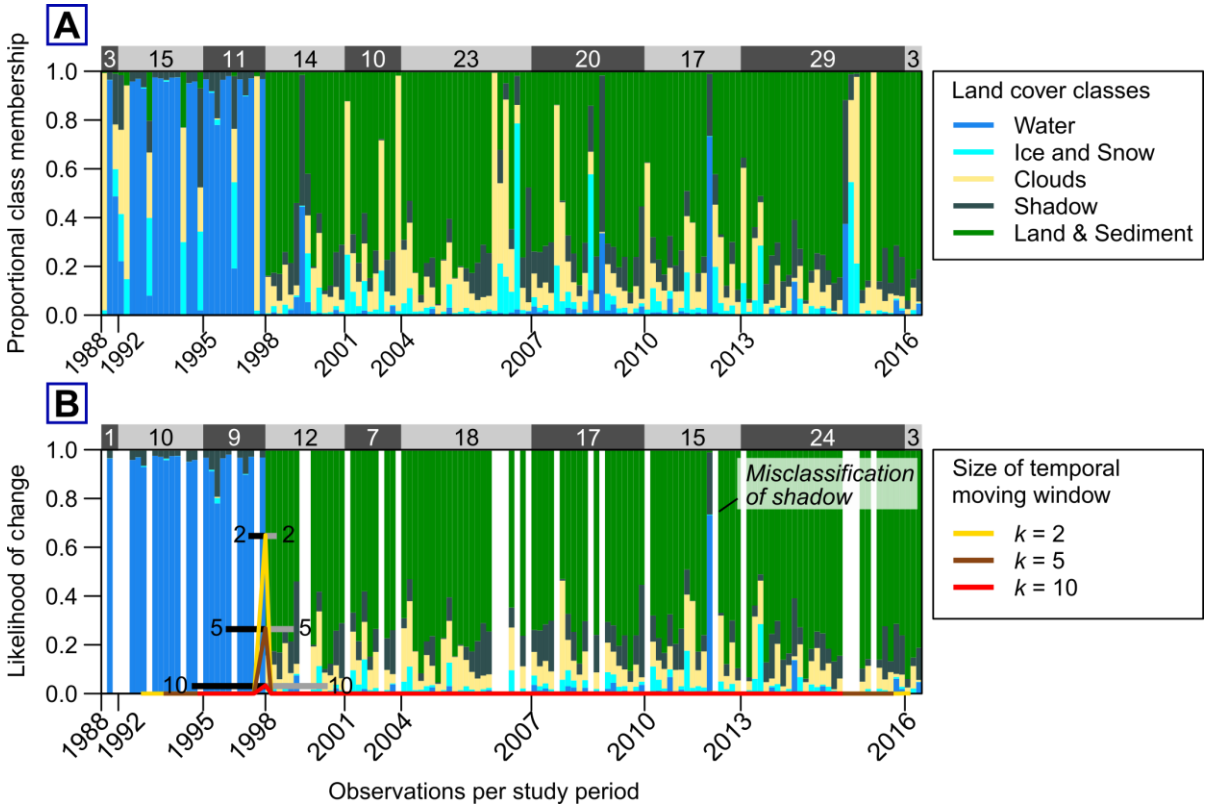

Figure 2-5: Example of pixel time series with a change from water to land and sediment for Sabai Tsho GLOF, October 1998. *A) Raw time series of estimated membership probability for the five land-cover classes. Note the differing number of observations in three-year intervals at the bar on top. B) Filtered pixel time series results of a change-point algorithm with different values of k (see text).*

We followed the recommendations of (Olofsson et al., 2013) to compute stratified error matrices that consider the proportion of land change area. We applied a stratified random sampling approach by collecting 20 samples for each of the *Water to Land* and *No Change* class from the eleven water change maps, resulting in a total of 440 samples. The *No Change* class was subsampled from pixels where the change-point algorithm revealed no transition. We visually identified the correct class on all images and labelled the pixels with the class value. After estimating the error matrix from raw sample counts, we weighted the matrix cells with the total area computed for the two classes to estimate the accuracy of area change.

We used the density-based clustering technique DBSCAN (Ester et al., 1996) to spatially aggregate pixels within a three-year period as change objects. DBSCAN joins spatially separated change pixels and removes spurious change pixels in regions with low pixel density. We set a minimum of four pixels and a maximum of 150 m to form a cluster of abruptly disappeared lake pixels. For all outburst candidates, we visually checked the corresponding images for sediment tails downstream of disappeared lake areas. For newly detected GLOFs, we gathered the information as in Table 2.1 and grouped the events into two categories based on our degree of confidence.

2.4. Results

2.4.1. Accuracy of land cover maps

The best models from 258 spatial cross-validation runs had a median weighted log loss of 0.1098 for Landsat TM/ETM+, and 0.0868 for Landsat OLI. According to this loss function, the two RF models would assign a class-membership probability of 0.896 (TM/ETM+) and 0.917 (OLI) for a particular observation. The estimated error matrices (Table 2.4 and Table 2.5) from hard land cover classes indicate a high overall accuracy of 91% (TM/ETM+) and 91% (OLI). The *Water* class is characterized by a comparable (good) UA and PA for TM/ETM+ (0.931/0.901) and OLI (0.929/0.945), confirming a high separability of water from all other land cover classes. Both classifiers showed their lowest performance for the *Cloud* class, mainly because of confusion with the *Land & Sediment* class. While PA and UA for *Ice & Snow* were similar, the results for *Land & Sediment* and *Shadow* diverged between the two classifiers. The number of samples per class in the training and test tiles differed between OLI and TM/ETM+, causing different sample sizes in the error matrices (Table 2.4 and Table 2.5).

Table 2.4: Error matrix for mapped (columns) and predicted (rows) land cover samples, as well as Producer's (PA) and User's (UA) accuracy for all land cover classes as discretisation of fuzzy to hard Landsat TM/ETM+ classification. *The accuracies were highest for the water class (blue) and lowest for the cloud class (red) due to confusion with the land & sediment class.*

		Reference							
		Water	**Land & Sediment**	**Ice & Snow**	**Cloud**	**Shadow**	**Total**	**PA**	**UA**
Prediction	**Water**	201	2	8	0	5	216	**0.931**	**0.901**
	Land & Sediment	0	560	16	**40**	19	635	0.882	0.927
	Ice & Snow	1	6	585	10	27	629	0.930	0.927
	Cloud	5	**29**	10	211	6	261	**0.808**	**0.808**
	Shadow	16	7	12	0	681	716	0.951	0.923
	Total	223	604	631	261	738	2457		

Table 2.5: Error matrix from mapped (columns) and predicted (rows) land cover samples, as well as Producer's (PA) and User's (UA) accuracy for all land cover classes as discretisation of fuzzy to hard Landsat OLI classification.

		Reference							
		Water	**Land & Sediment**	**Ice & Snow**	**Cloud**	**Shadow**	**Total**	**PA**	**UA**
Prediction	**Water**	171	3	2	0	8	184	0.929	0.945
	Land & Sediment	0	691	6	6	7	710	0.973	0.857
	Ice & Snow	1	9	292	4	9	315	0.927	0.945
	Cloud	3	74	7	395	1	480	0.823	0.975
	Shadow	6	29	2	0	218	255	0.855	0.897
	Total	181	803	307	405	243	1943		

2.4.2. Optimal time steps for change-point detection

For the eleven reference GLOFs, the change point algorithm showed decreasing mean success rates with increasing number of consecutive observations after noise removal (Figure 2-6-A). Success rates were highest for k = 2 (85%), then stepped towards a plateau for $k \in [3,4,5]$ (76-73%) and dropped below 50% for $k >= 8$. The rate of additionally detected change pixels (Figure 2-6-B) fell more steeply, showing a distinct kink at the transition to k = 3. We seek to maximize the rate of correctly detected change pixels, while minimizing the rate of additionally detected change pixels. We propose an optimum number of k = 3 time steps for change detection owing to the high rate of detected GLOF pixels and, at the same time, to the moderate rate of additionally detected pixels in the corresponding tiles.

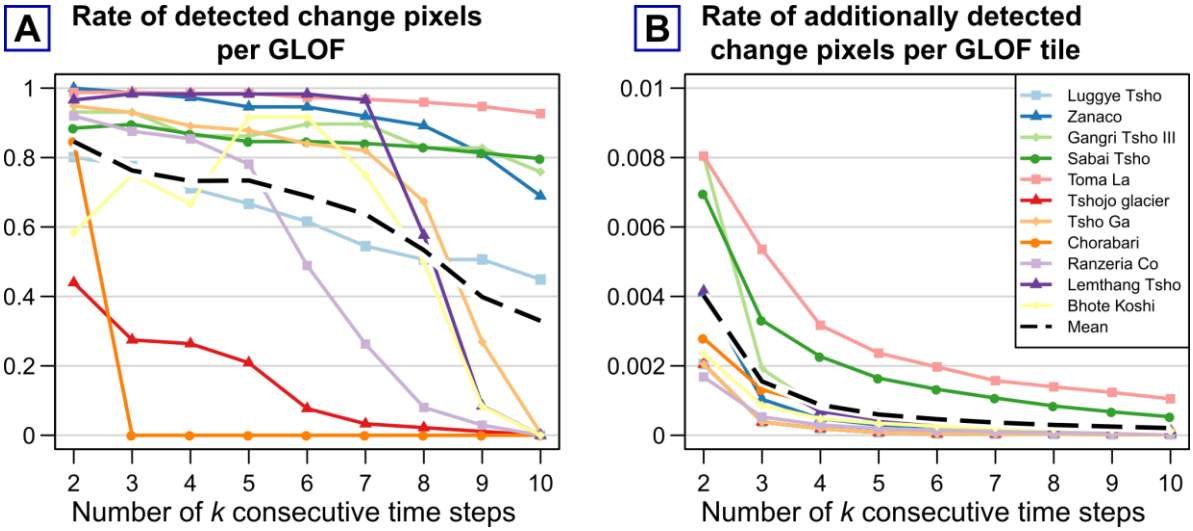

Figure 2-6: A) True positive rate expressed as the rate of detected change pixels by window size for all reference GLOFs; B) Rate of additionally detected change pixels within the GLOF tile expressed as the number of additionally detected pixels detected pixels divided by the number of all valid pixels per GLOF tile.

2.4.3. Accuracy of water change maps

Considering k = 3 time steps, our algorithm mapped 0.18% of the total area in the eleven GLOF tiles as a change from *Water to Land* (Table 2.6). The error matrix of the raw sample counts from the strata *Water to Land* shows that 70 out of 220 change pixels did not change. Area-weighted sample fractions had an overall accuracy of 99% (Table 2.7). The target class *Water to Land* class had a UA of 67% and a PA of 12%, while the *No Change* class had UA and PA of >99%.

Table 2.6: Error matrix for a total of 440 stratified samples randomly collected from the land cover change maps of the eleven GLOF tiles. *Water to Land is the change between the classes indicating a GLOF; No Change includes stable land cover of Water and Land, as well as all other changes in classes Cloud, Shadow and Ice & Snow. Map Area refers to the sum of all pixels of the change classes multiplied by a pixel size of 900 m². W_i is the proportion of the area mapped as change class i, divided by the total area.*

		Reference				
		Water to Land	**No Change**	**Total**	**Map Area [km²]**	W_i
Prediction	**Water to Land**	150	70	220	9.532	0.002
	No Change	2	218	220	5246.078	0.998
	Total	152	288	440	5255.61	1

Table 2.7: Estimated error matrix based on raw sample counts from Table 2.6. *Cell entries of the change classes Water to Land and No Change represent the estimated proportion of area calculated as the product of the raw sample fraction and class weights W_i given in Table 2.6.*

		Reference					
		Water to Land	**No Change**	**Total**	**UA**	**PA**	**Overall**
Prediction	**Water to Land**	0.0012	0.0006	0.0018	0.6667	0.1165	0.9903
	No Change	0.0091	0.9891	0.9982	0.9909	0.9994	
	Total	0.0103	0.9897	1			

2.4.4. Detection of GLOFs

The change point algorithm classified 38,009 change pixels in 68 image tiles. After spatial aggregation to candidate objects with DBSCAN, we investigated the images for sediment tails downstream, successfully identifying ten of the eleven reference GLOFs. For nine of the eleven reference GLOFs, our algorithm correctly detected >78% of the pixels that we had manually mapped as change pixels (Figure 2-6-A). The 2009 GLOF from Tshojo Glacier, Bhutan, was detected with a success of 30%, whereas the 2013 outburst from Lake Chorabari, India, remained undetected. The lake changes predicted by our detection algorithm agree well with independent manual mapping (Figure 2-7) to less than two pixels in width.

The change-point algorithm identified ten previously unreported GLOFs (Table 2.8), with nine of them in the central Himalayas and one in the Nyainqentanglha Mountains (Figure 2-8). Seven of these newly detected lake sources had distinct sediment tails downstream (Figure 2-10-A and B), which were more difficult to identify for three medium-confidence locations (Figure 2-10-C). We could identify outbursts from lake change maps involving as few as eight pixels (7,200 m^2, Table 2.8-H). We also detected a lake upstream of Luggye Tsho (Bhutan, Table 2.8-G) that had two outbursts with a major event in 1991, followed by refilling and a second minor event in 2010. We find that our method underestimates lake area changes by 9.4% on average; most of the lakes showed partial drainage (Table 2.8). Drained lakes areas of the newly detected GLOFs are below 120,000 m^2, corresponding to half of the maximum size of previously documented GLOFs (Figure 2-9).

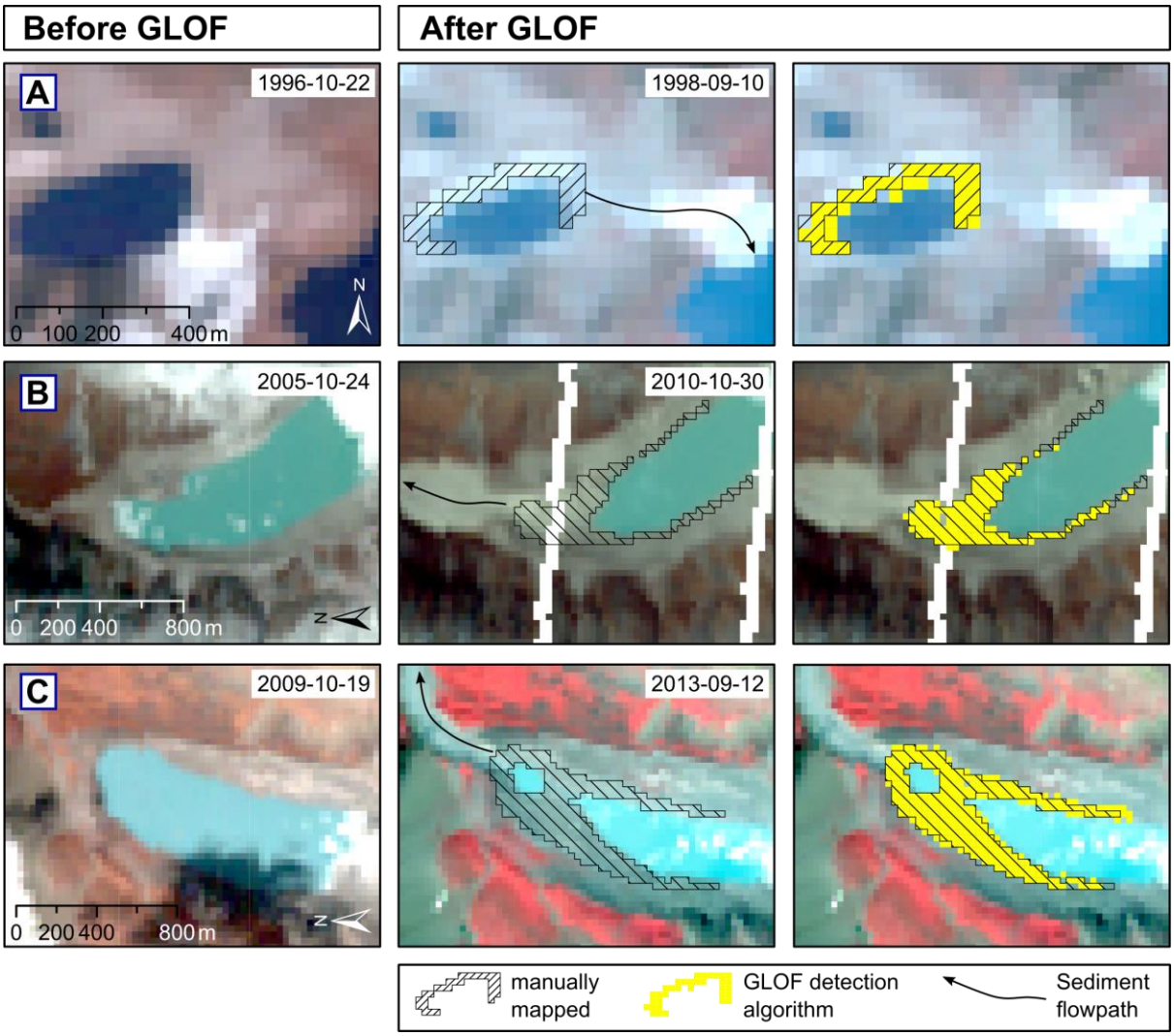

Figure 2-7: Glacial lake outbursts from A) Gangri Tsho III in 1998, B) Tsho Ga in 2009 and C) Ranzeria Co in 2013, showing the last noise-free image before (left panels) and the first noise-free image after the event (middle and right panels). *The appearance of sediment tails downstream is among our key criteria for detecting GLOFs. The post-GLOF image from Tsho Ga shows artefacts from the failure of the scan-line corrector of Landsat ETM+.*

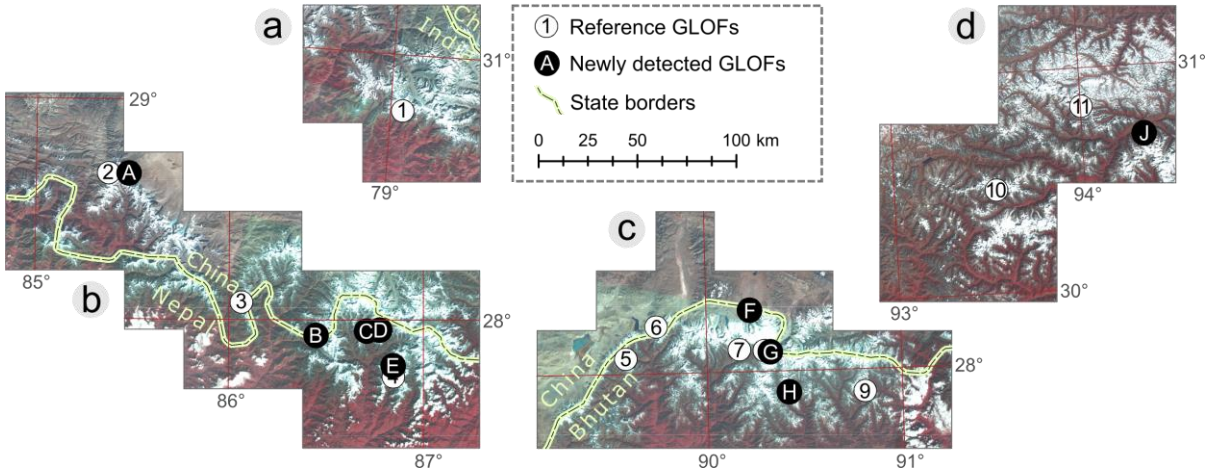

Figure 2-8: All reference GLOFs (Numbers 1-11) and newly detected GLOFs (letters A-J).

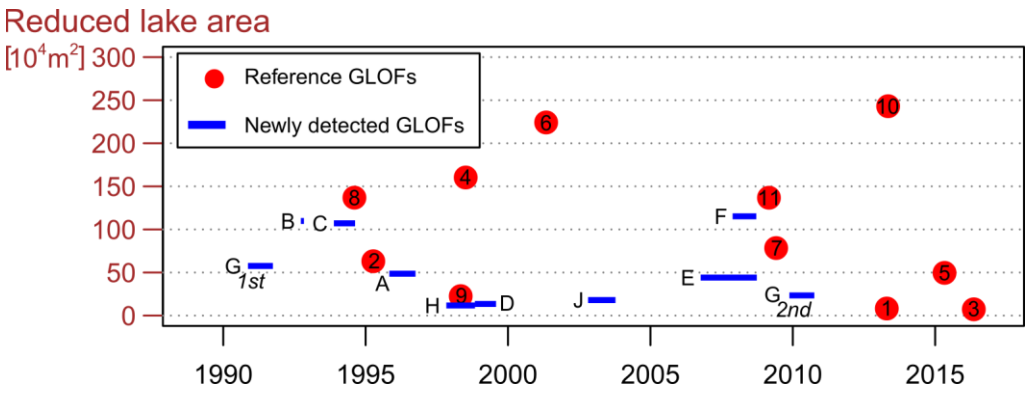

Figure 2-9 Comparison of drained lakes areas linked to previously documented (reference; Table 2.1) and newly detected GLOFs in a training area covering ~10% of the HKH. *Blue bars give intervals between noise-free images for newly detected GLOFs.*

Table 2.8: Previously unreported GLOFs from 1988 to 2016. *ID corresponds to labels in Figure 2-8. Elevations were extracted from SRTM data. Type of drainage is either complete (C) or partial (P). Column sums are given by ∑, and column means by μ.*

ID	Country	Long [°]	Lat [°]	Elevation [m a.s.l.]	Degree of confidence	Area change manually mapped [m²]	Area change predicted by CPA [m²]	Relative difference manual vs. predicted [%]	Maximum age	Minimum age	Difference between noise free images	Type of drainage
A	China	85.48	28.66	5,196	high	48,600	36,900	-24.1	1995-11-01	1996-10-02	336	P
B	China	86.45	27.93	5,192	medium	109,800	72,900	-33.6	1992-09-22	1992-11-01	40	P
C	Nepal	86.71	27.95	4,730	medium to high	107,100	107,100	0	1993-11-20	1994-08-19	272	C
D	Nepal	86.78	27.96	5,015	high	13,500	10,800	-20.0	1998-11-02	1999-08-01	272	C
E	Nepal	86.84	27.8	5,309	medium	44,100	41,400	-6.1	2006-10-07	2008-09-26	720	P
F	China	90.23	28.28	5,301	high	115,200	136,800	+18.75	2007-11-21	2008-09-20	304	P
G	Bhutan (1^{st})	90.33	28.1	4,706	high	57,600	52,200	-9.4	1990-11-14	1991-09-30	320	P
	(2^{nd})			4,706	high	23,400	20,700	-11.5	2009-11-18	2010-10-04	320	P
H	Bhutan	90.42	27.90	5,142	high	11,700	7,200	-38.5	1997-11-01	1998-11-04	368	P
J	China	94.32	30.69	4,117	high	18,000	21,600	+20.0	2002-10-24	2003-10-11	352	P
						Σ = 441,900	**Σ = 400,500**	**μ = -9.4**			**μ = 330**	

2.5. Discussion

2.5.1. Data quality

The success of our processing chain for automatically detecting past GLOFs in the HKH rests on a number of assumptions and simplifications. Time-series analysis requires co-registered Landsat imagery that we assumed to be sufficiently honoured by consistently using L1T imagery. Precise pixel alignment is most relevant for partial drainage with flow tracks only several pixels wide (Table 2.1 and Table 2.8). The resampling of overlapping Landsat scenes to the master projection (UTM Zone 45N) may also shift pixels by up to one pixel width, but this error does not negatively affect our change detection. We rarely observed such artefact offsets of lake shorelines that the change point algorithm interpreted as change events from water to land, causing an overestimation of change events. However, nearest neighbour is the only interpolation method for image resampling that preserves the original digital numbers (Parker et al., 1983). Other techniques such as cubic convolution or spline interpolation would blur the distinct transition between land and lake (Parker et al., 1983), compromising our ability to detect minor GLOFs.

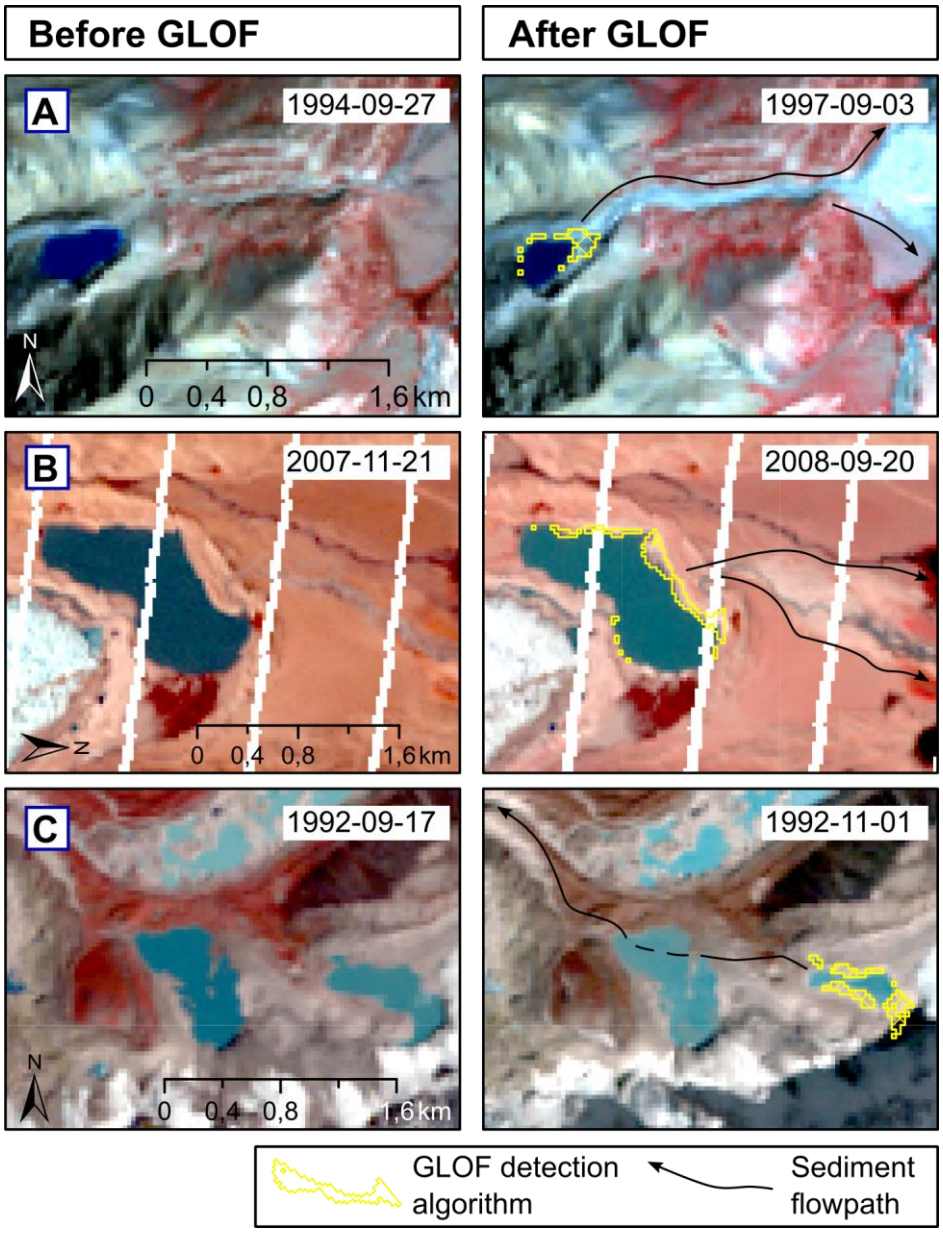

Figure 2-10: Examples of newly detected GLOFs with high confidence (A and B) and medium confidence (C). *Note the bright reflectance of sediments from the partially drained lakes in panels A and B (see Table 2.8-A and F). Panel C shows a distinct decrease of lake area, but uncertain outburst path. The change in colour of the lake downstream could imply a change in sediment concentration as an indicator for the GLOF event.*

2.5.2. Quality of fuzzy land cover maps

We chose a RF classifier because it is flexible, easy to use, robust against overfitting, while offering soft class membership estimates that express some of the uncertainties in the data. Moreover, RF performed robustly on comparable or smaller training data sets than ours (Rodriguez-Galiano et al., 2012). We avoided simpler and more transparent (parametric) classifiers, as these often perform worse in land-cover classification (Waske and Braun, 2009; Xu et al., 2014). Alternatives such as Support Vector Machines and Artificial Neural Networks have no or weakly

justified probabilistic output, while algorithm parametrization becomes less intuitive (Lippitt et al., 2008). Future work might compare the performance of different classifiers in our workflow, although such benchmarking depends heavily on the choice of data (Belgiu and Drăguţ, 2016). The error matrices (Table 2.4) indicate that confusing *Clouds* with *Land* is the most prominent classification error. Even a penalization could not fully avoid misclassifications. (Foga et al., 2017) suggested masking clouds from images with *CFmask*, but our tests with *CFmask* merely confirmed the known issue of confusing clouds with bright sediment surfaces. A possible solution might involve first predicting land cover on training images, followed by updating the classifier with samples from misclassified pixels along the lines of reinforcement learning. Collecting training data is the most labour-intense part in our processing chain, though it remains doubtful whether adding thousands of new training data would substantially increase our classification accuracy (Zhu et al., 2016). Spatial cross-validation with bootstrapping improves the performance of the RF classifier in diverse geographical settings, and is promising for transferring our approach to the whole HKH region.

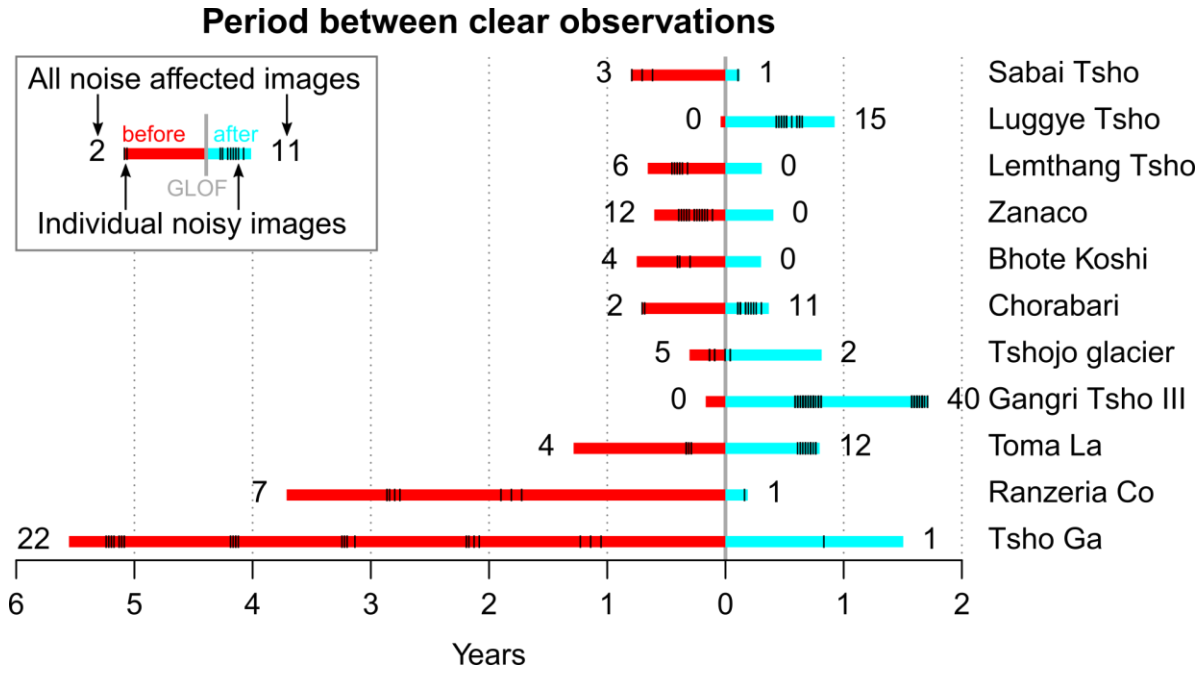

Figure 2-11: Period in years between clear images before (red) and after (cyan) the reference GLOFs. *Numbers at the end of the bars indicate the number of unsuitable images due to noise induced by clouds, shadows or lake freezing.*

2.5.3. Challenges of change-point detection

Calculating likelihoods in the change point algorithm assumes identically and independently distributed time steps. However, pixel time series involving multiple observations per year are temporally correlated and not equidistant due to noise. Other studies on change-point detection visually selected only one suitable image per year (Pflugmacher et al., 2012) or generated annual to

five-year image composites (Griffiths et al., 2014; Schroeder et al., 2011), likely concealing GLOFs within certain seasons (as for Sabai Tsho in September 1998 or Luggye Tsho in October 1994). Data availability for the reference GLOFs suggests that four to seven years without any clear view of the lakes are common (Tsho Ga and Ranzeria Co), and that high overpass rates (Gangri Tsho III) do not necessarily increase the chance of acquiring suitable images (Figure 2-11).

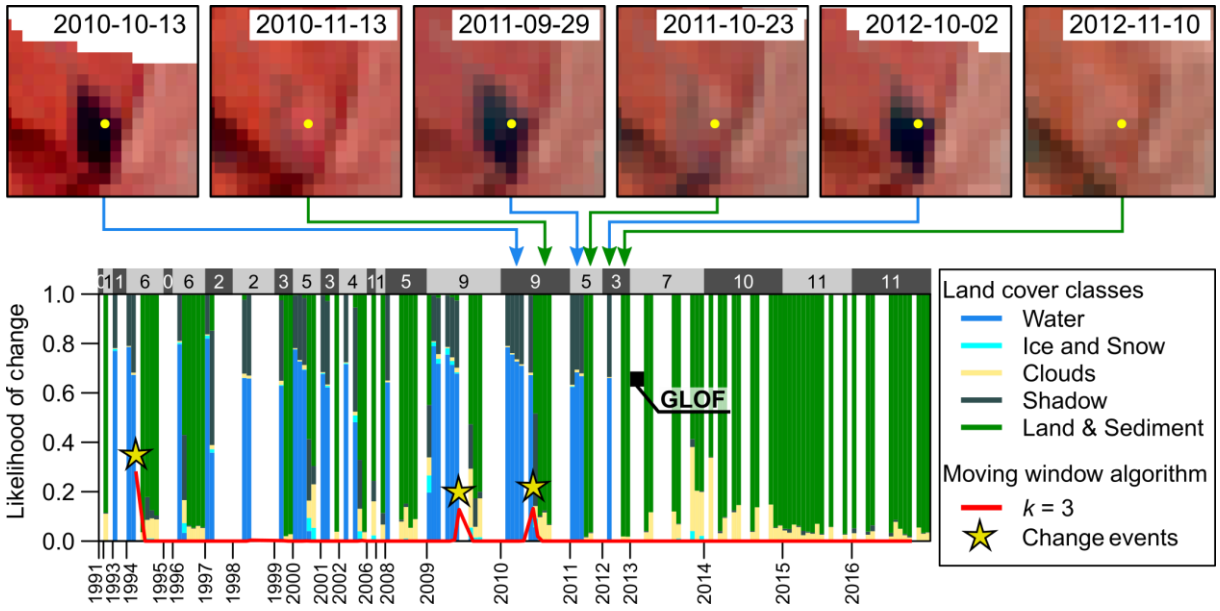

Figure 2-12: Noise-filtered pixel time series from Lake Chorabari (Table 2.1-1), extracted from yellow location pixel in top-row panels. *The algorithm correctly detected several changes from water to land (stars), but missed the GLOF because of noisy data in that year. A higher number of noise-free observations per year (see grey-shaded bar) allows better change detection. The lake had appeared and disappeared several times before the GLOF.*

The highly varying data availability in the HKH region led us to develop a change-point algorithm that differs from previously proposed methods; for example, for boreal environments comparable data gaps are less frequent (Hermosilla et al., 2016). Choosing k = 3 time steps of consecutive observations for computing the likelihoods of *Water* and *Land* is one of the few empirical steps in our processing chain, and may need further testing for larger areas. Our processing chain substantially decreases the influence of user-dependent decisions compared to other change-point algorithms that depend on a wide range of empirical parameters (Jamali et al., 2015; Kennedy et al., 2010). With the current parameter setting, we seem to overestimate the number of change pixels (Table 2.6), causing low PA of changed area (Table 2.7). Increasing k may decrease time-consuming visual validation, but also increase the risk of overlooking GLOFs. By contrast, any automated detection becomes difficult with less than three consecutive observations. The 2013 GLOF from Lake Chorabari, India, remained undetected because no noise-free image was available between lake filling and drainage (Figure 2-12).

Future work may involve a more flexible handling of time steps such that *k* becomes more (less) sensitive in regions where the number of observations in the pixel time series is low (high). The Chorabari time series also demonstrates how glacial lakes change their size without producing outburst floods. Desiccation, infilling, or subsurface drainage are processes that shrink or remove proglacial lakes in the HKH. Similarly, ponds on debris-covered glaciers can grow and shrink annually (Miles et al., 2017; Watson et al., 2016), though these and other, monsoonal, changes are beyond the scope of this study, given the seasonal preference of our satellite imagery.

Finally, determining whether a lake has drained catastrophically remains a time-consuming interactive step at the end of our processing chain. In most cases, Landsat imagery was our only data source for identifying tell-tale sediment tails. The resolution of Landsat data is often insufficient to reveal details about sediment dynamics in the outburst paths. In this context, the newly available Sentinel-2 data improve the situation for detecting GLOF events, offering a higher spatial resolution (up to 10m) and repeat rate of acquisition. Combining multi-sensor and multi-resolution datasets have become popular to map high-mountain glacial outlines and flow velocities (Holzer et al., 2015; Kääb et al., 2015; Shukla et al., 2010), but may also unlock more regional detail of glacial lake dynamics and resolve more, probably smaller events. Other drainage mechanisms such as vertical drops in lake level or the emptying of subglacial water pockets elude our analysis of optical imagery, but may be resolved with laser altimetry or radar techniques (Smith et al., 2009; Wingham et al., 2006). In any case, the ten newly detected GLOFs redefine the lower envelope of their potential activity in the HKH region.

2.6. Conclusions

Our newly developed processing chain allows a robust retrospective detection of glacial lake outburst floods (GLOFs) from Landsat time series in the Hindu Kush Himalayan (HKH). Fuzzy land-cover classification with Random Forests and a likelihood-based change point algorithm promise high accuracies in detecting independently documented GLOFs. We successfully detected ten of eleven reported GLOFs, as well as ten previously unreported ones. Though we analysed only 10% of the HKH, we were able to expand the current GLOF inventory by 91% for the past three decades. Ubiquitous cloud, ice and shadows in the HKH lead to data gaps that prohibit a comprehensive tracking of glacial lakes at regular intervals. We used shrinking lakes and exposed sediment tails as key indicators for GLOF detection that we time-stamped with a change-point algorithm that computes the likelihood of change from three consecutive observations of water to land. Thus exploring all valid observations in the stack of land cover maps is a novel approach for detecting changes in pixel time series and holds promise for mountainous environments with patchy Landsat

coverage. Data gaps and the limits of detection caused by 30 m resolution Landsat imagery call for multi-sensor and multi-resolution approaches including higher resolution imagery such as Sentinel-2 for future regional studies on GLOF detection. We robustly configured our processing chain using techniques of spatial-cross validation with bootstrapping for classifier training such that our methods are transferable to the whole HKH and mountain ranges elsewhere. The detection of ten previously unreported GLOFs confirms our initial hypothesis that the existing GLOF inventories underestimate significantly the number of GLOFs in the Himalayas. We thus set the basis towards a more complete GLOF inventory for the HKH, and towards objectively and systematically filling the gaps in the hitherto censored chronology of past GLOFs.

Acknowledgements

This research was funded by Deutsche Forschungsgemeinschaft (DFG) within the graduate research training group NatRiskChange (GRK 2043/1) at the University of Potsdam (http://www.natriskchange.de). SRTM and Landsat data were available from the U.S. Geological Survey. Landsat imagery were preprocessed via the Earth Resources Observation and Science (EROS) Center Science Processing Architecture (ESPA). Our computations were entirely based on the statistical software *R* (http://www.r-project.org/). We thank Adam Emmer and two anonymous referees for their helpful comments and Berry Boessenkool for computational support.

3. Unchanged frequency of moraine-dammed glacial lake outburst floods in the Himalaya

Authors
Georg Veh
Oliver Korup
Sebastian von Specht
Sigrid Roessner
Ariane Walz

Published as
Veh, G., Korup, O., von Specht, S., Roessner, S., Walz, A., 2019. Unchanged frequency of moraine-dammed glacial lake outburst floods in the Himalaya. *Nature Climate Change*, 9, 379-383.

ABSTRACT.

Shrinking glaciers in the Hindu Kush-Karakoram-Himalaya-Nyainqentanglha (HKKHN) region have formed several thousand moraine-dammed glacial lakes (Ives et al., 2010; Nie et al., 2017; Schwanghart et al., 2016b), some of them having grown rapidly in past decades (Nie et al., 2017; Wang et al., 2015). This growth might promote more frequent and potentially destructive glacial lake outburst floods (GLOFs) (Harrison et al., 2018; Huss et al., 2017; Richardson and Reynolds, 2000). Testing this hypothesis, however, is confounded by incomplete databases of few reliable, though selective case studies. Here we present a consistent Himalayan GLOF inventory derived automatically from all available Landsat imagery since the late 1980s. We more than double the known GLOF count and identify the southern Himalayas as a hotspot region, compared to the rarer affected Hindu Kush-Karakoram ranges. Yet the average frequency of 1.3 GLOFs per year has no credible posterior trend despite reported increases in glacial lake areas in most of the HKKHN (Gardelle et al., 2011), so that GLOF activity per unit lake area has decreased since the late 1980s. We conclude that learning more about the frequency and magnitude of outburst triggers rather than solely focusing on rapidly growing glacial lakes might improve appraisals of GLOF hazard.

3.1. Main article

Atmospheric warming and changing precipitation patterns will substantially change the contribution of glaciers to river runoff in the Himalayas and adjacent mountain belts within the next decades (Huss and Hock, 2018; Lutz et al., 2014). Terminal moraines and debris at the tongue of downwasting glaciers may trap meltwater, which is an immanent natural hazard if suddenly released in potentially destructive outburst floods (Richardson and Reynolds, 2000). Individual GLOFs in past decades attained runout distances of >120 km, causing up to hundreds of fatalities, destroying bridges and hydropower schemes, and locally causing channel incision and aggradation (Osti and Egashira, 2009; Richardson and Reynolds, 2000). Judging from Landsat imagery, which offers the longest continuous satellite record for the HKKHN since the late 1980s, several thousand moraine-dammed glacial lakes exist in the HKKHN today (Ives et al., 2010; Nie et al., 2017; Schwanghart et al., 2016b), being rare in the Karakoram, but abundant in the southern HKKHN (Gardelle et al., 2011). Since 1990, 401 new glacial lakes formed in the Western, Central and Eastern Himalayas, corresponding to an increase of 56.4 km^2 (+14.1%) in total area (Nie et al., 2017). Very large or rapidly growing glacial lakes have traditionally attracted hazard and risk assessments as these lakes may unleash exceptionally large flood volumes (Fujita et al., 2013; Wang et al., 2015). Recent approaches also account for lakes growing in loose debris or behind unconsolidated moraine dams, and for whether calving glacier ice, avalanches, landslides or rainstorms could potentially trigger outburst floods (GAPHAZ, 2017; Rounce et al., 2017). GLOFs from moraine-dammed lakes

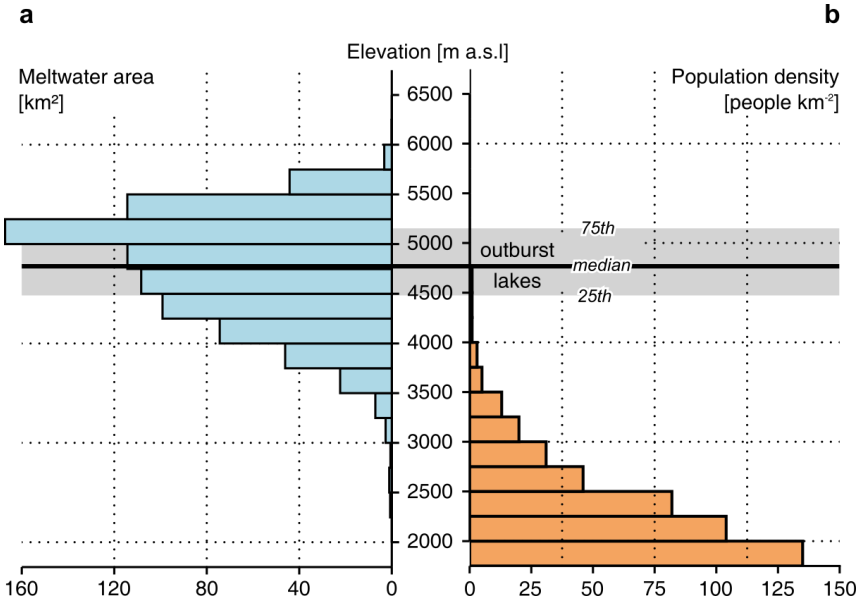

Figure 3-1: Elevation gap between meltwater areas and population density. a, *Unchanged meltwater areas (Pekel et al., 2016; Methods) in a 3-km buffer around glaciers and* ***b****, estimated population density from the LandScan™ (2014) Global Population Database in a 10-km buffer around glaciers. Thick black line is the median, and grey box is the interquartile range of lake elevation with reported outbursts (Figure 3-2).*

have drawn an increasing research interest over the past decades (Emmer, 2018), motivated by the hypothesis that a growing number and area of glacial lakes may raise GLOF frequency in the near future (Richardson and Reynolds, 2000). Counterintuitively, first-order global compilations on historical GLOFs dating back to the 19th century and beyond, indicate fewer GLOFs in past decades (Carrivick and Tweed, 2016; Harrison et al., 2018). Objectively estimating trends in GLOF frequency is challenging as many lakes form in terrain with limited access, making fieldwork impractical. In the HKKHN, outburst floods from glacier lakes initiated mainly between 4,500 and 5,200 m a.s.l., and some attenuated rapidly (Schwanghart et al., 2016b), possibly escaping notice in human settlements few thousand vertical meters below (Figure 3-1). Reliable reports of 40 GLOFs since 1935 are selective. We mapped these GLOFs, originally compiled by regional initiatives, highlighting 32 cases in the Central and Eastern Himalayas (Ives et al., 2010; Nie et al., 2018) in contrast to very few cases in the north-western Hindu-Kush-Karakoram and the Nyainqentanglha Mountains (Figure 3-2a, Supplementary Table 7.1). We speculate that these 40 reports preferentially covered large or destructive cases, which makes assessing their frequency difficult. In trying to account for this reporting bias, our objective is to estimate GLOF frequency and its changes from a systematic inventory covering the entire HKKHN.

We developed a Random Forest model for classifying land cover in Landsat images, and used a change-point analysis that successfully identified 10 out of 11 previously reported test cases (Veh et al., 2018; Methods). The analysed imagery covers the late 1980s to 2017, an interval that is conventionally used to study the response of natural hazards to climate change. Our analysis focuses on lakes dammed by moraines, but excludes water stored in subglacial pockets or seasonal and ephemeral water bodies that the optical images cannot resolve.

Systematically mining 8,210 Landsat images across the entire HKKHN, we added 22 newly detected GLOFs to the 17 GLOFs that had been reported since the beginning of the Landsat era in the late 1980s (Figure 3-2a, Supplementary Table 7.2). We thus more than doubled the existing GLOF count to a total of 39 cases in the past three decades, with most of the newly found GLOFs clustering between the Central Himalayas and the Nyainqentanglha Mountains (Figure 3-2a). Our analysis thus consolidates the regional contrast between low GLOF abundance in two northern regions (two new cases in the Hindu Kush-Karakoram, none in the Western Himalayas) and high GLOF abundance in three southern regions (20 new cases for the Central, Eastern Himalayas and Nyainqentanglha Mountains).

A swath analysis along the HKKHN (Figure 3-2b) reveals that the regional GLOF pattern correlates with the abundance of meltwater areas (Spearman's correlation coefficient ρ = 0.87) and the change of meltwater occurrence intensity (Pekel et al. 2016; see Methods), calculated as the difference between two epochs before and after the year 2000 (ρ = 0.77). Glacier cover (ρ = −0.18) and changes in mass balance (ρ = 0.26) are only weakly correlated with the number of GLOFs per swath (Arendt et al., 2015; Brun et al., 2017). The fraction of meltwater areas in the Central, Eastern Himalayas, and Nyainqentanglha Mountains is three to six times higher than that in northern basins

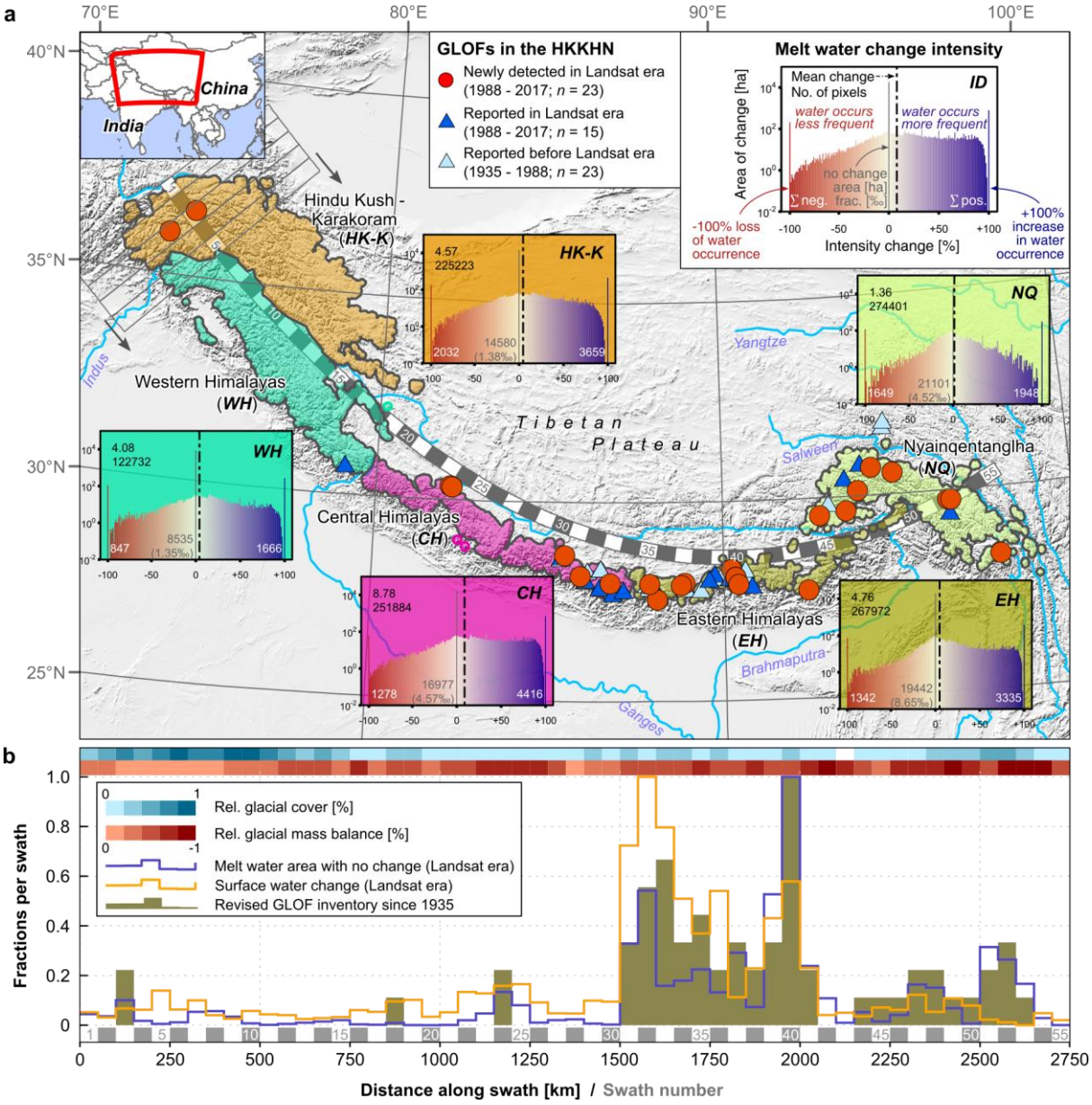

Figure 3-2: Revised map of Himalayan GLOFs. ***a****, Map of reported historic and newly detected GLOFs in five major drainage basins in the HKKHN in a 3-km buffer zone around glaciers. Insets show water change intensity for 1984-1999 and 2000-2015 of pixels classified as water at least once in one of these two periods (Pekel et al., 2016). All basins had posterior distributions with credible non-zero changes in meltwater areas.* ***b****, Statistics as above including present glacial cover (Arendt et al., 2015) and mass balance (Brun et al., 2017) from 2000-2016 (top bars), and GLOF frequency for 55 swaths (50 km × 700 km; see example at left figure margin in Figure 3-2). Fractions per swath are normalised so that 1 (or -1 for glacial mass balance) is the observed maximum. Blue line calculated from the spikes at zero in* ***a****; orange line is the sum of meltwater change intensity.*

(Figure 3-2). The Western Himalayas have some of the highest glacier melt rates (Brun et al., 2017) and meltwater-dependent runoff along the HKKHN (Kaser et al., 2010; Lutz et al., 2014), but GLOF abundance is low. The anomalously stable or advancing glaciers in the Karakoram Mountains (Gardelle et al., 2012) currently offer limited space for moraine-dammed lakes to form. Yet, glacier surges (Quincey et al., 2011) can locally form temporary ice dams and release GLOFs as observed at Kyagar or Khurdopin glacier during our study period (Hewitt and Liu, 2010; Round et al., 2017).

Only three of the 39 previously known and newly detected GLOFs originated from lakes that formed in the Landsat era, while nine lakes had been growing before they burst out. Expanding lake area alone thus did not warrant a high susceptibility to GLOFs. Yet, glacial lakes can grow again after an outburst and release more subsequent GLOFs, such as at Lakes Ayaco and Zhangzangbo, or a newly found GLOF in Bhutan that originated from the same lake location in 1991 and 2010 (Supplementary Table 7.2). Eight of the newly detected GLOFs occurred less than 16 km from previously known ones, but have gone unnoticed despite this proximity and a similar size. The posterior distributions of estimated mean flood volumes of new and GLOFs reported since the 1980s do not differ credibly (Figure 3-3; Supplementary Figure 7-3), indicating that large floods can still occur unnoticed today if not systematically monitored. Mean flood volumes of GLOFs predating the Landsat era were credibly larger, possibly because records of larger floods more likely entered

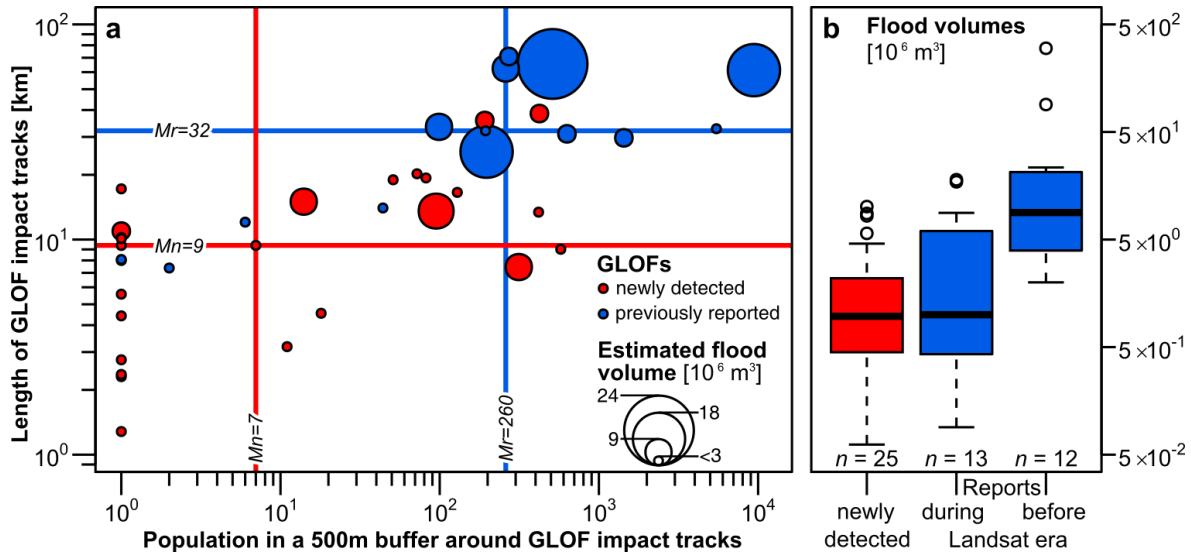

***Figure 3-3: Population density, impact tracks, and estimated flood volumes of GLOFs. a**, Red bubbles are 21 GLOFs detected in this study and four GLOFs from other remote sensing studies (Nie et al. 2018; Komori et al., 2012; Wang et al., 2011) blue bubbles are 15 previously reported GLOFs with mappable impact tracks and pre- and post-GLOF lake sizes. Population estimate is from the LandScan™ (2014) Global Population Database in a 500-m corridor. Thick lines are medians of new (M_n) and previously reported (M_r) GLOFs. Estimated zero population values are set to 1 due to logarithmic scale. **b**, Boxplots of flood volumes from newly detected (red) and previously reported GLOFs during and before the Landsat era (blue). Boxes span interquartile range; medians are thick black lines; whiskers encompass 1.5 times the interquartile range; circles are outliers. A Bayesian ANOVA shows no credible difference in mean GLOF volumes between newly found and previously known cases during the Landsat era.*

historic records. Besides flood volume, however, local population density, geomorphic impacts and associated damage may also influence reporting. To test this notion, we mapped traces of erosion and sedimentation by each GLOF in channels downstream, and compared these individual impact tracks with data from the LandScan™ (2014) Global Population Database. We find that newly found GLOFs had generally shorter impact tracks than previously reported ones and mostly affected river reaches with lower population density (Figure 3-3). Reports of Himalayan GLOFs thus largely favour damaging events: only twelve out of 40 published lake outbursts had caused no appreciable damage (Supplementary Table 7.1). Six newly detected GLOFs, for instance, drained into a larger lake further downstream, showing that large lakes can buffer impacts from smaller GLOFs.

From our revised database of 38 GLOFs between 1988 and 2017, we obtain an average rate of 1.3 GLOFs per year. Neither this overall nor the basin-wide GLOF frequencies in the Eastern Himalayas, the Central Himalayas or the Nyainqentanglha Mountains have changed credibly over these past three decades (Figure 3-4; Supplementary Figure 7-3); the HKKHN-wide trend is $-0.0006^{+0.0415}/_{-0.0394}$ yr^{-1} (95% highest density interval). Though remaining unchanged over the past three decades, the GLOF rate of 1.3 per year is the highest reported anywhere in the HKKHN. Our rate estimate differs from previous work proposing a global decrease in GLOF activity since the 1970s (Harrison et al., 2018) or the mid-1990s (Carrivick and Tweed, 2016), most likely because these studies considered selective reporting or detection negligible. The fraction of lakes that released GLOFs remained at ~0.7%, regardless of whether these lakes existed before or formed after 1990 (Nie et al., 2017). Yet the fraction of GLOFs per unit meltwater area has declined since 1990 (Figure

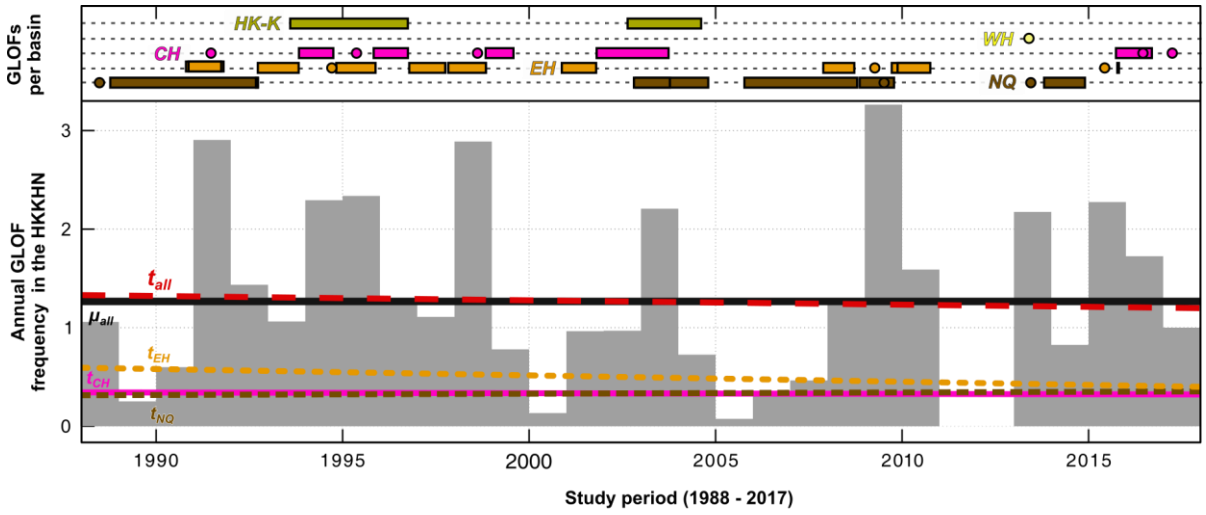

Figure 3-4: Unchanged GLOF frequency over the past three decades. *Grey histogram in lower panel shows annual GLOF frequency with posterior means μ_{all} and trends t_{all} estimated from Bayesian robust linear regression. Trends per basin (Figure 3-2a) are for the Central and Eastern Himalayas (t_{CH}, t_{EH}) and the Nyainqentanglha Mountains (t_{NQ}). Upper panel shows GLOFs with known dates as dots and newly detected GLOFs as bars spanning the intervals between suitable Landsat images. For these intervals, we assumed that each day was equally likely for the outburst date and added the probability mass of potential days to the number of dated cases to calculate the annual GLOF frequency.*

3-2), mainly because the expansion of few large moraine-dammed lakes dominated the total increase in meltwater area (Song et al., 2017; W. Wang et al., 2015). Even the most pronounced increase of meltwater areas in the southern Himalayas had no commensurate increase in GLOF activity (Figure 3-4). We infer that climate-driven rates of glacier melt and lake expansion may be unsuitable predictors of contemporary outburst potential, consistent with findings from the Patagonian Andes (Wilson et al., 2018). However, GLOF activity may lag behind glacier decay and lake growth that could have begun already at the end of the Little Ice Age (Harrison et al., 2018), an effect that our study period cannot cover.

An unchanged GLOF frequency may reflect some degree of resilience to climate-driven triggers, however. Calving glaciers and ice avalanches are the most frequently reported triggers for GLOFs (Nie et al., 2018), while elevated hydraulic pressure from sudden meltwater input or overspill from rainfall may exceed the shear resistance of moraine dams (Worni et al., 2012). The triggers of our 22 newly identified outburst floods remain unknown, but 16 of them came from pro- or supraglacial lakes within 300 m from their parent glaciers. With lakes gradually losing contact to their parent glacier, ice calving and avalanches become less relevant triggers (Nagai et al., 2017). This decoupling could explain why GLOF frequency has not increased with total meltwater area or the number of moraine-dammed lakes. Unless glacial lakes expanded substantially into the trajectories of avalanches and landslides, the growth of Nepal's largest lakes, for example, has only marginally changed their outburst hazard (Rounce et al., 2017). The projected average warming of 2.1 ± 0.1°C in Himalayan glacier regions until the end of the 21st century (Kraaijenbrink et al., 2017) will likely form new lakes (Linsbauer et al., 2016), and destabilise ice cores in moraines and permafrost in rock walls surrounding glacial lakes (Gruber et al., 2017; Haeberli et al., 2017). Whether and how these changes will alter GLOF frequency is open to future research, considering also the role of earthquakes and monsoonal storms triggering landslides and snow avalanches (Ballesteros-Cánovas et al., 2018). For example, severe ground shaking during the 2015 M_w 7.8 Ghorka earthquake did not trigger any GLOF in the Nepalese Himalayas, though nine landslides directly hit glacial lakes (Kargel et al., 2016). Finally, new lakes could have formed in stable bedrock depressions resistant to most GLOF triggers and hence less prone to outburst, similar to the Cordillera Blanca and the European Alps (Buckel et al., 2018; Emmer et al., 2016a). Desiccation, siltation, or subsurface drainage may shrink or obliterate lakes, though without diagnostic sediment tails from outburst floods. All major Himalayan basins also had distinct losses of meltwater area (Figure 3-2a), and 74 glacial lakes have disappeared in our study period without evidence of an outburst (Nie et al., 2017).

Our regional assessment emphasises that it is vital to learn more about the past and future frequency of such triggers to better understand controls on GLOF frequency. Characterizing succinctly the seismic, geomorphic, and glaciological setting of meltwater lakes may improve our understanding and predictions of GLOF frequency. Triggers of GLOFs may be difficult to derive on regional scales from Landsat imagery, but new generations of optical and radar satellite sensors and in-situ measurements push the way forward. Given that 20 out the 22 newly found GLOFs occurred in the monsoon season, our search algorithm is robust against data gaps due to cloud cover (Supplementary Figure 7-2). Yet higher resolution could shed light on potentially unobserved cases with released water volumes or lengths of sediment tails beyond the current limits of detection. Our method is readily applicable to other mountain belts with similar Landsat coverage, and thus allows objective comparisons between regional climate change and GLOF frequency. Multi-criteria guidelines may help to systematically categorise individual lake hazard, moving beyond the traditional approach of mapping lake expansion (GAPHAZ, 2017; Rounce et al., 2017). We conclude that our regional and objectively derived inventory adds systematic insights on the regional and temporal patterns of GLOFs in the HKKHN, and invite more focus on the triggers of this prominent Himalayan hazard.

Acknowledgements

This research was funded by Deutsche Forschungsgemeinschaft (DFG) within the graduate research training group NatRiskChange (GRK 2043/1) at the University of Potsdam (http://www.natriskchange.de). We used the freely available glacier outlines from the Randolph Glacier Inventory (https://www.glims.org/RGI/). Landsat, SRTM and GTOPO30 data were available from the US Geological Survey (https://www.earthexplorer.usgs.gov). Landsat images were preprocessed via the Earth Resources Observation and Science (EROS) Center Science Processing Architecture ESPA (https://www.espa.cr.usgs.gov). We used the LandScan™ (2014) High Resolution global Population Data Set copyrighted by UT-Battelle, LLC, operator of Oak Ridge National Laboratory under Contract No. DE-AC05-00OR22725 with the United States Department of Energy. Our spatial and statistical analysis was entirely based on the statistical software *R* (http://www.r-project.org/).

3.2. Methods

Landsat data and preprocessing. Our study area comprises a 3-km buffer around all HKKHN glaciers in the Randolph (version 5.0) and ICIMOD glacier inventories (Arendt et al., 2015; Bajracharya et al., 2011). We downloaded 8,210 images of Landsat TM, ETM+ and OLI images from

the *EarthExplorer* web portal (earthexplorer.usgs.gov), limited to <60% cloud cover and time stamps between September and November to avoid excess cloud cover during the South Asian summer monsoon and snow or ice cover in winter. Landsat Thematic Mapper (TM) imagery covers the Nyainqentanglha Mountains since 1986 and the Western Himalayas since 1994 (Supplementary Figure 7-1). Due to Landsat's commercial on-demand service until the mid-1990s and the lack of an on-board storage (Markham et al., 2004), image coverage over the HKKHN was irregular until the 21st century (Supplementary Figure 7-1). With the launch of the Enhanced Thematic Mapper (ETM+) in 1999, annually available imagery increased notably, but the failure of the Scan Line Corrector (SLC) in 2003 caused data loss of ~22% in ETM+ images (Wulder et al., 2012). Data availability shows another distinct kink in 2012 with the shutdown of Landsat TM, but improved one year later when the Landsat Operational Land Imager (OLI) was launched (Wulder et al., 2016). Any single pixel in our study area was overpassed 180 times on average during our study period, while the longitudinally overlapping orbits had a maximum of 449 views on any pixel (Supplementary Figure 7-1).

The images follow the USGS Collection-1 Tier 1 processing routines with terrain and precision correction with an image-to-image tolerance of <12-m radial root mean square error (RMSE) during geo-registration (USGS, 2018). The oblique semi-circular stretch of the HKKHN across six UTM zones (42N-47N) required re-projecting all images to an Oblique Mercator projection that minimizes projection distortions. The projection parameters were calculated using the coordinates of a discretised fourth-order polynomial fit through all glacier centroids along the HKKHN. We used a cubic convolution kernel to resample all images to 25-m pixel resolution using a Hotine Oblique Mercator projection routine as implemented as EPSG code 9812 in the Geospatial Data Abstraction Library (GDAL) (International Association of Oil & Gas Producers, 2016). All images were split subsequently into 940 tiles of 25 km × 25 km that covered the extent of our study area.

Summary of GLOF detection. The HKKHN is one of the most challenging regions for reliably detecting surface water bodies, discriminating them from other land-cover types, and tracking their changes over time (Veh et al., 2018). From a potential 16-day Landsat revisit cycle, annually available imagery narrows down to few (or even no) suitable scenes between September and November due to frequent post-monsoonal cloud cover in early autumn and lake freezing towards winter. We successfully trained, tested and validated a processing chain for GLOF detection in four spatially independent subsets in the Western, Central, Eastern Himalaya and Nyainqentanglha Mountains, comprising ~10% of the HKKHN (Veh et al., 2018). Here we show the application to the complete Himalayan range. In our customised workflow, we trained a Random Forest model to generate fuzzy land-cover maps containing the probabilities for the classes labelled as water, clouds, shadows, ice,

and land for each image tile. Our land cover maps had an overall accuracy of 91%, meeting our goal of robustly detecting water with a user's and producer's accuracy >90% for different Landsat sensors. Lakes decrease in area during GLOFs, involving an abrupt change from the classes 'water' to 'land' in our land-cover maps at the pixel scale. We defined a probability >0.5 for the classes 'cloud', 'shadow' and 'ice' as noise, and removed these observations from the pixel time series. For the remaining observations in the time series, we approximated the likelihood of change $p(C)$ by multiplying the likelihoods of belonging to the 'water' and 'land' class before and after each time step i:

$$p(C) = \prod_{i-3}^{i-1} P_i(w) \prod_{i}^{i+3} P_i(l) \quad (1)$$

where $P(w)$ is the probability of belonging to class 'water' for three time steps before i, and $P(l)$ is the probability of belonging to the class 'land' for three time steps after i. The likelihood of change $p(C)$ at time step i must exceed a specified threshold $T(C)$ to qualify as a change point. We set the threshold as

$$T(C) = 0.5^6 \quad (2)$$

where 0.5 is the random chance of belonging to a given class, and the exponent is the bandwidth of the change-point algorithm. Thus, our algorithm requires only six noise-free observations in a time series of pixels that can have a gap of several years. Hence the algorithm is robust against data gaps arising from the persistence of cloud, haze, snow, ice and shadow in Landsat images (Supplementary Figure 7-2). We set a lower limit of detection to clusters of six pixels, i.e. 3,750m^2, that simultaneously record a change event in their time series. We compared automatically detected with manually mapped change pixels for eleven known GLOFs, documenting >78% correctly detected pixels for nine cases, 30% for one case, and the case of Lake Chorabari (Kedernath) in 2013 remaining undetected (Veh et al., 2018). For tagging previously unknown GLOFs, we visually assessed Landsat images for tracks of geomorphic impact along channels and floodplains downstream of shrunken or disappeared water bodies. We term these GLOF impact tracks *sediment tails*, which are recorded by linear clusters of bright pixels that stand out from those of darker unaffected channels and valley floors. Consistent with field-based GLOF studies, we find that these sediment tails remained clearly visible also on Landsat images for years to decades after the lake outbursts. These persistent sediment tails below drained moraine-dammed lakes are thus a key diagnostic for detecting GLOFs in areas with longer data gaps.

Mapping change of meltwater areas. Abundant image noise and data gaps (Supplementary Figure 7-1, Supplementary Figure 7-2) in the HKKHN limit the production of annual maps of glacial lakes. We therefore assessed the long-term change of surface water in the HKKHN with the global map of surface water change (Pekel et al., 2016) (https://global-surface-water.appspot.com). Each pixel in this map marks the change in water occurrence intensity between two epochs (16 March 1984 to 31 December 1999, and 1 January 2000 to 10 October 2015) extracted from all available Landsat images. Only pairs of months with valid observations in both epochs were considered to calculate the occurrence difference between epochs. The average of all paired differences yields a map showing the intensity of change on surface water occurrence. We refined this dataset, clipping it to a 3-km buffer around glaciers and excluding all pixels from mountain rivers and streams on glaciers, as well as misclassifications mainly in terrain-shaded areas. All remaining pixels were assumed to relate to glacial meltwater and therefore termed *meltwater areas*. The histograms in Figure 3-2a show the full distribution of pixels within each basin where meltwater occurred more (1% to 100%), less frequent (-100% to -1%), or remained invariant (0) between the two epochs.

Outburst parameters of GLOF inventories. Our inventory on documented GLOFs contains cases with reported dates (day, year or specific period), location and, if available, damage. Following our visual image interpretation, some previously reported GLOFs, e.g. from Lake Kabache (Ives et al., 2010) or Lake Jialongco (Liu et al., 2013) were more likely debris flows as these floods originated from other sources upstream, and thus excluded from our historic GLOF inventory. For newly found and previously documented GLOFs, we digitised the corresponding lake areas from those Landsat images directly pre- and post-dating the outburst using ArcMap 10.5. We used the same scheme for historic GLOFs in the pre-Landsat era, where we added georeferencing information from Landsat images to 47 declassified black-and-white spy imagery (KH-4, -7, and -9) with an approximate spatial resolution of 20 to 30 feet (six to nine metres; lta.cr.usgs.gov/declass_1; lta.cr.usgs.gov/declass_2). The empirical relationship between lake area and volume (Cook and Quincey, 2015) was used to estimate pre- and post-GLOF lake volumes that we scaled to total flood volumes from their difference. In Figure 3-3, we show first-order values from the literature; our estimates were used only for floods with unknown flood volume. We furthermore manually digitised the centreline and the footprint of GLOF impact tracks from post-event Landsat images to calculate the length and area of impact tracks. The data in Figure 3-3a are a subset from reported cases for which we had complete information on pre- and post-GLOF lake areas and the lengths of the impact tracks (Supplementary Table 7.1). Lake elevations were extracted from the ALOS World 3D 30m V1.1 digital elevation model (eorc.jaxa.jp/ALOS/en/aw3d30/index.htm).

Differences in meltwater areas, GLOF size, and frequency. We used a one-way Bayesian ANOVA (which is the Bayesian variant of a *t*-test) to predict whether estimated (log-transformed) GLOF volumes differed credibly between reports predating the Landsat era (pre-1988) and after, and also between GLOFs documented in the Landsat era and our newly detected ones. The model estimates from the data the common mean over all groups of a nominal predictor x_i, and deviations from this common mean for each group. Our model setup had a normally distributed metric output (GLOF volume) $y \sim \mathcal{N}(\mu_i, \sigma^{-2})$ with mean $\mu_i = a_0 + a[x_i]$ and precision σ^{-2}, where $\sigma \sim \mathcal{U}(1,10)$ is uniformly distributed, and i is a group index. We set the hyperparameter $a_0 \sim \mathcal{N}(0,0.001)$ and similarly assumed normal distributions for the group weights $a \sim \mathcal{N}(0, \sigma_i^{-2})$ with σ_i being gamma distributed with shape s = 1.01005 and rate r = 0.1005, so that it has mode = 0.1 and standard deviation = 10. We also used this Bayesian ANOVA to check for credible non-zero changes in meltwater areas (Pekel et al., 2016) (Figure 3-2). To check whether annual GLOF frequency has changed during the Landsat period, we used a Bayesian robust linear regression, using a *t*-distributed target variable (annual GLOF frequency) to account for possible effects of outliers: $y \sim t(\mu, \tau, \upsilon)$, where the mean $\mu = b_0 + b_1 x$ is a linear combination of input x (year) with intercept $b_0 \sim \mathcal{N}(0, 10^{-12})$ and slope $b_1 \sim \mathcal{N}(0, 10^{-12})$; gamma distributed precision $\tau \sim \text{Gamma}(0.001,0.001)$, here with equal shape and rate parameters; and υ degrees of freedom. Lower values of υ are more robust to outliers, emphasising the tails of the *t*-distribution. We found that using $\upsilon \in [0.001, 100]$ hardly changed the posterior of the regression slope b_1. We numerically approximated all posterior distributions with a Markov Chain Monte Carlo sampling scheme implemented in the JAGS language (implemented in the package 'rjags' in the statistical programming software *R*) with three parallel chains of 100,000 iterations and a burn-in of 1,000 steps, and report here for the converged chains only the most relevant posterior distributions and their 95% highest density intervals.

4. Current and future hazard of Himalayan meltwater floods

Authors
Georg Veh
Oliver Korup
Ariane Walz

Under consideration as
Veh, G., Korup, O., Walz, A. Current and future hazard of Himalayan meltwater floods. In *Nature.*

ABSTRACT.

Sustainable development in the Himalayan region largely depends on how glaciers respond to atmospheric warming (Kraaijenbrink et al., 2017). Meltwater lakes have grown in size and number in past decades (Nie et al., 2017), and raised widely publicised concerns about more frequent, potentially destructive glacier lake outburst floods (GLOFs) (Harrison et al., 2018). More than 5,500 meltwater lakes dot the Himalayas today, and their number could nearly triple if glaciers disappeared. Yet regional projections of future flood hazards largely ignore the role of GLOFs. We use a Bayesian extreme-value model to estimate a current 100-year GLOF peak discharge of $20{,}600^{+2{,}200}/_{-2{,}300}$ m^3 s^{-1} in the greater Himalayan region, drawing on 0.3 trillion scenarios of likely dam-breach rates and outburst volumes. The GLOF hazard in terms of this return level could double to $41{,}700^{+5{,}500}/_{-4{,}700}$ $m^3 s^{-1}$ on average in the worst-case scenario of completely ice-free Himalayas, and even triple in the Karakoram mountains. We conclude that glacier melt alone could raise the risk from Himalayan GLOFs two- to threefold, even if the annual GLOF rate, vulnerability, and exposure were to remain unchanged.

4.1. Main article

Monsoonal floods are amongst the most destructive natural disasters in the Himalayas, and put the livelihoods of 240 million people at risk (Wester et al., 2019). Regional projections for the Indus, Ganges, and Brahmaputra rivers that drain most of the mountain belt, hold that flood frequencies will rise noticeably in the 21st century (Hirabayashi et al., 2013; Wijngaard et al., 2017). Such prognoses have largely disregarded episodic but potentially destructive floods that arise from the sudden emptying of meltwater lakes in Himalayan headwaters. In the past, such glacier lake outburst floods (GLOFs) have had discharges that surpassed hydro-meteorological discharges by orders of magnitude (Cenderelli and Wohl, 2001; Cook et al., 2018; Osti and Egashira, 2009). Lakes dammed by glacier moraines are particularly susceptible to outburst, triggered by ice or debris falling into the lake, strong earthquake shaking, internal piping or overtopping waves that exceed the shear resistance of the dam (Richardson and Reynolds, 2000). These triggers mostly happen unrecorded in remote terrain, eroding the impounding barriers within minutes to hours, and releasing sediment-laden floods that may travel >100 km downstream (Richardson and Reynolds, 2000). With little to no warning, communities and infrastructure downstream are often unprepared, and suffer loss of human lives and livestock, and damage to roads, buildings, and hydropower facilities (Allen et al., 2016; Watanabe and Rothacher, 1996). An objective and reproducible hazard assessment of such dam-break floods is key to human safety and sustainable development, and repeatedly emphasised in research and media coverage of atmospheric warming, dwindling glaciers, and growing meltwater lakes. GLOFs have gained growing attention in the Himalayas (Harrison et al., 2018; Nie et al., 2018), where these disasters have had the highest death toll worldwide (Carrivick and Tweed, 2016). Whether lake outbursts will become more frequent with atmospheric warming remains an open question, however. A global temperature rise of 1.5 °C could melt half of the Himalayan glacier mass until the end of the 21st century (Kraaijenbrink et al., 2017). Hence the thousands of Himalayan glacier lakes today (Nie et al., 2017) are likely to increase in number as presently ice-covered basins gradually become exposed and fill with meltwater (Linsbauer et al., 2016). Yet the average rate of GLOFs in the greater Himalayan region has remained unchanged in the past three decades (Veh et al., 2019), showing that rapid growth of glacier lakes alone is an unsuitable predictor of GLOF activity. This recognition reveals little about the current Himalayan GLOF hazard, let alone how this may change in the future. The high alpine conditions limit detailed fieldwork such that researchers have inferred GLOF characteristics mainly from the geometry of ice and moraine dams, the probability of avalanches or landslides entering a lake, or the water volumes released by outbursts (Emmer and Vilímek, 2013; Fujita et al., 2013; X. Wang et al., 2012). Increasingly detailed digital topographic data and satellite imagery allow measuring these variables,

but ranking key diagnostics for GLOF hazard appraisals has followed no common standard (GAPHAZ, 2017). While most research has been concerned with identifying glacier lakes that are most prone to outburst, we address instead the immediate physical consequence in terms of peak discharge Q_p [$m^3 s^{-1}$]. Guided by work on earthquakes, landslides, wildfires or floods, we express GLOF hazard using the frequency and magnitude of Q_p in a given area and period. We predict average return periods of Q_p from 0.3 trillion scenarios of physically plausible dam-breach rates and meltwater volumes released for glacier lakes in the greater Himalayan region. This number of simulations ensures that we have enough samples for fitting an extreme-value distribution to the simulated range of Q_p for each lake. Taking into account varying GLOF frequencies, we stack these simulations to predict GLOF hazard in terms of the 100-year peak discharge Q_{p100} for both the contemporary lake cover and the worst-case scenario of completely ice-free Himalayas (*Methods*).

We apply this simulation to the greater Himalayan region, including the mountain ranges of the Himalayas, Hindu Kush, Karakoram, Nyainqentanglha, and Hengduan Shan (Figure 4-1). From a manually mapped lake inventory (Zhang et al., 2015) and high-resolution maps of surface water (Pekel et al., 2016), we acquired a sample of 5,565 meltwater lakes >0.02 km^2 within 3 km of glacier margins between 2009 and 2015 (*Methods*). These lakes cover ~724 km^2, and are largest in the Eastern Himalayas and the Hengduan Shan (Figure 4-1). The ongoing shrinkage of >45,000 glaciers (Arendt et al., 2015) in these mountains may form new lakes where cirques, bedrock hollows, and

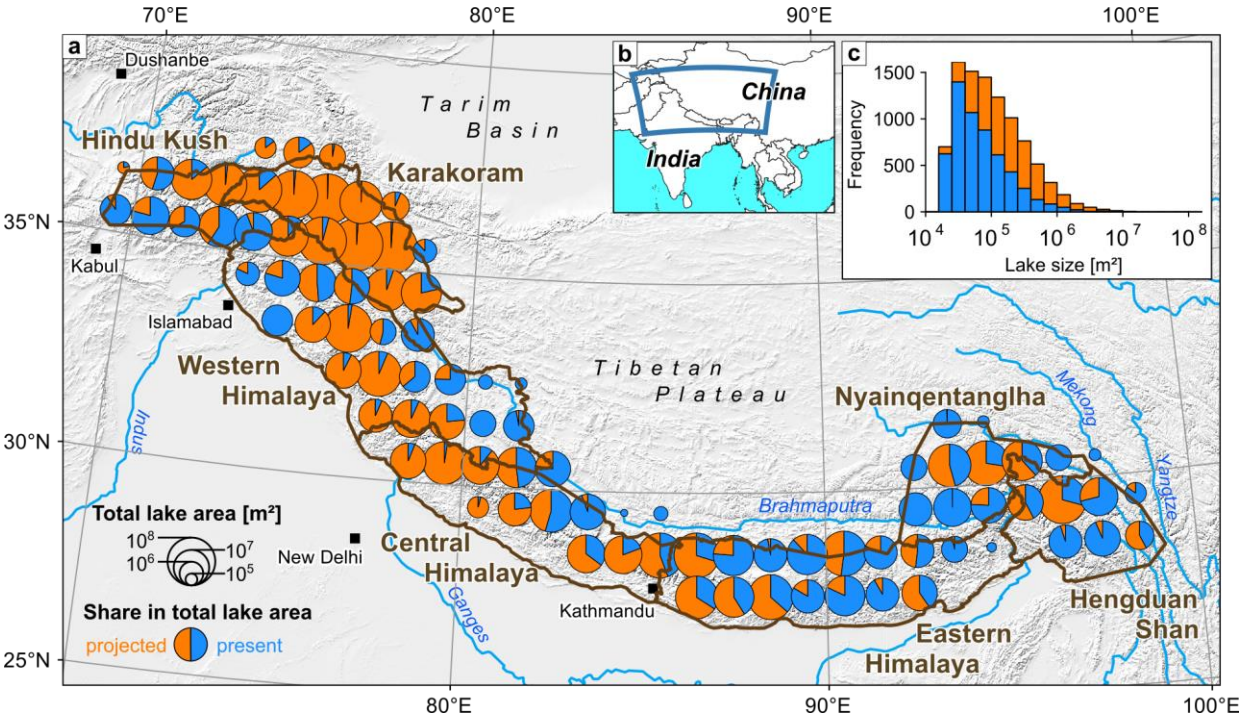

Figure 4-1: Present and projected future glacier lakes in the Himalayas. a, *Size of pie charts is scaled to the summed area of present and projected lakes within 3 km of glaciers (Arendt et al., 2015) in 1° × 1° bins for the worst-case scenario of completely ice-free Himalayas.* ***b,*** *Location of the Himalayas between the Indian subcontinent and the Tibetan Plateau.* ***c,*** *Histogram of present and projected glacier-lake areas.*

overdeepenings from subglacial erosion trap meltwater. We modelled the location and maximum size of such future lakes by subtracting the estimated ice thickness of all Himalayan glaciers >0.4 km^2 from digital ice-elevation data (*Methods*). We consider the worst case scenario, in which all presently ice-covered depressions fill to the brim with water in the future, which could form nearly 9,500 new lakes >0.02 km^2 that could store up to 123 km^3 of water in total. A completely ice-free greater Himalayan region might have three times more lakes covering five times more area than at present, and these projected lakes could grow largest in the Karakoram, Western, and Central Himalayas (Figure 4-1).

We used a physically motivated model to predict Q_p from the product of flood volume and dam-breach rate η (Supplementary Figure 7-4). Using data of 63 dam breaks from a wide range of topographic settings, we ran a robust Bayesian regression to obtain credible distributions of Q_p for each present or future lake in our study region. We calculated flood volumes for each meter drop in lake level and used the predictive posterior to compute Q_p for 100 physically plausible breach rates, deriving 10^5-10^8 posterior samples of Q_p for each lake. Thus predicted peak discharges span more than six orders of magnitude (Figure 4-2). Based on a mean posterior rate of 1.26 GLOFs yr^{-1} over the past three decades (Veh et al., 2019), we estimate a contemporary Q_{p100} of $20{,}500^{+2{,}200}/_{-2{,}300}$ m^3 s^{-1} (Supplementary Table 7.3) across all mountain ranges. Regionally differing GLOF rates cause variation in Q_{p100} (Figure 4-3). Correcting for this variation, we can explore how—for a fixed frequency—GLOF hazard changes as function of lake-size distribution (Figure 4-4): we find that, for

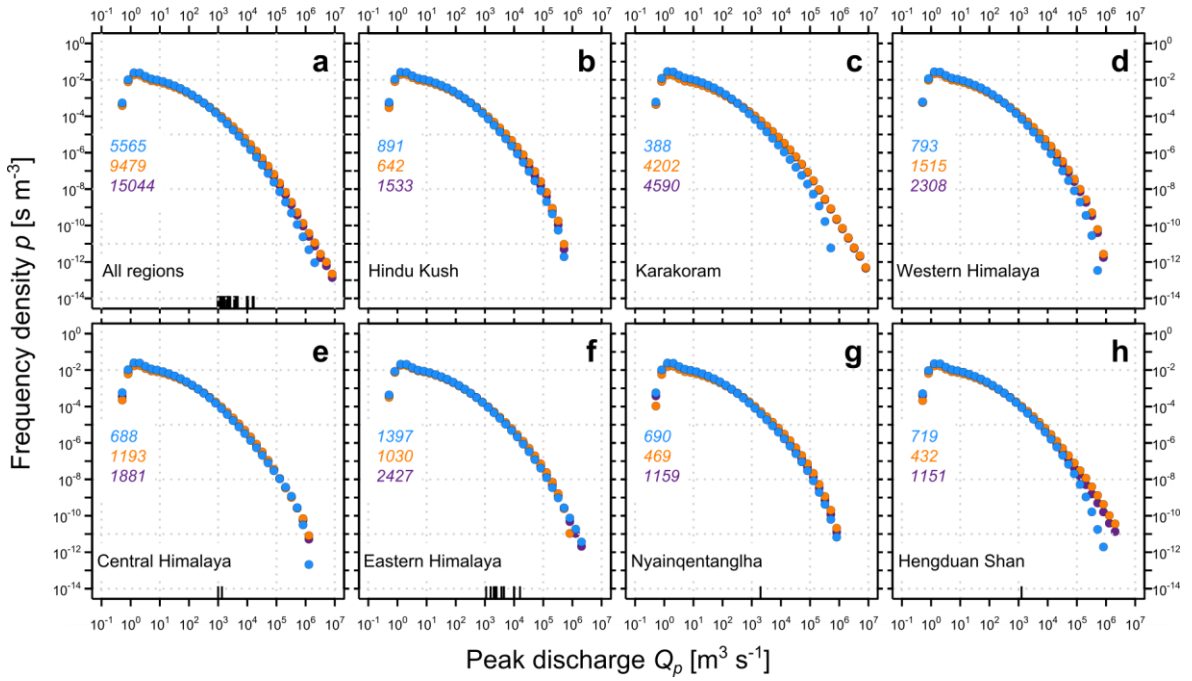

Figure 4-2: Frequency densities of simulated GLOF peak discharge Q_p for present and future Himalayan meltwater lakes. *Colour-coded numbers are numbers of present lakes (blue), projected lakes (orange), and the pooled estimate of present and projected lakes (dark orchid) in* ***a,*** *the entire study area and* ***b-h,*** *its seven subregions. Black ticks are 15 reported estimates of Q_p from moraine-dammed lakes in the study area since 1935.*

example, GLOF hazard in the Eastern Himalayas, which currently have most lakes and the highest GLOF activity in the past three decades (Veh et al., 2019), is more than 40% higher than the overall estimate. In contrast, the Western Himalayas had only one known outburst from moraine-dammed lakes in the past 30 years, while the rate-adjusted Q_{p100} there is still about 40% below that of the overall study area. Assuming that the annual GLOF rate remains constant, the changing size distribution of meltwater lakes in an ice-free scenario (and disregarding all present lakes) alone could raise Q_{p100} to $41{,}800^{+5{,}500}/_{-4{,}700}$ m^3 s^{-1}, essentially doubling the current GLOF hazard. If all current lakes survived until all Himalayan glaciers were gone, Q_{p100} would lie between these two end-member scenarios, though still at about 150% of the current estimate (Supplementary Table 7.3). All these projected changes in Q_{p100} involve the highest increase in GLOF peak discharges in the Karakoram mountains (Figure 4-2, Figure 4-3).

We offer a consistent and reproducible estimate of present and future GLOF hazard in the Himalayas. Our Bayesian prediction of Q_p explores the parameter space of plausible breach depths, breach rates, and associated flood volumes for any given lake, with up to hundreds of millions of outburst scenarios per lake. Thus predicted peak discharge allow a flexible and extendable hazard assessment (Rounce et al., 2016) that can accommodate changes in mean annual GLOF rates. Assuming that lakes will occupy all available topographic niches in ice-free Himalayas, our results

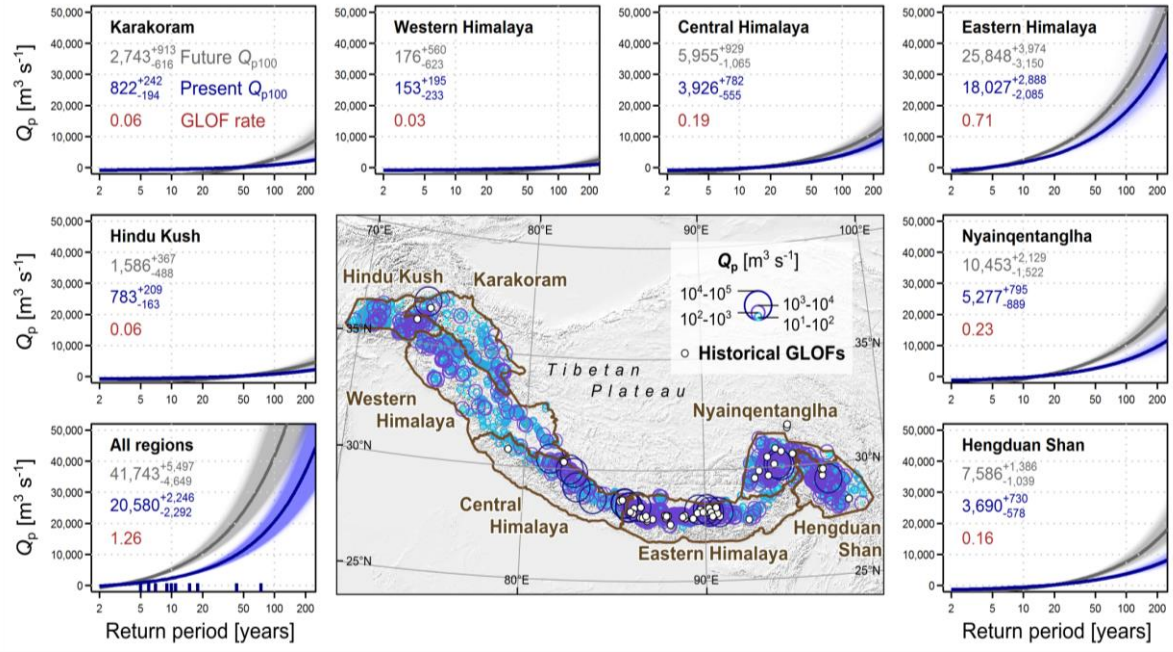

Figure 4-3: Present and future 100-year peak discharges from GLOFs in the greater Himalayan region. *Circles on map are present meltwater lakes with colours and radii scaled to the modes of the predicted distributions of Q_p for each lake. Insets show return periods of GLOF peak discharge for the entire study area (lower left) and its seven subregions. Curves are estimated GLOF return periods and numbers are the 100-year flood discharge for present lakes (blue) and projected future lakes (grey), assuming that the current GLOF rate per region (brown) remains unchanged. Thick lines are means of 200 simulations (thin lines) drawing on sampled time series of 10,000 years each. Black ticks are average return periods estimated for historic GLOFs since 1935.*

show the upper physical limit to future GLOF hazards. We identify the Hindu Kush, Karakoram, the Nyainqentanglha, and Hengduan Shan as potential hotspots with roughly twofold increases in future GLOF hazard, and robustly confirm previous notions for these regions (Prakash and Nagarajan, 2017; W. Wang et al., 2012).

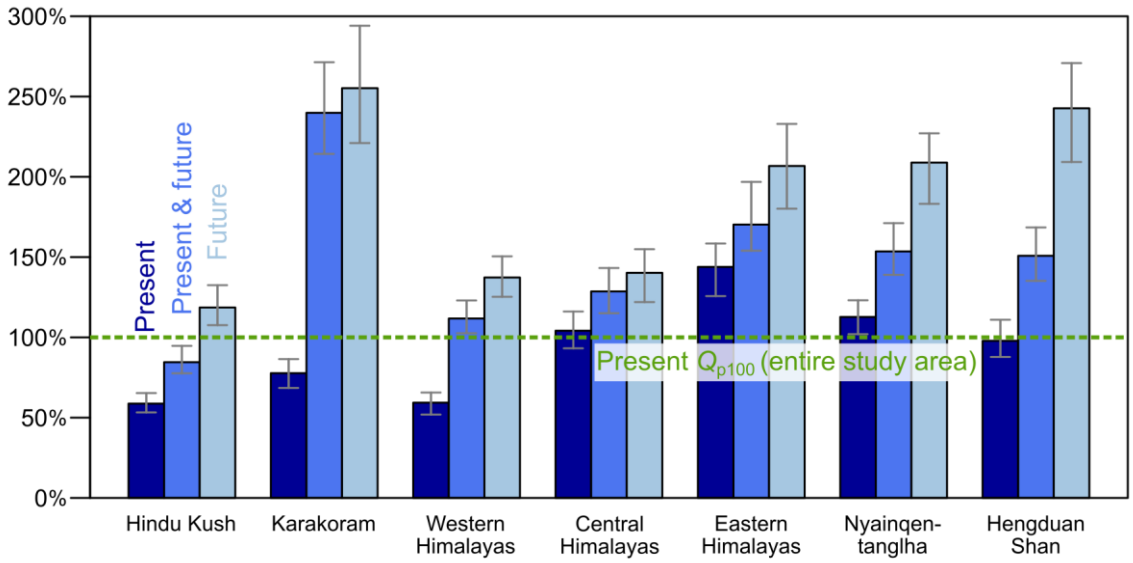

Figure 4-4: Regional estimates of Q_{p100} as fractions of the current Q_{p100} in the study area. *All estimates use a fixed mean rate of one GLOF per year to correct for regional differences in historically recorded GLOF frequencies (see Methods). This correction method highlights the effects of varying lake-size distributions in each region.*

Our regional estimates of GLOF return periods are consistent with the frequency of 15 reported GLOF discharges since 1935 (Figure 4-3). According to our estimates, the highest (15,920 $m^3 s^{-1}$ from Lake Zhangzangbo, China, in 1981) (Xu, 1988) had an average return period of about 75 years in the greater Himalayan region; the second highest peak discharges of ~10,000 $m^3 s^{-1}$ from Sangwang Co (1954) and Tam Pokhari (1998) were 45-year events (Osti and Egashira, 2009). Yet reports of Q_p rely largely on estimates from rating curves, eyewitness accounts, or measurements several kilometres downstream of the failing dams, thus compromising detailed, site-specific validation of our regional predictions. These uncertainties cause some of the scatter in the data that we based our model on (Supplementary Figure 7-4). However, our modelling approach explicitly propagates these uncertainties and robustly estimates Q_p from the distribution of meltwater lake areas in the entire Himalayan region. In the simplest case, we can resort to using this distribution of meltwater lake areas as a proxy of GLOF size conditional on outburst (Supplementary Figure 7-5). Lake area and volume will remain key determinants of GLOF hazard, regardless of whether we use alternative discharge rating curves (Supplementary Figure 7-5, Supplementary Figure 7-6), more elaborate numerical dam-breach simulations (Westoby et al., 2015), or any other metric of flood potential (Fujita et al., 2013).

Clearly, not all exposed overdeepenings in ice-free Himalayas may fill completely with water. Especially melting debris-covered glaciers will also contribute sediment, while premature dam failure, siltation or seepage similarly reduce the capacity to store water. Such processes likely reduce our predicted Q_p for shallower lakes, but contribute less to deeper lakes for which our breach scenarios accounted for a broader range of lake depths and flood volumes. In our simulations, all lake-level drops may occur equally likely, which is consistent with data from reported natural dam breaks (O'Connor and Beebee, 2009). To this end, we allowed for twice the range of documented breach rates to account for effects of failure mechanisms that may have remained unobserved. In our predictive model, each lake is equally likely to sudden outburst. Given more data about trigger and dam-failure mechanisms (GAPHAZ, 2017), our mixture model (*Methods*) is flexible enough to assign weighted outburst probabilities to the lakes.

In summary, our estimates of Himalayan GLOF hazard are snapshots prone to change. Both the number of glacier lakes and the annual GLOF rate could be undetectably higher, but are straightforward to change in our model. We conclude that the contemporary GLOF hazard in the greater Himalayan region could double because of sustained glacier melt, even if average GLOF frequency remained unchanged (Veh et al., 2019). In consequence, GLOF risk would also double in warmer Himalayas even if the vulnerability and exposure of downstream communities and infrastructure remained constant. Given the rapidly growing population, infrastructure, and hydropower projects in the Himalayas (Schwanghart et al., 2016b; Wester et al., 2019), our results quantify to first order the purely climate-driven contribution to GLOF hazard and risk.

Our predicted trajectories of future GLOF hazard and risk motivate a more dynamic assessment based on regular updates of outburst frequency and lake-size distribution. In this spirit, we offer a practical tool that is compatible with flood routing models, design codes, and hazard mitigation. Our appraisal of GLOF hazards complements projections of meteorological flood hazards in a warming climate for the sparsely instrumented Himalayan drainage network. Atmospheric warming is projected to increase mean daily and annual discharges in the Indus, Ganges, and Brahmaputra rivers only by few percent in this century (Lutz et al., 2014; Nepal and Shrestha, 2015), though the return periods for a given flood stage might drop by 50-90% in these rivers in the 21st century. Extreme runoff in headwaters (Wijngaard et al., 2017), and GLOFs in particular (Schwanghart et al., 2016b), has eluded such projections, and we show that changes to flood hazards and risk due to glacier melt require urgent attention in these projections.

4.2. Methods

Mapping present glacier lakes. We use '*glacier lake' and 'meltwater lake'* synonymously for water bodies fed by snow and ice within 3 km of 45,583 glaciers in seven regions defined by the Randolph Glacier Inventory (RGI) 5.0 (Arendt et al., 2015). We slightly modified the RGI outlines of the Central and Eastern Himalayas to include glaciers facing towards the Tibetan Plateau. We updated an inventory of 3,066 glacier lakes that were manually mapped from Landsat imagery between 2009 and 2011 in these regions (Zhang et al., 2015). We vectorised all water bodies >0.02 km^2 that persisted for at least two months between October 2014 and 2015, as classified in a high-resolution grid of global surface water (https://global-surface-water.appspot.com/). We excluded supraglacial ponds, and allowed for lakes protruding by up to 80% onto glacier boundaries, given that some glaciers were mapped as early as 1998. We removed water in rivers, channels, and floodplains with the masks from the Global River Width from Landsat (GRWL) data version 01.01 (https://doi.org/10.5281/zenodo.1297434). The GRWL stream network mostly covers higher-order channels, so that we removed river water pixels and other misclassified water bodies in headwaters manually.

Our automatically generated inventory contains 4,864 glacier lakes, and 76% of the 3,066 manually mapped lakes (Zhang et al., 2015). Omission errors were largest for small lakes, and half of the missed lakes were <0.032 km^2, due to the Landsat's sensor resolution (30 m), geometric pixel accuracy, mixed pixels, and natural oscillations of lake size (Supplementary Figure 7-7). Hence our lake inventory offers a conservative estimate of lake area. The median relative difference between automatically extracted and manually mapped lakes is –28%, but improves to –2% if accounting for half a pixel error for the manually mapped lakes (Zhang et al., 2015) (Supplementary Figure 7-7). We merged both inventories with the manually mapped lakes as the master, and added all non-overlapping, automatically extracted lakes, obtaining a final set of 5,565 glacier lakes.

Modelling future glacial overdeepenings. To estimate the size and distribution of glacier overdeepenings, we used gridded ice-thickness estimates from the GlabTop2 model for 16,140 glaciers >0.4 km^2 (http://mountainhydrology.org/data-nature-2017/). These data are based on the RGI glacier outlines, SRTM topography captured in 2000, and model assumptions of basal shear stress and local slope (Frey et al., 2014; Linsbauer et al., 2016). By subtracting the modelled ice thickness from the SRTM topography from, we obtain a first-order estimate of a completely ice-free Himalayan landscape. We smoothed DEM artefacts in this raw bedrock topography with a 5×5 median filter, filled all overdeepenings with a lake-fill algorithm, and thus obtained 9,871 overdeepenings >0.02 km^2. Local interpolation errors and SRTM data gaps form crater-like depressions that grossly overestimate parts of some depressions. Hence, we derived a volume-area

relationship from a global sample of 49 glacier lakes (Cook and Quincey, 2015) with a Bayesian robust linear regression, and removed 127 depressions with volumes outside the 95% highest density interval, as well as those <1 m deep (Supplementary Figure 7-8). We thus identified 9,479 depressions that could fill with meltwater in completely ice-free Himalayas.

Estimating peak discharge. Walder and O'Connor (1997) proposed a physically motivated model that predicts peak discharge during natural dam failure, based on the breach rate, breach depth, and volume of water released. They compiled data from 63 observed natural dam breaks in diverse settings, and found that the largest values of Q_p arise from dam breaches that fully develop before the lake level drops substantially. Such 'large' impoundments involve either large lake volumes relative to the breach depth or very rapid dam failure. In contrast, mountain valleys mostly store smaller volumes even behind high dams, so that peak discharge often occurs prior to complete dam incision (Walder and O'Connor, 1997). These two end members make up an asymptotic response of dimensionless peak discharge Q_{p*} when plotted against the dimensionless product η of lake volume and breach rate (Walder and O'Connor, 1997) (Supplementary Figure 7-4). From equations for critical flow, Walder and O'Connor inferred a model with the two key components dimensionless peak discharge $Q_p{}^* = Q_p g^{-1/2} h^{-5/2}$ and $\eta = V_0{}^* k^*$, where $V_0{}^* = V_0 h^{-3}$ is the dimensionless flood volume, $k^* = k g^{-1/2} h^{-1/2}$ is the dimensionless breach rate, g is the acceleration by gravity [m s^{-2}], h is the breach depth [m], and V_0 is the released water volume [m^3]. The breach rate k [m s^{-1}] subsumes lithologic conditions, the erodibility of the outflow channel, and the breach and downstream valley geometry, and has reported range of 2.5 orders of magnitude. The capped values of Q_{p*} express the model's idea that breach conditions primarily control peak discharge such that outflow deceleration or downstream ponding limit any further increase in discharge for a given breach geometry (Supplementary Figure 7-4).

Applying this model to larger datasets requires dealing with a substantial variance of Q_{p*} for a given η, and the poorly defined transition to the asymptotic behaviour at $0.6 < \eta < 1$, where data density is highest (O'Connor and Beebee, 2009). We learned a Bayesian robust piecewise regression model from the data on 63 dam breaks to capture the uncertainties of Q_p. We standardised the data and used a Hamiltonian Monte Carlo sampler (implemented in the STAN programming language; http://mc-stan.org/) with five parallel chains and 2,000 runs to produce marginal posteriors with effective sample sizes >4,000 each. The model has a linear trend and a constant separated by a break point assuming a Student t-distributed noise with 10 degrees of freedom to be robust against data outliers and a half-Cauchy prior on the scale parameter. Our prior on the breakpoint location was a truncated Gaussian $\mathcal{N}(-0.1, 0.1)$ on the interval $[-1, 0.5]$ informed by ref. (Walder and O'Connor, 1997). Having checked for convergence, we used 5,000 piecewise models from the 95% highest

density interval (HDI) of the posterior predictive distribution to estimate Q_{p*} for any given η of present and projected lakes in the Himalayas (Supplementary Figure 7-9). Values of η from single lakes encompass 100 physically plausible values of k based on a log-normal fit to reported breach rates (Walder and O'Connor, 1997), discretised breach depths h at 1-m steps and the associated flood volumes V_o. We finally cast Q_{p*} back into dimensional form to obtain physically plausible distributions of Q_p for each lake. For multiple lakes in a given region, we used a mixed distribution, assigning equal weights w_i to the posterior distribution of Q_p for each lake in our inventory, under the constraint that $\sum_{i=1}^{n} w_i = 1$.

To estimate the return periods of GLOF peak discharge (conditional upon lake outburst), we used a Bayesian Poisson-Generalised Pareto (PGB) model (Silva et al., 2017) that learns both the average return period of lake outbursts and their associated Q_p. We assume that the annual average rate λ of GLOFs is Poisson distributed (and thus randomly distributed in time) with a peak discharge taken from a Generalised Pareto distribution with a specified lower threshold. The assumption of a Poisson process is largely consistent with the history of reported GLOFs from moraine-dammed lakes in our study area. From 38 GLOFs in the past 30 years (1988-2017; Veh et al., 2019), we obtained a posterior annual rate of λ = 1.26 yr^{-1} that we used to simulate 10,000 years of data from the mixed posterior predictive distribution, and to fit the PGB model with a Markov Chain Monte Carlo sampler implemented in the package *extRemes* (Gilleland and Katz, 2016) in the statistical programming language *R*. We tested the sensitivity of the predictions to varying thresholds and used the 80th percentiles of the data as thresholds eventually, adjusting regional estimates by the appropriate regional values of λ. We repeated this sampling scheme 200 times for all Himalayan regions, and report the median from all estimated, average return periods and their 95% HDI. By design of our extreme-value model, changes in frequency directly change return periods. For example, a doubling of GLOF frequency in a given period shortens the return period of this discharge level by one half.

5. Discussion

Chapters 2, 3 and 4 aimed at **detecting** Himalayan Glacial Lake Outburst Floods (Chapter 2); quantifying their **frequency** since the late 1980s (Chapter 3); and appraising the contemporary and future outburst **hazard** from glacial lakes (Chapter 4). I summarize the core findings of these three research goals as follows:

- I developed a robust algorithm to detect automatically Glacial Lake Outburst Floods (GLOFs) in the Himalayas and adjacent mountain belts from a time series of Landsat images. With this method I generated the first systematic GLOF inventory for the region from 1988-2017.
- The method was able to more than double the existing GLOF count in the greater Himalayan region, and identified the southern Himalayas (mainly of Nepal and Bhutan) as a hotspot of GLOF activity in the past 30 years. Both overall and regional GLOF frequencies remained unchanged in this period despite ongoing glacier melt and growth of meltwater lakes in most of the study area.
- Finally, I proposed a first objective GLOF hazard appraisal for existing and projected future meltwater lakes in the Himalayan region. Estimates of the 100-year GLOF discharge assign the highest contemporary GLOF hazard to the southern Himalayas, consistent with the highest GLOF rate in the past three decades in that region. Projections show that the highest GLOF hazard could migrate towards the Karakoram, if the large glaciers there were to undergo severe to complete melting in the future.

Arguably, the unchanged GLOF frequency is an important, if not the most important, result of this thesis, because it questions many previous assumptions on how GLOF activity may respond to recently growing meltwater lakes. This counterintuitive finding that GLOF frequency has not changed in the past three decades, is directly relevant to my three research questions. It raises questions on methodological practice and validation of remotely detected cases; it is essential to discuss the response of GLOFs and their triggers to atmospheric warming on regional and global scales; and it is key input for quantifying contemporary and future GLOF hazard. In the following discussing, I refrain from revisiting the three research questions in sequence, but offer four questions that may directly follow from reading Chapters 2-4:

- What are the limits of GLOF detection with Landsat images and could these affect the completeness of the GLOF inventory? (Chapter 5.1)

- Can we use satellite images to validate, but also to learn from reported and newly detected cases? (Chapter 5.2)
- What are drivers of the regional GLOF pattern in the Himalayas and how does this pattern compare with other mountain ranges? (Chapter 5.3)
- How robustly can this proposed framework estimate GLOF hazard? (Chapter 5.4)

By answering each of these questions, I first chiefly give an overview to the problem and the main contribution from this thesis, before discussing remaining challenges and giving perspectives for future research.

5.1. Advances and challenges from a Landsat-based GLOF inventory

The finding that GLOF frequency remained unchanged in the past 30 years rests on the assumption that the change-point algorithm I used does not systematically miss GLOFs by a large number, and hence does not underestimate their distribution in time. Chapters 2 and 3 repeatedly stress the robustness of this algorithm, so that I offer here more supportive background.

5.1.1. Quantity and quality of Landsat images

Reliably detecting changes of glacial lakes, and hence outburst floods, in the Himalayas has the *"difficult*[y] *to obtain images covering the whole study area in a given year due to the highly frequent cloud cover across the region"* (Nie et al., 2017). Similar to other studies, I only used Landsat imagery outside of the monsoon season (September to November) to increase the chances for analysing images with low snow and ice cover in winter, or cloud cover during monsoon in spring and summer (Maharjan et al., 2018; Nie et al., 2017). Only four of 27 historical GLOFs with recorded dates happened outside of the monsoon season (Figure 5-1; Nie et al., 2018), so that the next available, cloud-free Landsat image after an outburst may come, in some cases, more than a year later. Yet these cases were robustly detected nevertheless. I emphasize that I designed the algorithm specifically to bridge data gaps such that it requires only six noise-free observations in a time series to detect shrinking water bodies. Supplementary Figure 7-2 shows that the algorithm successfully extracted 20 of the 22 newly detected GLOFs in the monsoon season, during which there were no

useful Landsat images. Furthermore, I found that GLOF detection neither depends on a high number of available pixels nor on a particularly low fraction of noise in the time series. Previously unknown GLOFs were detected in any interval in the three decades covered, even in the early 1990s when image coverage was lower and noise was higher than in the 21st century (Supplementary Figure 7-1; Supplementary Figure 7-2). Twelve of the 22 newly detected GLOFs occurred before 1998, and for that period I could use only Landsat 5 imagery. Although two Landsat sensors have been operating simultaneously since 1999 and thus have been offering a tighter coverage, I could not find any possibly commensurate increase in detected GLOFs. More than half of the newly detected GLOF traces had >50% noise in the images time series, and two cases even had >70% image noise. In six cases, the algorithm detected GLOFs over data gaps of more than two years (Figure 3-4, Supplementary Table 7.2). The Nyainqentanglha Mountains had the least available data and highest noise ratio, but the algorithm successfully detected the known cases from Tsho Ga and Ranzeria Co together with six previously unknown cases nevertheless.

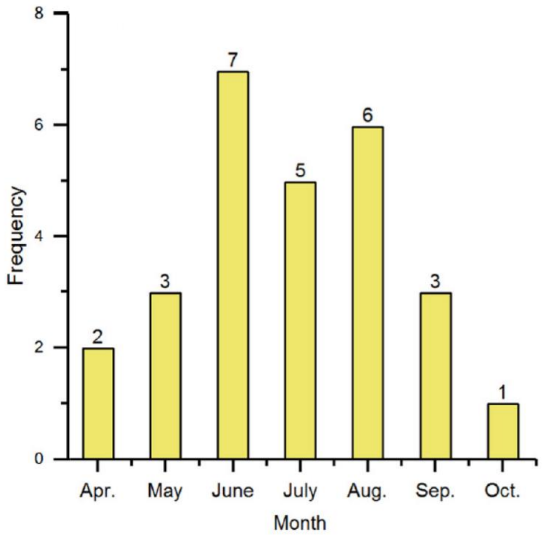

Figure 5-1: Seasonal frequencies of historical GLOFs in the Himalayas labelled with the number of cases per month. *Adapted from Nie et al. (2018).*

5.1.2. Limits of detection

I had given ample thought to design the change-point-algorithm with reproducible and validated rules, but different steps of image processing cannot circumvent some remaining caveats. One of these issues concerns image co-registration and re-projection. Landsat images offer a high geo-registration accuracy of less than half a pixel (<12m) radial root mean square error (USGS, 2018). But given the extent of my study area, my selection of Landsat images spanned six UTM zones, so that re-projection into one coordinate system was inevitable. This procedure can cause smoothing of edges and pixel shifts in Landsat images, plausibly adding to image noise at the shore lines of some lakes. I found that such spurious changes were not wider than a pixel, and that these changes contributed most to the false-positive ratio of the change-point algorithm (Table 2.6). I can rule out misidentified cases arising solely from this issue, because I visually cross-checked all change pixels in question for sediment tails downstream, regardless of how likely their change was. Another

approach to enhance confidence of true land cover change over image artefacts is to set a minimum area above which a change is regarded credible. I chose a threshold of 0.00375 km^2 or equivalently, six Landsat pixels, which is below most previous mapping exercises with Landsat images (Table 1.1), and allowed for detecting GLOFs with volumes below the smallest historic cases (Figure 3-3).

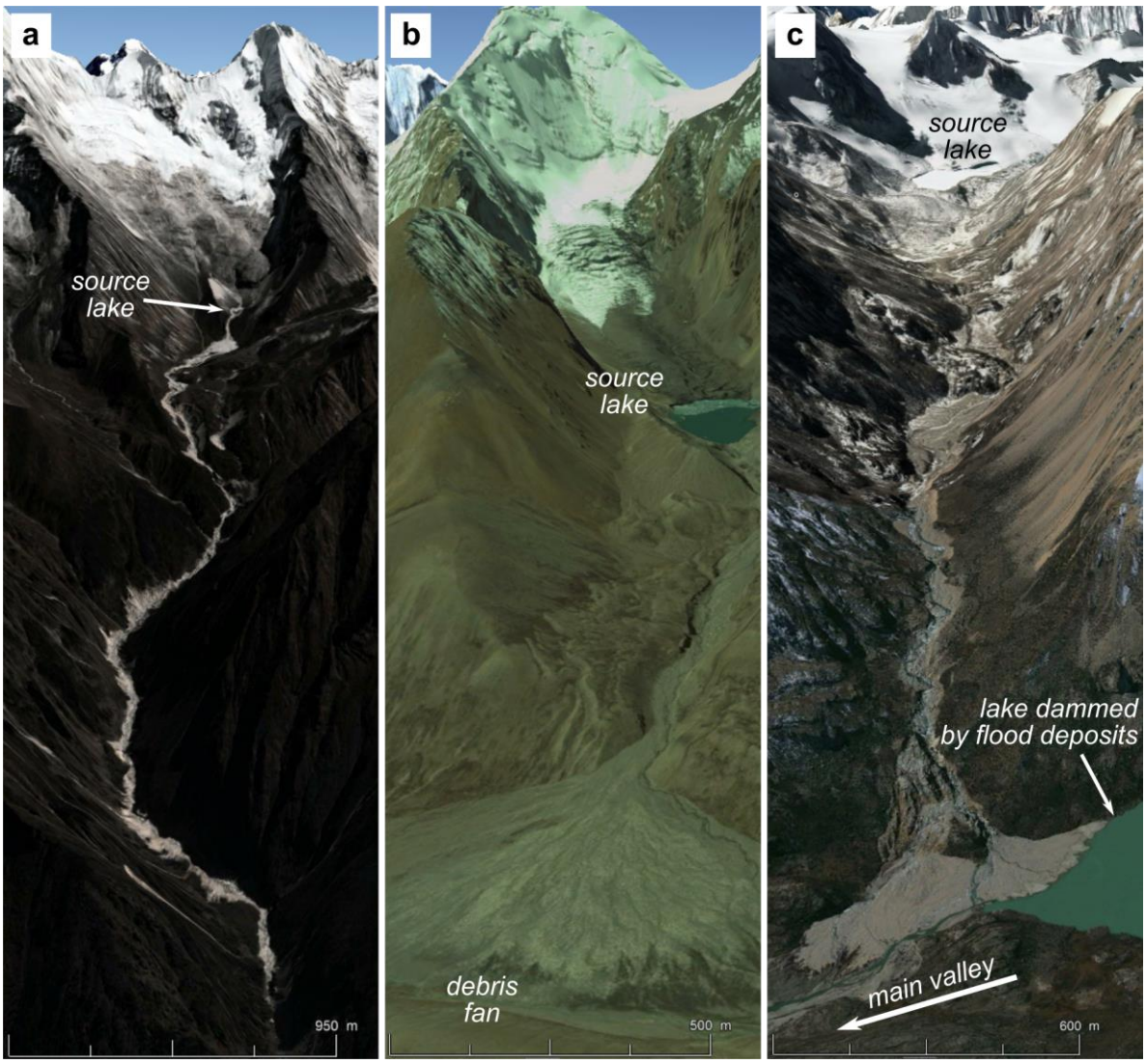

Figure 5-2: Geomorphic evidence from GLOFs. a, *Debris fan downstream of Gongbatongsha Tsho and further bank erosion and landslides along the channel downstream during and after the GLOF in July 2016. Image is from 24 Oct 2016.* ***b,*** *Debris fan deposited by a newly detected GLOF in 1996 (ID5), remaining visible in the image from 5 Oct 2011.* ***c,*** *Debris fan from a GLOF in tributary valley (1992; ID5) entering the trunk valley and damming a lake upstream. Image is captured 18 years later on 9 Nov 2010. All images are courtesy of Google LLC.*

Smaller outbursts could remain hidden in noise, unless no sediment tails appeared downstream of the lakes. I visually assessed Landsat or Google Earth images for such impact tracks, which involve well-documented signs of incision, reworking, and deposition of sediments in river channels (Cenderelli and Wohl, 2003; Cook et al., 2018; Kershaw et al., 2005). These traces of geomorphic impact remain visible on the Landsat images for years to decades after the lake outbursts. Indeed, many sediment tails from newly detected GLOFs dating back to the 1990s are still

present in recent satellite images (Figure 5-2). However, I can envisage three plausible cases for undetected GLOF tracks, assuming that the released flood volume (or equivalently the shrunken lake area) is below the resolution of my algorithm: (1) the first few kilometres downstream of a breached lake were already extensively reworked or active prior to the moraine-dam breach, so that erosion and deposition from the new flood pulse would not become apparent as a distinct change in contrast in satellite images; (2) the breach geometry favoured a slow or gradual release of the water volume, so that flood waves had insufficient energy to overspill or erode the channel banks downstream; (3) the downstream channel is cut largely into bedrock, so that only minor amounts of sediment can be entrained or deposited along the channel reach. Yet, such scenarios are unlikely for the first kilometers in Himalayan river channels, where steep hillslopes add debris to confined valley floors, promoting high flow depths and velocities for the released water masses (Korup and Tweed, 2007). The 2016 GLOF from Gongbatongsha Tsho, Nepal, for example, had the smallest reported flood volume (1.1×10^5 m^3), but caused bank erosion, landsliding, and an increase of the mean active channel width from 29.5 ± 3 m to 41.3 ± 3 m in the river over >40 km (Cook et al., 2018). My algorithm could successfully map this event from Landsat images (Figure 5-2a). Where flood waves enter alluviated reaches, GLOF sediments disperse rapidly and form large and highly reflective debris fans that clearly stand out from older deposits (Figure 5-2b,c).

Given all these diagnostics of algorithm performance and visual image interpretation, how complete is this updated GLOF inventory then? Only the GLOF from Kedarnath, India, in 2013 (Allen et al., 2016; Das et al., 2015) remained undetected, since the lake filled and burst out during a persistent period of cloud cover (Figure 2-11). Given 10 out of 11 successfully detected test cases, I assume that my inventory could roughly miss 10% of all GLOFs in the greater Himalayan region during the past three decades, but a more detailed estimate of missed cases remains elusive. Clearly, a complete GLOF inventory is beyond reach, and the demand for such an inventory cannot circumvent the need for defining a minimum threshold in terms of what qualifies as a GLOF. Nonetheless, I can warrant that my inventory is systematic and consistent above the chosen thresholds, and based on objectively reproducible and validated rules. Even if accepting that a complete GLOF inventory is beyond reach, using these simple rules allowed me to more than double the previously known GLOF count in the study region despite many years of satellite-based enquiry into this cryospheric hazard.

5.1.3. The minimum size of a GLOF from a hazard perspective

Discussing potential limits of detection is not merely a methodological detail, but directly linked to question of what is the smallest GLOFs we should worry about. Arbitrary lower size

thresholds will apply to any detection or mapping method, though practical applications would mostly be interested in the minimum size of GLOFs that we need to detect because of their hazard potential or geomorphic work. The literature reveals no key descriptors of GLOF sources, such as lake area, volume, depth, peak discharge or flood volume, which are part of the formal definition of GLOFs. For example, Emmer (2018) stated that GLOFs *"describe a sudden release of (part of the) water retained in a glacial lake, irrespective of the cause (trigger), mechanism (dam failure or dam overtopping) and glacial lake subtype involved"*. Figure 3-3 points at the possibility that it was most likely a combination of geomorphic impact and the people affected that motivated reports on GLOFs. Thus, damaging flows were recorded preferentially, whereas other events may have been noticed but not documented. The impact tracks from historic cases had a median length of 32 km and flood volumes $>5 \times 10^6$ m^3 (Figure 3-3), which might explain why researchers prioritised large, and in particular rapidly growing, lakes in hazard appraisals (Bolch et al., 2011; Prakash and Nagarajan, 2017; Rounce et al., 2017). However, one important lesson from the Kedarnath disaster in 2013 is that Nie et al. (2018) called for considering a wider range of GLOF sizes, specifically lakes >0.05 km^2, in hazard appraisals *"given that considerable damages could also be caused by the outburst of smaller lakes"*. Sticking to this threshold, however, would mean to ignore some 78% (or 23% of the total area) of glacial lakes in the Himalayas today (Figure 1-3, Maharjan et al., 2018). This threshold would further miss the GLOF from Gongbatongsha Tsho in 2016, which *"destroy*[ed] *the intake dam of a hydropower project, the Araniko highway, and numerous buildings"* (Cook et al., 2018). This case, together with ten newly detected GLOFs with flood volumes of the same order of magnitude, demonstrates that hazard assessment must not rely on large and destructive cases only. In this thesis, I contributed to quantify the frequency of lower GLOF magnitudes, which will improve hazard assessment, at least on regional scales. Half of the GLOFs–both in the newly and the complete historic inventory–had estimated flood volumes of $<10^6$ m^3 and may be at the lower end of potentially damaging events (Figure 3-3, Supplementary Table 7.1, Supplementary Table 7.2). Data on these smaller and commensurately more frequent flows make hazard appraisal more objective, especially in that the data might help us to learn more about the differences between damaging on non-damaging GLOFs.

5.2. Validating and extracting key diagnostics of GLOFs

5.2.1. Distinguishing GLOFs from other types of flow

Beyond tracing glacial lake changes and their outbursts, time series of satellite imagery can assist in validating historic cases with unknown or debated GLOF sources. In the Himalayas, large debris flows or flash floods have often been mistaken for GLOFs (and vice versa) (Nie et al., 2018), because these flows share similar characteristics such as sediment concentration and flow velocities. Cui et al. (2010) inferred from 18 historical GLOFs in Tibet that *"the general, sequential evolution of the flows can be described as from proximal GLOFs, to sediment-laden streamflow, to hyperconcentrated flow, to non-cohesive debris flow (viscous or cohesive debris flow only if sufficient fine sediment is present), and then, distally, back to hyperconcentrated flow and sediment-laden streamflow as sediment is progressively deposited"*. This spectrum of flows depends on the (changing) proportion of sediments in the flows, which in turn affects flow velocity, sediment transport capacity, and channel incision and aggradation (Coussot and Meunier, 1996). Previous studies thus may have misinterpreted the origin of the flood, if solely relying to field visits several kilometres downstream from the source. Such an example are two debris flows in Poiqu River basin, China, which Chen et al. (2007) regarded as GLOFs: *"On 23 May and 29 June, 2002, two large-scale*

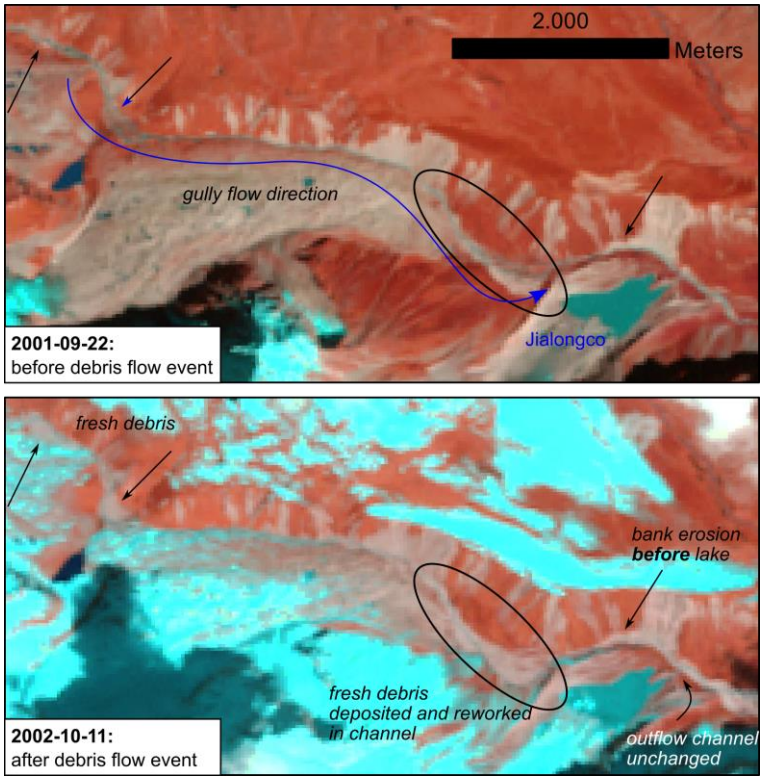

Figure 5-3: Landsat images of the Jialongco debris flow before the event (upper image) and after the event (lower image). *Arrows and ellipsis have the same position in both images. The debris flow flushed a gully from the upper left towards the lower right corner of the image. Sediment deposition and reworking along the channel clarify that this case is no GLOF from the lake in question.*

debris flows have burst in Chongdui gully and brought tremendous disasters to the hydropower station, the China–Nepal Highway, to communication establishment, and so on, resulting in economic loss above 7.5 million RMB. The two debris flows might have been caused by glacier thawing and moraine dam failure". Though widely cited later on (Ives et al., 2010; Liu et al., 2013; J.-J. Liu et al., 2014; Nie et al., 2018), I noticed that Lake Jialongco, the purported source lake of these two cases, has never been investigated in more detail. Landsat images show that the debris was already reworked and deposited upstream, while the moraine dam appears to be intact in the first image following the reported flood date (Figure 5-3). I can maintain that the present inventory of previously reported and newly detected cases holds solely cases where impact tracks give direct links to their sources.

5.2.2. Flood volumes

Some historical GLOFs have motivated detailed field work to recalculate flood volumes and flow stages (Byers et al., 2018; Cenderelli and Wohl, 2003; Cenderelli and Wohl, 2001; Lamsal et al., 2015), especially in ungauged headwater basins. What complicates the issue is that data access to long-term gauging data from Himalayan rivers is often proprietary. Making such data public could aid validating better the discharge of both previously known and newly detected GLOFs. Most historical estimates of flood volumes, and some newly detected cases in particular, are likely conservative minima, because triggers such as snow and ice avalanches, rockfalls or debris flows can add sediment to the released water volume right at the source, while additional sediments become entrained along the river channel via flow bulking (Byers et al., 2018; Cook et al., 2018; Kershaw et al., 2005). Estimating the contribution of these triggering processes to the total flood volumes is challenging, and the net flow bulking is next to impossible to derive from remote sensing images alone, especially if noise-free images are captured months after the incident. Without these data, we have to resort to the rough information contained in the bright sediment tails in post-event images, indicating only above-average flow widths, though without any further robust information on flood volume, flow depth or peak discharge.

5.2.3. Impact tracks and geomorphic work

The digitized impact tracks and lake surfaces provide readily available estimates of flow runout and the potential energy released. Inferring empirical relationships from these two parameters has been a key element in downstream risk analyses (Hungr, 1995; Rickenmann, 1999), but even the accuracy of this simple method suffers from the few available measured field data of GLOFs. While runout depends on local channel morphology, the mapped downstream reaches at

least provide an envelope estimate of the channel length that is impacted visibly as a function of outburst volume. We could in principle apply the same modeling approach that I used for learning Q_p from η to predict runout of flood volumes and hence offer a practical tool to estimate GLOF risk for the many lake volumes stored in inaccessible terrain.

The 22 new compiled impact tracks together with the compiled historical ones also inform the broader picture of geomorphic work by GLOFs. Initial work from Korup and Tweed (2007) on three large historic GLOFs (Nare, Dig Tsho and Tam Pokhari) suggests that the farthest active valley-floor widening was visible at 13 km downstream. I note that seven newly detected GLOFs had widened active channels over longer distances, while the 2009 GLOF from Tsho Ga (China) even left geomorphic traces over >70 km. In the Cordillera Blanca, only 5 of 29 reported GLOFs had channel impacts beyond 10 km downstream (Emmer, 2017), which was exceeded by 57% of all Himalayan cases since 1988. It is vital to test whether the apparent larger runout distances in the Himalayas are a consequence from larger flood volumes or from steeper channels. Our understanding of how far GLOFs can notably change channels will need more attention in the future, ideally to propose a metric of effective channel impact. A recent hypothesis–inferred from a single outburst flood at Gongbatongsha Tsho in 2016 (Figure 5-2a)–even states that *"GLOF impacts far exceed those of the annual summer monsoon, and GLOFs may dominate fluvial erosion and channel-hillslope coupling many tens of kilometers downstream of glaciated areas. Long-term valley evolution in these regions may therefore be driven by GLOF frequency and magnitude, rather than by precipitation"* (Cook et al., 2018). This notion is provocative, and perhaps in line with other case studies emphasizing the high geomorphic work by Holocene megafloods (Lang et al., 2013; Montgomery et al., 2004), but it is also testable. Quantifying the net mass balance of GLOFs in terms of budgeting sediment mobilization and export from river channels would ideally build on detailed pre-and post-event DEMs of the valley floor (Jacquet et al., 2017). Such repeat measurements will ultimately connect the geomorphologic response of GLOFs with hazard assessment, given that flood-induced changes in the channel bed can alter flow capacity and hence, potential inundation areas downstream (Slater et al., 2015).

5.3. Drivers of GLOF frequency on global and regional scales

Many studies issued largely qualitative or vague predictions or concerns about trends in GLOF occurrence, and rarely provided statistical tests to their conclusions. This is not only the case in the Himalayas, however. For this mountain belt, Nie et al. (2018) concluded without any statistical support *"that GLOF hazards increased from 1975 to 1995 and slightly decreased from 1995 to 2015"* (Figure 1-5). Subjective assertions such as a global *"apparent decline in the number of glacier floods*

recorded from the mid-1990s onwards" (Carrivick and Tweed, 2016) or an *"apparent increase in frequency of outbursts in the extratropical Andes"* (Iribarren Anacona et al., 2015) are common in recent work, but rarely supported by objective or formal proof. A wavelet analysis by Harrison et al. (2018) on a global GLOF record found *"that GLOF frequency increased dramatically and significantly around 1930 globally and between 1930 and 1960 regionally"*, but also conceded that *"the statistics of small numbers affect these regional, time-resolved records"*. In this thesis, I learned trends of GLOF frequency using a Bayesian regression of the annual GLOF count versus time. The Bayesian approach is capable of dealing with a small sample size, and thus directly addresses one caveat by Harrison et al. (2018). I selected a *t*-distributed noise in this model to account for possible outliers in the data. Thus my trend estimates are robust with respect to individual years of very high or very low GLOF abundance, or potentially missed cases. The posterior slope distributions of the regression models are centered on zero, and this ambiguity in the model coefficient is credible evidence of an unchanged GLOF frequency in the Himalayas (Supplementary Figure 7-2). I found no study–neither on the global nor the regional scale–that has postulated an unchanged GLOF frequency. With 20 additionally detected cases, the updated rate of 1.3 GLOFs per year on average exceeds all previous frequency estimates in the Himalayas. Considering GLOFs in the past three decades only, I more than doubled the estimate of 0.6 GLOFs yr^{-1} for the Western to Eastern Himalayas (Nie et al., 2018). The 38 Himalayan GLOFs since 1988 are as many as the 38 cases, which Harrison et al. (2018) collated worldwide for the same period. Considering the updated Himalayan GLOF count in global projections of GLOF frequencies is vital, because Harrison et al. (2018) argued that *"[…] the reduction in global GLOF frequency after the 1970s (especially in central Asia, HKH […]) is real, because the contemporary reporting is likely to be nearly complete given the scientific and policy interest in glacier hazards from the late 20th century"*. In this thesis, I maintain that the contemporary reporting is *unlikely* to be nearly complete, and that a large fraction of GLOFs has escaped attention. Such censoring may not be surprising, though noticeably revises our knowledge about average GLOF rates and trends in the greater Himalayan region, and also possibly beyond.

5.3.1. Comparing Himalayan with South American GLOF frequencies

Following a detailed search in the literature, I conclude that the Himalayas had the highest total abundance of GLOFs worldwide in the past three decades, and this is partly due to my large study area. Comparing my updated inventory with published estimates hence needs to adjust GLOF abundance, for example, to the total number of lakes per mountain belt. Only two GLOF inventories have covered the past three decades and used similar geomorphic diagnostics to cater for previously undetected cases. These databases list five GLOFs in the Cordillera Blanca, Peru, (CB; Emmer, 2017), and 25 cases in the Central and Patagonian Andes, Argentina and Chile (CPA; Iribarren Anacona et al., 2015; Wilson et al., 2018). Compared to the total lake abundance, Himalayan lakes had the lowest GLOFs count: out of 451, 2,170, and 7,314 moraine-dammed lakes in the CB, the CPA, and the Himalayas, I compute ratios of GLOFs versus lake abundance of 1.11, 1.15, and 0.52, respectively. The frequency of GLOFs compared to the regional sample of glacial lakes seems twice as high in South America as in Central Asia, which can have at least two reasons. First, the glaciers in the CPA cover

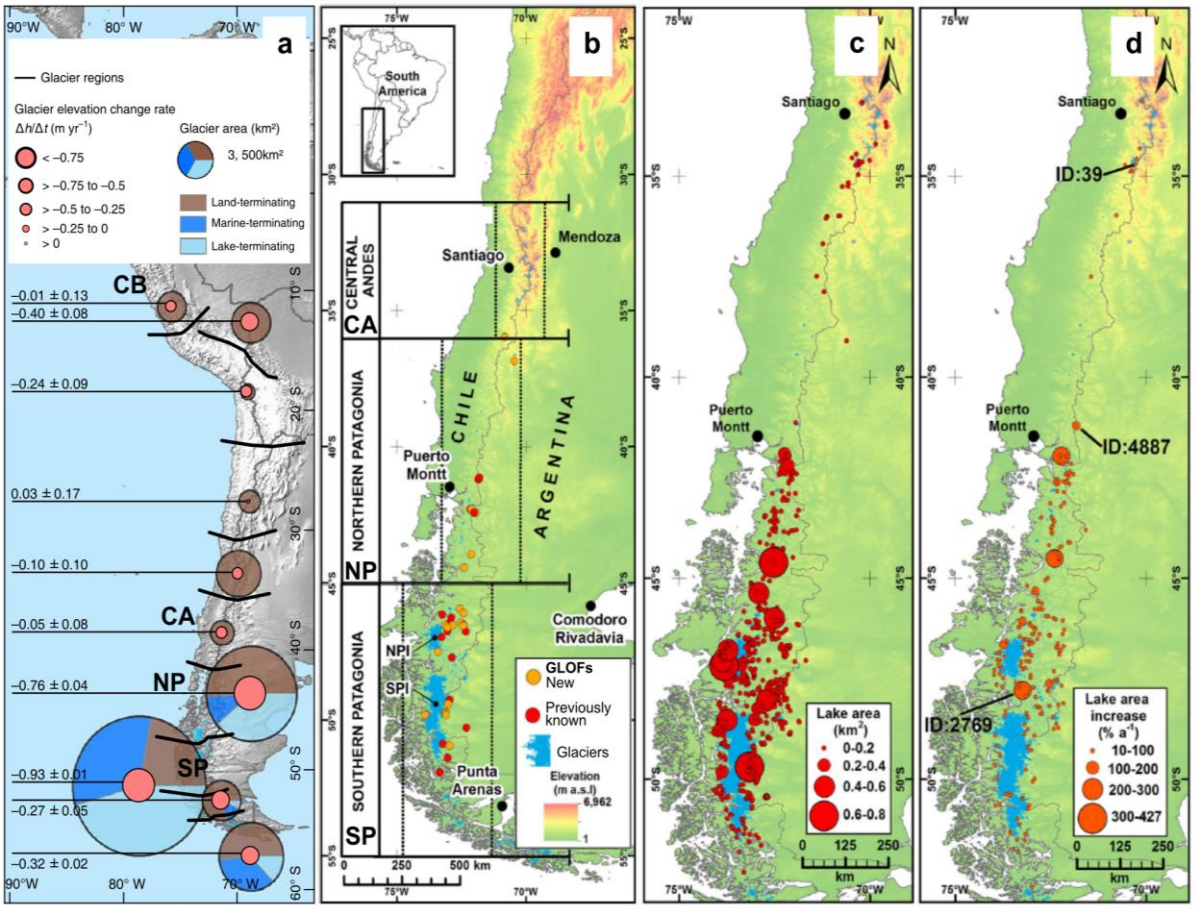

Figure 5-4: Glaciers, GLOFs and glacial lakes in South America. a, *Glacier cover (pie charts) and glacier elevation change rate (red circles), highlighting the four regions mentioned in the text: CB Cordillera Blanca; CA Central Andes; NP Northern Patagonia; SP Southern Patagonia.* ***b,*** *Outburst floods from moraine-dammed lakes as newly detected by Wilson et al (2018) in orange and previously reported by Iribarren Anacona et al. (2015) in red between Southern Patagonia and the Central Andes. SPI/ NPI – Southern/ Northern Patagonian Ice Sheet,* ***c,*** *Lake area.* ***d,*** *Increase in lake area. Highlighted IDs are rapidly expanding lakes, discussed in the original publication.*
Figures ***a,*** *are modified after Braun et al. (2019) and* ***b-d,*** *are after Wilson et al. (2018).*

<30,000 km^2, so that the study region is 42% smaller than the Himalayas. Assuming a fixed rate of missing GLOFs from satellite images, increasing the search range for GLOFs to larger areas such as the Himalayas is likely to commensurately raise the number of undetected GLOFs. This omission error cumulates with larger study areas. Second, considering the robust performance of the change-point algorithm, some of the regional difference in the GLOF-to-lake ratio could arise from the different orography, glacier cover, climate, and, hence varying response to atmospheric warming in the CPA. Mean annual losses of glacier masses in Southern and Northern Patagonia (– 0.79 ± 0.06 and −0.65 ± 0.07 meters water equivalent per year [m w.e. a^{-1}]) are larger than the estimates from the Nyainqentanglha and Bhutanese Himalayas (-0.62 ± 0.23 and -0.42 ± 0.20 m w.e. a^{-1}) (Braun et al., 2019; Brun et al., 2017). The total number of glacial lakes in the CPA increased by 43% in the past three decades (Wilson et al., 2018), and hence at a much faster pace than the rate of 8% newly forming lakes in the Himalayas (Nie et al., 2017). South American glaciers and glacial lakes may thus respond more dynamically to climate change than their counterparts in the Himalayas, perhaps expressed in the observed higher average frequency of GLOFs per lake. Despite these differences, the Andes share several similarities that confirm my findings of regional GLOF drivers in the Himalayas (see Figure 1-2, Figure 3-2, Figure 5-4):

1) regions with the highest glacier cover (Southern Patagonian Ice Field; Karakoram) do not host the most glacial lakes per unit area (Northern Patagonian Ice Field; Eastern Himalayas);
2) areas with the highest glacier cover (Southern Patagonian Ice Field; Karakoram) do not necessarily have the highest reported GLOF abundance (Northern Patagonian Ice Field, Eastern Himalayas);
3) the fastest growth in glacial lake number and areas (Northern Patagonian Ice Field; Eastern Himalayas) is not tied to the largest glacial mass losses (Southern Patagonian Ice Field; Nyainqentanglha);
4) only two lakes in the entire CPA and three lakes in the Himalayas formed and burst out in the past three decades;
5) GLOFs form local clusters (43% of all recorded cases occurred near the Northern Patagonian Ice Field; and 63% did in the Eastern Himalayas), while most of the remaining study areas had lower GLOF abundance (e.g. one in the Central Andes; one in the Western Himalayas).

5.3.2. Regional drivers for Himalayan GLOFs

Such pronounced contrasts of lake and GLOF abundance call for a more detailed discussion on drivers that raise regional GLOF frequencies, while other regions seem to be more resilient to GLOFs. In this regard, little attention has been paid to why, for example, 39 of all 62 reported GLOFs since 1935 originated from a set of ~2,200 moraine-dammed lakes in the Eastern Himalayas, but only one originated from the ~900 lakes in the Western Himalayas. Therefore, the total lake count per region alone appears to be a poor predictor for regional GLOF frequencies. Obviously, GLOFs must be tied to one or more local factors, otherwise we would expect GLOFs to occur proportional to the lake count per region.

Our understanding on GLOF drivers currently hinges on the notion that *"a trigger mechanism such as displacement wave from an ice or rock avalanche, or disintegrating ice-core within the dam is normally required"* (Richardson and Reynolds, 2000). Yet such triggers have been rarely witnessed in the field, fuelling debates on outburst mechanisms for many historic cases. One prominent example on contesting GLOF triggers is the failure of Tam Pokhari, Nepal, in 1998, which researchers attribute to landslides, while eyewitnesses observed an avalanche entering the lake (Osti et al., 2011; Osti and Egashira, 2009). Similar uncertainty applies to the asserted rockfall-induced GLOF from Langmale Lake, Nepal, in 2017, because "*the rockfall was not actually witnessed by anyone, partly because of the heavy fog that covered Saldim Peak that day"* (Byers et al., 2018). Nie et al. (2018) detected a previously unreported GLOF from Kongyangmi La Tsho (Eastern Himalaya) in 1997 by comparing pairs of Landsat images. They speculated that *"it is most likely that an ice avalanche occurred on the left side of the main glacier and that the mass movement of the ice avalanche plunged into the glacial lake, which triggered this GLOF event"*. Indeed, steep mountain walls surround the source lake, but whether this necessarily warrants an ice avalanche as the most plausible trigger still remains conjectural.

In the previous chapters, I refrained from speculating on triggers of specific (newly detected) GLOFs. Gathering information on these from satellite images remains problematic, given that monsoonal clouds often veil the site conditions at the time of the dam failure. Even inspection right after a GLOF may not readily guarantee to reveal its trigger(s): researchers visiting Lake Zhangzangbo three days after its breach in 1981 found blocks of floating ice in the lake, but remained uncertain whether these were also the remnants of a triggering ice avalanche (Xu, 1988). The challenge of identifying triggers will probably remain for most historic, but also future GLOFs, unless rock avalanches or debris flows, for example, leave clear signs of boulders entering the lakes (Byers et al., 2018; Hubbard et al., 2005). Given these caveats, I broaden the perspective to the regional

GLOF pattern in the following discussion instead, offering a systematic view on triggers and factors that could explain the regionally varying susceptibility to GLOFs.

5.3.2.1. Distribution and age of glacial lakes

A prominent concept concerning the resilience of lakes to triggers is that–with ongoing glacier retreat–lakes pass into a 'non-glacial' phase, when the distance to the parent glacier(s) increases and the contribution of glacial melt decreases (Emmer et al., 2016a, 2015). Today, 23% of all moraine-dammed lakes in the Himalayas are >1 km apart from their parent glacier(s), and such *"distal"* or *"unconnected"* lakes had lower rates of change than lakes with contact to their parent glacier(s) in past decades (Khadka et al., 2018; Song et al., 2016). Given that lake areas had grown least in the Western Himalayas since 1990 (Figure 5-5), we may thus speculate that glacial lakes are oldest there, lying at farer distances from their parent glaciers, and hence being more resilient to outbursts. This would confirm one of the earliest notions on GLOF hazard such that outburst susceptibility decreases with increasing lake age: *"glacier lakes, which occupy old glacier tongue basins of retreating glaciers, through valley glaciers and cirque glaciers with old, stabilized end-moraines formed during the Pleistocene period are relatively stable and outbursts less likely. On the other hand, glacier lakes which are in contact with an active glacier and which are dammed by unconsolidated moraines resulting from periods of recent glacier advances in the last 300 years, especially the last "Little Ice-Age" are potentially unstable and more prone for outbursts"* (Grabs and Hanisch, 1993).

The proximity to glaciers indeed seems to stimulate lake failure, not least since 16 of 22 newly detected GLOFs came from lakes within 300 m from their parent glaciers. Yet, the percentage of lakes within this distance (compared to the total regional lake count) is higher in the Western Himalayas (38%) than in the Eastern Himalayas (29%), where most historic outbursts occurred. Moreover, when and where, or if at all, this Little Ice Age has ended in the Himalayas is less clear, given that many glaciers in the Eastern Himalayas have remained at their maximum positions until today (Rowan, 2017), while others in the Karakoram are still advancing (Kääb et al., 2012). I roughly estimate the ages of Himalayan lakes from a sample of 341 lakes that formed between 1990 and 2015 in the Western, Central and Eastern Himalaya (Nie et al., 2017). Given a total abundance of 4,950 lakes in this region today, and ~14 lakes forming on average per year in this period, I would assume that Himalayan lakes started to spawn at least 350 years ago. Clearly, this is a minimum estimate, considering that anthropogenic warming may have accelerated annual meltwater and lake

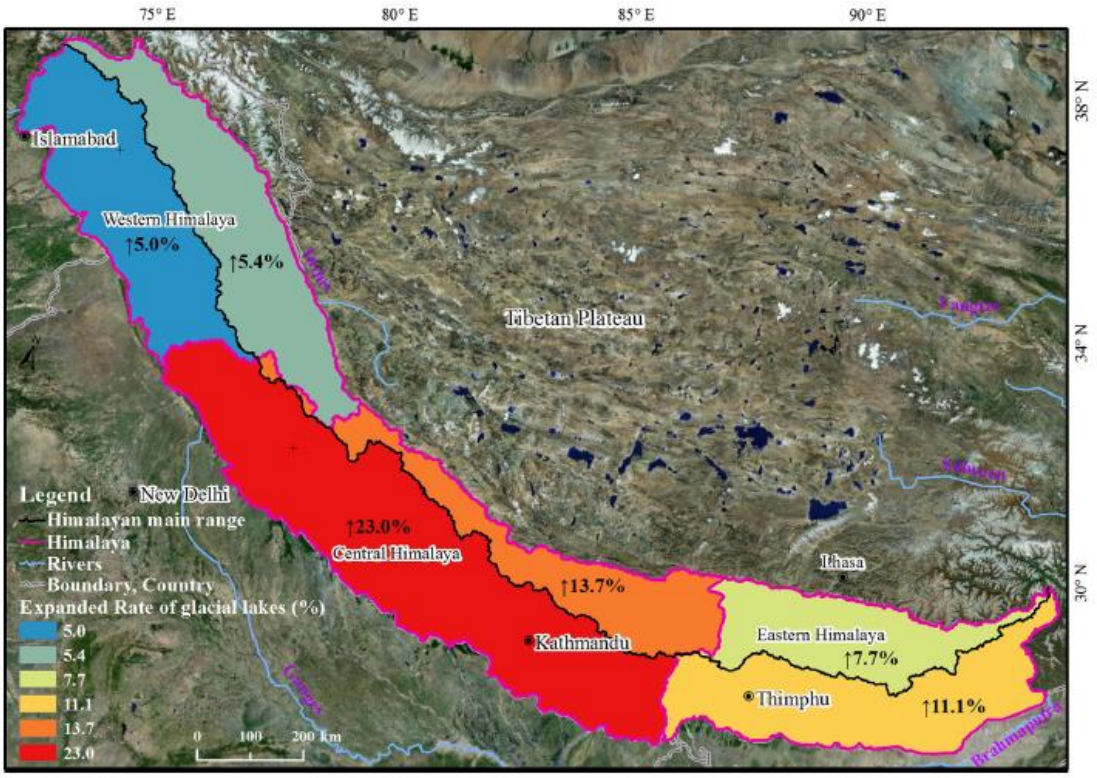

Figure 5-5: Glacial lake expansion in the Himalayas. *Adapted from Nie et al. (2017).*

production in recent decades (Gardelle et al., 2011). Whether the thousands of Himalayan glacial lakes today demand more systematic dating of their ages to appraise outburst hazard seems less expedient: In the Cordillera Blanca, Emmer (2017) found *"no obvious pattern between the age of the moraine dams and the timing of the GLOFs"*. There, lichenometric ages of ten breached moraine dams in the 20th century suggest that these moraines had been abandoned between 1400 and 1980, so that GLOFs can follow years to centuries after lake formation. Absolute (and particular 'young') ages of moraine dams thus remain an ambiguous predictor for GLOF frequency, not least that only three GLOFs in the Himalayas emerged and also burst out in the past three decades.

5.3.2.2. Climate and glaciers

Regional climate and its impact on glacier dynamics are two other factors that have been rarely coupled to the regional distribution of GLOFs. In general, the Himalayas act as an orographic barrier for the Indian Summer Monsoon, which expresses in a southeast-northwest gradient of precipitation (Bookhagen and Burbank, 2010). Precipitation peaks at values of >5,000 mm yr^{-1} at the foothills from the Hengduan Shan to the Eastern (Bhutanese) Himalayas, whereas the regions north of the range receive substantially less precipitation (Figure 5-6a). The Karakoram in the North is a generally cold and dry region, affected by the Westerlies. There, snowfall has the highest contribution to the total annual

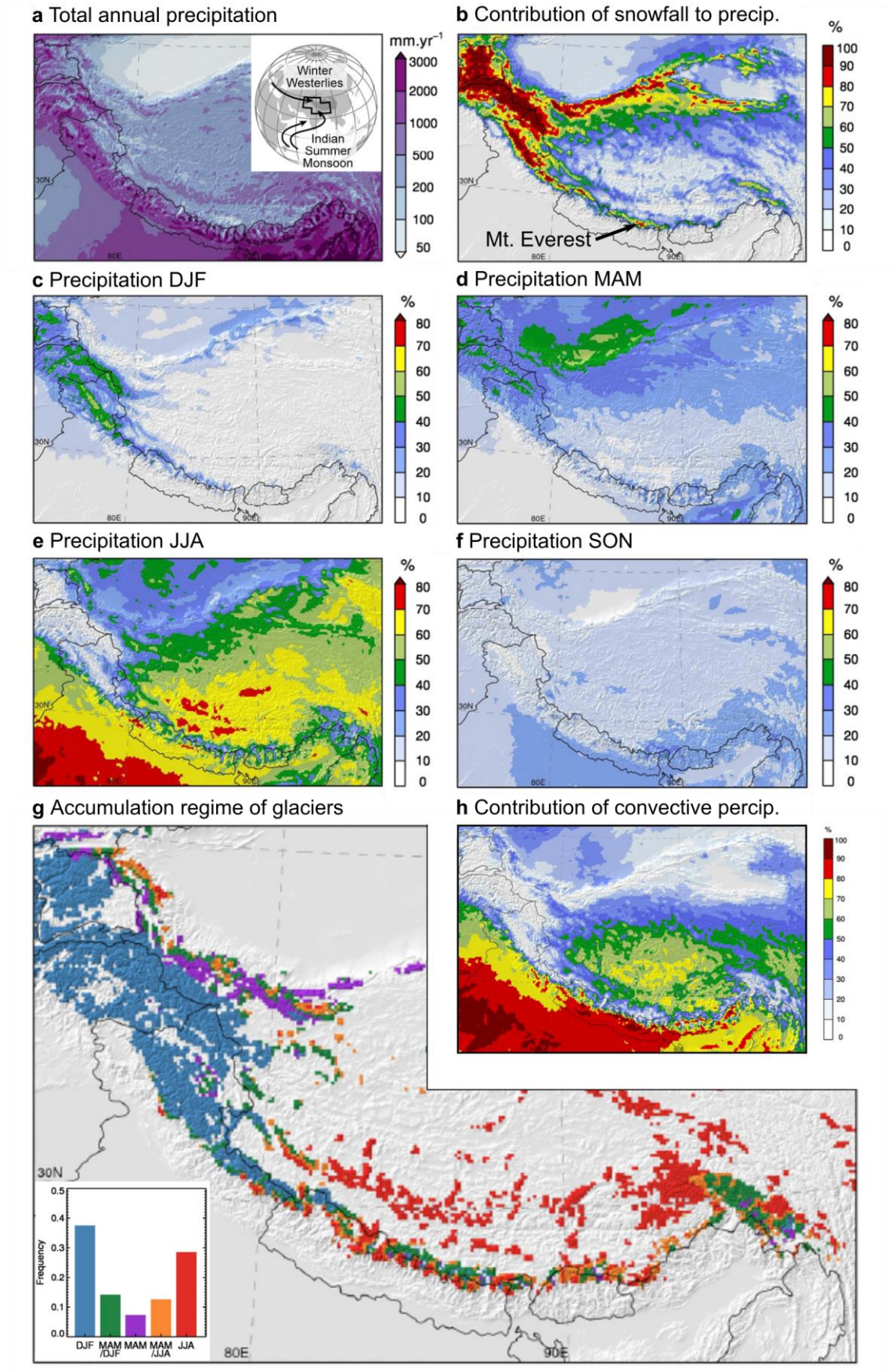
a Total annual precipitation
mm.yr⁻¹
3000
2000
1000
500
200
100
50
Winter Westerlies
Indian Summer Monsoon
30N
80E
b Contribution of snowfall to precip.
%
100
90
80
70
60
50
40
30
20
10
0
Mt. Everest
90E
c Precipitation DJF
d Precipitation MAM
e Precipitation JJA
f Precipitation SON
g Accumulation regime of glaciers
h Contribution of convective percip.
Frequency
0.5
0.4
0.3
0.2
0.1
0.0
DJF
MAM /DJF
MAM
MAM /JJA
JJA

◀ ***Figure 5-6: Precipitation, snowfall, and main accumulation period of glaciers. a,*** *Total annual precipitation in the Himalayas as a product of Winter Westerlies and Indian Summer Monsoon (see inset);* ***b,*** *Contribution of snowfall to the average amount of annual precipitation.* ***c-f,*** *Seasonal precipitation. Capitals are the initials of the months.* ***g,*** *Classification of glacier accumulation regimes according to precipitation seasonality. Inset histogram shows the relative occurrence of the classes in the map, which refer to preferred season(s) of accumulation.* ***h,*** *Contribution of convective precipitation to the total precipitation. All panels are adapted from Maussion et al. (2014).*

precipitation along the mountain belt, falling mostly between December and May (Figure 5-6b, Maussion et al., 2014). Glaciers in the Karakoram accumulate most of their masses in this period, whereas glaciers in the more southern regions (Central Himalayas to Hengduan Shan) gain mass from the summer monsoon (June to August) (Figure 5-6g). There, warmer and more humid conditions in summer favor glacier ice temperatures closer to the melting point, so that these 'temperate' glaciers can flow rapidly by basal sliding (Su and Shi, 2002). In contrast, glaciers in the Karakoram are widely considered (but rarely tested) as 'cold-based' glaciers, which flow less dynamic by ice creep (Quincey et al., 2011). A well-documented exception from this 'rule' are recent glacier surges in this region (Figure 5-7), which describe rapid increases in ice velocities driven by internal glacier instabilities, as opposed to clear climate signals (Rankl et al., 2014). These surges may have eroded moraine dams, which could explain why the Karakoram offers the lowest lake abundance (only 6% of all moraine-dammed lakes today), and hence only one of the lowest GLOF frequencies in my study region.

The timing and magnitude of precipitation (Figure 5-6a, c-f), and associated types of glacier flow along the Himalayas probably contribute much, if not most, to the striking difference in GLOF abundance between southern and northern regions. 95% of all historical GLOFs occurred in the southern regions (Central Himalaya to Hengduan Shan) and mostly during spring and summer (Figure 5-1), coinciding with a period of both accumulation and melt of snow and ice. The glaciers in the Central and Eastern Himalayas have 50-75% of their area below the contemporary equilibrium line altitude, where ablation dominates during summer (Figure 5-7; Kraaijenbrink et al., 2017). Excessive melt at the glacier termini and drainage of meltwater into lakes could temporally exceed the shear resistance of moraine dams and promote their failure. Brittle deformation of the flowing glacier mass (*crevasses*) is visible for many clean-ice glaciers in the southern Himalayas (Xin et al., 2008) and may enhance calving into lakes at their termini. At the same time, warm air masses during summer gradually thaw the frozen surfaces of lakes and moraine dams, making lakes less resilient to external impacts. However, this regional link between ablation and the occurrences of GLOFs only holds partly, given that Hindu Kush and the Hengduan Shan also have large glacier areas below the ELA, but little GLOF abundance.

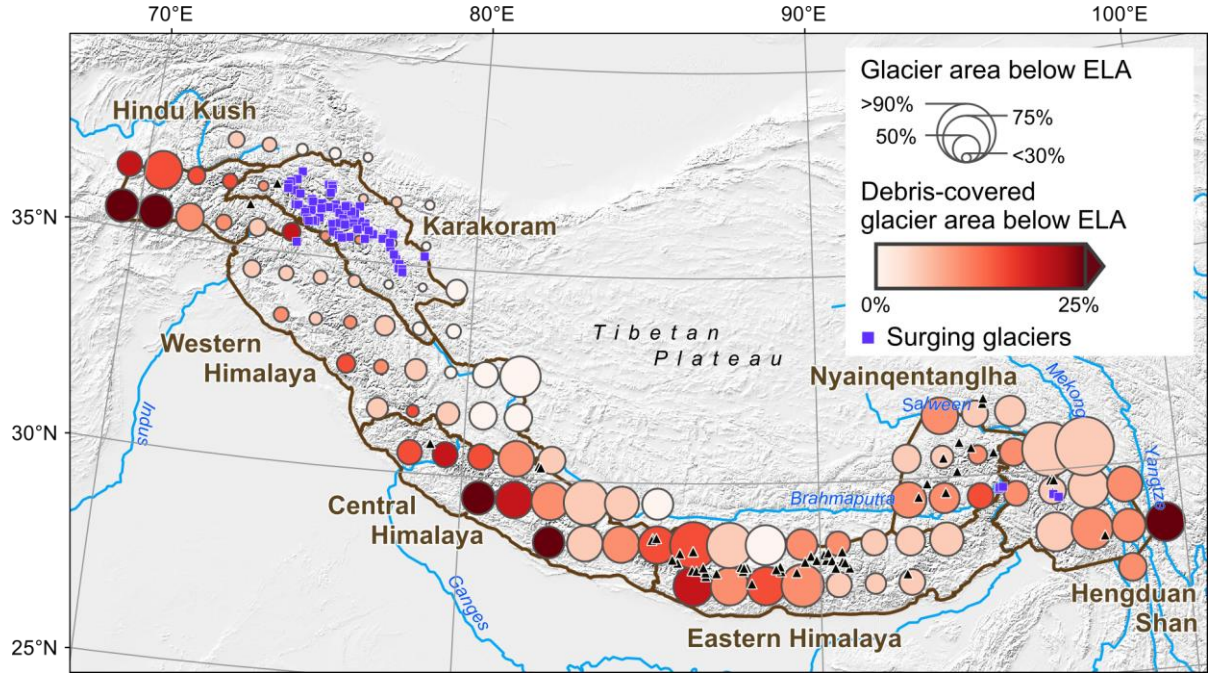

Figure 5-7: Glacier area and debris-covered glacier area below the Equilibrium Line Altitude (ELA). *Data are aggregated on a 1° × 1° grid, provided in Kraaijenbrink et al. (2017); http://mountainhydrology.org/data-nature-2017. Triangles are all 62 historic GLOFs. Surging glaciers are from Rankl et al. (2014) and Dehecq et al. (2019).*

Additionally, some regions in my study area have >20% debris cover on the glacier tongues (Figure 5-7). Debris shields the glacier ice from atmospheric warming, so that debris-covered glaciers can persist at lower elevations than their clean-ice counterparts and sustain meltwater production over much longer time scales (Rowan et al., 2015). With ongoing atmospheric warming, most of debris-covered glaciers had thinned at their termini and developed supraglacial ponds. If glaciers had gentle slopes (<2°) and low or no flow velocities (Quincey et al., 2007), these ponds eventually coalesce, grow in area and deepen to large terminal lakes. Prominent examples for this phenomenon are Imja Tsho, Luggye Tsho or Tsho Rolpa, which all expanded by >1 km^2 in less than 50 years (Komori, 2008; Sakai et al., 2000; Watanabe et al., 2009). Indeed, lakes in contact to debris-covered glaciers grew more than unconnected lakes in all southern Himalayan regions since 2000 (Song et al., 2017), including the Eastern Himalaya (Basnett et al., 2013), Nyainqentanglha (Song et al., 2016), and Hengduan Shan (Wang et al., 2017). Growing supraglacial ponds absorb up to 14 times more solar energy than their surrounding (Miles et al., 2018b) so that thermal erosion can undercut the adjacent ice and form steep cliffs (Watson et al., 2017). These could collapse into the ponds, while conduits between ponds have shown to pass >10^6 m^3 water within few hours through the glacier (Miles et al., 2018a; Rounce et al., 2017), possibly injecting additional water into lakes at the terminus and trigger GLOFs. Yet whether regional debris cover is a good predictor for GLOF activity remains unclear: I note that less than half (14) of all 38 GLOFs in the past three decades came from debris-covered glaciers. Regional debris cover matches with GLOF abundance in the Nepalese Himalayas,

while the Central Himalayas and the Hindu Kush, for example, offer regions with higher debris cover, but no GLOFs (Figure 5-7). One plausible reason is that these regions mostly have land-terminating glaciers where the interplay of thinning, surface gradient and flow velocity has not (yet) allowed a lake to form at the terminal moraine (King et al., 2018).

I had already outlined that glacial mass losses in the 21st century, expressed as average elevation change on glaciers, is most severe in the Western Himalayas and Nyainqentanglha (Brun et al., 2017; Figure 1-2). Glacier flow velocities, calculated for the same period, mimic the regional pattern of ice thinning (Figure 5-8): slowdown is largest in these two regions, followed by smaller reduction in flow speed between Western Nepal and Bhutan, while the stable or mass-gaining glaciers in the Karakoram show accelerated glacier flow velocities (Dehecq et al., 2019). Decreasing flow velocities suggest lower rates of ice transport towards the terminus, so that I would expect, in theory, optimal conditions for lakes to form where glaciers have become stagnant. Assuming that lakes grow in contact to retreating glaciers, such regions of low glacier flow velocities could be suitable predictors for GLOF activity. Yet, this is apparently not the case, given that glacial lakes in Western Himalaya, for example, grew slowest among all other regions in the main Himalayan mountain belt since 1990 (Figure 5-5). There, excess meltwater may have punctured moraine dams and impeded contemporary lake formation. In any case, this example shows that a general 'life cycle' of glacial lakes in high mountains (Emmer et al., 2016a, 2015), from glacier advance in the LIA to

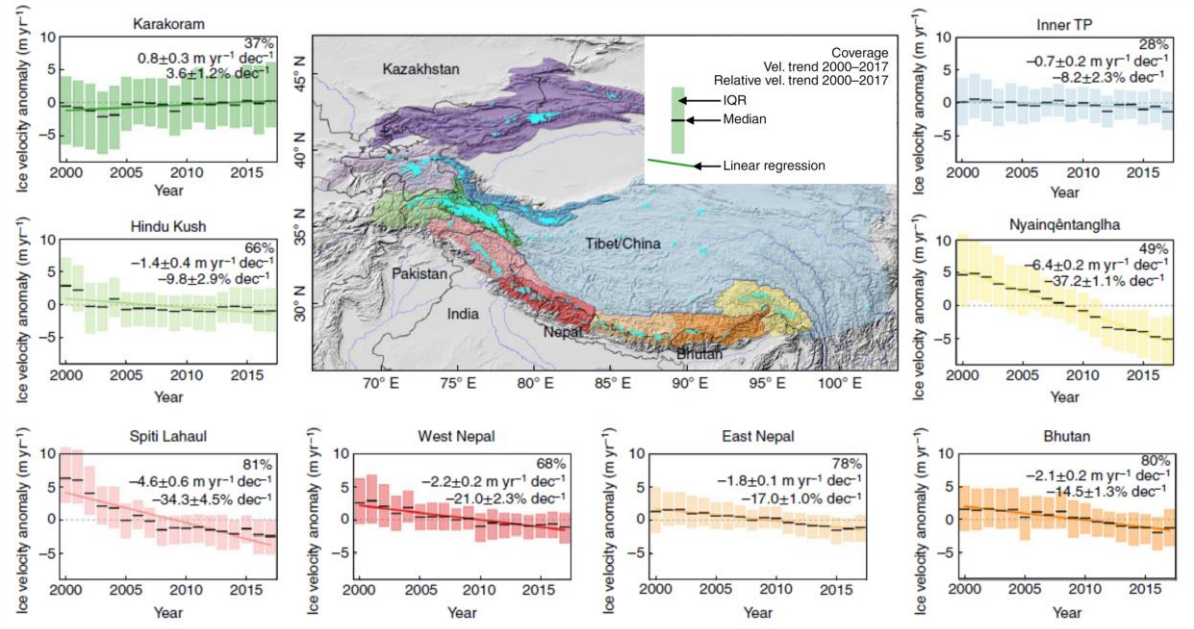

Figure 5-8: Annual glacier velocity anomalies for High Mountain Asia (2000–2017). *The centre map shows the study area from Dehecq et al. (2019), including eight subregions with glaciers highlighted in cyan. Each inset shows a time series of the annual velocity anomaly (change along flow direction relative to the mean velocity) for each subregion. Black lines represent the median anomaly, colour bars the interquartile range (IQR) and coloured lines the linear trend over 2000–2017. Coverage of observations common to all years (top), velocity trend (middle) and velocity trend relative to the mean velocity (bottom), with 68% confidence interval, are reported in each inset. Dec, decade. Figure and parts of the caption adapted from Dehecq et al. (2019).*

subsequent glacier retreat, lake formation behind moraines, and eventual catastrophic breaching is challenging, if not impossible to trace in the Himalayas.

5.3.2.3. Regional topography and rainfall

The topographic relief of the Himalayan mountain range constrains how far moist air masses can travel in altitude (Bookhagen and Burbank, 2010; Maussion et al., 2014). This orographic effect controls the amount of rainfall in regions where glacial lakes occur, which is vital to consider given that the sudden injection of rainwater has triggered lake failure elsewhere (Worni et al., 2012). Swath analysis along the strike of the Himalayas show that high-altitude rainfall is controlled by two characteristic orographic profiles (Figure 5-9A; Bookhagen and Burbank, 2010): parts of the Western Himalayas and the Eastern Himalayas have a one-step, i.e. more steadily rising, topography where most of the rainfall occurs at ~1,500-2,500 m a.s.l., and hence rarely reaches the characteristic elevation band for glacial lakes at 4,000-6,000 m a.s.l. (Figure 5-9B). Surprisingly, these two regions comprise a strongly contrasting GLOF record: the Eastern and the Western Himalaya had the highest and lowest historic GLOF count, respectively, so that orographic rainfall seems less appropriate to characterize the regional GLOF pattern. The Central Himalayas, in turn, offer a two-step topography, allowing moist air masses to travel beyond >4,000 m a.s.l. where glacial lakes preferentially form and fail (Figure 5-9C). Large proportions of rainfall in the high-mountains of Nepal occur in convective rainstorms (Figure 5-6h). However, my search in literature revealed no evidence that any historic GLOF was related to rainfall in this region. Furthermore, 17 GLOFs in the Central and Eastern Himalayas occurred north of the main topographic divide, where precipitation is substantially lower (Figure 5-9). The GLOF at Kedarnath (Das et al., 2015), lying at the transition from Central to Western Himalaya, is the only reliably documented rainfall-triggered GLOF in the Himalayas, which these swaths did not cover.

Given the sparsely instrumented meteorological network, I here presented satellite-based rainfall estimates that had an original resolution of several tens of kilometres and were downscaled to 10 or one km resolution using statistical relationships or regional climate circulation models (Bookhagen and Burbank, 2010; Maussion et al., 2014). The only climate station above 5,000 m a.s.l. near Mount Everest (Nepal) records that 90% of the annual precipitation (~400 mm) occurs as rainfall between June and September. This high contribution of rainfall at these altitudes suggests

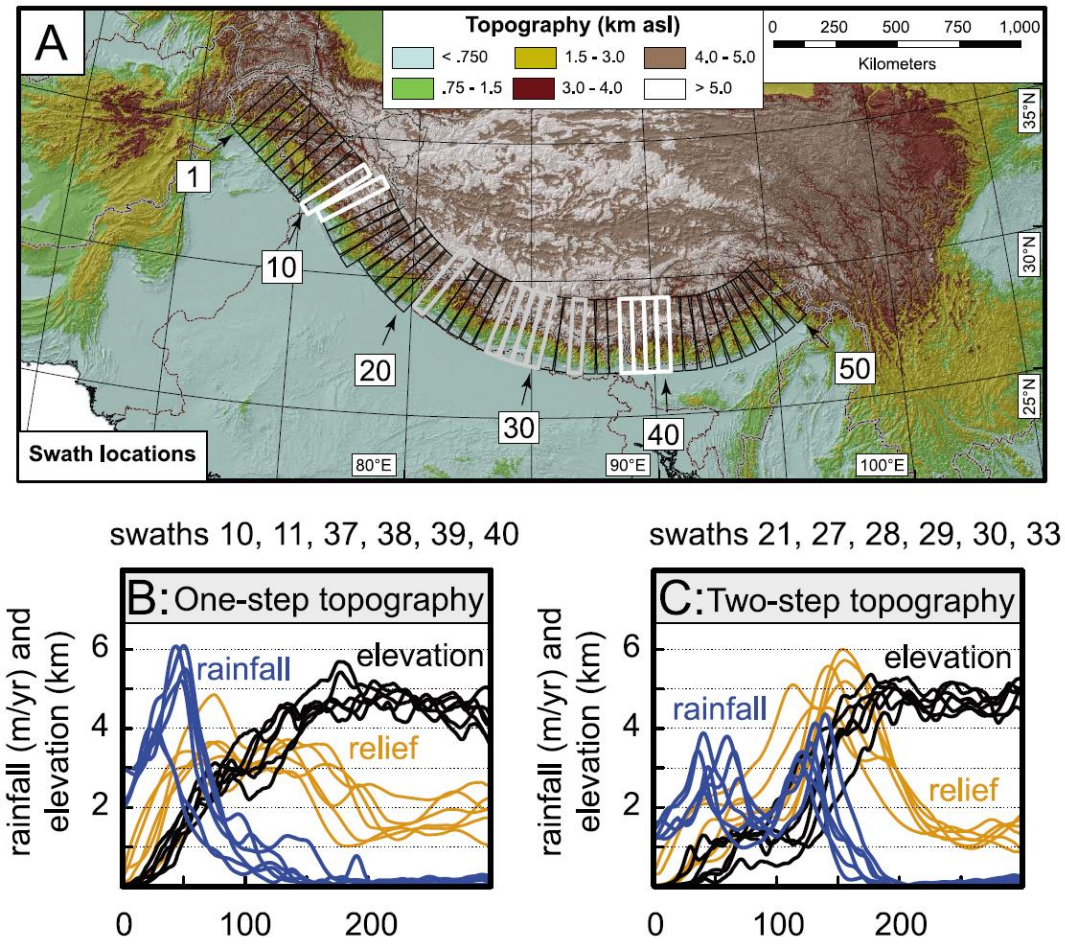

Figure 5-9: Rainfall, relief, and topography in the Himalayas. A, *Location of numbered, 50 km wide and 300 km long swaths, representative for the two end-members from the distribution of topography, relief, and rainfall.* ***B)*** *One-step topography with steadily rising topographic profile results in a single high-amount rainfall peak (white swaths in A). Orange lines of relief are the variation of elevation within a 5 km radius.* ***C)*** *Two-step morphology coinciding with the Lesser Himalaya units and Higher (Greater) Himalaya forming two rainfall peaks (grey swaths in A). Figure adapted from Bookhagen and Burbank (2010).*

that–in some regions–the amount and frequency of rainfall at glacial lakes could be higher than such coarse-scale products may estimate. The role of rainfall as a GLOF trigger thus remains an open question. Nevertheless, such reanalysis data offer estimates of several climate parameters beyond precipitation such as temperature or heat flux at sub-daily resolution, which are vital to analyse for anomalies in the days prior to historic GLOFs.

The 19 reported GLOFs in the Central Himalayas could possibly relate to a zone of world's highest relief, offering detachment zones with high potential energy, so that mass flows could enter lakes despite long runout distances. Glacier ice entrained by rock avalanches can reduce bulk friction, and even increase flow extents (Schneider et al., 2011). Such a case occurred at Mount Hualcán (Cordillera Blanca) in 2010, when a rock-ice avalanche (~5 × 10^5 m^3) dropped over ~1,000 m vertically into Laguna 513, causing a flood wave ~25 m high (Carey et al., 2012; Schneider et al., 2014). Two newly detected GLOFs in the Nyainqentanglha and Eastern Himalaya showed bright

sediment tails entering the lakes in the post-event images, suggesting that debris flows could also have contributed to lake failure in some cases. Contrary to this theory, the Eastern Himalayas have lower relief than the Central Himalayas, but even higher GLOF abundance, so that relief seems to be a rather vague predictor for the regional GLOF pattern.

5.3.2.4. Earthquakes

Apart from atmospheric triggers such as rainfall, earthquakes may play a dominant role in releasing such mass movements. At least one historic GLOF in Patagonia in 2000 (Harrison et al., 2006) and five historic GLOFs in the Cordillera Blanca–one in 1725 and four in 1970 (Emmer, 2017; Lliboutry et al., 1977)–have been attributed to a seismic origin, either directly by reduced cohesion in moraine dams or indirectly by landslides or rockfalls entering lakes. In the Nepal Himalaya, valley infills at Pokhara have likely preserved repeated catastrophic GLOFs following three magnitude *M*8 earthquakes in ~1100, 1255, and 1344 AD (Schwanghart et al., 2016a). It is hence surprising that earthquakes have been rarely regarded as a potential trigger for Himalayan GLOFs in the literature. Exceptions confirm this rule, and Gurung et al. (2017) contemplate that the 2015 Lemthang Tsho GLOF (Bhutan) could relate to a *M*5.1 earthquake that occurred on the same day at an epicentral distance and depth of 187 km and 27 km, respectively. They state that its *"role […] is difficult to confirm or discount in absence of first-hand information, but seems unlikely due to weak intensity of shaking"*. They conclude that, with *"the region being seismically very active zone, the role of earthquake as a trigger of GLOF cannot be overlooked"*. The failure of Sabai Tsho in the Nepal Himalayas has been attributed to co-seismic mass movements into the lake, since at least four earthquakes with magnitudes from 4.1 to 5.6 were recorded at the same day within 15 km from the lake (Osti et al., 2011).

At least 6,694 discrete earthquake shocks with $M>4$ and depths <150 km had their epicentres in a 150 km wide corridor along my study area between 1985 and 2017 (Figure 5-10a). The regional pattern of earthquakes, however, only partly complies with GLOF abundance: While the GLOF cluster in the Nepalese Himalayas is densely covered with seismic records, such signals are missing (or were at least not recorded) in the Bhutanese Himalayas, where GLOF abundance is highest. I also note frequent earthquake tremors in the Central Himalayas and the regions north of it, where only three GLOFs occurred in total (including the rainfall-triggered GLOF at Kedarnath in 2013).

A more detailed look at the seismic record shows that at least 748 earthquakes occurred within 150 km of newly detected and historic GLOFs, and at most two years before the outbursts occurred (Figure 5-10b). Without further analysis of the associated local ground acceleration or displacement, I hypothesise that these shocks could at least have preconditioned some triggers of the observed GLOFs that were recorded days, months or years later. Many smaller earthquakes (M~4) occurred less than 100 days before the GLOFs, but mostly at distances >50 km from the source lakes. Other

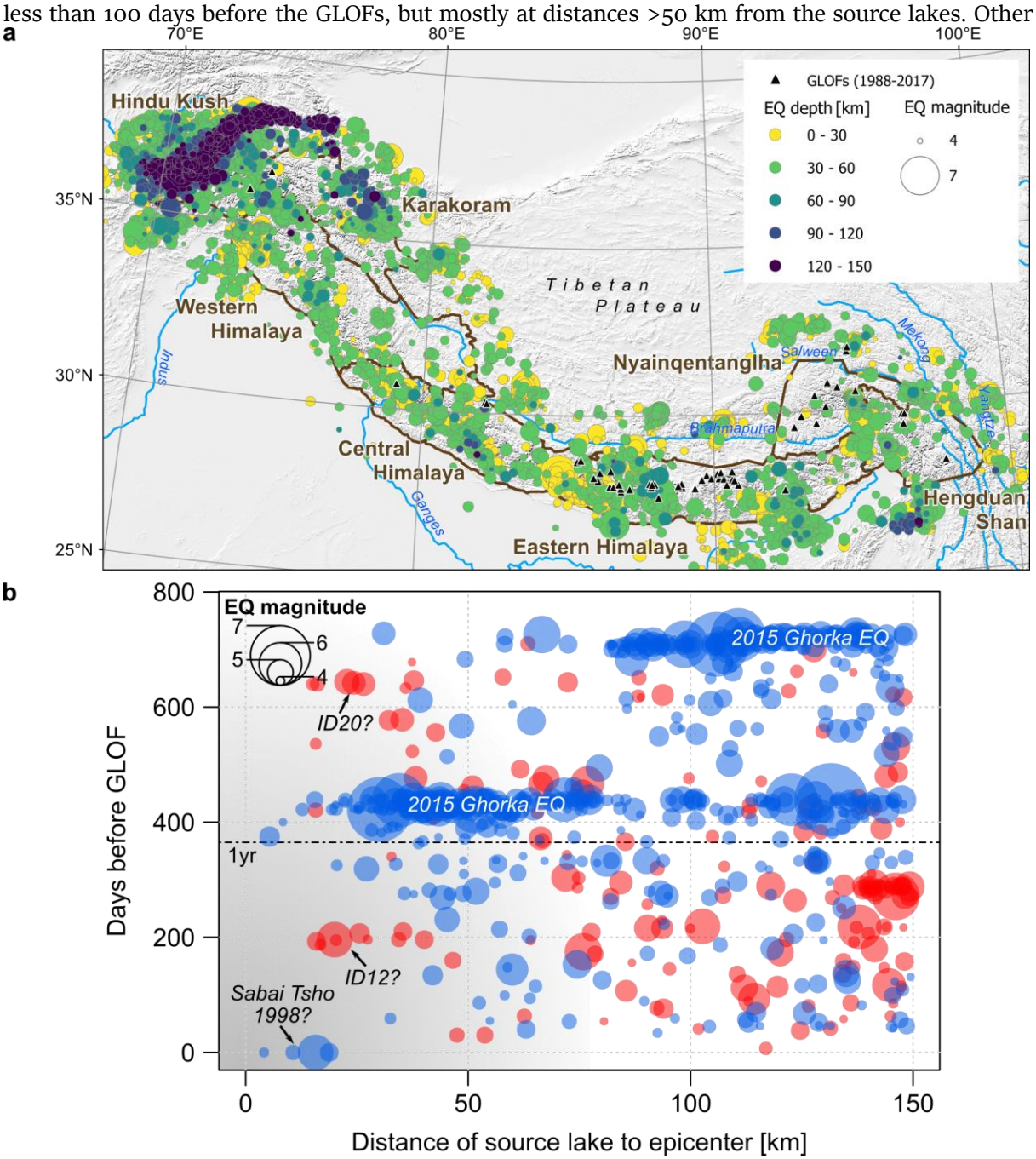

Figure 5-10: Earthquakes in the Himalayas (1985-2017). a, *Epicenters with depths <150 km and magnitudes >4 in a 150-km buffer around the study region (brown). Data from USGS (https://earthquake.usgs.gov/earthquakes/search; accessed 09 March 2019)* ***b,*** *Distance of GLOFs to earthquake epicenters in space and time. Bubbles are epicenters within 150 km (disregarding earthquake depth) and less than two years before newly detected (red) and previously known (blue) GLOFs. Grey color gradient highlights earthquakes that occurred both spatially and temporally close to the GLOFs. Large earthquakes such as the Ghorka earthquake in Nepal 2015 form clusters because of aftershocks.*

GLOFs (ID12 and 20) had sequences of shocks of >M4.8 between 200 and 650 days prior (Figure 5-10b). These cases might call for investigating post-seismic triggers with methods similar to those used in studies after the Ghorka earthquake in 2015: high-resolution satellite images showed no outbursts despite direct impacts from landslides into lakes (Kargel et al., 2016), whereas field visits from Byers et al. (2017) *"identified worrisome cracks near the Tsho Rolpa outlet channel"*. New advances in capturing earthquake-related mass movements may come from recently launched optical satellite constellations such as Copernicus Sentinel-2 or PlanetScope CubeSat. These missions have resolutions of 10 and 3 m, and repeat rates of five days or even on demand (ESA, 2015; Planet Labs, 2018). While optical imagery may still suffer from monsoonal clouds, radar missions such as Sentinel-1 or ALOS-2 point the way forward: Interferometric Synthetic Aperture Radar (InSAR) can penetrate clouds and detect earthquake-induced horizontal and vertical displacements with millimeter accuracy (Klees and Massonnet, 1998).

5.3.2.5. Triggers and global warming

GLOFs have been widely expected (Bajracharya and Mool, 2010; Cook et al., 2018; Richardson and Reynolds, 2000) or predicted (Harrison et al., 2018) to occur more frequently with ongoing atmospheric warming. Attributing GLOFs to climate change needs to consider two processes independently of each other: One of these is the presence and growth of glacial lakes, which we may assume to result from climate-driven glacier melt. Following the prevailing concept in GLOF research, we need, second, a trigger that causes some of these emerging lakes to fail catastrophically. Harrison et al. (2018) proposed a theory that predicts outbursts to lag behind lake formation. In this theory, triggers could occur randomly in time, from a year to centuries after lakes had started to grow. This notion may give a hint, why the rate of GLOFs per unit time has not increased commensurately with the number and area of glacial lakes during my study period. If triggers are a prerequisite for GLOFs, but come with delay to lake formation, this could support my hypothesis that the number of trigger events per unit lake must have declined in the past three decades.

Triggers could also increase their frequency with atmospheric warming. However, I assume that this has happened less likely in the past 30 years, at least not with a magnitude or frequency that could have changed GLOF frequency in the past 30 years. Ice avalanches have dominated the historic record of triggers (Nie et al., 2018), which are challenging to attribute to atmospheric warming. My search in literature could not identify whether ice avalanches may change their frequency with ongoing global warming and glacier retreat. Projections of less or no ice in high mountains (Huss et al., 2017) may ask not least, which mechanisms could trigger GLOFs when all ice is gone eventually.

One option for increasing GLOF frequencies in the future are landslides, which could occur more often in high mountains because of atmospheric warming (Huggel et al., 2012). A recent hypothesis expects that thawing permafrost at high elevations may initate a process chain, in which steep mountain walls become unstable, so that landslides may detach and enter meltwater lakes eventually (Haeberli et al., 2017). However, testing such a process cascade in the Himalayas is difficult, not least since few long-term, regionally distributed datasets exist for these single components. I also found no study that systematically analysed landslide occurrences at elevations >4,000 m a.s.l., which is where impacts into glacial lakes may play a role. Judging from annual mapping in Nepal, monsoon-induced landslides Himalayas showed no change in frequency between 2000 and 2018 (Marc et al., 2019). Regarding atmospheric warming, Krishnan et al. (2019) found that *"during 1901–2014, annual mean surface air temperature increased significantly in the HKH at a rate of about 0.104 °C/decade"*, but they evaluated only climate stations outside the high mountains. Maps of permafrost distribution in the Himalayas only come from models with coarse spatial resolution (>1 km), given that *"direct observations of permafrost in mountains of the HKH are sparse"* (Gruber et al., 2017). These authors note that the minimum elevation of permafrost could be anywhere between 3,500 and 6,000 m a.s.l. in the Himalayas, depending on local topography, aspect and temperature. As a consequence, even less is known on the local changes of the lower permafrost limit in past decades (Fukui et al., 2007). Huggel et al. (2012) conclude that there is still no unambiguous evidence that the landslide frequency may increase with atmospheric warming. Yet glacial lakes are expected to persist for hundreds to thousands of years in mountain landscapes (Haeberli et al., 2017). Whether they survive long enough to become targets of possibly changing landslide frequencies is an essential question for future research.

Landslides, however, could also have a non-climatic background: the 2015 Ghorka earthquake alone featured 5-8 times more landslides compared to the pre-earthquake period (Marc et al., 2019). In the Cordillera Blanca, four GLOFs from the 1970 Ancash earthquake have disproportionally added to the total count and average rate of GLOFs (Emmer, 2017). Earthquakes and other non-climate driven mass movements are essential to consider when it comes to attributing GLOFs and their triggers to climate change. Harrison et al. (2018) summarised this issue appropriately: *"The difficulty of attributing individual GLOF behaviour to climate change relates to the presence of non-climatic factors affecting GLOF behaviour, such as moraine dam geometry and sedimentology, climate-independent GLOF triggers (e.g. earthquakes) and the timescales related to destabilization of mountain slopes, producing mass movements into lakes"*. I note that the baseline behaviour of GLOF triggers in absence of climate change remains largely unknown, given that reports on GLOFs are widely unsystematic before the 1980s (Ives et al., 2010; Nie et al., 2018). In any case, I recommend

to account for both climatic and non-climatic triggers, including their changes, when projections of future GLOF frequency, hazard, and risk are demanded.

5.4. Robustness of the hazard framework

Understanding the physics of regional GLOF frequencies is one of the most urgent tasks to quantify GLOF hazard and risk. Though I could only speculate on regional GLOF drivers in the previous chapters, I maintain that the regionally varying susceptibility to GLOFs directly becomes apparent in my hazard appraisal: regions with higher (lower) historic GLOF abundance have higher (lower) contemporary GLOF hazard, which I expressed as the discharge that occurs on average once in 100 years. The concept of the 100-year GLOF discharge may sound unfamiliar at first view, probably because it has not been used for this type of natural hazard in the literature before. In essence, my approach for estimating GLOF hazard does not deviate from other hazard appraisals for hydro-meteorological floods, earthquakes, tsunamis, wildfires or asteroid impacts. Clearly, estimating the exceedance probability of an event of a given magnitude or larger is most widely applied in flood hydrology. Gauging equipment often log discharge for decades, so that return periods for any flood discharge of interest in a catchment can be readily inferred from distributions fitted to the extreme values (over a threshold or in defined blocks) from the recorded data.

For historic GLOFs, such reported values of peak discharge are less reliable, given that they were often measured or approximated many tens of kilometres downstream, either visually or with gauging equipment prone to malfunction or blackouts during such high flows. Other studies estimated peak discharge from hydraulic step-backwater models; critical-depth methods; entrainment velocities of flow-transported boulders; super-elevation geometries; or empirical breach relationships (Korup and Tweed, 2007). Given these different methodologies, such estimates of peak discharge are challenging to integrate into a single time series of peak discharge. For the 22 newly detected GLOFs, values of peak discharge are completely missing, which–in sum–made applying the traditional extreme-value approach in hydrology impractical. My solution to estimate GLOF return periods was to combine the inferred GLOF frequencies with simulations of flood magnitudes from possible GLOF sources. This approach is widely used for example in tsunami hazard appraisals, in which historic earthquake catalogues provide the frequency, while models of wave propagation from rupture zones yield an estimate of tsunami magnitude (Horspool et al., 2014).

5.4.1. Predictions of peak discharge

My estimates of GLOF magnitudes hinge on simplified hydraulic principles of critical flow, which Walder and O'Connor (1997) expressed in a physically motivated dam break model. They assumed that data from 63 breached reservoirs had sufficiently well recorded breach depths, rates and volumes to offer sufficient confirmation of these principles. Given the challenges to measure peak discharge at the breach, these cases include no uncertainties or measurement errors. Nevertheless, I can readily implement these uncertainties as prior information in the Bayesian piece-wise regression model that I learned from these data (Supplementary Figure 7-4). The individual cases therein encompass a wide range of dam and breach geometries, lake volumes, and topographic settings. Moraine dams are only one among eight dam types that entered this model, and this imbalance could explain some of the scatter of Q_{p*} over nearly two orders of magnitude for a given η, the product of breach volume and released flood volume. This variance would decrease possibly, if applying the model solely to moraine-dammed failures. Limiting the model in this way, however, would also mean that we had fewer data points available, and that the posterior predictive distributions would likely become broader. Outbursts from landslide dams dominate the data points used in the model, and only two GLOFs, one from the Tien Shan and one from Midui Lake in the Nyainqentanglha Mountains, contributed to learning the model, because breach erosion rates had been rarely measured at the dam failure. Despite this caveat, the detailed compilation by O'Connor and Beebee (2009) demonstrated that the reported data on moraine-dammed lakes do not form any distinct group outside of the overall trend of natural dam failures. Any differences to landslide dams, for example, in terms of overall geometry, are part of the overall scatter.

Using this model to predict Q_p for any other lake of interest needs to consider a complete distribution of plausible breach erosion rates, particularly if no physical properties of the dam are known. Empirical breach erosion rates from natural dam breaks vary by more than two orders of magnitude (O'Connor and Beebee, 2009), so that predictions of Q_p will spread across a similar or larger range for a given flood volume. My Bayesian approach expresses all the major uncertainties in the shape of its marginal posterior distributions and offers richer information than any traditional point estimate from an empirical discharge-rating curve could do. For the GLOF at Kedarnath, for example, Das et al. (2015) compared 20 predictions of best-fit or envelope-based equations, and found Q_p–for a fixed volume and breach depth–to vary by an order of magnitude. They also compared the sensitivity towards input data and found lake depth to vary by 36%, whereas lake volume varied by 60%. In my approach, the posterior distributions of Q_p, predicted for any Himalayan lake, explicitly propagate these uncertainties as I calculated flood volumes from lake level drops in 1-m steps (Supplementary Figure 7-9).

Validating model predictions with reported peak discharge will remain unrewarding, not least due to missing breach erosion rates for historical Himalayan GLOFs. Yet with increasing computational capacities, the inference of Q_p for historic (and also newly detected) cases should increasingly benefit from numerical and probabilistic models that include physically plausible scenarios of dam failure and flood-wave routing (Watson et al., 2015; Westoby et al., 2014; Westoby et al., 2015). In parallel, laboratory experiments have been increasingly successful to represent some of the key physical boundary conditions in such models (Carrivick, 2010; Carrivick et al., 2011). Even without further constraining these unknowns, I was able to learn from the data both the inflection point and credible error margins for the model by Walder and O'Connor (1997). These uncertainties are essential to know for predicting GLOF hazard, but have eluded detailed treatment in the original (Walder and O'Connor, 1997) or subsequent publications (O'Connor and Beebee, 2009). Yet they can be readily implemented into the current model setup, while still maintaining its original intention "*for rapid prediction of plausible values of peak discharge"* (Walder and O'Connor, 1997).

5.4.2. Size distribution of glacial lakes

Appraising performances and improvements of this model must not distract from the regional and size distribution of glacial lakes, which may be even more robust indicators for GLOF hazard than peak discharge. In essence, my estimates of peak discharge are only a proxy for lake area with the goal of expressing hazard in a more tangible way than lake area alone. Assuming that my inferred GLOF rates are correct to first order, the regional abundance and size of glacial lakes will remain the main control on regional GLOF hazard, regardless of which metric we use to estimate hazard. If we seek for reducing uncertainties in the peak-discharge model and its input data, we could ask in the simplest case: what is the 100-year lake area that bursts out in the Himalayas? Such a metric of hazard is even more straightforward to obtain with currently available lake inventories (Table 1.1), and will probably only marginally change the regional distribution of hazard that I estimated. While single scenarios of peak discharge from my, but also any other, model remain difficult to validate, the large sample of 0.3 billion scenarios is what makes my regional hazard appraisal robust. Numerical simulations show that increasing sizes of lake impacts or flood volumes produce higher discharges and runouts (Frey et al., 2018; Somos-Valenzuela et al., 2016), so that hazard–ignoring the temporal probability for the sake of the argument–is again tied to lake volumes, and hence lake areas.

A similar scaling relationship may also apply to the overdeepenings that I extracted from ice thickness data (Kraaijenbrink et al., 2017; Linsbauer et al., 2016). From the basic concepts in the associated ice flow model (inverse flow law, coupling of surface slope with local ice thickness via

basal shear stress), the largest glaciers in the Karakoram can be expected to erode and expose the largest overdeepenings, if they have completely melted in the future (Linsbauer et al., 2016). Here, the strongest increase of GLOF hazard is thus not surprising to see, given that the size of overdeepenings correlates with glacier area (Supplementary Figure 7-5). Clearly, the extent and depth of single overdeepenings can be prone to errors. Validation of the ice thickness model, which I used, with 86 in-situ measurements shows that ice thicknesses are likely underestimated by -25.7 m on average (Frey et al., 2014). Hence, modelled depressions could be deeper than I assumed, which could translate into higher future GLOF hazard in some regions, if these depressions do not fill by sediments or dry out. In any case, given that such ice thickness models can robustly represent the regional distribution of overdeepenings, the present glacier areas alone may provide a first-order appraisal of future GLOF hazard, without any conversion to other diagnostics of flood magnitude.

5.5. Conclusion and future research questions

In this thesis, I proposed a framework for estimating GLOF hazard in the Himalayas on regional scales. Appraising GLOF hazard hinges on the number of observed GLOFs in a given region, and could be strongly underestimated, if not systematically corrected for unreported cases. In this spirit, I collated the first consistent GLOF inventory for the Himalayas between the late 1980s and 2017. By more than doubling the GLOF count to a total of 38 cases since 1988, I consolidated the regional contrast between higher GLOF abundance in the southern regions, and comparatively fewer GLOFs in the northern Hindu-Kush Karakoram range. Hence, the southern parts of the Himalayas have a higher contemporary GLOF hazard, which is not least due to a larger number and area of glacial lakes today. I find that GLOF rates and the regional size distribution of glacial lakes have a principal control on GLOF hazard, regardless of whether we express hazard by the 100-year return period of GLOF peak discharge, which I introduced here, or any other quantitative metric.

These findings raised the question of how GLOF hazard changes in the future, if glaciers keep retreating as they mostly did in past decades. I show that the region-wide GLOF hazard could double in future when all glaciers in the Himalayas have melted eventually. While this is probably no worst-case scenario any more, I maintain that glacier melt alone could raise the risk from Himalayan GLOFs two- to threefold, even if the annual GLOF rate, vulnerability, and exposure were to remain unchanged. Given the rapidly growing population, infrastructure, and hydropower projects in the Himalayas, this finding quantifies to first order the purely climate-driven contribution to GLOF hazard and risk.

In this thesis, I presented an unprecedented GLOF inventory and a novel approach to estimate GLOF hazard. These outcomes motivate some future research directions at the interface of geomorphology and hazard assessment:

1/ Geomorphology: What are the magnitude and frequency of GLOFs beyond the Landsat era?

My evaluation of the Landsat archive covered images from the past three decades, an interval that is conventionally used to study the response of natural hazards to climate change. However, glaciers have thinned, retreated and lost mass in many regions of the Himalayas–except for the Karakoram–since the 1970s or even earlier (Bolch et al., 2019), a period which my methodology could not cover. Quantifying the response times of glacial lakes and GLOFs to climate change is not only essential for hazard assessment. Outburst floods from moraine-dammed lakes are major conveyors of sediment in the Himalayan sediment routing system, probably taking an even larger role in the annual sediment yield than 'normal' monsoon-driven floods (Cook et al., 2018). Though I gave a first idea on sediment redistribution by mapping such sediment tails downstream of breached lakes, a more detailed quantification of their geomorphic effectiveness, especially for the pre-Landsat era, has remained an open question in this thesis. Appraising the landscape response to GLOFs needs to investigate their magnitude and frequency on a longer timeframe than the past 30 years.

Systematically extending the Himalayan GLOF inventory could make use of declassified satellite or aerial images to identify previously unreported cases (Komori et al., 2012; Nie et al., 2018). Such images mostly give the geomorphic impact after the flood, which calls for field work to approximate the year of occurrence. Vital information on GLOF ages can come from buried trees in sediment deposits (Stolle et al., 2017), from flood impacts in tree rings (Ballesteros-Cánovas et al., 2015), or from local documents or chronologies (Emmer, 2017). Estimating historic GLOF magnitudes needs to quantify eroded and deposited sediment volumes in river channels. For this purpose, a widely unexplored resource are repeated historical digitial elevation models from stereo-photographs and aerial images (Maurer and Rupper, 2015; Maurer et al., 2016). Such an expanded GLOF inventory could ideally answer at least three key questions in geomorphology: (1) How do sediment yields from single GLOFs compare with basin-wide, monsoon-driven erosion rates in the Himalayas? (2) How long do mountain rivers need to evacuate sediment and, hence, recover to pre-GLOF conditions? (3) Regarding the differences in flood volumes of GLOFs before and in the Landsat era (Figure 3-3b), how do magnitudes of glacier-related floods change with atmospheric warming?

Moving beyond the Landsat era also means to improve our understanding of future GLOF frequency. Given that individual GLOFs are still difficult to attribute to atmospheric warming, I find that learning more on outburst susceptibility of glacial lakes could be a first step forward.

2/ Susceptibility: What are the factors that make glacial lakes prone to outburst?

This thesis has put together the most complete GLOF inventory in the Himalayas, which can be used as a stepping stone to learn the variables that make lakes susceptible to outbursts. Statistical learning techniques such as logistic regression are appropriate tools to identify the predictors that best discriminate drained lakes from undrained lakes (McKillop and Clague, 2007). The main input for such models are parameters that describe lake-specific characteristics (dam type and geomeotry, lake size), and its surrouding topography, geology, or climate (Prakash and Nagarajan, 2017). By training the Random Forest model (Chapter 2.3.2) and analysing regional GLOF drivers (Chapter 5.3.2), I already have generated or obtained many of these key variables. Learning the decisive variables for lake outbursts should be then readily practicable for future work. With logistic regression models, I can also objectively estimate the breach probabilities (or better susceptibilities) for the thousands of undrained lakes. These probabilities could add a vital update to the regional hazard model (Chapter 4). For example, simulations of peak discharge could be sampled according to the probability of failure from a given lake.

Statistical modelling of outburst susceptibility is not necessarily tied to the Himalayas alone. I hypothesize that globally collated cases (Harrison et al., 2018) can inform such susceptibility models, in which regional differences in climate, for example, can be appropriately represented as another predicting variable. This would be a first step forward not only to objectively estimate the outburst probability for a recently compiled sample of 13,000 glacial lakes worldwide (Shugar et al., 2019). It also calls for a global application of my hazard framework.

3/ Hazard and risk: How can we couple the regional estimates of the 100-year flood discharge to local scales?

I infer that my presented hazard appraisal can robustly quantify GLOF return periods at regional scales, but comes with little information on hazard and risk on the local scale. The 100-year GLOF discharge hitherto quantifies the peak discharge at a breach location in the headwaters. To be a more useful diagnostic for practitioners, this discharge needs to be routed downstream. Simulations of GLOF peak discharge need to include the baseflow of high mountain rivers, possibly with monsoonal flood discharges adding to these peak flows. Current model frameworks can estimate hydro-meteorological flood discharges from freely available data on topography, rainfall

and river networks in fully automated manner (Sampson et al., 2015). In this regard, future work may aim at implementing GLOF runout models (Watson et al., 2015) as an additional module in such hydro-meteorological frameworks. With exposure data becoming increasingly available (Sieg, 2019), hazard and risk from GLOFs could hence be probabilistically estimated at finer spatial scales, from districts, to cities and even single houses.

6. Bibliography

Allen, G.H., Pavelsky, T.M., 2018. Global extent of rivers and streams. Science 361, 585–588.

Allen, S.K., Rastner, P., Arora, M., Huggel, C., Stoffel, M., 2016. Lake outburst and debris flow disaster at Kedarnath, June 2013: hydrometeorological triggering and topographic predisposition. Landslides 13, 1479–1491. https://doi.org/10.1007/s10346-015-0584-3

Arendt, A., Bliss, A., Bolch, T., Cogley, J., Gardner, A., Hagen, J., Hock, R., Huss, M., Kaser, G., Kienholz, C., 2015. Randolph Glacier Inventory–A dataset of global glacier outlines: Version 5.0. Glob. Land Ice Meas. Space Boulder Colo. USA.

Ashraf, A., Naz, R., Roohi, R., 2012. Glacial lake outburst flood hazards in Hindukush, Karakoram and Himalayan Ranges of Pakistan: implications and risk analysis. Geomat. Nat. Hazards Risk 3, 113–132. https://doi.org/10.1080/19475705.2011.615344

Bajracharya, B., Shrestha, A.B., Rajbhandari, L., 2007. Glacial Lake Outburst Floods in the Sagarmatha Region: Hazard Assessment Using GIS and Hydrodynamic Modeling. Mt. Res. Dev. 27, 336–344. https://doi.org/10.1659/mrd.0783

Bajracharya, S.R., Maharjan, S.B., Shrestha, F., 2011. Clean Ice and Debris covered glaciers of HKH Region.

Bajracharya, S.R., Mool, P., 2010. Glaciers, glacial lakes and glacial lake outburst floods in the Mount Everest region, Nepal. Ann. Glaciol. 50, 81–86.

Bajracharya, S.R., Mool, P.K., Shrestha, B.R., 2006. The impact of global warming on the glaciers of the Himalaya, in: Proceedings of the International Symposium on Geodisasters, Infrastructure Management and Protection of World Heritage Sites. pp. 231–242.

Ballesteros-Cánovas, J.A., Stoffel, M., St George, S., Hirschboeck, K., 2015. A review of flood records from tree rings. Prog. Phys. Geogr. Earth Environ. 39, 794–816. https://doi.org/10.1177/0309133315608758

Ballesteros-Cánovas, J.A., Trappmann, D., Madrigal-González, J., Eckert, N., Stoffel, M., 2018. Climate warming enhances snow avalanche risk in the Western Himalayas. Proc. Natl. Acad. Sci. 115, 3410–3415. https://doi.org/10.1073/pnas.1716913115

Basnett, S., Kulkarni, A.V., Bolch, T., 2013. The influence of debris cover and glacial lakes on the recession of glaciers in Sikkim Himalaya, India. J. Glaciol. 59, 1035–1046. https://doi.org/10.3189/2013JoG12J184

Belgiu, M., Drăguţ, L., 2016. Random forest in remote sensing: A review of applications and future directions. ISPRS J. Photogramm. Remote Sens. 114, 24–31. https://doi.org/10.1016/j.isprsjprs.2016.01.011

Benn, D.I., Bolch, T., Hands, K., Gulley, J., Luckman, A., Nicholson, L.I., Quincey, D., Thompson, S., Toumi, R., Wiseman, S., 2012. Response of debris-covered glaciers in the Mount Everest region to recent warming, and implications for outburst flood hazards. Earth-Sci. Rev. 114, 156–174. https://doi.org/10.1016/j.earscirev.2012.03.008

Bolch, T., Buchroithner, M.F., Peters, J., Baessler, M., Bajracharya, S., 2008. Identification of glacier motion and potentially dangerous glacial lakes in the Mt. Everest region/Nepal using spaceborne imagery. Nat. Hazards Earth Syst. Sci. 8, 1329–1340.

Bolch, T., Kulkarni, A., Kääb, A., Huggel, C., Paul, F., Cogley, J.G., Frey, H., Kargel, J.S., Fujita, K., Scheel, M., others, 2012. The state and fate of Himalayan glaciers. Science 336, 310–314.

Bolch, T., Peters, J., Yegorov, A., Pradhan, B., Buchroithner, M., Blagoveshchensky, V., 2011. Identification of potentially dangerous glacial lakes in the northern Tien Shan. Nat. Hazards 59, 1691–1714. https://doi.org/10.1007/s11069-011-9860-2

Bolch, T., Pieczonka, T., Mukherjee, K., Shea, J., 2017. Brief communication: Glaciers in the Hunza catchment (Karakoram) have been nearly in balance since the 1970s. The Cryosphere 11, 531–539. https://doi.org/10.5194/tc-11-531-2017

Bolch, T., Shea, J.M., Liu, S., Azam, F.M., Gao, Y., Gruber, S., Immerzeel, W.W., Kulkarni, A., Li, H., Tahir, A.A., 2019. Status and change of the cryosphere in the Extended Hindu Kush Himalaya Region, in: The Hindu Kush Himalaya Assessment. Springer, pp. 209–255.

Bookhagen, B., Burbank, D.W., 2010. Toward a complete Himalayan hydrological budget: Spatiotemporal distribution of snowmelt and rainfall and their impact on river discharge. J. Geophys. Res. 115. https://doi.org/10.1029/2009JF001426

Braun, M.H., Malz, P., Sommer, C., Farías-Barahona, D., Sauter, T., Casassa, G., Soruco, A., Skvarca, P., Seehaus, T.C., 2019. Constraining glacier elevation and mass changes in South America. Nat. Clim. Change 9, 130–136. https://doi.org/10.1038/s41558-018-0375-7

Breiman, L., 2001. Random forests. Mach. Learn. 45, 5–32.

Brun, F., Berthier, E., Wagnon, P., Kääb, A., Treichler, D., 2017. A spatially resolved estimate of High Mountain Asia glacier mass balances from 2000 to 2016. Nat. Geosci. 10, 668–673. https://doi.org/10.1038/ngeo2999

Buchroithner, M.F., Jentsch, G., Wanivenhaus, B., 1982. Monitoring of recent geological events in the Khumbu area (Himalaya, Nepal) by digital processing of Landsat MSS data. Rock Mech. Rock Eng. 15, 181–197.

Buckel, J., Otto, J.C., Prasicek, G., Keuschnig, M., 2018. Glacial lakes in Austria - Distribution and formation since the Little Ice Age. Glob. Planet. Change 164, 39–51. https://doi.org/10.1016/j.gloplacha.2018.03.003

Byers, A.C., Byers, E.A., McKinney, D.C., Rounce, D.R., 2017. A field-based study of impacts of the 2015 earthquake on potentially dangerous glacial lakes in Nepal. HIMALAYA J. Assoc. Nepal Himal. Stud. 37, 7.

Byers, A.C., McKinney, D.C., Somos-Valenzuela, M., Watanabe, T., Lamsal, D., 2013. Glacial lakes of the Hinku and Hongu valleys, Makalu Barun National Park and Buffer Zone, Nepal. Nat. Hazards 69, 115–139. https://doi.org/10.1007/s11069-013-0689-8

Byers, A.C., Rounce, D.R., Shugar, D.H., Lala, J.M., Byers, E.A., Regmi, D., 2018. A rockfall-induced glacial lake outburst flood, Upper Barun Valley, Nepal. Landslides. https://doi.org/10.1007/s10346-018-1079-9

Carey, M., Huggel, C., Bury, J., Portocarrero, C., Haeberli, W., 2012. An integrated socio-environmental framework for glacier hazard management and climate change adaptation: lessons from Lake 513, Cordillera Blanca, Peru. Clim. Change 112, 733–767. https://doi.org/10.1007/s10584-011-0249-8

Carrivick, J.L., 2010. Dam break – Outburst flood propagation and transient hydraulics: A geosciences perspective. J. Hydrol. 380, 338–355. https://doi.org/10.1016/j.jhydrol.2009.11.009

Carrivick, J.L., Jones, R., Keevil, G., 2011. Experimental insights on geomorphological processes within dam break outburst floods. J. Hydrol. 408, 153–163. https://doi.org/10.1016/j.jhydrol.2011.07.037

Carrivick, J.L., Tweed, F.S., 2016. A global assessment of the societal impacts of glacier outburst floods. Glob. Planet. Change 144, 1–16. https://doi.org/10.1016/j.gloplacha.2016.07.001

Cenderelli, D.A., Wohl, E.E., 2003. Flow hydraulics and geomorphic effects of glacial-lake outburst floods in the Mount Everest region, Nepal. Earth Surf. Process. Landf. 28, 385–407. https://doi.org/10.1002/esp.448

Cenderelli, D.A., Wohl, E.E., 2001. Peak discharge estimates of glacial-lake outburst floods and "normal" climatic floods in the Mount Everest region, Nepal. Geomorphology 40, 57–90.

Che, T., Xiao, L., Liou, Y.-A., 2014. Changes in Glaciers and Glacial Lakes and the Identification of Dangerous Glacial Lakes in the Pumqu River Basin, Xizang (Tibet). Adv. Meteorol. 2014, 1–8. https://doi.org/10.1155/2014/903709

Chen, F., Zhang, M., Tian, B., Li, Z., 2017. Extraction of Glacial Lake Outlines in Tibet Plateau Using Landsat 8 Imagery and Google Earth Engine. IEEE J. Sel. Top. Appl. Earth Obs. Remote Sens. 10, 4002–4009. https://doi.org/10.1109/JSTARS.2017.2705718

Chen, W., Doko, T., Fukui, H., Yan, W., 2013. Changes in Imja Lake and Karda Lake in the Everest Region of Himalaya. Nat. Resour. 4, 449–455. https://doi.org/10.4236/nr.2013.47055

Chen, X., Cui, P., Li, Y., Yang, Z., Qi, Y., 2007. Changes in glacial lakes and glaciers of post-1986 in the Poiqu River basin, Nyalam, Xizang (Tibet). Geomorphology 88, 298–311. https://doi.org/10.1016/j.geomorph.2006.11.012

Clague, J.J., Evans, S.G., 2000. A review of catastrophic drainage of moraine-dammed lakes in British Columbia. Quat. Sci. Rev. 19, 1763–1783.

Clague, J.J., O'Connor, J.E., 2015. Glacier-related outburst floods, in: Snow and Ice-Related Hazards, Risks and Disasters. Elsevier, pp. 487–519.

Cogley, J.G., Kargel, J.S., Kaser, G., van der Veen, C.J., 2010. Tracking the source of glacier misinformation. Science 327, 522–522.

Conrad, O., Bechtel, B., Bock, M., Dietrich, H., Fischer, E., Gerlitz, L., Wehberg, J., Wichmann, V., Böhner, J., 2015. System for Automated Geoscientific Analyses (SAGA) v. 2.1.4. Geosci. Model Dev. 8, 1991–2007. https://doi.org/10.5194/gmd-8-1991-2015

Cook, K., Andermann, C., Gimbert, F., Hovius, N., Adhikari, B., 2017. Impacts of the 2016 outburst flood on the Bhote Koshi River valley, central Nepal. Geophys. Res. Abstr. 19.

Cook, K.L., Andermann, C., Gimbert, F., Adhikari, B.R., Hovius, N., 2018. Glacial lake outburst floods as drivers of fluvial erosion in the Himalaya. Science 362, 53–57.

Cook, S.J., Quincey, D.J., 2015. Estimating the volume of Alpine glacial lakes. Earth Surf. Dyn. 3, 559–575. https://doi.org/10.5194/esurf-3-559-2015

Costa, J.E., Schuster, R.L., 1988. The formation and failure of natural dams. Geol. Soc. Am. Bull. 100, 1054–1068.

Coussot, P., Meunier, M., 1996. Recognition, classification and mechanical description of debris flows. Earth-Sci. Rev. 40, 209–227.

Cui, P., Dang, C., Cheng, Z., Scott, K.M., 2010. Debris Flows Resulting From Glacial-Lake Outburst Floods in Tibet, China. Phys. Geogr. 31, 508–527. https://doi.org/10.2747/0272-3646.31.6.508

Das, S., Kar, N.S., Bandyopadhyay, S., 2015. Glacial lake outburst flood at Kedarnath, Indian Himalaya: a study using digital elevation models and satellite images. Nat. Hazards 77, 769–786. https://doi.org/10.1007/s11069-015-1629-6

Dehecq, A., Gourmelen, N., Gardner, A.S., Brun, F., Goldberg, D., Nienow, P.W., Berthier, E., Vincent, C., Wagnon, P., Trouvé, E., 2019. Twenty-first century glacier slowdown driven by mass loss in High Mountain Asia. Nat. Geosci. 12, 22–27. https://doi.org/10.1038/s41561-018-0271-9

DeVries, B., Verbesselt, J., Kooistra, L., Herold, M., 2015. Robust monitoring of small-scale forest disturbances in a tropical montane forest using Landsat time series. Remote Sens. Environ. 161, 107–121. https://doi.org/10.1016/j.rse.2015.02.012

Emmer, A., 2018. GLOFs in the WOS: bibliometrics, geographies and global trends of research on glacial lake outburst floods (Web of Science, 1979–2016). Nat. Hazards Earth Syst. Sci. 18, 813–827. https://doi.org/10.5194/nhess-18-813-2018

Emmer, A., 2017. Geomorphologically effective floods from moraine-dammed lakes in the Cordillera Blanca, Peru. Quat. Sci. Rev. 177, 220–234. https://doi.org/10.1016/j.quascirev.2017.10.028

Emmer, A., Klimeš, J., Mergili, M., Vilímek, V., Cochachin, A., 2016a. 882 lakes of the Cordillera Blanca: An inventory, classification, evolution and assessment of susceptibility to outburst floods. CATENA 147, 269–279. https://doi.org/10.1016/j.catena.2016.07.032

Emmer, A., Merkl, S., Mergili, M., 2015. Spatiotemporal patterns of high-mountain lakes and related hazards in western Austria. Geomorphology 246, 602–616. https://doi.org/10.1016/j.geomorph.2015.06.032

Emmer, A., Vilímek, V., 2013. Review Article: Lake and breach hazard assessment for moraine-dammed lakes: an example from the Cordillera Blanca (Peru). Nat. Hazards Earth Syst. Sci. 13, 1551–1565. https://doi.org/10.5194/nhess-13-1551-2013

Emmer, A., Vilímek, V., Huggel, C., Klimeš, J., Schaub, Y., 2016b. Limits and challenges to compiling and developing a database of glacial lake outburst floods. Landslides. https://doi.org/10.1007/s10346-016-0686-6

ESA, 2015. Sentinel-2 User Handbook, ESA Standard Document.

Ester, M., Kriegel, H.-P., Sander, J., Xu, X., others, 1996. A density-based algorithm for discovering clusters in large spatial databases with noise., in: Proceedings of 2nd International Conference on Knowledge Discovery and Data Mining (KDD-96). Presented at the 2nd International Conference on Knowledge Discovery and Data Mining (KDD-96), pp. 226–231.

Foga, S., Scaramuzza, P.L., Guo, S., Zhu, Z., Dilley, R.D., Beckmann, T., Schmidt, G.L., Dwyer, J.L., Joseph Hughes, M., Laue, B., 2017. Cloud detection algorithm comparison and validation for operational Landsat data products. Remote Sens. Environ. 194, 379–390. https://doi.org/10.1016/j.rse.2017.03.026

Foody, G.M., Boyd, D.S., 1999. Detection of partial land cover change associated with the migration of inter-class transitional zones. Int. J. Remote Sens. 20, 2723–2740. https://doi.org/10.1080/014311699211769

Fraser, R., Olthof, I., Kokelj, S., Lantz, T., Lacelle, D., Brooker, A., Wolfe, S., Schwarz, S., 2014. Detecting Landscape Changes in High Latitude Environments Using Landsat Trend Analysis: 1. Visualization. Remote Sens. 6, 11533–11557. https://doi.org/10.3390/rs61111533

Frey, H., Huggel, C., Chisolm, R.E., Baer, P., McArdell, B., Cochachin, A., Portocarrero, C., 2018. Multi-Source Glacial Lake Outburst Flood Hazard Assessment and Mapping for Huaraz, Cordillera Blanca, Peru. Front. Earth Sci. 6. https://doi.org/10.3389/feart.2018.00210

Frey, H., Machguth, H., Huss, M., Huggel, C., Bajracharya, S., Bolch, T., Kulkarni, A., Linsbauer, A., Salzmann, N., Stoffel, M., 2014. Estimating the volume of glaciers in the Himalayan-Karakoram region using different methods. The Cryosphere 8, 2313–2333. https://doi.org/10.5194/tc-8-2313-2014

Fujita, K., Sakai, A., Takenaka, S., Nuimura, T., Surazakov, A.B., Sawagaki, T., Yamanokuchi, T., 2013. Potential flood volume of Himalayan glacial lakes. Nat. Hazards Earth Syst. Sci. 13, 1827–1839. https://doi.org/10.5194/nhess-13-1827-2013

Fujita, K., Suzuki, R., Nuimura, T., Sakai, A., 2008. Performance of ASTER and SRTM DEMs, and their potential for assessing glacial lakes in the Lunana region, Bhutan Himalaya. J. Glaciol. 54, 220–228.

Fukui, K., Fujii, Y., Ageta, Y., Asahi, K., 2007. Changes in the lower limit of mountain permafrost between 1973 and 2004 in the Khumbu Himal, the Nepal Himalayas. Glob. Planet. Change 55, 251–256. https://doi.org/10.1016/j.gloplacha.2006.06.002

GAPHAZ, 2017. Assessment of Glacier and Permafrost Hazards in Mountain Regions – Technical Guidance Document. Prepared by Allen, S., Frey, H., Huggel, C. et al. Standing Group on Glacier and Permafrost Hazards in Mountains (GAPHAZ) of the International Association of Cryospheric Sciences (IACS) and the International Permafrost Association (IPA). Zurich, Switzerland / Lima, Peru.

Gardelle, J., Arnaud, Y., Berthier, E., 2011. Contrasted evolution of glacial lakes along the Hindu Kush Himalaya mountain range between 1990 and 2009. Glob. Planet. Change 75, 47–55. https://doi.org/10.1016/j.gloplacha.2010.10.003

Gardelle, J., Berthier, E., Arnaud, Y., 2012. Slight mass gain of Karakoram glaciers in the early twenty-first century. Nat. Geosci. 5, 322–325. https://doi.org/10.1038/ngeo1450

Gilleland, E., Katz, R.W., 2016. extRemes 2.0: An Extreme Value Analysis Package in R. J. Stat. Softw. 72. https://doi.org/10.18637/jss.v072.i08

Gimbert, F., Cook, K., Andermann, C., Hovius, N., Turowski, J., 2017. Using seismic arrays to quantify the physics of a glacial outburst flood and its legacy on upland river dynamics. Geophys. Res. Abstr. 19.

Grabs, W.E., Hanisch, J., 1993. Objectives and Prevention Methods for Glacier Lake Outburst Moods (GLOFs). Snow Glacier Hydrol, IAHS Publications 218, 341–352.

Griffiths, P., Kuemmerle, T., Baumann, M., Radeloff, V.C., Abrudan, I.V., Lieskovsky, J., Munteanu, C., Ostapowicz, K., Hostert, P., 2014. Forest disturbances, forest recovery, and changes in forest types across the Carpathian ecoregion from 1985 to 2010 based on Landsat image composites. Remote Sens. Environ. 151, 72–88. https://doi.org/10.1016/j.rse.2013.04.022

Gruber, S., Fleiner, R., Guegan, E., Panday, P., Schmid, M.-O., Stumm, D., Wester, P., Zhang, Y., Zhao, L., 2017. Review article: Inferring permafrost and permafrost thaw in the mountains of the Hindu Kush Himalaya region. The Cryosphere 11, 81–99. https://doi.org/10.5194/tc-11-81-2017

Gurung, D.R., Khanal, N.R., Bajracharya, S.R., Tsering, K., Joshi, S., Tshering, P., Chhetri, L.K., Lotay, Y., Penjor, T., 2017. Lemthang Tsho glacial Lake outburst flood (GLOF) in Bhutan: cause and impact. Geoenvironmental Disasters 4, 4–17. https://doi.org/10.1186/s40677-017-0080-2

Haeberli, W., Schaub, Y., Huggel, C., 2017. Increasing risks related to landslides from degrading permafrost into new lakes in de-glaciating mountain ranges. Geomorphology 293, 405–417. https://doi.org/10.1016/j.geomorph.2016.02.009

Haritashya, U., Kargel, J., Shugar, D., Leonard, G., Strattman, K., Watson, C., Shean, D., Harrison, S., Mandli, K., Regmi, D., 2018. Evolution and Controls of Large Glacial Lakes in the Nepal Himalaya. Remote Sens. 10, 798. https://doi.org/10.3390/rs10050798

Harrison, S., Glasser, N., Winchester, V., Haresign, E., Warren, C., Jansson, K., 2006. A glacial lake outburst flood associated with recent mountain glacier retreat, Patagonian Andes. The Holocene 16, 611–620.

Harrison, S., Kargel, J.S., Huggel, C., Reynolds, J., Shugar, D.H., Betts, R.A., Emmer, A., Glasser, N., Haritashya, U.K., Klimeš, J., Reinhardt, L., Schaub, Y., Wiltshire, A., Regmi, D., Vilímek, V., 2018. Climate change and the global pattern of moraine-dammed glacial lake outburst floods. The Cryosphere 12, 1195–1209. https://doi.org/10.5194/tc-12-1195-2018

Harrison, S., Kargel, J.S., Huggel, C., Reynolds, J., Shugar, D.H., Betts, R.A., Emmer, A., Glasser, N., Haritashya, U.K., Klimeš, J., Reinhardt, L., Schaub, Y., Wilyshire, A., Regmi, D., Vilímek, V., 2017. Climate change and the global pattern of moraine-dammed glacial lake outburst floods. Cryosphere Discuss. 1–28. https://doi.org/10.5194/tc-2017-203

Hermosilla, T., Wulder, M.A., White, J.C., Coops, N.C., Hobart, G.W., 2015. An integrated Landsat time series protocol for change detection and generation of annual gap-free surface reflectance composites. Remote Sens. Environ. 158, 220–234. https://doi.org/10.1016/j.rse.2014.11.005

Hermosilla, T., Wulder, M.A., White, J.C., Coops, N.C., Hobart, G.W., Campbell, L.B., 2016. Mass data processing of time series Landsat imagery: pixels to data products for forest monitoring. Int. J. Digit. Earth 1–20. https://doi.org/10.1080/17538947.2016.1187673

Hewitt, K., 2014. Glaciers of the Karakoram Himalaya, Advances in Asian Human-Environmental Research. Springer Netherlands, Dordrecht.

Hewitt, K., Liu, J., 2010. Ice-Dammed Lakes and Outburst Floods, Karakoram Himalaya: Historical Perspectives on Emerging Threats. Phys. Geogr. 31, 528–551. https://doi.org/10.2747/0272-3646.31.6.528

Hirabayashi, Y., Mahendran, R., Koirala, S., Konoshima, L., Yamazaki, D., Watanabe, S., Kim, H., Kanae, S., 2013. Global flood risk under climate change. Nat. Clim. Change 3, 816–821. https://doi.org/10.1038/nclimate1911

Holzer, N., Vijay, S., Yao, T., Xu, B., Buchroithner, M., Bolch, T., 2015. Four decades of glacier variations at Muztagh Ata (eastern Pamir): a multi-sensor study including Hexagon KH-9 and Pl?iades data. The Cryosphere 9, 2071–2088. https://doi.org/10.5194/tc-9-2071-2015

Horspool, N., Pranantyo, I., Griffin, J., Latief, H., Natawidjaja, D.H., Kongko, W., Cipta, A., Bustaman, B., Anugrah, S.D., Thio, H.K., 2014. A probabilistic tsunami hazard assessment for Indonesia. Nat. Hazards Earth Syst. Sci. 14, 3105–3122. https://doi.org/10.5194/nhess-14-3105-2014

Hubbard, B., Heald, A., Reynolds, J.M., Quincey, D., Richardson, S.D., Luyo, M.Z., Portilla, N.S., Hambrey, M.J., 2005. Impact of a rock avalanche on a moraine-dammed proglacial lake: Laguna Safuna Alta, Cordillera Blanca, Peru. Earth Surf. Process. Landf. 30, 1251–1264. https://doi.org/10.1002/esp.1198

Huggel, C., Clague, J.J., Korup, O., 2012. Is climate change responsible for changing landslide activity in high mountains? Earth Surf. Process. Landf. 37, 77–91. https://doi.org/10.1002/esp.2223

Hungr, O., 1995. A model for the runout analysis of rapid flow slides, debris flows, and avalanches. Can. Geotech. J. 32, 610–623.

Huss, M., Bookhagen, B., Huggel, C., Jacobsen, D., Bradley, R.S., Clague, J.J., Vuille, M., Buytaert, W., Cayan, D.R., Greenwood, G., Mark, B.G., Milner, A.M., Weingartner, R., Winder, M., 2017. Toward mountains without permanent snow and ice. Earths Future 5, 418–435. https://doi.org/10.1002/2016EF000514

Huss, M., Hock, R., 2018. Global-scale hydrological response to future glacier mass loss. Nat. Clim. Change 8, 135–140. https://doi.org/10.1038/s41558-017-0049-x

International Association of Oil & Gas Producers, 2016. Geomatics Guidance Note 7, part 2: Coordinate Conversions & Transformations including Formulas (No. 373-7–2).

IPCC, 2007. Climate change 2007: the physical science basis: contribution of Working Group I to the Fourth Assessment Report of the Intergovernmental Panel on Climate Change, M.L. Parry, O.F. Canziani, J.P. Palutikof, P.J. van der Linden and C.E. Hanson, Eds. Cambridge University Press, Cambridge ; New York.

Iribarren Anacona, P., Mackintosh, A., Norton, K.P., 2015. Hazardous processes and events from glacier and permafrost areas: lessons from the Chilean and Argentinean Andes. Earth Surf. Process. Landf. 40, 2–21. https://doi.org/10.1002/esp.3524

Iturrizaga, L., 2011. Glacier Lake Outburst Floods, in: Singh, V.P., Singh, P., Haritashya, U.K. (Eds.), Encyclopedia of Snow, Ice and Glaciers. Springer Netherlands, Dordrecht, pp. 381–399.

Iturrizaga, L., 2005. Historical glacier-dammed lakes and outburst floods in the Karambar valley (Hindukush-Karakoram). GeoJournal 63, 1–47.

Ives, J.D., Shrestha, R., Mool, P., others, 2010. Formation of glacial lakes in the Hindu Kush-Himalayas and GLOF risk assessment. ICIMOD Kathmandu.

Jacquet, J., McCoy, S.W., McGrath, D., Nimick, D.A., Fahey, M., O'kuinghttons, J., Friesen, B.A., Leidich, J., 2017. Hydrologic and geomorphic changes resulting from episodic glacial lake outburst floods: Rio Colonia, Patagonia, Chile. Geophys. Res. Lett. 44, 854–864. https://doi.org/10.1002/2016GL071374

Jain, S.K., Lohani, A.K., Singh, R.D., Chaudhary, A., Thakural, L.N., 2012. Glacial lakes and glacial lake outburst flood in a Himalayan basin using remote sensing and GIS. Nat. Hazards 62, 887–899. https://doi.org/10.1007/s11069-012-0120-x

Jamali, S., Jönsson, P., Eklundh, L., Ardö, J., Seaquist, J., 2015. Detecting changes in vegetation trends using time series segmentation. Remote Sens. Environ. 156, 182–195. https://doi.org/10.1016/j.rse.2014.09.010

Jóhannesson, T., Raymond, C., Waddington, E.D., 1989. Time–scale for adjustment of glaciers to changes in mass balance. J. Glaciol. 35, 355–369.

Kääb, A., Berthier, E., Nuth, C., Gardelle, J., Arnaud, Y., 2012. Contrasting patterns of early twenty-first-century glacier mass change in the Himalayas. Nature 488, 495–498. https://doi.org/10.1038/nature11324

Kääb, A., Treichler, D., Nuth, C., Berthier, E., 2015. Brief Communication: Contending estimates of 2003-2008 glacier mass balance over the Pamir-Karakoram-Himalaya. The Cryosphere 9, 557–564. https://doi.org/10.5194/tc-9-557-2015

Kargel, J.S., Leonard, G.J., Shugar, D.H., Haritashya, U.K., Bevington, A., Fielding, E.J., Fujita, K., Geertsema, M., Miles, E.S., Steiner, J., Anderson, E., Bajracharya, S., Bawden, G.W., Breashears, D.F., Byers, A., Collins, B., Dhital, M.R., Donnellan, A., Evans, T.L., Geai, M.L., Glasscoe, M.T., Green, D., Gurung, D.R., Heijenk, R., Hilborn, A., Hudnut, K., Huyck, C., Immerzeel, W.W., Liming, J., Jibson, R., Kaab, A., Khanal, N.R., Kirschbaum, D., Kraaijenbrink, P.D.A., Lamsal, D., Shiyin, L., Mingyang, L., McKinney, D., Nahirnick, N.K., Zhuotong, N., Ojha, S., Olsenholler, J., Painter, T.H., Pleasants, M., Pratima, K.C., Yuan, Q.I., Raup, B.H., Regmi, D., Rounce, D.R., Sakai, A., Donghui, S., Shea, J.M., Shrestha, A.B., Shukla, A., Stumm, D., van der Kooij, M., Voss, K., Xin, W., Weihs, B., Wolfe, D., Lizong, W., Xiaojun, Y., Yoder, M.R., Young, N., 2016. Geomorphic and geologic controls of geohazards induced by Nepals 2015 Gorkha earthquake. Science 351, aac8353-1-10. https://doi.org/10.1126/science.aac8353

Kaser, G., Gro\s shauser, M., Marzeion, B., 2010. Contribution potential of glaciers to water availability in different climate regimes. Proc. Natl. Acad. Sci.

Kattelmann, R., 2003. Glacial lake outburst floods in the Nepal Himalaya: a manageable hazard? Nat. Hazards 28, 145–154.

Kattelmann, R., Watanabe, T., 1997. Draining Himalayan glacial lakes before they burst. IAHS Publ.-Ser. Proc. Rep.-Intern Assoc Hydrol. Sci. 239, 337–344.

Katz, R.W., Parlange, M.B., Naveau, P., 2002. Statistics of extremes in hydrology. Adv. Water Resour. 25, 1287–1304.

Kennedy, R.E., Yang, Z., Cohen, W.B., 2010. Detecting trends in forest disturbance and recovery using yearly Landsat time series: 1. LandTrendr — Temporal segmentation algorithms. Remote Sens. Environ. 114, 2897–2910. https://doi.org/10.1016/j.rse.2010.07.008

Kershaw, J.A., Clague, J.J., Evans, S.G., 2005. Geomorphic and sedimentological signature of a two-phase outburst flood from moraine-dammed Queen Bess Lake, British Columbia, Canada. Earth Surf. Process. Landf. 30, 1–25. https://doi.org/10.1002/esp.1122

Khadka, N., Zhang, G., Thakuri, S., 2018. Glacial Lakes in the Nepal Himalaya: Inventory and Decadal Dynamics (1977–2017). Remote Sens. 10, 1913. https://doi.org/10.3390/rs10121913

King, O., Dehecq, A., Quincey, D., Carrivick, J., 2018. Contrasting geometric and dynamic evolution of lake and land-terminating glaciers in the central Himalaya. Glob. Planet. Change 167, 46–60. https://doi.org/10.1016/j.gloplacha.2018.05.006

Klees, R., Massonnet, D., 1998. Deformation measurements using SAR interferometry: potential and limitations. Geol. En Mijnb. 77, 161–176.

Komori, J., 2008. Recent expansions of glacial lakes in the Bhutan Himalayas. Quat. Int. 184, 177–186. https://doi.org/10.1016/j.quaint.2007.09.012

Komori, J., Koike, T., Yamanokuchi, T., Tshering, P., 2012. Glacial lake outburst events in the Bhutan Himalayas. Glob. Env. Res 16, 59–70.

Korup, O., Tweed, F., 2007. Ice, moraine, and landslide dams in mountainous terrain. Quat. Sci. Rev. 26, 3406–3422. https://doi.org/10.1016/j.quascirev.2007.10.012

Kraaijenbrink, P.D.A., Bierkens, M.F.P., Lutz, A.F., Immerzeel, W.W., 2017. Impact of a global temperature rise of 1.5 degrees Celsius on Asia's glaciers. Nature 549, 257–260. https://doi.org/10.1038/nature23878

Krishnan, R., Shrestha, A.B., Ren, G., Rajbhandari, R., Saeed, S., Sanjay, J., Syed, M.A., Vellore, R., Xu, Y., You, Q., 2019. Unravelling Climate Change in the Hindu Kush Himalaya: Rapid

Warming in the Mountains and Increasing Extremes, in: The Hindu Kush Himalaya Assessment. Springer, pp. 57–97.
Lala, J.M., Rounce, D.R., McKinney, D.C., 2018. Modeling the glacial lake outburst flood process chain in the Nepal Himalaya: reassessing Imja Tsho's hazard. Hydrol. Earth Syst. Sci. 22, 3721–3737. https://doi.org/10.5194/hess-22-3721-2018
Lamsal, D., Sawagaki, T., Watanabe, T., Byers, A.C., McKinney, D.C., 2015. An assessment of conditions before and after the 1998 Tam Pokhari outburst in the Nepal Himalaya and an evaluation of the future outburst hazard. Hydrol. Process.
Lang, K.A., Huntington, K.W., Montgomery, D.R., 2013. Erosion of the Tsangpo Gorge by megafloods, eastern Himalaya. Geology 41, 1003–1006.
Lewin, J., Macklin, M.G., 2003. Preservation potential for Late Quaternary river alluvium. J. Quat. Sci. 18, 107–120. https://doi.org/10.1002/jqs.738
Li, J., Sheng, Y., 2012. An automated scheme for glacial lake dynamics mapping using Landsat imagery and digital elevation models: a case study in the Himalayas. Int. J. Remote Sens. 33, 5194–5213. https://doi.org/10.1080/01431161.2012.657370
Linsbauer, A., Frey, H., Haeberli, W., Machguth, H., Azam, M.F., Allen, S., 2016. Modelling glacier-bed overdeepenings and possible future lakes for the glaciers in the Himalaya—Karakoram region. Ann. Glaciol. 57, 119–130. https://doi.org/10.3189/2016AoG71A627
Lippitt, C.D., Rogan, J., Li, Z., Eastman, J.R., Jones, T.G., 2008. Mapping selective logging in mixed deciduous forest. Photogramm. Eng. Remote Sens. 74, 1201–1211.
Liu, J., Tang, C., Cheng, Z., 2013. The two main mechanisms of Glacier Lake Outburst Flood in Tibet, China. J. Mt. Sci. 10, 239–248. https://doi.org/10.1007/s11629-013-2517-8
Liu, J.-J., Cheng, Z.-L., Su, P.-C., 2014. The relationship between air temperature fluctuation and Glacial Lake Outburst Floods in Tibet, China. Quat. Int. 321, 78–87. https://doi.org/10.1016/j.quaint.2013.11.023
Liu, S.S., Donghui, S., Junli, X., Xin, W., Xiaojun, Y., Zongli, J., Wanqin, G., Anxin, L., Shiqiang, Z., Baisheng, Y., Zhen, L., Junfeng, W., Lizong, W., 2014. Glaciers in China and Their Variations, in: Kargel, J.S., Leonard, G.J., Bishop, M.P., Kääb, A., Raup, B.H. (Eds.), Global Land Ice Measurements from Space. Springer Berlin Heidelberg, Berlin, Heidelberg, pp. 583–608.
Lliboutry, L., Arnao, B.M., Pautre, A., Schneider, B., 1977. Glaciological problems set by the control of dangerous lakes in Cordillera Blanca, Peru. I. Historical failures of morainic dams, their causes and prevention. J. Glaciol. 18, 239–254.
Lutz, A.F., Immerzeel, W.W., Shrestha, A.B., Bierkens, M.F.P., 2014. Consistent increase in High Asia's runoff due to increasing glacier melt and precipitation. Nat. Clim. Change 4, 587–592. https://doi.org/10.1038/nclimate2237
Maharjan, S.B., Mool, P.K., Lizong, W., Xiao, G., Shrestha, F., Shrestha, R.B., Khanal, N.R., Bajracharya, S.R., Joshi, S., Shai, S., 2018. The Status of Glacial Lakes in the Hindu Kush Himalaya-ICIMOD Research Report 2018/1. Kathmandu: ICIMOD.
Marc, O., Behling, R., Andermann, C., Turowski, J.M., Illien, L., Roessner, S., Hovius, N., 2019. Long-term erosion of the Nepal Himalayas by bedrock landsliding: the role of monsoons, earthquakes and giant landslides. Earth Surf. Dyn. 7, 107–128. https://doi.org/10.5194/esurf-7-107-2019
Markham, B.L., Storey, J.C., Williams, D.L., Irons, J.R., 2004. Landsat sensor performance: history and current status. IEEE Trans. Geosci. Remote Sens. 42, 2691–2694. https://doi.org/10.1109/TGRS.2004.840720
Martinuzzi, S., Gould, W.A., González, O.M.R., 2007. Creating cloud-free Landsat ETM+ data sets in tropical landscapes: cloud and cloud-shadow removal.
Maurer, J., Rupper, S., 2015. Tapping into the Hexagon spy imagery database: A new automated pipeline for geomorphic change detection. ISPRS J. Photogramm. Remote Sens. 108, 113–127. https://doi.org/10.1016/j.isprsjprs.2015.06.008

Maurer, J.M., Rupper, S.B., Schaefer, J.M., 2016. Quantifying ice loss in the eastern Himalayas since 1974 using declassified spy satellite imagery. The Cryosphere 10, 2203–2215. https://doi.org/10.5194/tc-10-2203-2016

Maussion, F., Scherer, D., Mölg, T., Collier, E., Curio, J., Finkelnburg, R., 2014. Precipitation seasonality and variability over the Tibetan Plateau as resolved by the High Asia Reanalysis. J. Clim. 27, 1910–1927.

McFeeters, S.K., 1996. The use of the Normalized Difference Water Index (NDWI) in the delineation of open water features. Int. J. Remote Sens. 17, 1425–1432. https://doi.org/10.1080/01431169608948714

McKillop, R.J., Clague, J.J., 2007. Statistical, remote sensing-based approach for estimating the probability of catastrophic drainage from moraine-dammed lakes in southwestern British Columbia. Glob. Planet. Change 56, 153–171. https://doi.org/10.1016/j.gloplacha.2006.07.004

Metternicht, G., 1999. Change detection assessment using fuzzy sets and remotely sensed data: an application of topographic map revision. ISPRS J. Photogramm. Remote Sens. 54, 221–233.

Miles, E.S., Watson, C.S., Brun, F., Berthier, E., Esteves, M., Quincey, D.J., Miles, K.E., Hubbard, B., Wagnon, P., 2018a. Glacial and geomorphic effects of a supraglacial lake drainage and outburst event, Everest region, Nepal Himalaya. The Cryosphere 12, 3891–3905. https://doi.org/10.5194/tc-12-3891-2018

Miles, E.S., Willis, I., Buri, P., Steiner, J.F., Arnold, N.S., Pellicciotti, F., 2018b. Surface Pond Energy Absorption Across Four Himalayan Glaciers Accounts for 1/8 of Total Catchment Ice Loss. Geophys. Res. Lett. 45, 10,464-10,473. https://doi.org/10.1029/2018GL079678

Miles, E.S., Willis, I.C., Arnold, N.S., Steiner, J., Pellicciotti, F., 2017. Spatial, seasonal and interannual variability of supraglacial ponds in the Langtang Valley of Nepal, 1999-2013. J. Glaciol. 63, 88–105. https://doi.org/10.1017/jog.2016.120

Montgomery, D.R., Hallet, B., Yuping, L., Finnegan, N., Anders, A., Gillespie, A., Greenberg, H.M., 2004. Evidence for Holocene megafloods down the tsangpo River gorge, Southeastern Tibet. Quat. Res. 62, 201–207. https://doi.org/10.1016/j.yqres.2004.06.008

Mool, P.K., 1995. Glacier Lake Outburst Floods in Nepal. J. Nepal Geol. Soc. 11, 273–280.

Mueller, N., Lewis, A., Roberts, D., Ring, S., Melrose, R., Sixsmith, J., Lymburner, L., McIntyre, A., Tan, P., Curnow, S., Ip, A., 2016. Water observations from space: Mapping surface water from 25years of Landsat imagery across Australia. Remote Sens. Environ. 174, 341–352. https://doi.org/10.1016/j.rse.2015.11.003

Nagai, H., Ukita, J., Narama, C., Fujita, K., Sakai, A., Tadono, T., Yamanokuchi, T., Tomiyama, N., 2017. Evaluating the Scale and Potential of GLOF in the Bhutan Himalayas Using a Satellite-Based Integral Glacier–Glacial Lake Inventory. Geosciences 7, 77. https://doi.org/10.3390/geosciences7030077

Nepal, S., Shrestha, A.B., 2015. Impact of climate change on the hydrological regime of the Indus, Ganges and Brahmaputra river basins: a review of the literature. Int. J. Water Resour. Dev. 31, 201–218. https://doi.org/10.1080/07900627.2015.1030494

Nie, Y., Liu, Q., Liu, S., 2013. Glacial lake expansion in the Central Himalayas by Landsat images, 1990–2010.

Nie, Y., Liu, Q., Wang, J., Zhang, Y., Sheng, Y., Liu, S., 2018. An inventory of historical glacial lake outburst floods in the Himalayas based on remote sensing observations and geomorphological analysis. Geomorphology 308, 91–106. https://doi.org/10.1016/j.geomorph.2018.02.002

Nie, Y., Sheng, Y., Liu, Q., Liu, L., Liu, S., Zhang, Y., Song, C., 2017. A regional-scale assessment of Himalayan glacial lake changes using satellite observations from 1990 to 2015. Remote Sens. Environ. 189, 1–13. https://doi.org/10.1016/j.rse.2016.11.008

Nitze, I., Grosse, G., 2016. Detection of landscape dynamics in the Arctic Lena Delta with temporally dense Landsat time-series stacks. Remote Sens. Environ. 181, 27–41. https://doi.org/10.1016/j.rse.2016.03.038

O'Connor, J.E., Beebee, R.A., 2009. Floods from natural rock-material dams. Megaflooding Earth Mars 128–163.

O'Connor, J.E., Clague, J.J., Walder, J.S., Manville, V., Beebee, R.A., 2013. Outburst Floods, in: Treatise on Geomorphology. Elsevier, pp. 475–510.

Olofsson, P., Foody, G.M., Stehman, S.V., Woodcock, C.E., 2013. Making better use of accuracy data in land change studies: Estimating accuracy and area and quantifying uncertainty using stratified estimation. Remote Sens. Environ. 129, 122–131. https://doi.org/10.1016/j.rse.2012.10.031

Olthof, I., Fraser, R.H., Schmitt, C., 2015. Landsat-based mapping of thermokarst lake dynamics on the Tuktoyaktuk Coastal Plain, Northwest Territories, Canada since 1985. Remote Sens. Environ. 168, 194–204. https://doi.org/10.1016/j.rse.2015.07.001

Osti, R., Bhattarai, T.N., Miyake, K., 2011. Causes of catastrophic failure of Tam Pokhari moraine dam in the Mt. Everest region. Nat. Hazards 58, 1209–1223. https://doi.org/10.1007/s11069-011-9723-x

Osti, R., Egashira, S., 2009. Hydrodynamic characteristics of the Tam Pokhari glacial lake outburst flood in the Mt. Everest region, Nepal. Hydrol. Process. 23, 2943–2955. https://doi.org/10.1002/hyp.7405

Parker, J.A., Kenyon, R.V., Troxel, D.E., 1983. Comparison of interpolating methods for image resampling. IEEE Trans. Med. Imaging 2, 31–39.

Pekel, J.-F., Cottam, A., Gorelick, N., Belward, A.S., 2016. High-resolution mapping of global surface water and its long-term changes. Nature 540, 418–422. https://doi.org/10.1038/nature20584

Pfeffer, W.T., Arendt, A.A., Bliss, A., Bolch, T., Cogley, J.G., Gardner, A.S., Hagen, J.-O., Hock, R., Kaser, G., Kienholz, C., Miles, E.S., Moholdt, G., Mölg, N., Paul, F., Radić, V., Rastner, P., Raup, B.H., Rich, J., Sharp, M.J., 2014. The Randolph Glacier Inventory: a globally complete inventory of glaciers. J. Glaciol. 60, 537–552. https://doi.org/10.3189/2014JoG13J176

Pflugmacher, D., Cohen, W.B., E. Kennedy, R., 2012. Using Landsat-derived disturbance history (1972–2010) to predict current forest structure. Remote Sens. Environ. 122, 146–165. https://doi.org/10.1016/j.rse.2011.09.025

Planet Labs, 2018. Planet Imagery Product Specifications.

Prakash, C., Nagarajan, R., 2017. Outburst susceptibility assessment of moraine-dammed lakes in Western Himalaya using an analytic hierarchy process: GLOF susceptibility assessment using AHP. Earth Surf. Process. Landf. 42, 2306–2321. https://doi.org/10.1002/esp.4185

Qi, J., Chehbouni, A., Huete, A.R., Kerr, Y.H., Sorooshian, S., 1994. A modified soil adjusted vegetation index. Remote Sens. Environ. 48, 119–126.

Quincey, D.J., Braun, M., Glasser, N.F., Bishop, M.P., Hewitt, K., Luckman, A., 2011. Karakoram glacier surge dynamics. Geophys. Res. Lett. 38, 1–6. https://doi.org/10.1029/2011GL049004

Quincey, D.J., Richardson, S.D., Luckman, A., Lucas, R.M., Reynolds, J.M., Hambrey, M.J., Glasser, N.F., 2007. Early recognition of glacial lake hazards in the Himalaya using remote sensing datasets. Glob. Planet. Change 56, 137–152. https://doi.org/10.1016/j.gloplacha.2006.07.013

Rankl, M., Kienholz, C., Braun, M., 2014. Glacier changes in the Karakoram region mapped by multimission satellite imagery. The Cryosphere 8, 977–989. https://doi.org/10.5194/tc-8-977-2014

Richardson, S.D., Reynolds, J.M., 2000. An overview of glacial hazards in the Himalayas. Quat. Int. 65, 31–47.

Rickenmann, D., 1999. Empirical relationships for debris flows. Nat. Hazards 19, 47–77.

Riggs, G.A., Hall, D.K., Salomonson, 1994. A snow index for the Landsat Thematic Mapper and Moderate Resolution Imaging Spectroradiometer. Presented at the Geoscience and Remote Sensing Symposium, 1994. IGARSS '94. Surface and Atmospheric Remote Sensing: Technologies, Data Analysis and Interpretation, pp. 1942–1944 vol.4. https://doi.org/10.1109/IGARSS.1994.399618

Rodriguez-Galiano, V.F., Ghimire, B., Rogan, J., Chica-Olmo, M., Rigol-Sanchez, J.P., 2012. An assessment of the effectiveness of a random forest classifier for land-cover classification. ISPRS J. Photogramm. Remote Sens. 67, 93–104. https://doi.org/10.1016/j.isprsjprs.2011.11.002

Rounce, D., Byers, A.C., Byers, E.A., McKinney, D.C., 2017a. Brief communication: Observations of a glacier outburst flood from Lhotse Glacier, Everest area, Nepal. The Cryosphere 11, 443–449. https://doi.org/10.5194/tc-11-443-2017

Rounce, D., Watson, C., McKinney, D., 2017b. Identification of Hazard and Risk for Glacial Lakes in the Nepal Himalaya Using Satellite Imagery from 2000–2015. Remote Sens. 9, 654. https://doi.org/10.3390/rs9070654

Rounce, D.R., McKinney, D.C., Lala, J.M., Byers, A.C., Watson, C.S., 2016. A new remote hazard and risk assessment framework for glacial lakes in the Nepal Himalaya. Hydrol. Earth Syst. Sci. 20, 3455–3475. https://doi.org/10.5194/hess-20-3455-2016

Round, V., Leinss, S., Huss, M., Haemmig, C., Hajnsek, I., 2017. Surge dynamics and lake outbursts of Kyagar Glacier, Karakoram. The Cryosphere 11, 723–739. https://doi.org/10.5194/tc-11-723-2017

Rouse Jr, J., Haas, R.H., Schell, J.A., Deering, D.W., 1974. Monitoring vegetation systems in the Great Plains with ERTS.

Rover, J., Ji, L., Wylie, B.K., Tieszen, L.L., 2012. Establishing water body areal extent trends in interior Alaska from multi-temporal Landsat data. Remote Sens. Lett. 3, 595–604. https://doi.org/10.1080/01431161.2011.643507

Rowan, A.V., 2017. The "Little Ice Age"in the Himalaya: A review of glacier advance driven by Northern Hemisphere temperature change. The Holocene 27, 292–308.

Rowan, A.V., Egholm, D.L., Quincey, D.J., Glasser, N.F., 2015. Modelling the feedbacks between mass balance, ice flow and debris transport to predict the response to climate change of debris-covered glaciers in the Himalaya. Earth Planet. Sci. Lett. 430, 427–438. https://doi.org/10.1016/j.epsl.2015.09.004

Sakai, A., Chikita, K., Yamada, T., 2000. Expansion of a moraine-dammed glacial lake, Tsho Rolpa, in Rolwaling Himal, Nepal Himalaya. Limnol. Oceanogr. 45, 1401–1408.

Salerno, F., Thakuri, S., D'Agata, C., Smiraglia, C., Manfredi, E.C., Viviano, G., Tartari, G., 2012. Glacial lake distribution in the Mount Everest region: Uncertainty of measurement and conditions of formation. Glob. Planet. Change 92–93, 30–39. https://doi.org/10.1016/j.gloplacha.2012.04.001

Sampson, C.C., Smith, A.M., Bates, P.D., Neal, J.C., Alfieri, L., Freer, J.E., 2015. A high-resolution global flood hazard model. Water Resour. Res. 51, 7358–7381. https://doi.org/10.1002/2015WR016954

Scherler, D., Munack, H., Mey, J., Eugster, P., Wittmann, H., Codilean, A.T., Kubik, P., Strecker, M.R., 2014. Ice dams, outburst floods, and glacial incision at the western margin of the Tibetan Plateau: A> 100 ky chronology from the Shyok Valley, Karakoram. Geol. Soc. Am. Bull. 126, 738–758.

Schneider, D., Huggel, C., Cochachin, A., Guillén, S., García, J., 2014. Mapping hazards from glacier lake outburst floods based on modelling of process cascades at Lake 513, Carhuaz, Peru. Adv. Geosci. 35, 145–155. https://doi.org/10.5194/adgeo-35-145-2014

Schneider, D., Huggel, C., Haeberli, W., Kaitna, R., 2011. Unraveling driving factors for large rock-ice avalanche mobility. Earth Surf. Process. Landf. 36, 1948–1966. https://doi.org/10.1002/esp.2218

Schroeder, T.A., Wulder, M.A., Healey, S.P., Moisen, G.G., 2011. Mapping wildfire and clearcut harvest disturbances in boreal forests with Landsat time series data. Remote Sens. Environ. 115, 1421–1433. https://doi.org/10.1016/j.rse.2011.01.022

Schwanghart, W., Bernhardt, A., Stolle, A., Hoelzmann, P., Adhikari, B.R., Andermann, C., Tofelde, S., Merchel, S., Rugel, G., Fort, M., Korup, O., 2016a. Repeated catastrophic valley infill following medieval earthquakes in the Nepal Himalaya. Science 351, 147. https://doi.org/10.1126/science.aac9865

Schwanghart, W., Worni, R., Huggel, C., Stoffel, M., Korup, O., 2016b. Uncertainty in the Himalayan energy–water nexus: estimating regional exposure to glacial lake outburst floods. Environ. Res. Lett. 11, 74005. https://doi.org/10.1088/1748-9326/11/7/074005

Senese, A., Maragno, D., Fugazza, D., Soncini, A., D'Agata, C., Azzoni, R.S., Minora, U., Ul-Hassan, R., Vuillermoz, E., Asif Khan, M., Shafiq Rana, A., Rasul, G., Smiraglia, C., Diolaiuti, G.A., 2018. Inventory of glaciers and glacial lakes of the Central Karakoram National Park (CKNP – Pakistan). J. Maps 14, 189–198. https://doi.org/10.1080/17445647.2018.1445561

Shrestha, A.B., Eriksson, M., Mool, P., Ghimire, P., Mishra, B., Khanal, N.R., 2010. Glacial lake outburst flood risk assessment of Sun Koshi basin, Nepal. Geomat. Nat. Hazards Risk 1, 157–169. https://doi.org/10.1080/19475701003668968

Shrestha, B.B., Nakagawa, H., Kawaike, K., Baba, Y., Zhang, H., 2013. Glacial hazards in the Rolwaling valley of Nepal and numerical approach to predict potential outburst flood from glacial lake. Landslides 10, 299–313. https://doi.org/10.1007/s10346-012-0327-7

Shugar, D.H., Burr, A., Haritashya, U.K., Kargel, J.S., Watson, C., Bevington, A., Steiner, N., Betts, R.A., Harrison, S., Strattman, K., Kennedy, M., 2019. Where are the world's glacial lakes and how big are they?, in: Geophysical Research Abstracts. Presented at the European Geosciences Union General Assembly, Vienna, Austria, p. EGU2019-6153.

Shukla, A., Arora, M.K., Gupta, R.P., 2010. Synergistic approach for mapping debris-covered glaciers using optical thermal remote sensing data with inputs from geomorphometric parameters. Remote Sens. Environ. 114, 1378–1387. https://doi.org/10.1016/j.rse.2010.01.015

Sieg, T., 2019. Reliability of Flood Damage Estimations across Spatial Scales (cumulative). University of Potsdam, Potsdam.

Silva, A.T., Portela, M.M., Naghettini, M., Fernandes, W., 2017. A Bayesian peaks-over-threshold analysis of floods in the Itajaí-açu River under stationarity and nonstationarity. Stoch. Environ. Res. Risk Assess. 31, 185–204. https://doi.org/10.1007/s00477-015-1184-4

Slater, L.J., Singer, M.B., Kirchner, J.W., 2015. Hydrologic versus geomorphic drivers of trends in flood hazard. Geophys. Res. Lett. 42, 370–376. https://doi.org/10.1002/2014GL062482

Smith, B.E., Fricker, H.A., Joughin, I.R., Tulaczyk, S., 2009. An inventory of active subglacial lakes in Antarctica detected by ICESat (2003–2008). J. Glaciol. 55, 573–595.

Somos-Valenzuela, M.A., Chisolm, R.E., Rivas, D.S., Portocarrero, C., McKinney, D.C., 2016. Modeling a glacial lake outburst flood process chain: the case of Lake Palcacocha and Huaraz, Peru. Hydrol. Earth Syst. Sci. 20, 2519–2543. https://doi.org/10.5194/hess-20-2519-2016

Somos-Valenzuela, M.A., McKinney, D.C., Byers, A.C., Rounce, D.R., Portocarrero, C., Lamsal, D., 2015. Assessing downstream flood impacts due to a potential GLOF from Imja Tsho in Nepal. Hydrol. Earth Syst. Sci. 19, 1401–1412. https://doi.org/10.5194/hess-19-1401-2015

Song, C., Sheng, Y., Ke, L., Nie, Y., Wang, J., 2016. Glacial lake evolution in the southeastern Tibetan Plateau and the cause of rapid expansion of proglacial lakes linked to glacial-hydrogeomorphic processes. J. Hydrol. 540, 504–514. https://doi.org/10.1016/j.jhydrol.2016.06.054

Song, C., Sheng, Y., Wang, J., Ke, L., Madson, A., Nie, Y., 2017. Heterogeneous glacial lake changes and links of lake expansions to the rapid thinning of adjacent glacier termini in the Himalayas. Geomorphology 280, 30–38. https://doi.org/10.1016/j.geomorph.2016.12.002

Stolle, A., Bernhardt, A., Schwanghart, W., Hoelzmann, P., Adhikari, B.R., Fort, M., Korup, O., 2017. Catastrophic valley fills record large Himalayan earthquakes, Pokhara, Nepal. Quat. Sci. Rev. 177, 88–103. https://doi.org/10.1016/j.quascirev.2017.10.015

Su, Z., Shi, Y., 2002. Response of monsoonal temperate glaciers to global warming since the Little Ice Age. Quat. Int. 97, 123–131.

Sun, M., Liu, S., Yao, X., Li, J., 2014. The cause and potential hazard of glacial lake outburst flood occurred on July 5, 2013 in Jiali County, Tibet. J. Glaciol. Geocryol. 36, 158–165.

Thompson, S.S., Benn, D.I., Dennis, K., Luckman, A., 2012. A rapidly growing moraine-dammed glacial lake on Ngozumpa Glacier, Nepal. Geomorphology 145–146, 1–11. https://doi.org/10.1016/j.geomorph.2011.08.015

Tulbure, M.G., Broich, M., Stehman, S.V., Kommareddy, A., 2016. Surface water extent dynamics from three decades of seasonally continuous Landsat time series at subcontinental scale in a semi-arid region. Remote Sens. Environ. 178, 142–157. https://doi.org/10.1016/j.rse.2016.02.034

USGS, 2018. Landsat Collections (Report No. 2018–3049), Fact Sheet. Reston, VA.

Veh, G., Korup, O., Roessner, S., Walz, A., 2018. Detecting Himalayan glacial lake outburst floods from Landsat time series. Remote Sens. Environ. 207, 84–97. https://doi.org/10.1016/j.rse.2017.12.025

Veh, G., Korup, O., von Specht, S., Roessner, S., Walz, A., 2019. Unchanged frequency of moraine-dammed glacial lake outburst floods in the Himalaya. Nat. Clim. Change 9,379-383. https://doi.org/10.1038/s41558-019-0437-5

Verbesselt, J., Zeileis, A., Herold, M., 2012. Near real-time disturbance detection using satellite image time series. Remote Sens. Environ. 123, 98–108. https://doi.org/10.1016/j.rse.2012.02.022

Vuichard, D., Zimmermann, M., 1987. The 1985 Catastrophic Drainage of a Moraine-Dammed Lake, Khumbu Himal, Nepal: Cause and Consequences. Mt. Res. Dev. 7, 91. https://doi.org/10.2307/3673305

Walder, J.S., O'Connor, J.E., 1997. Methods for predicting peak discharge of floods caused by failure of natural and constructed earthen dams. Water Resour. Res. 33, 2337–2348.

Wang, S., Qin, D., Xiao, C., 2015. Moraine-dammed lake distribution and outburst flood risk in the Chinese Himalaya. J. Glaciol. 61, 115–126. https://doi.org/10.3189/2015JoG14J097

Wang, W., Gao, Y., Iribarren Anacona, P., Lei, Y., Xiang, Y., Zhang, G., Li, S., Lu, A., 2018. Integrated hazard assessment of Cirenmaco glacial lake in Zhangzangbo valley, Central Himalayas. Geomorphology 306, 292–305. https://doi.org/10.1016/j.geomorph.2015.08.013

Wang, W., Xiang, Y., Gao, Y., Lu, A., Yao, T., 2015. Rapid expansion of glacial lakes caused by climate and glacier retreat in the Central Himalayas. Hydrol. Process. 29, 859–874. https://doi.org/10.1002/hyp.10199

Wang, W., Yao, T., Gao, Y., Yang, X., Kattel, D.B., 2011a. A First-order Method to Identify Potentially Dangerous Glacial Lakes in a Region of the Southeastern Tibetan Plateau. Mt. Res. Dev. 31, 122–130. https://doi.org/10.1659/MRD-JOURNAL-D-10-00059.1

Wang, W., Yao, T., Yang, W., Joswiak, D., Zhu, M., 2012. Methods for assessing regional glacial lake variation and hazard in the southeastern Tibetan Plateau: a case study from the Boshula mountain range, China. Environ. Earth Sci. 67, 1441–1450. https://doi.org/10.1007/s12665-012-1589-z

Wang, W., Yao, T., Yang, X., 2011b. Variations of glacial lakes and glaciers in the Boshula mountain range, southeast Tibet, from the 1970s to 2009. Ann. Glaciol. 52, 9–17.

Wang, X., Chai, K., Liu, S., Wei, J., Jiang, Z., Liu, Q., 2017. Changes of glaciers and glacial lakes implying corridor-barrier effects and climate change in the Hengduan Shan, southeastern Tibetan Plateau. J. Glaciol. 63, 535–542. https://doi.org/10.1017/jog.2017.14

Wang, X., Liu, S., Ding, Y., Guo, W., Jiang, Z., Lin, J., Han, Y., 2012. An approach for estimating the breach probabilities of moraine-dammed lakes in the Chinese Himalayas using remote-sensing data. Nat. Hazards Earth Syst. Sci. 12, 3109–3122. https://doi.org/10.5194/nhess-12-3109-2012

Waske, B., Braun, M., 2009. Classifier ensembles for land cover mapping using multitemporal SAR imagery. ISPRS J. Photogramm. Remote Sens. 64, 450–457. https://doi.org/10.1016/j.isprsjprs.2009.01.003

Wasson, R.J., Sundriyal, Y.P., Chaudhary, S., Jaiswal, M.K., Morthekai, P., Sati, S.P., Juyal, N., 2013. A 1000-year history of large floods in the Upper Ganga catchment, central Himalaya, India. Quat. Sci. Rev. 77, 156–166. https://doi.org/10.1016/j.quascirev.2013.07.022

Watanabe, T., Lamsal, D., Ives, J.D., 2009. Evaluating the growth characteristics of a glacial lake and its degree of danger of outburst flooding: Imja Glacier, Khumbu Himal, Nepal. Nor. Geogr. Tidsskr. - Nor. J. Geogr. 63, 255–267. https://doi.org/10.1080/00291950903368367

Watanabe, T., Rothacher, D., 1996. The 1994 Lugge Tsho Glacial Lake Outburst Flood, Bhutan Himalaya. Mt. Res. Dev. 16, 77. https://doi.org/10.2307/3673897

Watanbe, T., Rothacher, D., 1996. The 1994 Lugge Tsho Glacial Lake Outburst Flood, Bhutan Himalaya. Mt. Res. Dev. 16, 77. https://doi.org/10.2307/3673897

Watson, C.S., Carrivick, J., Quincey, D., 2015. An improved method to represent DEM uncertainty in glacial lake outburst flood propagation using stochastic simulations. J. Hydrol. https://doi.org/10.1016/j.jhydrol.2015.08.046

Watson, C.S., Quincey, D.J., Carrivick, J.L., Smith, M.W., 2016. The dynamics of supraglacial ponds in the Everest region, central Himalaya. Glob. Planet. Change 142, 14–27. https://doi.org/10.1016/j.gloplacha.2016.04.008

Watson, C.S., Quincey, D.J., Smith, M.W., Carrivick, J.L., Rowan, A.V., James, M.R., 2017. Quantifying ice cliff evolution with multi-temporal point clouds on the debris-covered Khumbu Glacier, Nepal. J. Glaciol. 63, 823–837. https://doi.org/10.1017/jog.2017.47

Weiss, A., 2001. Topographic position and landforms analysis. Presented at the Poster presentation, ESRI user conference, San Diego, CA.

Wester, P., Mishra, A., Mukherji, A., Shrestha, A.B. (Eds.), 2019. The Hindu Kush Himalaya Assessment: Mountains, Climate Change, Sustainability and People. Springer International Publishing, Cham.

Westoby, M.J., Brasington, J., Glasser, N.F., Hambrey, M.J., Reynolds, J.M., Hassan, M.A.A.M., Lowe, A., 2015. Numerical modelling of glacial lake outburst floods using physically based dam-breach models. Earth Surf. Dyn. 3, 171–199. https://doi.org/10.5194/esurf-3-171-2015

Westoby, M.J., Glasser, N.F., Brasington, J., Hambrey, M.J., Quincey, D.J., Reynolds, J.M., 2014. Modelling outburst floods from moraine-dammed glacial lakes. Earth-Sci. Rev. 134, 137–159. https://doi.org/10.1016/j.earscirev.2014.03.009

Westoby, M.J., Glasser, N.F., Hambrey, M.J., Brasington, J., Reynolds, J.M., Hassan, M.A.A.M., 2014. Reconstructing historic Glacial Lake Outburst Floods through numerical modelling and geomorphological assessment: Extreme events in the Himalaya. Earth Surf. Process. Landf. 1675–1692. https://doi.org/10.1002/esp.3617

Wijngaard, R.R., Lutz, A.F., Nepal, S., Khanal, S., Pradhananga, S., Shrestha, A.B., Immerzeel, W.W., 2017. Future changes in hydro-climatic extremes in the Upper Indus, Ganges, and Brahmaputra River basins. PLOS ONE 12, e0190224. https://doi.org/10.1371/journal.pone.0190224

Wilson, R., Glasser, N.F., Reynolds, J.M., Harrison, S., Anacona, P.I., Schaefer, M., Shannon, S., 2018. Glacial lakes of the Central and Patagonian Andes. Glob. Planet. Change 162, 275–291. https://doi.org/10.1016/j.gloplacha.2018.01.004

Wingham, D.J., Siegert, M.J., Shepherd, A., Muir, A.S., 2006. Rapid discharge connects Antarctic subglacial lakes. Nature 440, 1033–1036. https://doi.org/10.1038/nature04660

Worni, R., Huggel, C., Stoffel, M., 2013. Glacial lakes in the Indian Himalayas — From an area-wide glacial lake inventory to on-site and modeling based risk assessment of critical glacial lakes. Sci. Total Environ. 468–469, S71–S84. https://doi.org/10.1016/j.scitotenv.2012.11.043

Worni, R., Stoffel, M., Huggel, C., Volz, C., Casteller, A., Luckman, B., 2012. Analysis and dynamic modeling of a moraine failure and glacier lake outburst flood at Ventisquero Negro, Patagonian Andes (Argentina). J. Hydrol. 444–445, 134–145. https://doi.org/10.1016/j.jhydrol.2012.04.013

Wulder, M.A., Masek, J.G., Cohen, W.B., Loveland, T.R., Woodcock, C.E., 2012. Opening the archive: How free data has enabled the science and monitoring promise of Landsat. Remote Sens. Environ. 122, 2–10. https://doi.org/10.1016/j.rse.2012.01.010

Wulder, M.A., White, J.C., Loveland, T.R., Woodcock, C.E., Belward, A.S., Cohen, W.B., Fosnight, E.A., Shaw, J., Masek, J.G., Roy, D.P., 2016. The global Landsat archive: Status, consolidation, and direction. Remote Sens. Environ. 185, 271–283. https://doi.org/10.1016/j.rse.2015.11.032

Xin, W., Shiyin, L., Wanqin, G., Junli, X., 2008. Assessment and Simulation of Glacier Lake Outburst Floods for Longbasaba and Pida Lakes, China. Mt. Res. Dev. 28, 310–317. https://doi.org/10.1659/mrd.0894

Xin, W., Shiyin, L., Wanqin, G., Xiaojun, Y., Zongli, J., Yongshun, H., 2012. Using Remote Sensing Data to Quantify Changes in Glacial Lakes in the Chinese Himalaya. Mt. Res. Dev. 32, 203–212. https://doi.org/10.1659/MRD-JOURNAL-D-11-00044.1

Xu, D., 1988. Characteristics of debris flow caused by outburst of glacial lake in Boqu River, Xizang, China, 1981. GeoJournal 17, 569–580.

Xu, L., Li, J., Brenning, A., 2014. A comparative study of different classification techniques for marine oil spill identification using RADARSAT-1 imagery. Remote Sens. Environ. 141, 14–23. https://doi.org/10.1016/j.rse.2013.10.012

Yamada, T., Sharma, C.K., 1993. Glacier lakes and outburst floods in the Nepal Himalaya. IAHS Publ.-Publ. Int. Assoc. Hydrol. Sci. 218, 319–330.

Yamanokuchi, T., Tadono, T., Komori, J., Kawamoto, S., Tomiyama, N., 2011. Temporal monitoring of supraglacial lakes on Tshojo Glacier at Bhutan, in: IEEE International Geoscience and Remote Sensing Symposium, Vancouver, Canada.

Yan, W., Liu, J., Zhang, M., Hu, L., Chen, J., 2017. Outburst flood forecasting by monitoring glacier-dammed lake using satellite images of Karakoram Mountains, China. Quat. Int. 453, 24–36. https://doi.org/10.1016/j.quaint.2017.03.019

Yao, X., Liu, S., Sun, M., Wei, J., Guo, W., 2012. Volume calculation and analysis of the changes in moraine-dammed lakes in the north Himalaya: a case study of Longbasaba lake. J. Glaciol. 58, 753–760. https://doi.org/10.3189/2012JoG11J048

Zevenbergen, L.W., Thorne, C.R., 1987. Quantitative analysis of land surface topography. Earth Surf. Process. Landf. 12, 47–56.

Zhang, G., Yao, T., Xie, H., Wang, W., Yang, W., 2015a. An inventory of glacial lakes in the Third Pole region and their changes in response to global warming. Glob. Planet. Change 131, 148–157. https://doi.org/10.1016/j.gloplacha.2015.05.013

Zhu, Z., Gallant, A.L., Woodcock, C.E., Pengra, B., Olofsson, P., Loveland, T.R., Jin, S., Dahal, D., Yang, L., Auch, R.F., 2016. Optimizing selection of training and auxiliary data for operational land cover classification for the LCMAP initiative. ISPRS J. Photogramm. Remote Sens. 122, 206–221. https://doi.org/10.1016/j.isprsjprs.2016.11.004

Zhu, Z., Wang, S., Woodcock, C.E., 2015. Improvement and expansion of the Fmask algorithm: cloud, cloud shadow, and snow detection for Landsats 4–7, 8, and Sentinel 2 images. Remote Sens. Environ. 159, 269–277. https://doi.org/10.1016/j.rse.2014.12.014

Zhu, Z., Woodcock, C.E., 2012. Object-based cloud and cloud shadow detection in Landsat imagery. Remote Sens. Environ. 118, 83–94. https://doi.org/10.1016/j.rse.2011.10.028

7. Supplementary Information

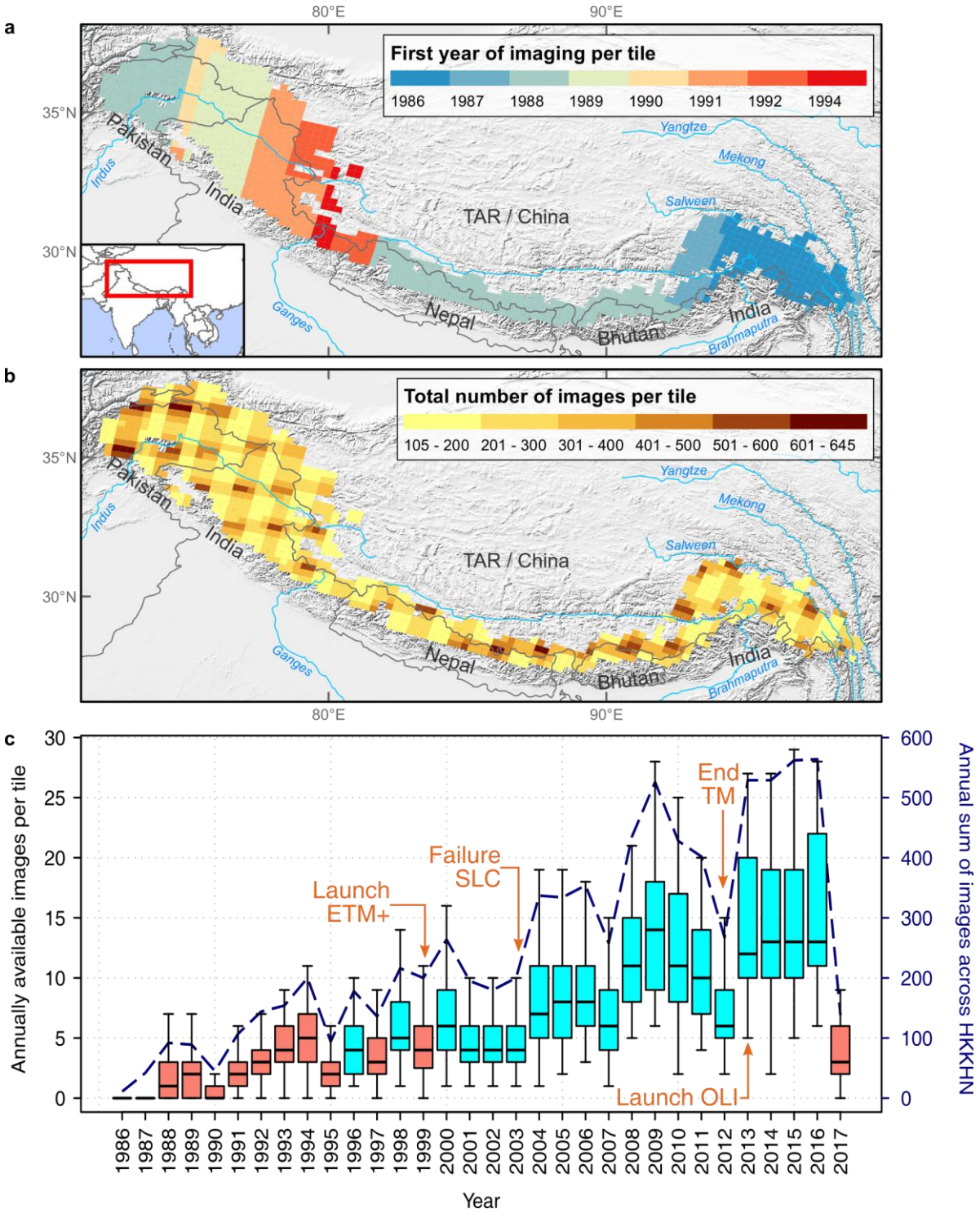

Supplementary Figure 7-1: Temporal and geographic coverage of Landsat imagery over the HKKHN. *Data given in 25 km ×25 km tiles.* ***a****, Year of first available image per tile.* ***b****, Total number of images per tile.* ***c****, Available images per tile and year along the HKKHN. Boxes span interquartile range; medians are thick black lines; whiskers encompass 1.5 times the interquartile range. Blue and red boxes express years with complete and incomplete image coverage across all tiles. Dashed line refers to right vertical axis.*

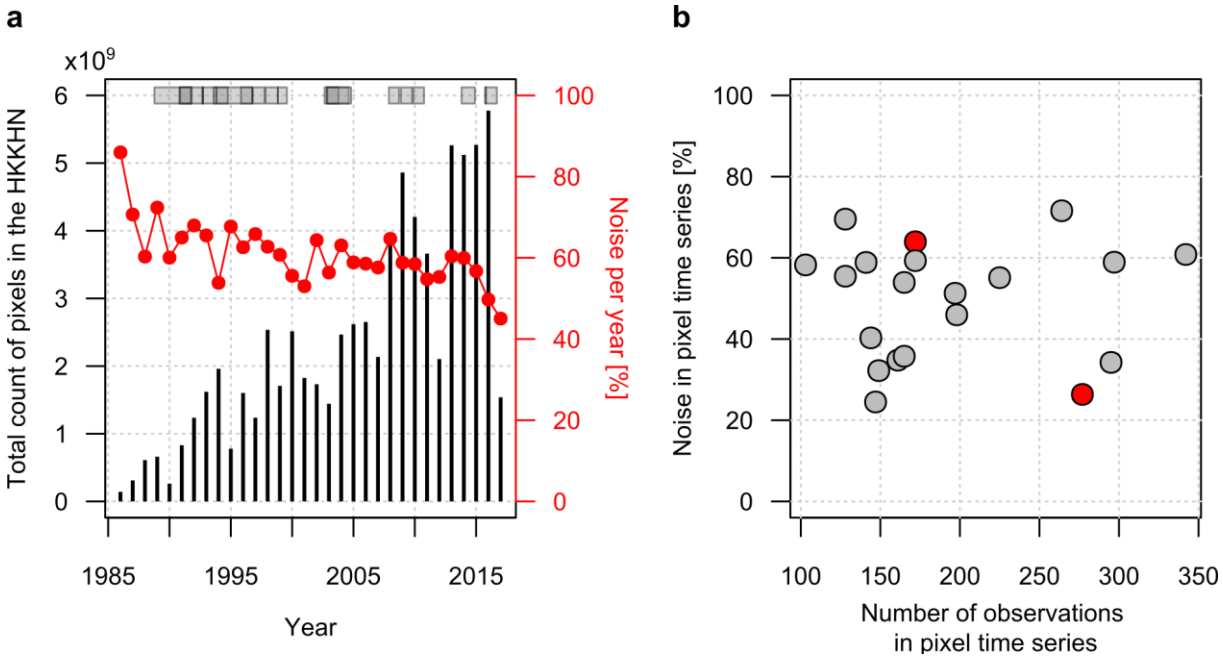

Supplementary Figure 7-2: Noise in Landsat images and GLOF times series. a, *Summary statistics on all classified Landsat pixels. Black lines are the annual sums of available Landsat pixels in the HKKHN and red line is the annual fraction of noise (snow, ice, clouds and shadow) as classified by the Random Forest classifier. The fraction of noise is 58.7% across the total of 74.5 × 10^9 classified pixels. Grey bars on top are time intervals between suitable Landsat images for newly detected GLOFs, which do not correlate with the total amount of pixels or their noise-free fraction.* ***b,*** *Fraction of noise in GLOF pixel time series. Dots show newly detected GLOFs, represented by a randomly selected pixel that changed from water to land after the GLOF. The algorithm successfully extracted GLOFs in pixel time series with >70% noise, regardless of available amount of pixels in the time series. 20 of the 22 newly detected GLOFs happened in the monsoon season (grey dots), demonstrating that the algorithm can successfully bridge missing images during the periods of extended cloud cover.*

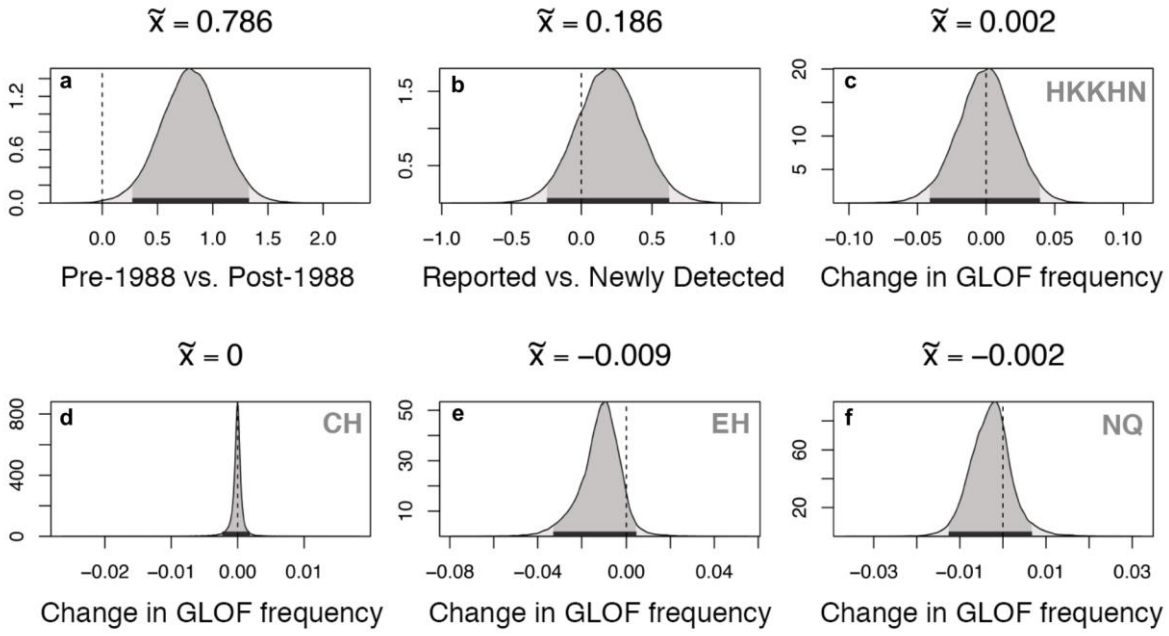

Supplementary Figure 7-3: Posterior distributions of GLOF characteristics. *Horizontal black thick line and dark grey shade highlight 95% highest density intervals (HDI); vertical dashed line marks zero values; modal values are given on top of each distribution; y-axes have arbitrary units.* ***a****, Deviations from the common mean of estimated (log-transformed) GLOF volumes between for the pre-Landsat era (pre-1988) and younger (post-1988) are credibly non-zero (the zero value is outside of the 95% HDI).* ***b****, Deviations from the common mean of estimated (log-transformed) GLOF volumes in the Landsat era for reported and newly detected cases cannot be credibly distinguished.* ***c****, Slope of Bayesian robust linear regression indicating average annual GLOF frequency in the HKKHN cannot be credibly distinguished from zero.* ***d-f****, Corresponding regression slopes for the Central Himalayas (CH), eastern Himalayas (EH), and Nyainqentanglha Mountains (NQ); none of the parts of the HKKHN have had credible increases in GLOF frequency since the late 1980s.*

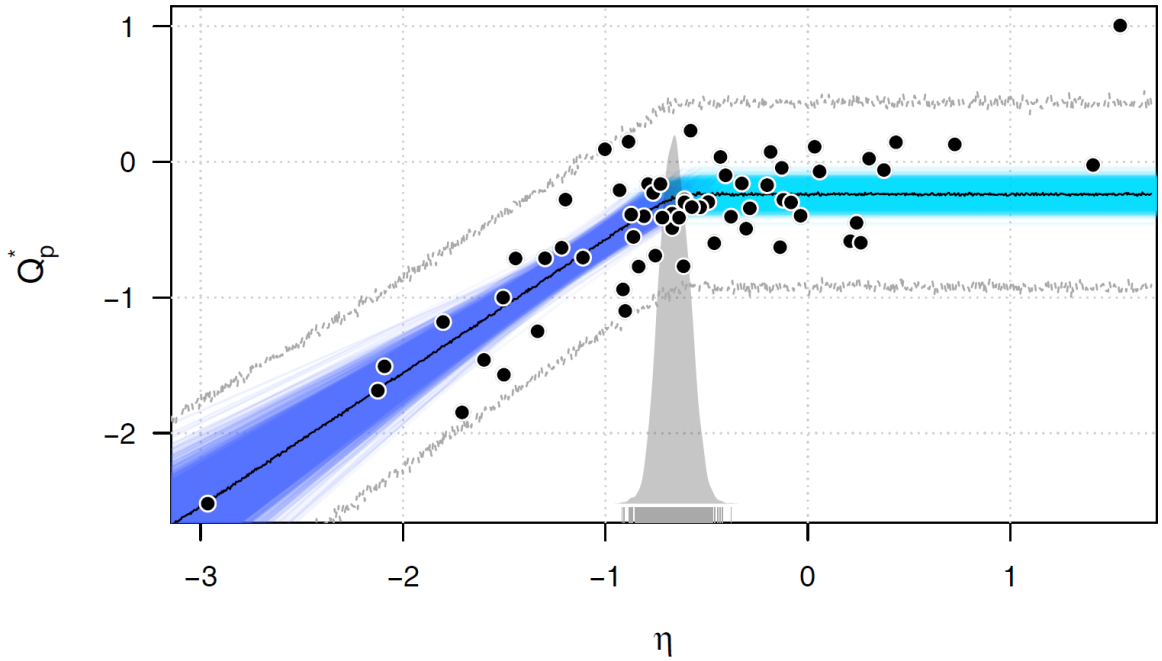

Supplementary Figure 7-4: Bayesian piecewise linear regression for predicting peak discharge Q_{p^*} from η, the product of breach rate and released flood volume (all dimensionless). *Lines are mean predictive posteriors of 5,000 samples of piecewise models with linear increase below (dark blue) and a constant asymptote above (light blue) a breakpoint learned from 63 data on dam failures (black dots). Grey probability density estimates the posterior breakpoint locations (grey ticks). Solid black line is the median of predictive posteriors, and dashed envelope is piecewise 95% highest density interval.*

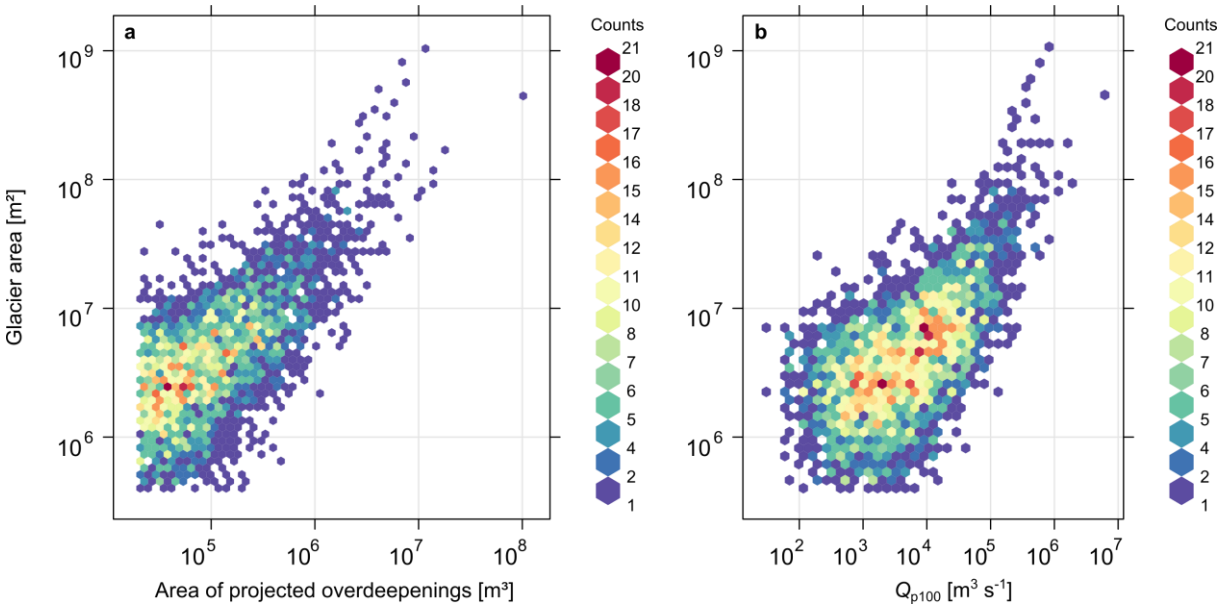

Supplementary Figure 7-5: Glacier area versus area of overdeepenings and Q_{p100}. a, *Glacier area correlates positively (on log scale) with the area of the largest projected overdeepening per glacier with a Pearson's correlation coefficient of ρ = 0.685.* ***b,*** *Glacier area correlates positively (on log scale) with the mode of predicted Q_p per glacier, showing a Pearson's correlation coefficient of ρ = 0.63.*

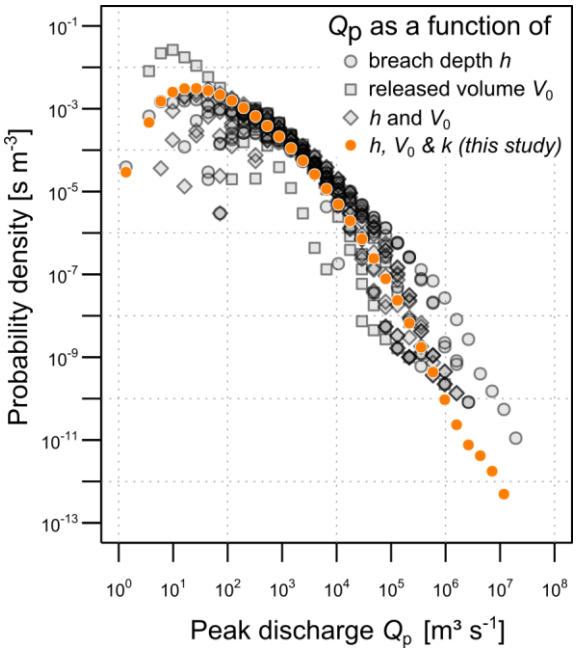

Supplementary Figure 7-6: Estimated probability densities of Q_p for ~9,500 projected Himalayan glacial overdeepenings. *We assumed complete drainage and breach to the lake beds, and predicted Q_p with our approach and 21 empirical equations complied in Das et al. (2015). Symbols refer to whether peak discharge is a function of breach depth h, released volume V_0 or a combination of both. Estimates of Q_p from empirical equations are consistent within ~10²-10⁴ m³ s^{-1}, but spreads over more than two orders of magnitudes for larger GLOF discharges.*

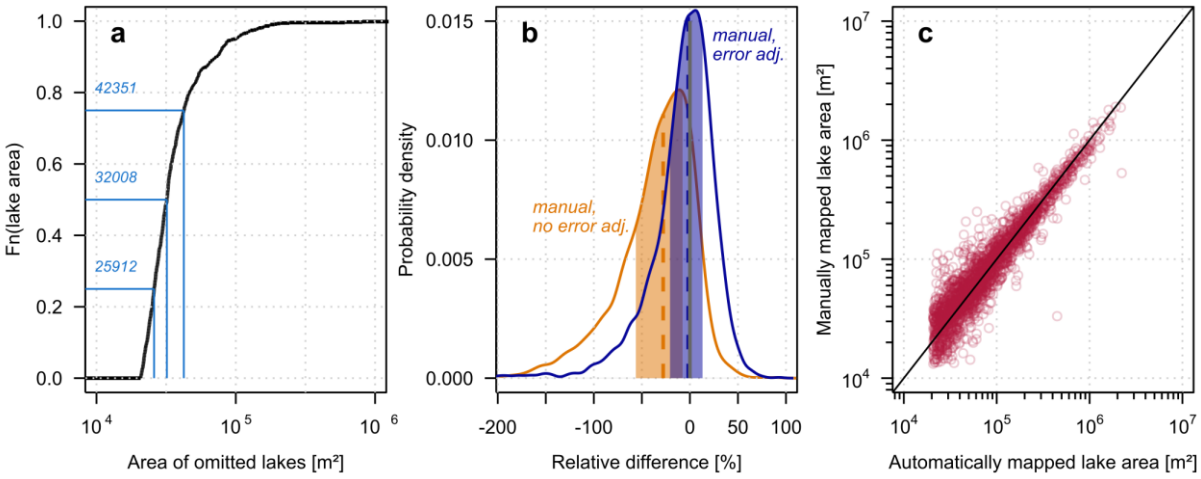

Supplementary Figure 7-7: Accuracy assessment for the present-day lake inventory. a, *Empirical cumulative distribution function of 737 lakes that we omitted using our automatic mapping approach. Lines show the median, and the 25th and 75th percentiles of omitted lake areas.* ***b,*** *Probability density of relative area difference between automatically and manually mapped lakes. Blue curves account for half a pixel mapping error in manually mapped lakes, whereas the orange curve is without error adjustment. Colour fills are the interquartile ranges, and dashed lines are the medians.* ***c,*** *Area of automatically mapped lakes versus area of manually mapped lakes (n = 2,329).*

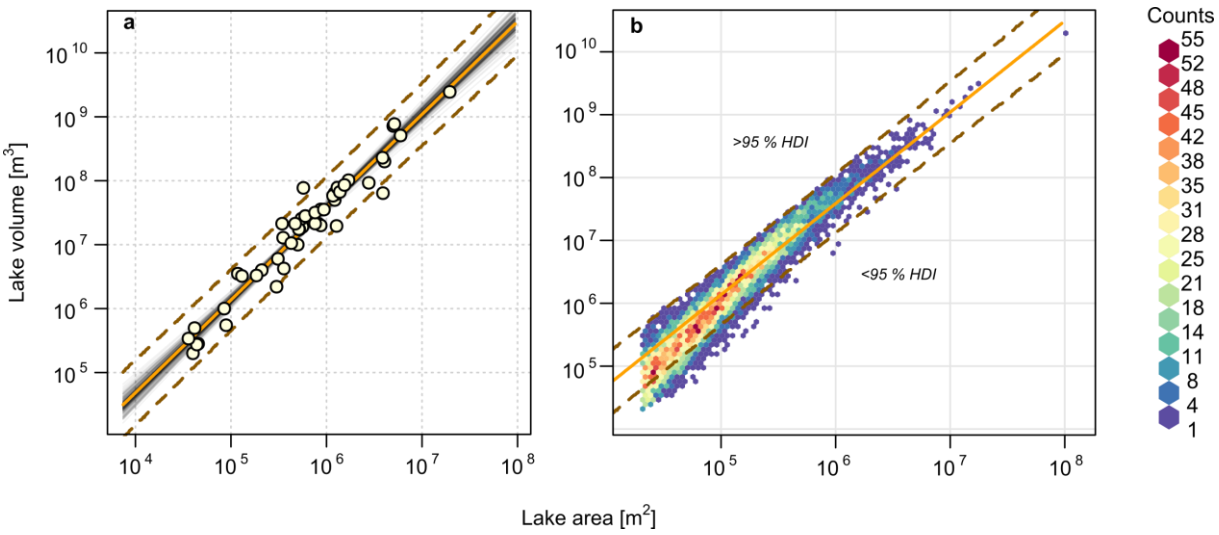

Supplementary Figure 7-8: Area-volume relationship of bathymetrically surveyed lakes and modelled overdeepenings. a, *Sample of 49 bathymetrically surveyed glacial lakes (light yellow circles; from Cook and Quincey et al., 2015). Semi-transparent black lines are a sample of 500 median predictive posteriors from 100,000 linear models of lake area versus lake volume. Solid light green line is the median of all mean predictive posteriors and dashed dark green envelope is the 95% highest density interval.* ***b,*** *Distribution of projected overdeepenings after lakes above the 95% HDI and <1 m deep had been removed from the initial distribution.*

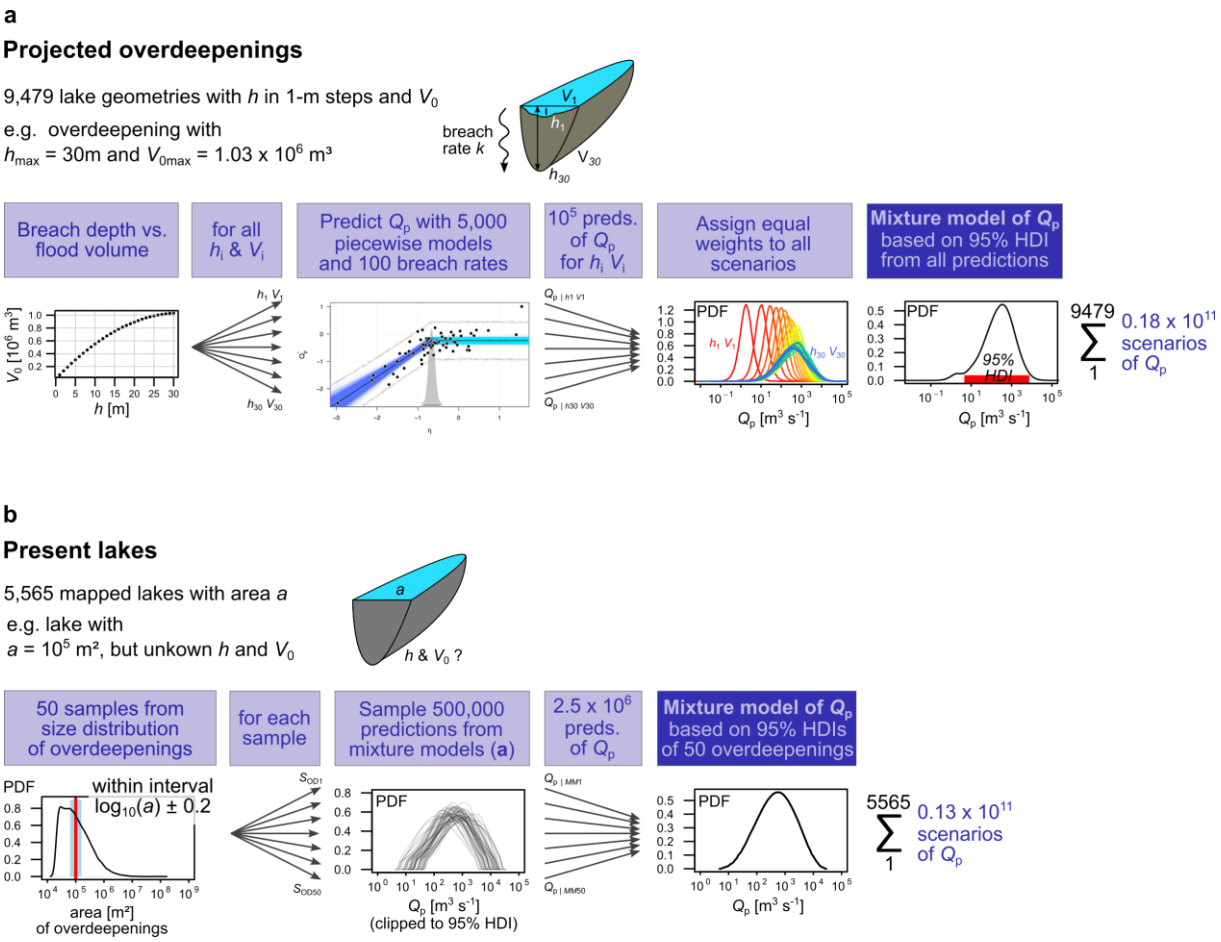

Supplementary Figure 7-9: Scheme for predicting Q_p for projected overdeepenings and present lakes. a, *Projected overdeepenings offer well-constraint geometries in terms of lake depths and volumes. For every 1-m drop in lake level, we calculated the associated flood volume and predicted Q_p with a piecewise Bayesian regression, obtaining a mixture model of Q_p from equally weighted outburst scenarios.* ***b****, Present lakes only offer mapped surface areas, but lack information on depths and volumes. From all overdeepenings, we randomly sampled 50 overdeepenings within an interval around the areas of present lakes and extracted the associated values of Q_p, obtaining again a mixture model of Q_p.*

Supplementary Table 7.1: Reported GLOFs along the HKKHN in chronological order. *Estimated volumes were derived from digitised lake areas with empirical lake area to volume relationship (Cook and Quincey, 2015). Asterisks for total flood volumes denote estimates from literature. Thick line denotes the beginning of the Landsat era.*

ID	Lake	Country	Basin	Lat [°]	Lon [°]	Altitude [m a.s.l.]	Date	Vol. before [10^6 m^3]	Vol. after [10^6 m^3]	Total flood vol. [10^6 m^3]	Length of impact track [km]	Reported fatalities, damages and economic loss	Reference
1	Taraco	China	CH	28.30	86.13	5245	1935-08-06			3* - 63*		66,700 m^2 of wheat field, livestock	(Ives et al., 2010; S. S. Liu et al., 2014; X. Wang et al., 2012)
2	Qubixiamaco/ Qiongbihema Tsho	China	EH	27.85	88.92	4764	1940-07-10			12.4*		Street and buildings	(S. S. Liu et al., 2014; X. Wang et al., 2012)
3	Lure Co	China	EH	28.27	90.59	5415	1950s						(S. S. Liu et al., 2014)
4	Sangwangco	China	EH	28.24	90.11	5130	1954-07-16			300*		691 people and 8,679 livestock, 170 villages destroyed	(Gurung et al., 2017; Ives et al., 2010; Osti and Egashira, 2009; X. Wang et al., 2012)
5	Cuoalong glacier	Bhutan	EH	28.06	90.61	4864	1955 - 1966					Devastation 28 km downstream	(Komori et al., 2012)
6	Tarina Tsho	China	EH	28.11	89.90	4274	1957					Punakha Dzong building, 75 km downstream	(Komori et al., 2012)
7	Bachamancha	Bhutan	EH	28.03	90.68	4797	1960s						(Ives et al., 2010)
8	Longdaco	China	CH	28.62	85.35	5115	1964-08-28			10.8*			(Bajracharya et al., 2006; Chen et al., 2013)
9	Gelhaipuco/ Jilaico	China	EH	27.96	87.81	5248	1964-09-21	9.64	2.27	7.36 / 23.4*	65.5	Nepal–China Highway, 12 trucks	(J.-J. Liu et al., 2014; X. Wang et al., 2012)
10	Damenhaico	China	NQ	29.87	93.04	5219	1964-09-26			2*		villages and blocked the Niyang River for 16 h	(Ives et al., 2010)
11	Zhangzangbo/ Cirenmaco 1st	China	CH	28.07	86.07	4630	1964						(J.-J. Liu et al., 2014; Wang et al., 2018)
12	name unknown	Bhutan	EH	27.82	89.35	4474	1966 - 1974						(Komori et al., 2012)
13	Ayaco 1st	China	CH	28.35	86.49	5529	1968-08-15			90*		Roads and one concrete bridge damaged as far as 40 km away	(J.-J. Liu et al., 2014; X. Wang et al., 2012)
14	Ayaco 2nd	China	CH	28.35	86.49	5529	1969-08-17						(J.-J. Liu et al., 2014; X. Wang et al., 2012)
15	Ayaco 3rd	China	CH	28.35	86.49	5529	1970-08-18						(J.-J. Liu et al., 2014; X. Wang et al., 2012)
16	Pogeco	China	NQ	31.74	94.73	4322	1972-07-23					Few minor bridges	(S. S. Liu et al., 2014)
17	Bogeco	China	NQ	31.86	94.76	4332	1974-07-06					Roads, wooden bridges	(S. S. Liu et al., 2014)
18	Nare	Nepal	CH	27.83	86.83	4596	1977-09-03			4.9*		Mini hydropower plant, bridges and trails	(Buchroithner et al., 1982; Cenderelli and Wohl, 2001; X. Wang et al., 2012)
19	Nagma Pokhari	Nepal	EH	27.87	87.87	4926	1980-06-23	19.46	16.46	3	70.7	Villages destroyed 71 km from source	(Fujita et al., 2013; Ives et al., 2010; X. Wang et al., 2012)
20	Zharico	China	EH	28.30	90.61	5353	1981-06-24					Mills, hydropower station, bridges, and houses	(Ives et al., 2010; S. S. Liu et al., 2014; X. Wang et al., 2012)
21	Zhangzangbo/ Cirenmaco 2nd	China	CH	28.07	86.07	4630	1981-07-11			19*		Killed 200 people, buildings, bridges and a hydropower station	(Wang et al., 2018)

22	Yindapu Co	China	EH	27.95	87.91	5168	1982-08-27	23.49	16.46	7.03	33.4	~1,600 head of livestock, 20 ha of cultivated fields, houses in eight villages	(Gurung et al., 2017; S. S. Liu et al., 2014; Nie et al., 2018)
23	Dig Tsho	Nepal	CH	27.87	86.59	4376	1985-08-04	9.09	6.18	2.90/ 5*	29.7	Hydroelectric power plant, 14 bridges, ~30 houses, many hectares of farmland, trail network	(Cenderelli and Wohl, 2003; Vuichard and Zimmermann, 1987)
24	Guangxieco	China	NQ	29.47	96.50	3833	1988-07-15	8.28	2.55	5.72/ 6*	31.0	Killed 5 people and 50 livestock; 18 bridges; NY 0.1 billion damage	(J.-J. Liu et al., 2014; X. Wang et al., 2012)
25	Chubung	Nepal	CH	27.88	86.47	4615	1991-07-12			0.5* - 1*		Few houses	(Kattelmann, 2003; X. Wang et al., 2012)
26	Luggye Tsho	Bhutan	EH	28.09	90.30	4511	1994-10-07	32.21	24.11	8.09 / 17.2*	25.6	Houses in different villages	(Fujita et al., 2008)
27	Zanaco	China	CH	28.66	85.37	4732	1995-06-07	0.66	0.00	0.66	12.0	28 km stretch of a highway	(J.-J. Liu et al., 2014; Nie et al., 2018)
28	Tam Pokhari/ Sabai Tsho	Nepal	CH	27.74	86.84	4411	1998-09-03	10.03	4.59	5.44/ 19.5*	61.3	Human lives and more than NRs 156 million	(Ives et al., 2010; Lamsal et al., 2015; Osti and Egashira, 2009)
29	Kongyangmi La Tsho	India	EH	27.90	88.78	5115	1995	11.16	2.86	8.30	7.5	n.a. (found by image analysis)	(Nie et al., 2018)
30	Gangri Tsho III	Bhutan	EH	27.90	90.81	4810	1998	0.64	0.11	0.53/ 1*	10.1	n.a. (found by image analysis)	(Komori et al., 2012)
31	Chongbaxia Tsho/ Longjiu Co	China	EH	28.21	89.74	4882	2001	18.23	9.49	8.75/ 7.8*	15.0	n.a. (found by image analysis)	(Fujita et al., 2013; Komori et al., 2012; S. S. Liu et al., 2014; Nie et al., 2018)
32	Unnamed	China	NQ	29.75	96.47	5062	2005-09	2.02	0.84	1.18	5.6	n.a. (found by image analysis)	(Wang et al., 2011b)
33	Tsho Ga/ Cuoga	China	NQ	30.83	94.00	4737	2009-07-29	10.46	4.56	5.90	70.9	Killed 2 people; destroyed 27 kms of road, 6 bridges; 19 cars and motorcycles	(S. S. Liu et al., 2014; Nie et al., 2018)
34	Tshojo glacier	Bhutan	EH	28.10	90.16	4267	2009-04-29			1.47*		None	(Komori et al., 2012; Yamanokuchi et al., 2011)
35	Geiqu	China	EH	27.95	87.99	5488	2010	0.41	0.04	0.37	7.4	Roads and a bridge	(S. S. Liu et al., 2014)
36	Chorabari	India	WH	30.75	79.06	3889	2013-06-17	0.29	0.00	0.29/ 0.43*	32.7	Hundreds to thousands of people, hydropower plants, roads, buildings	(Allen et al., 2016; Das et al., 2015)
37	Ranzeria Co	China	NQ	30.47	93.53	5013	2013-07-05	13.22	4.37	8.85	62.4	Killed several people and livestock; concrete bridge; economic loss ~CNY 0.25 billion	(Sun et al., 2014)
38	Lemthang Tsho	Bhutan	EH	28.07	89.58	4257	2015-06-28	0.72	0.00	0.72/ 0.37*	14.0	4 horses; 4 bridges, 1 acre of land, 1 km of trail	(Gurung et al., 2017)
39	Gongbatongsha Tsho	China	CH	28.08	86.06	4619	2016-07-07	0.09	0.00	0.09	8.1	Hydropower station	(Cook et al., 2018)
40	Langmale lake	Nepal	CH	27.81	87.14	4790	2017-04-20	0.93	0.28	0.65	32.0	Three buildings, bridges, many hectares of farmland	(Byers et al., 2018)

Supplementary Table 7.2: Newly detected GLOFs. *Period of outburst is given by the last clear image before and the first clear Landsat image after the GLOF. Estimated volumes were derived from digitised lake areas with empirical lake area to volume relationship (Cook and Quincey, 2015).*

ID	Country	Ba-sin	Lat [°N]	Lon [°E]	Alti-tude [m.a.s.l.]	Date of last clear image before GLOF	Date of next clear image after GLOF	Vol. before [10^6 m^3]	Vol. after [10^6 m^3]	Total flood vol. [10^6 m^3]	Length of impact track [km]
1	China	NQ	30.13	93.90	4,197	1976-01-04 (KH image)	1987-11-08	2.21	1.25	0.96	20.2
2	China	NQ	29.55	92.79	5,283	1988-10-09	1992-09-25	0.10	0.00	0.10	2.8
3	China	EH	27.97	88.89	5,433	1990-10-20	1991-10-23	8.76	4.18	4.58	38.5
4 (1st)	Bhutan	EH	28.09	90.33	4,706	1990-11-14	1991-09-30	1.61	0.38	1.22	2.4
5	China	NQ	29.75	96.56	5,122	1992-09-04	1992-09-20	15.32	5.20	10.12	13.6
6	India	EH	27.56	88.11	4,717	1992-09-23	1993-10-28	0.96	0.29	0.67	9.0
7	Pakistan	HKK	36.03	73.20	4,555	1993-08-06	1996-10-01	0.07	0.01	0.06	16.6
8	China	CH	30.34/ 30.36	82.14/ 82.12	5,451	1993-10-31	1994-10-02	6.61	2.21	4.40	10.9
9	China	CH	28.66	85.48	5,199	1995-11-01	1996-10-02	1.65	0.48	1.17	19.3
10	India	EH	27.70	92.39	5,060	1996-10-15	1997-10-02	1.12	0.15	0.97	19.0
11	Bhutan	EH	27.90	90.42	5,130	1997-11-01	1998-11-04	0.46	0.01	0.45	17.2
12	Nepal	CH	27.96	86.78	5,003	1998-11-02	1999-08-01	0.10	0.00	0.10	3.2
13	China	CH	28.14	85.92	4,858	2001-10-24	2003-09-28	0.35	0.35	NA	4.4
14	Pakistan	HKK	36.61	73.90	3,778	2002-08-23	2004-08-12	2.03	0.04	1.99	13.4
15	China	NQ	30.68	94.32	4,118	2002-10-24	2003-10-11	2.29	1.77	0.51	4.5
16	China	NQ	29.63	93.55	4,660	2002-11-09	2004-10-21	0.65	0.27	0.38	9.4
17	Bhutan	EH	28.28	90.23	5,302	2007-11-21	2008-09-20	28.76	23.05	5.71	35.8
18 (2nd)	Myanmar	NQ	28.32	97.84	4,187	2008-11-12	2009-10-14	1.08	0.84	0.24	2.3
19	Bhutan	EH	28.09	90.33	4,705	2009-11-18	2010-10-04	1.28	0.85	0.43	1.3
20	China	NQ	30.54	94.94	3,876	2013-10-23	2014-11-27	0.78	0.00	0.78	8.0
21	China	CH	30.31	82.20	5,534	2015-09-26	2016-09-12	4.98	2.79	2.18	10.2
22	China	EH	27.94	87.90	5,494	2015-10-09	2015-10-25	1.73	0.69	1.04	9.4

Supplementary Table 7.3: Estimated 100-year GLOFs for present and projected future meltwater lakes.

	Contemporary Q_{p100} [m³ s⁻¹]	**Possible future Q_{p100} [m³ s⁻¹]**	**Pooled estimate of present and future Q_{p100} [m³ s⁻¹]**	**Average contemporary GLOF rate [n yr⁻¹]**
All regions	20,607 $^{+2219}/_{-2320}$	41,817 $^{+5,423}/_{-4,723}$	31,169 $^{+4,347}/_{-3,413}$	1.26
Hindu Kush	786 $^{+206}/_{-166}$	1,587 $^{+366}/_{-489}$	1,091 $^{+259}/_{-263}$	0.06
Karakoram	831 $^{+233}/_{-203}$	2,782 $^{+873}/_{-656}$	2,610 $^{+736}/_{-646}$	0.06
Western Himalaya	136 $^{+213}/_{-215}$	271 $^{+465}/_{-718}$	90 $^{+458}/_{-458}$	0.03
Central Himalaya	3,940 $^{+768}/_{-568}$	5,991 $^{+893}/_{-1,101}$	5,289 $^{+1,102}/_{-826}$	0.19
Eastern Himalaya	18,159 $^{+2,757}/_{-2217}$	25,930 $^{+3,891}/_{-3,233}$	21,493 $^{+2,858}/_{-2,675}$	0.71
Nyainqentanglha	5,283 $^{+789}/_{-895}$	10,566 $^{+2,017}/_{-1,634}$	7,362 $^{+1,303}/_{-1168}$	0.23
Hengduan Shan	3,708 $^{+712}/_{-596}$	7,600 $^{+1,371}/_{-1,053}$	5,049 $^{+970}/_{-971}$	0.13